Studies of molecular responses in models of successful ageing

Thesis submitted in accordance with the requirements of the University of Liverpool for the degree of Doctor of Philosophy

By

Shaun Calvert

December 2017

Abstract

Ageing is a major socioeconomic concern and a risk factor in most diseases. As such, a better understanding of the ageing process could provide major insights into many disease treatments and prognoses. It is still not completely clear why organisms age, though multitudes of theories exist. There is large variation within and between species in lifespan and ageing progression. Superior maintenance of cognitive and physical function with age and avoidance of age-related morbidities is known as successful ageing. Understanding how this successful ageing occurs could be key to manipulating the ageing phenotype and mitigating age-related morbidity.

Caloric restriction has been shown to increase lifespan in a number of organisms and delay the ageing phenotype. This is regarded as the most robust intervention for the extension of lifespan to date. Caloric restriction is difficult to implement in humans, so the use of drugs that mimic the effects of caloric restriction are needed to take advantage of this intervention. We performed a microarray analysis of nematode worms (*Caenorhabditis elegans*) undergoing caloric restriction or being treated with predicted caloric restriction mimetics. These compounds act similarly to caloric restriction, but a large number of differentially expressed genes were observed between treatments and calorically restricted worms. This suggests that these compounds act through distinct mechanisms to caloric restriction. This was principally due to variations in worm development likely caused by varying levels of developmental delay. In addition to this developmental caveat, cell cycle and cell surface genes were found to be differentially expressed in a number of comparisons particularly with worms treated with the caloric restriction mimetic rapamycin.

The naked mole rat (*Heterocephalus glaber,* NMR) is the longest-lived rodent, living over 30 years. It is also cancer resistant. This lifespan is considerably longer than similarly sized mice (*Mus musculus*) at up to 4 years and comes with a delayed ageing phenotype. NMR cells have been reported to be more resistant to DNA damage, which is thought to be a major contributor to ageing and cancer. We hypothesise that this DNA damage resistance is responsible for the NMR's long-lived and cancer-resistant phenotype. By studying cells derived from these animals, comparative studies can be performed to identify potential causes for the observed differences in lifespan. As DNA damage is thought to be a causative factor in ageing we performed survival assays and calculated LD50 (the dose at which 50% of the cells die, known as the 'lethal dose 50') values for two DNA damaging compounds, camptothecin and chromium (vi) oxide in mouse and NMR cells. NMR cells appear to have higher LD50 values for both compounds and hence are more resistant as has been previously shown. NMR cells surviving treatment were also less prone to become irreversibly senescent. RNAseq was performed on the mouse and NMR primary fibroblast treated with camptothecin or chromium (vi) oxide. NMR

skin fibroblasts appear to show reduced expression of DNA damage repair genes, in contrast to what has been reported previously in NMR liver cells. Functional enrichment revealed significant differences at the cell surface between the two species. Cell adhesion genes were found to be expressed significantly greater in the NMR. NMR cells were shown to adhere to a culture plate more slowly than mouse cells after genotoxic treatment, confirming differences in cellular adhesion dynamics. We conclude that differences in mouse and NMR phenotype are not down to differences in DNA damage repair gene expression. Instead, we propose the hypothesis that the observed differences in cell surface chemistry contribute to the NMR's cancer-resistant phenotype.

Acknowledgements

I would like to thank my supervisor Dr João Pedro De Magalhães as well as Dr Aoife Doherty and Dr Robi Tacutu for their advice and guidance throughout this project. Additionally, I would like to thank Carl Wright and Tom Heyes for their support in the lab.

I would also like to thank my friends and family for their support and encouragement.

Finally, I would like to thank the Biotechnology and Biological Sciences Research Council for financially supporting this project through the DTP studentship (BB/J014516/1).

Table of contents

List of figures

List of tables

List of abbreviations

ACC – cetyl-coA carboxylase

aff-1 – AF4/FMR2 Family Member

AKT– protein kinase B

AMP – adenosine monophosphate

AMPK – AMP-activated protein kinase

ANOVA – Analysis of variance

APE1 – *Ape1*– AP endonuclease 1

ARE – Antioxidant Response Elements

Asm-3 – acid sphingomyelinase

ATM – Ataxia Telangiectasia Mutated

ATP – adenosine triphosphate

ATR – Ataxia Telangiectasia and Rad3-Related Protein

A2m – alpha2-macroglobulin

BER – Base Excision Repair

BLAST – Basic Local Alignment Search Tool

BRCA1 – *Brca1*– breast cancer associated 1

CAM – Cell Adhesion Molecule

cam – camptothecin

CAR – Coxsackie and Adenovirus Receptor

CDC25 – cell division cycle 25A

Cdkn1c – Cyclin Dependent Kinase Inhibitor 1C

Cdkn2a – Cyclin Dependent Kinase Inhibitor 2A

Cdkn2b – Cyclin Dependent Kinase Inhibitor 2B

CDK – Cyclin-Dependent Kinase

cDNA – Complementary DNA

C. elegans – Caenorhabditis elegans

Cenpf – Centromere Protein F

CGC – Caenorhabditis Genetics Centre

Cm – centimetre

CPD – cyclobutane pyrimidine dimers

Cr^{6+}– hexavalent chromium

ct – cycle threshold

CTN-1 – ctn-1 – alpha catulin

CUL4 – Cullin-4

C5 – Cyclopurines form when carbon 5

DDB1 – *Ddb1* – DNA-binding protein 1

DDB2 – DNA-binding protein 2

Dcc – Deleted in Colorectal Cancer

Δct – delta ct

DDS – DNA damage signalling

DE – Differentially Expressed

DMEM – Dulbecco's Modified Eagle's medium

DMSO – Dimethyl Sulfoxide

DNA – Deoxyribose Nucleic Acid

DoE – design of experiments

Dpp10 – Dipeptidyl Peptidase Like 10

DSB – Double-strand Breaks

DSBR – Double-Strand Break Repair

E. coli – *Escherichia coli*

EDTA – Ethylenediaminetetraacetic acid

Efna5 – Ephrin A5

EME1 – Essential Meiotic Structure-Specific Endonuclease 1

EPCAM – epithelial cell adhesion molecule

ERCC1 – Excision Repair Cross-Complementation Group 1

ERK – extracellular signal-regulated kinase

EXO1 – exonuclease 1

Ezr – Ezrin

Fam135b – family with sequence similarity 135 member B

FBS – Foetal Bovine Serum

FSC – Forward scatter

FDR – False Discovery Rate

FE – Functional Enrichment

FEN1 – flap endonuclease 1

FGF2 – fibroblast growth factor 2

FOXO – *Foxo* – Forkhead box protein

FRTA – Free Radical Theory of Ageing

FU – Fluorescence Units

g – standard gravity

Gadd45 – growth arrest and DNA damage-inducible alpha

Gas1 – Growth arrest-specific protein 1

GDP – Guanosine-diphosphate

GEN1 – Gen Endonuclease Homolog 1

GEO – Gene Expression Omnibus

ggNER – global genome NER

GH – growth hormone

GHR – Growth Hormone Receptor

GLUT4 – Glucose transporter type 4

GO– Gene Ontology

Gpr19 – G protein-coupled receptor 19

Grik2 – glutamate receptor, ionotropic, kainate 2

GTP – Guanosine-triphosphate

HA – Hyaluronan

H. glaber – Heterocephalus glaber

hMLH – MutL homolog

hMSH – mutS homolog

Hoxc10 – Homeoprotein C10

Hprt1 – Hypoxanthine Phosphoribosyltransferase 1

Hr – hour

HSC – haematopoietic stem cell

IARC – International Agency for Research on Cancer

Ifit1 – Interferon Induced Protein With Tetratricopeptide Repeats 1

IGF-1 – insulin like growth factor 1

IGF1R – insulin-like growth factor 1 receptor

IR-A – insulin receptor alpha

KEGG – Kyoto Encyclopedia of Genes and Genomes

LD50 – Lethal Dose 50

Lig4 – DNA Ligase 4

LQ – Longevity Quotient

MAPK – mitogen-activated protein kinase

MEF – Mouse Embryonic Fibroblasts

MEK – Mitogen-activated protein kinase kinase

MEM – Minimum Essential Media

miRNA – micro RNAs

mJ – millijoules

ml – millilitres

Mlst8 – Target of rapamycin complex subunit

MMEJ – Microhomology-Mediated End Joining

mm – millimetre

MMR – Mismatch Repair

M. musculus – *Mus musculus*

MRE11 – Meiotic Recombination 11

mRNA – messenger RNA

mTOR – Mammalian Target of Rapamycin

mTORC – mammalian target of rapamycin complex

Muc5ac – Mucin-5 Subtype AC, Tracheobronchial

MUS81 – Crossover Junction Endonuclease

Myo1c – Myosin IC

NAD+ – nicotinamide adenine dinucleotide

NBS1 – Nijmegen Breakage Syndrome 1

NCBI – National Centre for Biotechnology Information

NER – Nucleotide Excision Repair

NF-κB – nuclear factor kappa-light-chain-enhancer of activated B cell

Ng – nanograms

NGM – nematode growth medium

NHEJ – Non-Homologous End Joining

Nhej1 – Non-homologous end-joining factor 1

NIA – National Institute on Ageing

NRF2 – *Nrf2*– Nuclear factor like 2

µl – microlitre

µM – micro Moles

NMN – nicotinamide mononucleotide

NMR – Naked Mole Rat

nt – Nucleotides

Ostn – Osteocrin

PARP1 – Poly ADP-ribose polymerase 1

PCNA – Proliferating Cell Nuclear Antigen

PCR – Polymerase Chain Reaction

Pik3r6 – Phosphoinositide-3-Kinase Regulatory Subunit 6

PI3K – *Pi3k* – phosphoinositide-3-kinase

Pmaip1 – Phorbol-12-Myristate-13-Acetate-Induced Protein 1

POLβ – DNA Polymerase beta

POLδ – DNA Polymerase delta

POLε – DNA Polymerase Epsilon

POLL – DNA Polymerase Lambda

pRB – retinoblastoma protein

qPCR – quantitative Polymerase Chain Reaction

RBX1 – Ring-Box 1

RFC – replication factor C

RIN – RNA integrity number

RMA – Multi-Array Average

RNA – Ribose Nucleic Acid

RNAseq – RNA sequencing

RPA – replication protein A

rpm – rotations per minute

rRNA – Ribosomal RNA

ROS – Reactive Oxygen Species

R3hcc1 – R3H Domain And Coiled-Coil Containing 1

SCFs – SKP1-Cullin-F-box protein ligases

SD – Standard Deviation

Selplg – Selectin P Ligand

Serpinb2 – Serpin Family B Member 2

SDSA – Synthesis-Dependent Strand Annealing Pathway

SIRT1 – sirtuin 1

SKP1 – S-phase kinase-associated protein 1

Slamf1 – signalling lymphocytic activation molecule family member 1

SLX1 – Structure-Specific Endonuclease Subunit 1

SLX4 – Structure-Specific Endonuclease Subunit 4

Smad3 – SMAD family member 3

Sox5 – SRY (sex determining region Y)-box 5

SSB – Single-Strand Break

ssDNA – single-stranded DNA

TAg – SV40 large T antigen

Tbp – TATA-Box Binding Protein

tcNER – transcription-coupled NER

TEP1 – *Tep1* – telomerase-associated protein 1

TERF1 – *Terf1* – Telomeric repeat-binding factor 1

TGF-β – Transforming growth factor beta

tmax – maximum lifespan

TNC – Tenascin C

TOPO-1 – topoisomerase 1

TOP2A – Top2a – DNA topoisomerase 2-alpha

TOR – Target of Rapamycin

TSC2 – tuberous sclerosis 2

U/mL – Units Per Millilitre

UV – ultra violate

UV-DDB – UV-damaged DNA-binding protein

UW – University of Wisconsin

WEE1 – WEE1 G2 Checkpoint Kinase

WST-1 – Water-soluble Tetrazolium salt 1

YAP – Yes-Associated Protein

XLF – XRCC4-Like Factor

XPA – xeroderma pigmentosum group A protein

XPC – xeroderma pigmentosum group C

XPF – Excision Repair Cross-Complementation Group 4

XPG – DNA repair protein complementing XP-G cells

XRCC1 – X-ray repair cross-complementing protein 1

8-oxo-dG – 8-oxo-2'deoxyguanosine

°C – degrees Celsius

Chapter 1: Introduction

1.1 Ageing

One of the major challenges facing the developed world is how to deal with the ageing population. The proportion of elderly individuals is increasing and, as such, the cost to support them increases. Ageing, defined here as the progressive decline in cellular and organismal function over time, is a major risk factor for many complex chronic diseases such as cancer. Additionally, age can serve as a risk factor for infectious diseases and injury due to poorer immune responses and wound healing in elderly individuals. The aim of ageing research is to identify why we age, to develop interventions that could slow the ageing process to improve the quality of life of elderly individuals and to reduce the economic burden of the ageing population.

It is still unclear why organisms age at all, however, a number of theories have been proposed. Possibly the most promising and widely accepted is the free radical theory of ageing proposed over 60 years ago (1). This theory states that ageing is a result of cellular damage caused by reactive oxygen species (ROS). ROS are oxygen-containing free radicals (molecules with an unpaired electron) and are produced primarily in the mitochondria (90% of ROS) (2). During oxidative phosphorylation, oxygen is reduced to water by the addition of four electrons. The addition of one, two or three electrons only, known as partial reduction, results in the production of superoxide ion, hydrogen peroxide and hydroxyl radicals, respectively. Additionally, ionising radiation, typically ultraviolet radiation can also generate ROS by removing an electron from water to generate hydroxyl radicals. These ROS damage the cell through redox reactions with cellular components as the free radical takes electrons to complete its electron pair. This can happen to lipids, proteins and nucleic acids.

Lipid peroxidation occurs when the free radical steals an electron from a lipid in the cell, typically at the lipid bilayer of cellular membranes. The lipid molecule becomes a free radical as a result and in turn, steals an electron from another molecule in a chain reaction through the membrane. This can damage the membrane and end products of this lipid peroxidation can go on to damage DNA (Deoxyribonucleic acid) (3). Oxidation of the amino acids in proteins can result in changes to the protein's 3D structure and hence alter the protein's ability to function and prevent enzymatic functionality (4, 5). This oxidation can also result in cross-linking, aggregation and fragmentation of the proteins (5). ROS also damage DNA, resulting in loss of nucleotides, modification of the bases and strand breaks. Any damage to the DNA that is not repaired can result in mutations and cell death. DNA damage is thought to be a major contributing factor to ageing and cancer. ROS can be removed by the activity of antioxidants which give up an electron to complete the free radical's electron pair. Alternatively, enzymes can act to neutralise specific ROS; the main enzymes are superoxide dismutase,

catalase, and Glutathione peroxidase, which act on superoxide, hydrogen peroxide and hydroxyl radical, respectively.

Evidence for the free radical theory of ageing mainly comes in the form of correlations of increased oxidative damage with age and decreased levels of oxidative damage in longer-lived animals (6-8). However, studies in which levels of antioxidants are altered either through genetic intervention or feeding of antioxidants have given mixed results. For example, low doses of the antioxidant vitamin E extended lifespan in *Drosophila melanogaster*, but larger doses did not (9). ROS are important signalling molecules (10, 11) and so some ROS are required for basic cellular functions. Some long-lived animals show exceptionally high levels of oxidative stress, bringing this theory into question (12).

Alternative, but not necessarily mutually exclusive, theories of ageing consider the ageing process to be genetically coded. The developmental theory of ageing states that genes that promote survival and early reproductive success (typically through fast growth and development) will be selected for even if they have deleterious effects in later life as evolutionary selection acts primarily at reproduction (13). This would explain why diseases such as Huntington's disease that are autosomal dominant and lethal can persist because the gene is passed on before the disease develops. Evidence for this theory comes from the large number of genes that affect lifespan. According to the GenAge database (build 18), a database of ageing associated genes, there are over 2,000 genes that are known to affect lifespan or ageing when individually manipulated (14).

Ageing seems to occur in a similar fashion between different species with several hallmarks of ageing present in different species. The following nine hallmarks of ageing appear conserved between different species: genomic instability, epigenetic alterations, loss of proteostasis, mitochondrial dysfunction, deregulated nutrient sensing, telomere shortening, cellular senescence (described in detail in Chapter 5.1.2), altered intercellular communication, and stem cell exhaustion (15).

DNA damage accumulates over time and hence increases with age (16). Defects in DNA damage repair genes can result in premature ageing diseases, linking DNA damage and ageing (17). DNA damage may lead to mutations that, in turn, can inhibit the gene's function and hence result in cellular dysfunction. Accumulation of such damaged cells would lead to tissue dysfunction and hence ageing. DNA damage and the repair of DNA damage will be discussed in more detail in Chapter 1.3. In addition to changes to the DNA itself, changes to epigenetic markers are also associated with ageing. There are several common changes in these markers with increased age in mammals, such as increased histone H4K16 acetylation (18). Genetic alterations of genes affecting methylation or acetylation of DNA or histone proteins have been shown to increase lifespan (19).

Defects in proteostasis, the maintenance of appropriate levels of correctly folded proteins, have been associated with ageing and some ageing-associated diseases (20). Proteostasis involves the activity of protein stabilisers called chaperones that promote correct protein folding, and mechanisms of protein degradation to remove misfolded proteins. Decreased chaperone activity through mutations have been shown to decrease lifespan (21), and increased chaperone activity has been shown to increase lifespan (22, 23). Protein degradation pathways show decreased activity with age (24, 25). One such pathway, chaperone-mediated autophagy, has been shown to be required for lifespan extension in flies treated with caloric restriction mimetics (26).

A number of nutrient sensing pathways have been found to alter lifespan; these are described in more detail in Chapter 1.1.1.

Mitochondria, which were discussed earlier in this chapter, are a major source of ROS. As organisms age the efficiency of the electron transfer chain decreases, leading to greater electron leakage, ROS generation and decreased ATP (adenosine triphosphate) production (27). ROS-induced damage to the mitochondria may increase the amount of ROS it produces, thus forming a positive feedback loop.

The regeneration of tissues with fresh cells is reduced in ageing individuals. This is due to decreased stem cell function that would otherwise serve to renew tissues. This functional attrition has been shown in mouse studies to affect a wide array of tissues, including the skin (28), bone (29), and brain (30), among others. For example, haematopoietic stem cells (HSCs) show reduced proliferation with age which may result in anaemia, myeloid malignancies and reduced competency of the adaptive immune system due to a preferential shift away from the lymphoid lineage (31, 32). HSCs show an increased level of signalling lymphocytic activation molecule family member 1 (*Slamf1*) expression with age. *Slamf1* is a membrane glycoprotein that is thought to mediate bacterial detection and phagocytosis (33). Isolation of HSC's expressing low or high levels of *Slamf1* through florescence-associated cell sorting allowed the selective transplantation into lethally irradiated congenic recipient mice. Both high and low *Slamf1* expressing cells showed HSC activity. However, cells expressing high *Slamf1* showed a bias towards the myeloid cell lineage (31). In older age, fewer cells of the adaptive immune system will be available, and hence the adaptive immune system will be less capable of mediating an immune response. Studies with mouse HSCs have shown that the decrease in proliferation that occurs with age correlates with increased DNA damage and p16 expression as detected by quantitative PCR (qPCR) (34, 35). HSCs derived from p16 knockout mice showed increased proliferative capacity compared to wild-type HSC of the same age (35). It is not simply the increase of stem cell proliferation that is beneficial to organismal health, but also maintenance of appropriate

levels of proliferation and quiescence. An increase in stem cell proliferation can be detrimental to tissue maintenance by exhausting the stem cell niche and ultimately reducing the proliferative capacity later on in life. This has been shown in *p21*-deficient mice in which levels of HSC and neural stem cells were increased in young animals, but this ultimately led to decreased levels later in life compared to wild-type mice, resulting in susceptibility to myelotoxic insults (36, 37). Similarly, fibroblast growth factor 2 (FGF2) signalling in old muscle tissue was shown to promote stem cell proliferation and depletion that was rescued by inhibition of FGF2 (38). Transferring young stem cells into ageing individuals can increase lifespan and reduce degenerative phenotypes in mice, even in tissues in which donor cells are not detected (39). This suggests an additional mechanism by which stem cells may rejuvenate tissues, potentially through the activity of secreted factors. This idea is backed up by parabiosis experiments in which the vasculature of old and young mice is connected. Old skeletal muscle stem cells typically show decreased proliferation with age due to reduced Notch signalling. However, exposure to young serum has been shown to increase proliferation and notch signalling within these cells in old mice (40). It should be noted that this process also appears to work in reverse, with one study looking at neural stem cells in young mice showing decreased neurogenesis, neural stem cell abundance, and learning in young mice when connected to old mice (41). Finally, the lifespan extending intervention, caloric restriction, or treatment with caloric restriction mimetics (described in more detail in Section 1.1.1) can affect stem cell activity. Studies in mouse skeletal muscle have shown enhanced availability of muscle stem cells and muscle repair in both young and old animals undergoing caloric restriction (42). Similarly, treatment with rapamycin, a compound thought to be a caloric restriction mimetic, improved haematopoiesis and self-renewal of HSC in old mice through inhibition of mTOR (mammalian target of rapamycin) and reduction in p16 expression (43). The maintenance of stem cell activity is affected by the other hallmarks of ageing, such as DNA damage, which has been implicated in limiting the regenerative capacity of stem cells with genes, such as Ataxia Telangiectasia Mutated (ATM) that serves to maintain genomic stability being implicated in protecting stem cell populations (44). Similarly, nutrient sensing pathways, such as mTOR (as described in Section 1.1.1) and insulin growth factor (IGF) signalling pathway (described in Section 1.1.1), have also been seen to affect stem cell functionality with reduced IGF signalling resulting in lower stem cell activity in serially transplanted HSCs (45).

Ageing is associated with an increased level of inflammation and inflammatory signalling. Increasing such inflammation results in a premature ageing phenotype in mice (46). Additionally, inhibition of one such inflammatory pathway, the NF-κB (nuclear factor kappa-light-chain-enhancer of activated B cell) pathway, led to the rejuvenation of ageing skin in transgenic mice (47). Interleukin 6 is a proinflammatory cytokine and has been shown to accumulate in sera with age (48, 49). Studies

in elderly people have indicated that higher levels of interleukin 6 correlate with increased risk of death and morbidity (50, 51). A study in mice showed that this increase is reduced in mice undergoing caloric restriction (49). Taken together this indicates inflammation is both a causative factor and a resulting symptom of ageing and such would form a positive feedback loop promoting the ageing process.

Clearly, ageing is a complex multi-factorial process. Fortunately, the above factors appear interlinked with treatments aimed to improve one aspect, such as modifying nutrient sensing pathway activity, having widespread effects on other aspects of the ageing phenotype.

1.1.1 Caloric restriction

The environment of an organism can also affect lifespan. Caloric restriction, the reduction in food intake without malnutrition, can extend lifespan. This was first discovered in the 1930s in white rats that were restricted in calorie intake from birth or after weaning (52), though the level of feed restriction in this study was not consistent as the researchers were aiming to maintain a given weight. This lifespan extension has been confirmed in an array of other species, including, yeast, worms, and mice (53-55) indicating a conserved mechanism. Not only is lifespan extended, but so is health span, in that age-related diseases such as cancer develop later (56). This was first shown in adult-onset restriction in rats 50 years after an initial study in which mice on ab libitum or ~77% or ~58% ab libitum diets were shown to have decreased cancer incidence and slower age-related declines in the immune system through assays such as immunofluorescent labelling of T cells (57, 58). Caloric restriction may not be as ubiquitous as previously thought, however, as some species and mice strains appear resistant to the life-extending effects of caloric restriction and in some cases have reduced lifespan (59, 60). Caloric restriction without malnutrition is difficult to implement, and different methods can have different effects and even stimulate different genetic pathways (61). Additionally, caloric restriction has a number of side effects including reduced muscle mass and depression, and as such is unlikely to be adopted by humans even if proven effective (62, 63).

Studies in model organisms may not be representative of humans due to evolutionary dissimilarities. Rhesus monkeys, however, are an excellent model to represent humans as their genome shares approximately 93% sequence identity with that of humans (64). They also possess similar age-related pathologies as experienced by humans, for example, cataracts (65). Two major studies started in the 1980s that raised rhesus monkeys on either approximate *ad libitum* or caloric restriction (~30% reduction in calorie intake) diets are providing interesting results. One of these

studies conducted by the University of Wisconsin (UW) found that caloric restriction reduced both age-related and all-cause mortality (66). However, the other study conducted by the National Institute on Ageing (NIA), concluded that caloric restriction did not affect either age-related or all-cause mortality (60). These differences in the results are likely due to a number of differences between the two studies. Firstly, though both studies provided an approximately 30% reduction in calories, the method of calculating this amount varied between the studies. Furthermore, the actual food provided and its percentage make up of carbohydrates, protein and fat differed between the two studies. The UW study created an ad libitum value for each individual by monitoring food intake over 3-6 month and reduced this value by 30% to induce CR, whereas the NIA study used established data on rhesus monkey nutrition (67) to predict an ab libitum value based on the size and age of the individuals and reduced this value by 30% in caloric restriction conditions. Additionally, feeding regimes in the NIA study resulted in one study groups (old females) having similar food intake between control and caloric restriction treated individuals which would result in lower levels of CR. Secondly, the origin of the animals used varied with the UW using only India derived animals and the NIA study using both India and China derived animals which show both genetic and physiological variation (68, 69). Finally, the level of medical treatment provided to animals with known conditions varied with the UW study treating conditions and the NIA study not until later in the study when this was changed. This lack of treatment would account for non-age-related morbidity and mortality particularly in non-breeding females that are prone the potentially fatal endometriosis (70) (this was reduced in the UW study by using females that had already had children). In addition to changes in survival, both studies reported improvements in the health of the animals on caloric restriction with improved fasting glucose and reduced cancer incidence. Taken together these studies highlight not only the difficulty of studying caloric restriction but also the difficulty of implicating this rigorous intervention in higher order mammals; as the same reduction in calories performed in a slightly different way may give very different results. Furthermore, these studies support the idea that caloric restriction may provide health benefits in the evolutionarily similar humans.

The use of organisms in research provided ethical, as well as financial challenges particularly in higher organisms such as mice and monkeys. Hence an alternative method of studying caloric restriction is often used whereby the effects are monitored in cell culture. Caloric restriction is induced in cell culture by exposing the cells to serum derived from animals undergoing caloric restriction. One such study exposed rat, human and mouse cells to serum derived from rats or rhesus monkeys undergoing either caloric restriction or *ab libitum* feeding. This study found cells exposed to serum from caloric restriction animals had increased oxidative and heat stress resistance, which was partially removed by supplementation of IGF-1 (71). This is what we would expect from cells undergoing caloric

restriction as IGF-1 is reduced in caloric restriction, as we will discuss later in this section. This indicates these cells are responding as though they are undergoing caloric restriction and hence can serve as a model for study into the mechanisms of caloric restriction.

The evolutionary rationale for this increased lifespan in response to reduced calorie intake is as follows. While food is bountiful, an organism should maximise growth and reproduction to produce offspring which will have a better chance of surviving while food is in good supply. However when food is limited, and the organism is hence calorically restricted, the focus shifts to survival to endure the period of scarcity and survive until food becomes more prevalent. During such famine, it makes little sense to focus on unnecessary growth or to produce offspring that will likely starve.

Caloric restriction mimetics aim to emulate the life-extending effect of caloric restriction without these side effects or the need to change diet. A number of compounds have been identified as caloric restriction mimetics, such as rapamycin, allantoin (72) (described in more detail in Section 2.1.1) and NMN (nicotinamide mononucleotide). NMN is essentially a precursor to NAD+ (nicotinamide adenine dinucleotide) that in turn boosts DNA damage repair through binding of DBC1 (deleted in breast cancer 1) inhibiting its inhibition of PARP1 (Poly ADP-ribose polymerase 1) that contributes to BER (described in Section 1.3) (73). Treatment with NMN boosts NAD+ levels which are seen to decline with age (74). Additionally, NMN treatment may activate SIRT1 (sirtuin 1) by providing SIRT1 with its rate limiting substrate NAD+ (74). SIRT1 contributes to caloric restriction (discussed later in this section). Despite a lack of data on the effects of NMN treatment on lifespan directly this candidate caloric restriction mimetic is currently undergoing stage one human clinical trials to assess the safety and bioavailability of NMN in human treatment (75).

The exact mechanism of caloric restriction is still not clear, but a number of pathways have been implicated (76). Perhaps unsurprisingly these pathways feature nutrient-sensing components.

The first genetic pathway shown to affect lifespan is the IGF-1 signalling pathway first identified in *Caenorhabditis elegans* (*C. elegans)* when temperature-sensitive mutations of *daf-2* (an IGF-1 receptor ortholog) were found to increase lifespan by approximately double in worms. These worms also showed prolonged movement and pharyngeal pumping which have been shown to decline with age, indicating slower ageing (77). This lifespan extension was shown to require daf-16 which is a FOXO (Forkhead box protein) family transcription factor (77). The FOXO transcription factor family is conserved between invertebrates and mammals, but where *C. elegans* have one FOXO transcription factor (DAF-16), mammals have four, (FOXO1, 3, 4 and 6) (78). A reduction in IGF-1 signalling is observed during caloric restriction of rats showing that pathways are conserved in mammals (79).

Growth hormone receptor (GHR) knockout mice have reduced IGF-1 and have reduced cancer incidence and increased lifespan, as do growth hormone deficient Ames dwarf mice (80, 81). These experiments indicate the importance of IGF-1 in lifespan extension and also identify growth hormone (GH) and GHR as upstream components of the IGF-1 pathways. IGF-1 deficient mice do not have further increased lifespan when on caloric restriction, showing the necessity of IGF-1 in caloric restriction (81). High serum IGF-1 is also associated with cancer risk in humans (81). GH is produced in the pituitary gland and can bind to GHR in the liver to stimulate IGF-1 production; this has been confirmed in cultured rat hepatocytes (82). This explains the observations in GHR knockout mice and Ames dwarf mice. IGF-1 is transported around the body via the circulatory system allowing access throughout the body, which explains how this pathway can have profound systemic effects in multiple tissues. IGF-1 binds its receptor, insulin-like growth factor 1 receptor (IGF1R) or insulin receptor alpha (IR-A), at the cell membrane. According to the human protein atlas, a database of protein expression and localisation within the human body, IGF1R is present in a wide array of tissues including liver, skin, the digestive system, and the respiratory system (83). IGF1 binding to these receptors results in activation of phosphoinositide 3-kinase (PI3K), which in turn activates protein kinase B (AKT) via phosphorylation. This activity was shown through immunoprecipitation of AKT derived from muscle cells with or without PI3K activity and with or without IGF-1 exposure (84).

Active AKT phosphorylates the FOXO proteins inhibiting their activity. This was first shown in the *C. elegans* (85, 86), but has subsequently been shown in mammals as well (87-89). When phosphorylated, these FOXO bind 14-3-3 chaperone proteins and become sequestered in the cytoplasm. The creation of FOXO-GFP fusion proteins has confirmed this nuclear exclusion for FOXO 1 and 3, however, this was not seen in response to AKT activity in FOXO6 (90). Furthermore, in situ hybridisation has shown FOXO6 expression appears limited to the nervous system (90). A 30% reduction in calorie intake resulted in no difference in lifespan in mice that were *Foxo3*$^{+/-}$ or *Foxo3*$^{-/-}$. However, these mice did show a decreased incidence of cancer (91). This indicated that *Foxo3* is required for the life-extending effect of caloric restriction, but not the cancer-preventive effect. A similar experiment that looked at a heterozygous *Foxo1* knock out mouse strain found the opposite effect, with caloric restriction having the same effect on lifespan, but a loss of the anti-cancer effect of caloric restriction in the mutant mice (92). This suggests that *Foxo1* is required for the anti-cancer effects of caloric restriction, but not the lifespan-extension effects. One of the response genes confirmed to be only upregulated in the wild-type mice in response to caloric restriction was p21, suggesting this to be a gene responsible for the anti-cancer effects of caloric restriction (92). FOXO1 and 3 are repressed through deacetylation directly and deacetylation of a transcriptional coactivator p300 by the SIRT1 protein (93). This is counter-intuitive as caloric restriction has been shown to induce

SIRT1 expression (94, 95) and SIRT1 knockout mice do not live any longer on caloric restriction compared to control mice (96). This suggests that SIRT1 may serve to limit FOXO activity to appropriate levels to facilitate longevity. This idea is backed up by experiments in *Akt*$^{-/-}$ mice that have increased FOXO expression; these mice were shown to be more sensitive to damage-induced apoptosis and genotoxic stress (97). This is likely due to inappropriate entry into apoptosis as a result of increased FOXO activity. SIRT1 may also act through deacetylation of the DNA damage repair factor KU70 to prevent apoptosis and promote autophagy (94, 98). IGF-1's role in caloric restriction has been brought into question as chronic reduction in serum IGF-1 has been observed to have deleterious effects on health and lifespan (99).

Polymorphisms of FOXO3 have been shown to be positively associated with increased life-spans in humans through genotyping studies on centenarian (100 or more years old), or long-lived (95-106 year old) populations and young control individuals (100, 101). A similar study looking at 761 Chinese centenarians and 1,056 younger controls also identifies polymorphisms in FOXO1 that were negatively correlated with lifespan in females (102). These studies highlight the significance of the FOXO transcription factors in human longevity.

By combining 75 genome-wide expression profiles (derived from 5 different studies), it has been indicated that daf-16 upregulates 1,663 genes and downregulates 1,733 genes (103). These upregulated genes were enriched for those involved with oxidation reduction and carbohydrate metabolism. The downregulated genes were enriched for growth, reproduction and development. A similar meta-analysis looking at 12 immunoprecipitation followed by sequencing (ChIP-seq) datasets found ~7,000 genes were targeted by FOXO transcription factors in mice (104). These genes showed enrichment for apoptosis, p53 signalling, oxidative stress and metabolism. These results imply increased oxidative stress resistance, which may prolong lifespan by prevention of cellular damage in accordance with the free radical theory of ageing (detailed in Section 1.1), may be the key mode of action in these genes.

In addition to inhibition of the FOXO transcription factors, AKT also phosphorylates and inactivates tuberous sclerosis2 (TSC2) that would otherwise inhibit mTOR (105). Hence the reduction in IGF-1 signalling would result in increased TSC2 activity and hence reduced mTOR activity. The *C. elegans* homolog of mTOR is let-363, also known as TOR (target of rapamycin). RNAi knock down of TOR increases adult lifespan (106). Caloric restriction decreased mTOR expression and activity in mice (95, 107). The mTOR protein associates with others to form one of two complexes known as mTOR complex 1 and 2 (mTORC1 and 2). In mice, reduced mTORC1 (in the form of double heterozygous

mutations for mTOR and Target of rapamycin complex subunit (*Mlst8*)) results in increased lifespan (108). Inhibition of mTOR in rat cells results in decreased protein synthesis, cell cycle arrest and selective apoptosis of some types of tumour cells (109).

Autophagy has been shown to be necessary for lifespan extension through caloric restriction or genetic manipulations of IGF-1 and TOR (110). Impaired autophagy through reduction of key regulator genes results in accelerated ageing in a wide array of species including flies, worms and rat cells (111-113). Autophagy decreases with age in human and rat cell cultures (114). Increased autophagy is sufficient to increase lifespan in many organisms including human cells (115, 116).

Another signalling pathway that may play a role in caloric restriction and ageing is the Ras signalling pathway. Ras can be thought of as inactive (GDP (Guanosine-diphosphate) bound) or active (GTP (Guanosine-triphosphate) bound). Active Ras bind to effector molecules including Raf that initiates a phosphorylation cascade via MEK (Mitogen-activated protein kinase kinase), mitogen-activated protein kinase (MAPK) and extracellular signal-regulated kinase (ERK). Studies in mice undergoing a 20% reduction in calorie intake have shown a reduction in both Ras and MAPK (117). It is yet to be determined if this reduction in Ras signalling is necessary or sufficient for lifespan extension. Ras is capable of binding PI3K, activating it (118) and ERK can promote the phosphorylation and subsequent degradation of FOXO3 (119). This indicates that this pathway can inhibit FOXO transcription factor activity and hence inhibit longevity. In addition, ERK has been shown to phosphorylate TSC2, inhibiting its ability to inhibit mTOR (120). Hence Ras signalling has the capacity to limit lifespan by interacting with both the IGF-1 and mTOR pathways. Ageing tissues show elevated MAPK and ERK activity (121), though it is not clear if this is a cause or consequence of ageing. Inhibition of RAS by the generation of knock out mutants of RASGRF1 (a RAS activator) increases lifespan in mice (122), supporting the idea that this pathway inhibits longevity.

AMP-activated protein kinase (AMPK) is, as the name suggests, a protein kinase that is activated by binding with AMP (adenosine monophosphate) (123). Its activity is reduced by binding to ATP and hence AMPK acts as an energy sensor, becoming active when the ratio of AMP to ATP increases. It primarily acts to maintain the energy balance of the cell through a number of mechanisms. In muscle cells, active AMPK increases glucose uptake by promoting translocation of the glucose transporter GLUT4 to the plasma membrane (124). Glycogen synthesis is decreased through phosphorylation of glycogen synthase (125), and fatty acid oxidation is increased through phosphorylation of cetyl-coA carboxylase (ACC) by active AMPK (126). In *C. elegans* AMPK is necessary for the lifespan-extending effects of caloric restriction (127) and rats experiencing caloric restriction

(40% calorie reduction) had increased AMPK activity in older age compared to controls (128). AMPK increases SIRT1 activity indirectly by increasing the availability of NAD^+, a rate-limiting substrate for SIRT1 (129). AMPK can also affect FOXO signalling, as it has been shown to directly phosphorylate FOXO3 in 6 locations promoting its activity (130). Finally, AMPK is a potent inhibitor of mTOR. This inhibition acts through phosphorylation of Raptor (a component of the TORC1 complex) (131) and TSC2 (a regulator of mTOR) (132). Taken together, this shows AMPK to be a potent regulator of ageing pathways and shows the interconnected nature of these CR-related pathways.

Caloric restriction induces the activity of NRF2 (Nuclear factor like 2) which activates various anti-oxidant pathways and mice deficient in NRF2 lose the cancer-protecting effect of caloric restriction, but not the life-extending effect (133).

1.1.2 Successful ageing

Rowe and Kahn's model of successful ageing (134) states that successful ageing constitutes low probability of disease and disease-related morbidities, high cognitive and physical functional capacity and active engagement of life. It has been proposed that 'positive spirituality', the level of life satisfaction, be added to the model, as centenarians do not meet the conventional requirements for successful ageing (135, 136). This model is focused on successful ageing in humans and factors such as active engagement or positive spirituality are not relevant or difficult to assess in other organisms. Hence, for the purpose of this thesis successful ageing is defined as the maintenance of cognitive and physical function with age and avoidance of age-related morbidities in a manner that is greater than expected. Caloric restriction can be considered a model of successful ageing as it delays age-related morbidities (56). Additionally, long-lived organisms that elicit delays in age-related morbidity development are also considered to be successfully ageing.

1.1.3 Cancer

Cancer, so called because of solid tumours' similarity in appearance to a crab, with a central mass and leg-like vasculature at the edges, is a key age-related morbidity and major source of mortality responsible for 7.98 million deaths in 2010 (137). It is the uncontrolled growth of cells with the potential to spread to other parts of the body. As such, benign tumours which do not spread are not classed as cancer.

Cancer is a very diverse disease that is typically categorised by the cell type of origin to give five broad categories. These are carcinomas (arising from epithelial cells), sarcoma (arising from connective tissues), lymphomas and leukaemias (arising from haematopoietic cells), blastomas (arising from precursor cells or embryonic tissues) and germ cell tumours (arising from pluripotent germ cells). These vary further between specific cell type, and even cancer cells within the same tumour can show genetic variation (138).

Cancer can be caused by a wide array of factors including pathogens, chemicals, ionising radiation and hormones (139). Ultimately cancer is caused by genetic mutations and/or epigenetic abnormalities (140).

There are a number of natural barriers cells must overcome to become cancerous. Cells usually require growth signals such as hormones to grow and divide. However, cancer cells can grow without such external signals. They do so by either producing these signals themselves, losing activity of growth-inhibiting pathways or through the excessive activity of growth-promoting pathways (141). These cancer cells must also be insensitive to both external and internal anti-growth signals. Cells can normally only replicate a limited number of times, this is known as the Hayflick limit (142). This is due to the repetitive DNA sequences at the end of chromosomes called telomeres being shortened after each round of division. This shortening can extend into the coding region of the chromosome resulting in crisis that kills most cells. Cancer cells are thought to overcome this through the expression of telomerase that replace the lost telomeres (143). Abnormal cells that are damaged or infected by pathogens are removed through apoptosis, the process of cellular self-destruction, but cancer cells that are often malformed do not undergo apoptosis. This may be due to defects in damage detection or apoptosis initiation (144). Cancerous cells can be removed by both the innate and adaptive immune system (145, 146). Hence, cancer cells must evade the immune system. This may be done through disabling aspects of the immune system through TGF-β (Transforming growth factor beta) or other immunoregulatory factors or potentially through recruitment of regulatory immune cells (147-149). Cancer cells need to undergo metabolic changes that also facilitate greater growth rates (150). Finally, cancer cells need to induce angiogenesis and lymphangiogenesis to provide oxygen and nutrients to the tumour, remove waste and facilitate metastasis (151, 152).

Cancer kills through inhibition of key biological functions, for example, a tumour in the lungs can prevent oxygen absorption, or through major disruptions in homeostasis such as hypercalcemia induced by various lymphomas and leukaemias (153).

1.2 Model organisms in ageing

There is a great deal of plasticity in the rate of ageing between different species. For example, the longest-lived mammal, the bowhead whale is predicted to live for 211 years. This is around a hundred times longer than the lifespan of the shortest-lived mammal, the forest shrew, that lives for only 2.1 years (values from AnAge, a database of ageing and life history in animals) (14). In nature, a positive trend is observed by which body size and lifespan correlate (Figure 1.1) (154). Evolutionarily, this makes sense as larger animals would take longer to grow and reach sexual maturity and their larger size would mean they would be less susceptible to predation. The lower the level of predation, the greater the selective pressure for longer life. From this trend, we can create a longevity quotient (LQ) as a measure of how well an animal matches this trend. An LQ of 1 would indicate that an animal lives as long as we would expect based on its size, a higher value indicates a long-lived animal that may have unique anti-ageing mechanisms. Birds for example often have a longer lifespan than we would expect based off body mass alone, as do bats. This has likely evolved because of their ability to avoid predators by flying (155). Humans are also an exception to the rule, living to 122 years. This gives us an LQ of around 4 meaning we can live up to four times longer than we would expect based on our body size alone, which is in part due to our advanced healthcare.

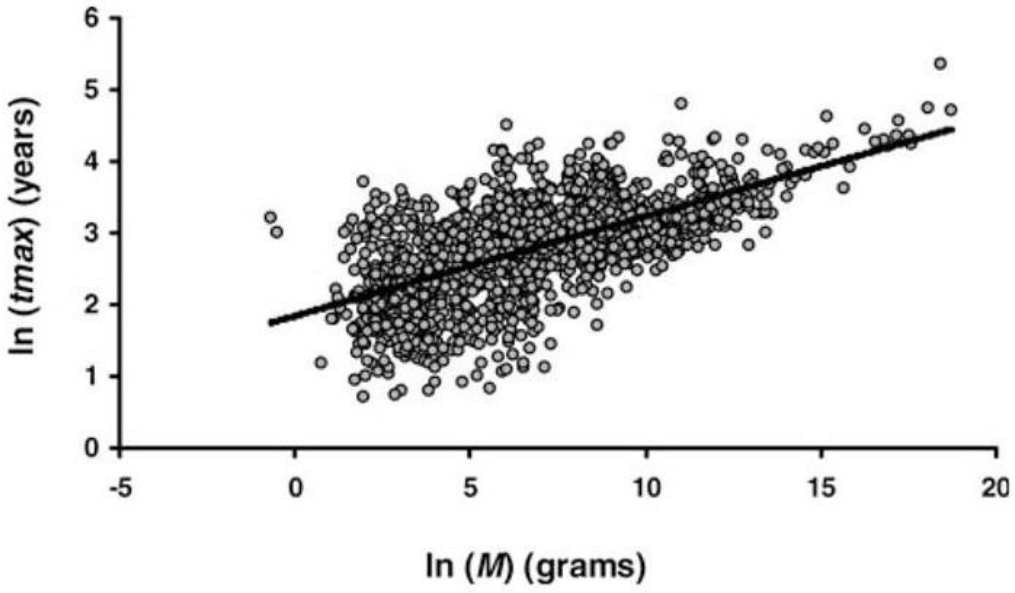

Figure 1.1. Plot of natural log-transformed maximum lifespan (tmax) and body mass (M) of all mammals, birds, reptiles and amphibians in AnAge (n=1,456). Taken with permission from (154).

1.2.1 *Caenorhabditis elegans*

When studying ageing, it is often useful to study short-lived animals, to identify why they are so short-lived, but also to allow experiments aiming to observe changes in lifespan to be completed within a researcher's career and/or lifetime. *Caenorhabditis elegans* is a soil-dwelling nematode worm found worldwide and are mostly self-fertilising, egg-laying hermaphrodites, though some males are present in the population (<0.2%) (156). *C. elegans* have a maximum lifespan of ~58 days (14), are approximately 1mm long, are easy to maintain in large numbers and have a well-annotated, sequenced genome making them excellent model organisms. Additionally, they are transparent making observations of internal tissues and cells possible in living organisms. Worms kept at lower temperature live longer until a certain threshold (54) showing clear plasticity of lifespan within this species. The *C. elegans* lifecycle is well documented (Figure 1.2). Eggs hatch after about 9 hours post-laying. The newly hatched worms (known as L1s) undergo multiple moults during which a new life-stage-specific cuticle is formed, and the old cuticle is shed (157). Worms become adults after 4 moults. As *C. elegans* has an invariant number of somatic cells, studies have tracked the lineage of each cell from fertilisation to adulthood (158, 159). Developing worms can enter a developmentally-arrested dauer diapause stage, which is considered to be an un-ageing state. Worms can survive in this dauer state for up to four months and then have the same adult lifespan once development continues. Entering this dauer state can essentially increase the worm's lifespan by up to ~200%. Genetic interventions can also affect lifespan, for example, a mutation of the insulin IGF-1 receptor, *daf-2* can result in approximately doubled lifespan (77). This lifespan effect was discovered in *C. elegans* and later found to control longevity in flies and mice showing that discoveries in *C. elegans* may also apply to other organisms, potentially even humans (160). There are 838 genes in GenAge that are associated with ageing in *C. elegans* (14).

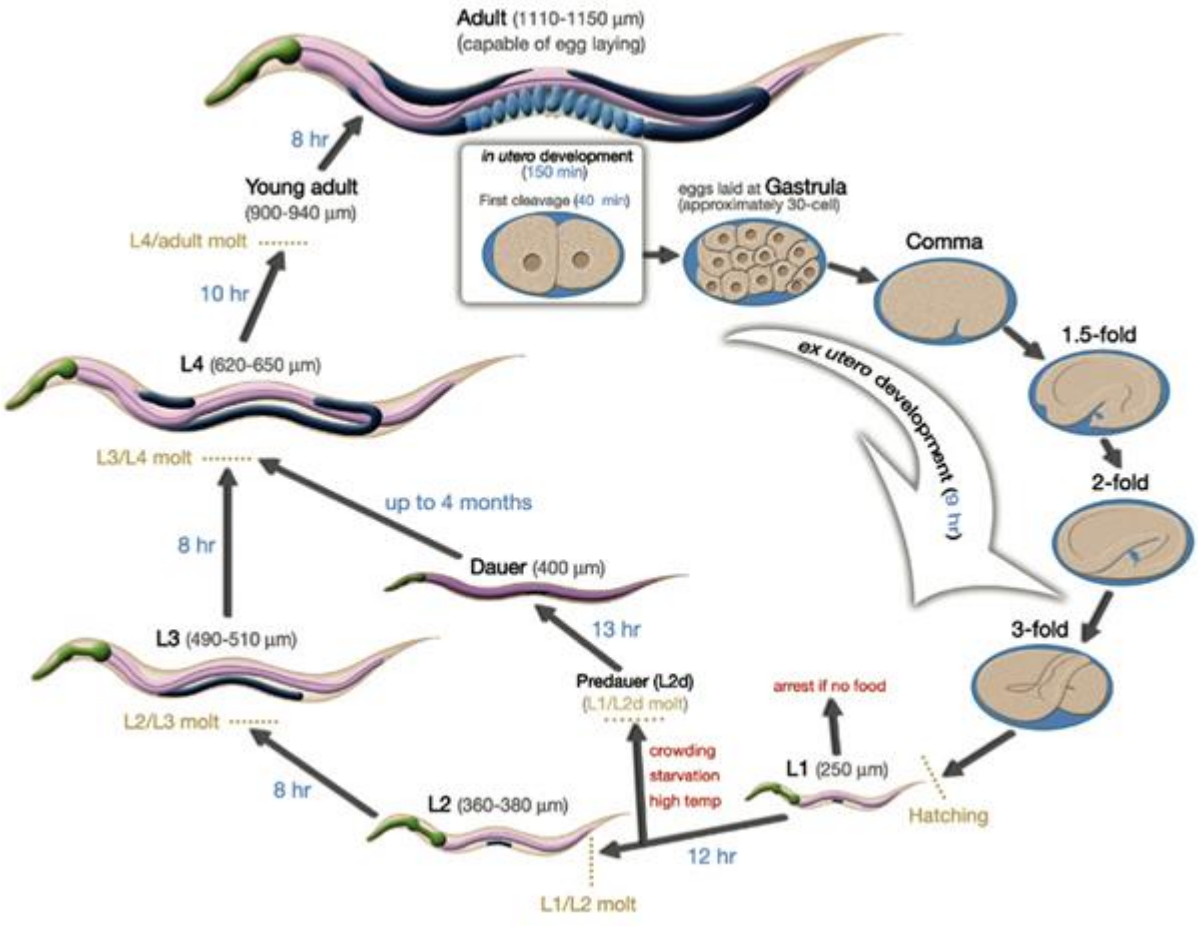

Figure 1.2. Caenorhabditis elegans lifecycle at 22°C. Blue numbers indicate the time spent at each life stage; red text indicates factors that can result in developmental arrest. Only the hermaphrodite adult is shown. Taken with permission from (161).

Caloric restriction can increase worm lifespan by up to 150% depending on the method used to induce caloric restriction (61). The simplest method of caloric restriction and the method used in this study is to use *eat-2* mutant worms. The ligand-gated ion channel *eat-2* is located post synoptically in the pharyngeal pump, controlling the rate of pump contraction (162, 163). Mutation of *eat-2* results in decreased pharyngeal pumping and hence decreased food intake, inducing caloric restriction (61, 163, 164). Caloric restriction can also be induced by dilution of food source (*E. coli* (*Escherichia coli)*), use of chemically defined liquid media or reducing *E. coli* growth by reducing peptone in agarose plates (61). *Eat-2* mutants are long-lived, and this lifespan extension does not require *daf-16* or AMPK (61, 164). Caloric restriction by dilution of *E. coli* or peptone, however, does require both *daf-16* and AMPK (61). This indicates that these methods of caloric restriction have varying mechanisms and that comparisons between them may be inaccurate. *E. coli* often accumulates in the pharynx and intestine of older worms (165). Feeding worms *E. coli* that have been killed through antibiotic treatment or UV exposure, or *E. coli* treated with bacteriostatic

agents that prevent its proliferation increases worm lifespan (165, 166). It is thought this mortality is caused by the production of toxins in proliferating *E. coli* and hence it is plausible that reduced intake of *E. coli* in caloric restriction could result in a lifespan increase, in part through reduced *E. coli* build up. Hence performing caloric restriction on worms provided with killed *E. coli* removes this confounding factor and has been shown to increase lifespan (72, 167). It is also of note that *E. coli* serve not only as a source of calories but also essential nutrients. Therefore caloric restriction through reduced *E. coli* intake also reduces the intake of these nutrients and hence caloric restriction through this method in *C. elegans* is often referred to as dietary restriction.

1.2.2 *Heterocephalus glaber*

Heterocephalus glaber (Figure 1.3) also known as the naked mole rat (NMR) is the longest-lived rodent with a lifespan of 31 years (LQ = 4.9) which is much larger than the similarly sized mouse, *Mus musculus* with a lifespan of only 4 years (LQ = 0.7) (14, 168, 169). This lifespan is longer than we would expect based on the NMR's body size and has likely evolved as a result of a number of different traits. NMRs are native to the horn of Africa and are subterranean, living in burrows that protect them from both predators and extremes in temperature reducing early mortality. They have limited ability to thermoregulate and have a lower body temperature then mice; they typically move to different areas of the burrow or huddle to keep warm allowing for lower basal metabolism (170, 171). NMRs are remarkably resistant to hypoxia surviving at 5% oxygen with no observed ill effects. Mice, however, die after 10 minutes at 5% oxygen. Additionally, NMRs are capable of surviving for 18 minutes under total anoxia (no oxygen) (172). This increased survival is down to a shift to anaerobic metabolism of fructose, likely an adaption to living in burrows that frequently have poor ventilation and hence reduced oxygen content (172). This adaption further reduces the risk of mortality in the NMR's subterranean niche. NMRs are eusocial animals living in colonies with one breeding female (the queen) and one to three breeding males. These breeders are further protected from predation by the workers, and since these are the only individuals that reproduce, a long lifespan will be selected for. In addition to their long lifespan, the NMR seems to be cancer resistant, with some colonies having no observed incidences of cancer (173, 174). The breeding females also show no decline in fertility with age and NMRs appear healthy even at old age and hence NMRs are considered to exhibit negligible

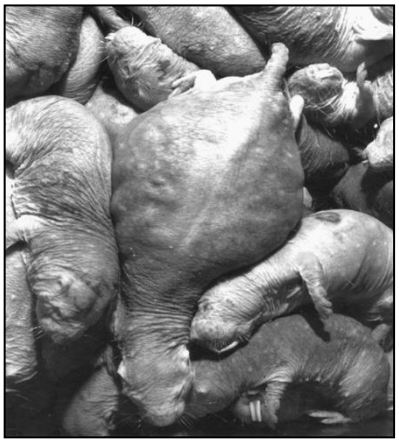

Figure 1.3. A sleeping NMR colony. Centre is the pregnant queen (12).

senescence (174). NMRs also appear resistant to DNA damage as skin fibroblasts from NMRs treated with DNA damaging agents require a higher dose to kill half of the cells (LD50) than fibroblasts from mice (175). These traits have been attributed to a number of features.

NMR's resistance to cancer has been suggested to be due in part to high molecular mass hyaluronan (HA) (176). This extracellular substance is five times larger in NMR compared to mice. It likely evolved to allow the NMR skin to be more stretchable for squeezing through tunnels. It may act as a physical barrier preventing cell over-growth or may act through its strong interaction with CD44 on the surface of the cell to activate anti-cancer pathways.

NMRs have been shown to have better translational accuracy than mice, with fewer incorrect amino acids being incorporated in newly-synthesised proteins than mice, with a similar rate of synthesis (177). This increased accuracy would result in a more stable proteome and hence could result in longer lifespan by reducing the rate of defective protein accumulation.

NMRs have high levels of the proteins NRF2 and p53 that may play a central role in longevity. The transcription factor NRF2 acts in response to stresses such as oxidative stress. In response to oxidative stress, NRF2 is translocated to the nucleus of the cell to activate transcription of various antioxidant response elements (ARE) (178). NMR cells have a higher basal level of NRF2 compared to mice and the increase observed in response to oxidative stress is larger than that in mice (179). p53 is capable of regulating cell cycle, cellular senescence and DNA responses, and increasing p53 activity has been shown to both increase cancer resistance and lifespan in mice (180, 181).

Fibroblasts derived from NMRs have shown remarkable resistance to oncogenic transformation. Induced expression of the oncogenes SV40 large T antigen (TAg) and Ras^{G12V} together is sufficient to induce full malignant transformation of mouse and rat cells (182, 183). However, when this oncogenic combination is expressed in NMR cells, they fail to form colonies in soft agar (an assay for tumorigenicity) and rapidly undergo crisis when transplanted into immunodeficient mice (184, 185). Crisis is a period of genomic instability in which most if not all cells die and is caused by excessive shortening of the telomeres due to excessive proliferation. This crisis phenotype was rescued by the addition of human telomerase reverse transcriptase (185). This rapid entry of cells into crisis after oncogenic transformation may be an important defence mechanism against cancer in the NMR.

NMR cells show decreased or halted proliferation when in contact with other cells (186). This is termed contact inhibition of proliferation (will henceforth be referred to as contact inhibition). NMR cells have been reported to undergo contact inhibition at a much lower cell density than those from mice or humans (184). This early contact inhibition requires p53 and pRB (retinoblastoma protein)

tumour suppressor pathways, as well as signalling via p16 (184). This early contact inhibition may provide an extra layer of protection against cancer by preventing excessive cell growth. A study of NMR skin and lung fibroblasts showed they divided slower than those derived from mice (187). This study found a population doubling time of 8.13 days in NMR while mice were found to have a population doubling time of 3.46 days. Additionally, this study concluded that neither mouse nor NMR cells undergo replicative senescence as this was not detected after 200 days of cell culture. However replicative senescence may still occur under different conditions or after further cell divisions. This study grew both cell lines at 5% CO2 and 3% oxygen, but mouse cells were grown at 37°C, and NMR cells were grown at 35°C which may affect the results (187). This study combined data from 4 inbred mice and 1 wild mouse. Another study looking at growth rates in skin and lung fibroblasts from NMR and mouse cells used the same temperature of 37°C to grow the cells and examined the growth rate at 21 and 3% oxygen. This study also examined data from inbred lab strains and wild-derived mice separately. NMR fibroblasts showed a population doubling time of 6.26 days at low oxygen and 12.62 at high oxygen, while lab mice had a population doubling time of 2.68 days at low oxygen and 11.92 days at high oxygen (188) and wild-derived mice had a population doubling time of 3.66 days at low oxygen and 5.97 days at high oxygen. NMR fibroblasts appear to divide slower than those derived from mice in a consistent manner under varying conditions. The increased sensitivity to oxygen of NMR cells to wild mouse cells is likely a result of their natural environment in burrows that may have low oxygen contents. The increased sensitivity of lab mouse strains may be due to loss of oxidative resistance genes due to inbreeding.

The NMR nuclear and mitochondrial genomes have been sequenced with a sequencing depth of 98.6% and over a 20-fold assembly (189). This sequencing has provided a number of insights about the NMR's remarkable features. For example, 244 pseudogenes were identified, and these showed enrichments for terms including visual perception. Loss of gene activity in such genes may explain the poor sight of NMRs that arose as a result of living in dark tunnels. By looking at positively-selected genes, we can glean information regarding the evolution of particular traits. This study found 141 positively-selected genes (at a false discovery rate of 0.05). These include the genes *Tep1* (telomerase associated protein 1), a telomerase component and *Terf1* (Telomeric repeat-binding factor 1), a telomeric repeat binding factor. *Terf1* has been shown to regulate telomere length in a human tumour cell line with increased activity shortening telomere length and decreased activity increasing this length (190). The study also looked at genes that possessed amino acid residues unique to NMR when compared to homologs from 36 different vertebrates (including humans, mice and rats). Top2a (DNA topoisomerase 2-alpha), a DNA topoisomerase, was one such gene. TOP2A along with TERF1 and TEP1 form a 5-protein complex that regulates telomere length (191). Changes in telomere maintenance

may be relevant to both the NMR's lifespan and cancer resistance, as telomere shortening limits the number of divisions a cell can undergo and hence can prevent cancerous cell overgrowth. Additional genes found to possess unique polymorphisms include the DNA damage repair enzyme AP endonuclease 1 (*Ape1*) (discussed in Section 1.3) which is involved in Base excision repair (BER). BER is the DNA repair pathway responsible for repairing UV-induced DNA damage and alterations of such genes may explain the NMR's perceived susceptibility to UV-induced DNA damage (175). This study also looked at p16, a gene shown to be required for NMR cell culture's early contact inhibition. They found low similarity between exon three between mouse and NMR and predicted stop codons in exon 2 resulting in a shorter (14Kd) protein, but functional domains were thought to be preserved. Such changes may affect the activity of this protein to facilitate its role in early contact inhibition. Genome sequencing can identify candidate genes for further research such as genes present in only NMRs, genes with polymorphisms and genes that have undergone positive selection. Such genes may contribute to the unique traits found in the NMR.

The use of RNA sequencing, a technique that identifies the expression levels of an organism's genes (detailed in Section 1.4) has been conducted on NMR cells (189, 192, 193). One study that looked at RNAseq data from brain, liver and kidney in 4 and 20-year-old NMRs showed fewer changes between the two groups compared to data in humans or mice that looked at young and old organisms (189). For example, only 24 genes changed in expression with age in the brain, compared to54 in humans, and two of these genes had an opposite change in expression in NMRs. *Smad3* (SMAD family member 3) is downregulated in the human brain sample but upregulated in NMR brains with age. *Smad3* modulates cell cycle progression and hence may contribute to the NMR's cancer resistance by modulating correct cell cycle progression.

Another study extracted liver cells from 3 young NMRs (2-3 years) and 3 wild mice (6.5 months) for RNAseq (192). This study was conducted before the availability of the NMR genome, and hence orthologs were mapped to the mouse genome via the Basic Local Alignment Search Tool (BLAST) (194). This resulted in the caveat that genes with reduced expression in the NMR relative to mice may simply have poor coverage from the assembly used. As such, only genes with increased expression in NMR were identified. An interesting gene found to be upregulated in this study is alpha2-macroglobulin (*A2m*). *A2m* shows a positive correlation with age in humans and has been associated with Alzheimer's disease with inherited deletions increasing the risk of developing Alzheimer's (195, 196). This suggests a protective role of *A2m* and may contribute to the NMR's apparent resistance to age-related morbidities. Among the over-expressed genes, those related to the mitochondria were overrepresented (66 genes) and included the ageing-related gene succinate dehydrogenase cytochrome b560 subunit. Mutation of this gene decrease lifespan in *C. elegans* and can promote

tumorigenesis is mouse cell cultures (197, 198). In accordance with the free radical theory of ageing, changes to the mitochondria that are the primary source of ROS may affect the rate of ageing. NMRs show higher levels of markers of oxidative stress to proteins (cysteine oxidation observed in liver cells (199) and protein carbonyls observed in multiple tissues (200)), lipids (isoprostanes detected in urine and malondialdehyde detected in liver samples (201)), and DNA (8-oxo-2'deoxyguanosine (8-oxo-dG) (200)) than mice. Hence NMRs seem to have a high basal level of oxidative stress (12), suggesting this is not the case. The largest change in expression found in this study was a 300-fold increase in epithelial cell adhesion molecule (EPCAM). This is counter-intuitive as EPCAM is associated with cancer through inhibition of cadherin cell adhesion and promoting cell cycle progression (202). Such a large difference in expression of a gene involved in cell adhesion may suggest a contributory role to the NMR's exceptional phenotype as cell adhesion can affect cell cycle, and cancer development (detailed in Section 5.1.1).

An RNAseq study compared NMR, mouse and human liver cells derived from 3 different individuals per species. This study used the inbred Balb/C mouse strain as opposed to wild-derived mice which is less comparable to wild animals and hence differences in gene expression may be due to this inbreeding. The availability of a sequenced NMR genome allowed for data on genes with lower expression in NMRs to be utilised unlike the previous study in NMR liver cells. This study focused on DNA damage genes and found upregulation of DNA damage genes, particularly those involved in homologous recombination and non-homologous end joining (NHEJ) (193). This increased expression of genes involved in repairing double-strand breaks (DSB) may explain why NMR fibroblasts seem particularly resistant to agents that induce DSB (175).

As NMRs are typically 8-10cm long and live in colonies that contain 20-300 (average of 75) individuals, it is more practical to study their cells and extrapolate back to the animal. Fibroblasts can easily be grown in culture flasks with appropriate media to allow for study outside the animal. We predict that the NMR's apparent DNA damage resistance is integral to their long lifespan and cancer resistance.

1.3 DNA damage and repair

DNA can be damaged by both endogenous and environmental factors, and estimations in mice predict that, under normal conditions, cells undergo ~14,000 – 22,000 DNA lesions per day (203). DNA damage if unrepaired can induce apoptosis, senescence and create mutations that can lead to cellular dysfunction and hence cancer and ageing. Defects in DNA repair pathways can cause premature ageing syndromes which, as the name suggests, show an accelerated ageing phenotype supporting the idea that ageing is at least in part caused by DNA damage (17).

The main source of endogenous DNA damage is ROS. ROS oxidise DNA resulting in oxidised bases, abasic sites and strand breaks (204). Environmental sources of DNA damage include chemical agents, viruses and ionising radiation. The main form of radiation organisms are exposed to is UV radiation, which primarily induces cyclopurines and (6-4) photoproducts.

Oxidised bases are, as the name suggests, nucleotide bases that are oxidised. This can lead to mutations. One study, focusing on 8-oxo-dG, which is often used as a biomarker for oxidative stress, found that 8-oxo-dG led to mutations (single base deletions, G:C to T:A or G:C to C:G transversions or larger deletions) 14% of the time (205). Oxidised bases are repaired via BER.

Abasic sites are points in DNA in which the nucleotide base is lost, leaving the DNA backbone intact. These occur due to either spontaneous hydrolysis of the *N*-glycosyl bond, or through deliberate enzymatic cleavage of this bond to remove inappropriate bases (206, 207). These sites can block transcription and DNA replication making them cytotoxic (208). Additionally, these sites are mutagenic leading to many single base substitutions (209). Abasic sites can also give rise to single-strand breaks (208). Abasic sites are repaired primarily by BER, but nucleotide excision repair (NER) may also play a role.

Strand breaks, which include both single and double-strand breaks, are breaks in the DNA backbone. Single-strand breaks (SSB) are caused either by damaging agents or as an intermediate of BER. SSB can result in mutations and chromosomal aberrations (210). If DNA containing an SSB undergoes replication, DSB may be formed. SSB are repaired through BER. DSB may form as a result of DNA damaging agents either directly or indirectly or as an intermediate in normal biological processes. DSB can induce apoptosis, mutations and chromosomal rearrangements (211, 212). Chromosomal rearrangements caused by DSB have been associated with some forms of cancer (213, 214). DSB are repaired through NHEJ, microhomology-mediated end joining (MMEJ), and homologous recombination.

Cyclopurines form when carbon 5 (C5) of ribose in DNA is turned into a free radical (loses an electron). C5 takes an electron from the C8-N7 double bond resulting in C5-C8 bond, distorting the nucleotides shape and hydrogen bonding with its adjacent nucleotide (215). Accumulation of cyclopurines can block mammalian RNA polymerase II and replicative DNA polymerases and can result in misincorporation of the adjacent nucleotide during DNA replication (216, 217). Cyclopurines are repaired through NER.

(6-4) photoproducts form when two pyrimidine bases on DNA strand undergo a photochemical reaction with UV radiation and bond to each other as opposed to their adjacent bases

(218). This can result in misincorporation of adjacent bases, typically an adenine being paired with cytosine resulting in a CC to TT mutation after replication. (6-4) photoproducts are repaired through NER.

DNA adducts are points in the DNA with a chemical agent covalently attached. A wide array of DNA adduct and DNA adduct inducing compounds have been identified and the severity of the damage these induce to DNA varies between them (219). DNA adducts can induce mutations either during error-prone DNA repair or DNA replication at the adduct site (220). The method of repair also varies between adducts. Mismatch repair (MMR) (221), NER (222), BER (223), and a chemical reaction by which O6-Methylguanine DNA methyltransferase removes methyl and ethyl adducts from guanine bases (224) have all been identified as removing DNA adducts.

DNA crosslinking occurs when a DNA nucleotide is covalently linked via a DNA crosslinking agent to a nucleotide from either the same strand (intrastrand crosslinking) or opposite strand (interstrand crosslinking). Intrastrand crosslinks can result in mutations as nucleotide bases are often misincorporated in the opposite strand during DNA synthesis (225, 226). Interstrand crosslinking holds the two strands together blocking transcription and DNA replication. Interstrand crosslinks can be repaired through NER (227). The repair of intrastrand crosslinking depends on the cell's position in the cell cycle. During late S or G2 phase where an intact sister chromatid is available, a combination of NER and homologous repair act to remove the crosslink (228). When an intact sister chromatid is not available, NER is utilised to remove the lesion from one strand, and new DNA is synthesised using the remaining strand as a template (229, 230). This remaining strand is then removed and the gap filled as before. This DNA synthesis utilises lesion bypass DNA polymerase which has a relatively high mutation rate (230, 231).

DNA damage cannot simply be replaced like other cellular components; it must last the lifespan of the cell, and hence any damage to the cell's DNA needs to be repaired. As DNA is so vital to an organism's survival, a number of sophisticated mechanisms have evolved to repair DNA damage.

During NER, appropriate DNA damage is recognised, and a short single-strand of DNA containing the lesion is removed, leaving the undamaged strand intact. DNA polymerase then replaces the removed strand using the intact strand as a template. Then DNA ligase connects the newly synthesised strand to the end of the old strand. There are two types of NER, global genome NER (ggNER) that occurs anywhere in the genome and transcription-coupled NER (tcNER) that occurs on the transcribed strand of active genes. DNA damage needs to be detected before it can be repaired. For ggNER this recognition is performed by the XPC complex (232) that has been shown to be made up of xeroderma pigmentosum group C (XPC), either RAD23A or RAD23B and centrin 2 through co-

immunoprecipitation analysis (233). This complex binds to DNA with a greater affinity at site of DNA damage. This has been shown through biochemical assays using purified XPC complex, and have shown increased binding at 6-4 photoproducts (232), abasic sites (234) and N-acetyl-2-aminofluorene adducts (235). This XPC binds poorly to UV-induced cyclobutane pyrimidine dimers (CPD) even though these are repaired through ggNER, hence additional factors are required for damage detection. UV-damaged DNA-binding protein (UV-DDB) is a protein complex made up of DNA-binding protein 1 and 2 (DDB1 and 2) (236, 237). Purified UV-DDB has been shown to bind CPD and 6-4 photoproducts (238). UV-DDB contributes to the $CRL4^{DDB2}$ complex (made up of DDB2, DDB1, Cullin-4 (CUL4) and Ring-Box 1 (RBX1)) that also serves as damage sensor (239). Detection of DNA damage in tcNER is initiated by stalling of RNA polymerase II. The $CRL4^{CSA}$ complex (made up of CSA-DDB1-CUL4-RBX1) is recruited to the site of damage and acts similarly to the $CRL4^{DDB2}$ complex. These GRL4 complexes promote ubiquitination of histone proteins, clearing them from the site of damage (239). Both tcNER and ggNER result in the recruitment of the TFIIH complex that is made up of 10 proteins, and acts to promote unwinding and opening of the DNA strand into an open bubble structure (240). This open structure allows incisions to be made by the endonucleases ERCC1-XPF (Excision Repair Cross-Complementation Group 1 - Excision Repair Cross-Complementation Group 4) and XPG (DNA repair protein complementing XP-G cells). ERCC1-XPF is thought to perform the initial 5' incision and XPG the later 3' incision ~24-32 bases away (241, 242). Xeroderma pigmentosum group A protein (XPA) and replication protein A (RPA) act to prevent cleavage in the undamaged strand by preferentially binding it (243). The damaged strand is released and replaced by DNA polymerases. The 3' nick is then ligated by DNA ligase.

Mechanistically NER and BER are very similar: both cut out a single-strand of DNA containing DNA damage and replace the strand using DNA polymerase and DNA ligase. Their main difference is how the damage is recognised. NER proteins recognise distortions in the DNA structure, whereas BER relies on specific glycosylases to detect the lesion and cut the base out to create an abasic site or create a single-strand break marking the strand for BER. BER can remove a single base (short patch) or multiple bases (long strand). Humans possess at least 11 glycosylases. The glycosylases gently nip the DNA strand while scanning them causing the strand to bend, which at sites of damaged bases cause the base to pop out of the DNA strand and enter the glycosylases binding site in a process known as 'base flipping'(244). Mono-functional glycosylases rely on a water molecule to act as a nucleophile and attack the aromatic carbon of the target base resulting in an abasic site. Bi-functional glycosylases exhibit enzymatic cleavage of the base and cut the DNA strand leaving a single-strand break. Next, the abasic site has an incision made at its 5' side by endonucleases, if not already done by bi-functional glycosylases. The major endonuclease responsible for these incisions in mammals is the

APE1endonuclease which accounts for >95% of this activity (245). APE1 can also remove blocking groups, such as 3'- phosphoglycolate, and creates a 3'-OH group required for repair (246). The missing base is replaced by DNA polymerase. POL*β* is the primary polymerase responsible for short patch BER though POLL can also fulfil this role (247, 248). In long patch BER, more nucleotides (~2-12) are replaced. POLδ and POLε perform strand displacement synthesis in which new bases are made, and the old ones are essentially pushed out the way creating an overhang in the old strand. This allows the creation of multiple new bases when only a single base gap is present. These polymerases are aided by proliferating cell nuclear antigen (PCNA) that serves as a processivity-promoting factor (249). The overhang is then removed by structure-specific nucleases; this is primarily flap endonuclease 1 (FEN1) (250). Finally, the newly synthesised strand is ligated to the rest of the strand. In short patch BER this is primarily done by DNA ligase I, and in long patch BER, this is primarily done by DNA ligase IIIα (251). DNA ligase IIIα requires X-ray repair cross-complementing protein 1 (XRCC1), a scaffold protein (252). In additionPARP1 is thought to contribute to this relegation step in select types of damage as these are repaired with reduced capacity when PARP1 is inhibited (253). It is not clear how PARP1 acts in BER but may serve to stabilise XRCC1 (254).

Homologous recombination occurs when a double-strand break is present when sister chromatids are available to be copied. First, both 5' ends of the DNA break are cut away in a process known as resection. This creates unpaired single-strand DNA which can now invade the DNA of the identical sister chromatin, and anneal to the equivalent section of DNA. DNA polymerase then adds the DNA to the 3' end. This occurs for both strands of the broken DNA. With all the gaps filled in, the strands can either be ligated to the DNA strand to which they were originally connected or more commonly to the strand of the other chromatid resulting in crossover. Homologous recombination repair begins with pre-synapsis in which 3' overhang is generated at the DSB. Some sources of strand breaks, such as ionising radiation, result in modified bases at the 5' and 3' end of the break. Such modifications need to be removed and this is done by the MRX (Meiotic Recombination 11 (MRE11), Rad50 and Xrs2) complex and exonuclease 1 (EXO1) in *saccharomyces cerevisiae* (MRX is replaced with the MRN complex in mammals, as Nijmegen Breakage Syndrome 1 (NBS1) replaces Xrs2) which is not required for repair of DSBs that lack these modifications (255-257). RPA binds ssDNA (single-stranded DNA) and inhibits the formation of secondary structure to facilitate homologous repair (258). Rad51 binds to ssDNA forming a helical nucleoprotein filament on the DNA (259). This binding requires the activity of co-factors including Rad52, and complexes of Rad51 paralogs (XRCC2, XRCC3, RAD51B, RAD51C and RAD51D) (260, 261). Deletion of any of these paralogs results in inhibition of delivery of Rad51 to the DNA strand (260). BRCA1 (breast cancer associated 1) and 2 also contributes to the activity of Rad51, as they are capable of direct binding (262, 263). Mutations of BRCA1 and 2 are

associated with cancer (a disease in part caused by DNA damage) (264), decreased homologous recombination (265-267) and decreased Rad51 accumulation in response to DNA damage (268, 269).

Next homology is searched for before invasion of the homologous DNA takes place and is collectively termed synapsis. The RPA/Dmc1 filament around the ssDNA forms a complex with the DNA strand of the sister chromatin to allow invasion by the ssDNA and allows searching for homology through annealing of the bases. The final stage, termed post-synapses, involves the generation of new DNA and relegation of the DNA strands. Rad54 aids the formation of the Rad51 DNA complex but also serves to remove Rad51 from the ssDNA after successful homologous annealing (270). This allows the entry of DNA polymerase to extend the 3' end of the invading DNA strand. From here homologous recombination diverges into 2 distinct pathways; the Double-Strand Break Repair (DSBR) pathway and the Synthesis-Dependent Strand Annealing Pathway (SDSA). In SDSA the DNA strand retreats from the invaded dsDNA and re-anneals to its original DNA strand. In DSBR the ssDNA that did not invade the dsDNA anneals to its homologous sequence in the invaded DNA forming a 'double Holliday junction'. This annealing means that both strands are connected and to resolve this an enzyme, termed a resolvase, is required to cut both junctions in either the opposite (resulting in crossing over) or the same direction. In mammals, Gen Endonuclease Homolog 1 (GEN1), Crossover Junction Endonuclease (MUS81)-Essential Meiotic Structure-Specific Endonuclease 1 (EME1), and Structure-Specific Endonuclease Subunit 1 and 4 (SLX1 and 4) have been implicated as filling this role (271). Finally, the DNA is reconnected by DNA ligase 1 to produce two intact strands of dsDNA (272). PARP1 appears to have a regulatory role in HR as PARP1 knock out cells show increased Rad51 loci formation but otherwise normal homologous recombination (273).

NHEJ occurs when double-strand breaks form and no DNA copies exist to serve as a template. Instead, overhangs at the break site are used that will be homologous to the opposing overhang and are known as microhomologies. If these are not present, then MMEJ occurs, which is essentially the same as NHEJ except the DNA is cut away to create these overhangs. Typically, this is less accurate as it can lead to deletions of the DNA between the microhomologies. The first step in NHEJ is binding by the Ku heterodimer (Ku70 and Ku80, also known as XRCC5 and 6) to the broken DNA strand. Ku, when bound to DNA, has a greater binding capacity for other proteins including the nuclease DNA-dependent protein kinase catalytic subunit (DNA-PKcs) in complex with Artemis, polymerase μ and λ, and DNA ligase 4 in complex with XRCC4-Like Factor (XLF) and XRCC4 (274). Hence Ku recruits and stabilises the enzymatic components required for NHEJ. Artemis possesses a 5' endonuclease activity, and the Artemis, DNA-PKcs complex possesses both 5' and 3' endonuclease activity (275). This complex can bind DNA strand ends but does so with greater affinity when the Ku complex is present (276). DNA-PKcs autophosphorylates itself and Artemis when bound to the DNA, facilitating Artemis'

endonuclease activity and causing conformational changes that facilitate binding of other NHEJ proteins (277, 278). Additionally, this complex is capable of opening up hairpin loops that are necessary for NHEJ (275). The endonuclease activity creates overhangs in the DNA structure. The polymerases μ and λ act to extend the DNA strand after annealing in a template-dependent manner and polymerase μ can act template-independently to create random microhomologies (279). These polymerase can display template slippage that can result in repeats forming which is often seen in NHEJ (274). Once homology and annealing have been achieved it is the job of DNA ligase 4 to ligate the DNA strands together in a manner that is dependent on XRCC4 activity (280). DNA ligase 4 can also ligate blunt ends together (281). XLF stimulates XRCC4-DNA ligase 4's ability to ligate the DNA strand (282). XRCC4-DNA ligase 4 shows remarkable flexibility. It can mediate ligation on a single-strand of the double-stranded DNA which is useful if the other strand is unligatable (283). It can ligate across gaps (279). Finally, it can ligate incompatible DNA that lacks homology (284).

MMR aims to detect and correct mismatched bases. A number of proteins act to detect these errors, but the question remains as to which is the correct base and which the error. In gram-negative bacteria, differences in stand methylation mark the newly synthesised DNA strand and hence which side the error is on. In eukaryotes, the picture is less clear, but it is thought that nicks in the newly synthesised strand serve this stand-labelling role (285). Recognition of DNA damage in humans is conducted by two heterodimers of mutS homolog (hMSH) 2 with either hMSH3 or hMSH6 to form the complexes hMutSβ or hMutSα, respectively (286). These complexes recruit more components of the repair pathway including heterodimeric complexes of MutL homolog (hMLH) 1 with PMS1 protein homolog (hPMS) 2, hPMS1, or hMLH3 to form hMutLα, hMutLβ, or hMutLγ, respectively. Only hMurlα contributes to MMR and acts to make an incision 5' of the mismatch. Additionally, the hMutS complexes recruit PCNA that interacts with hMSH2, 3 and 6 (287). This PCNA interaction is required for 3' nick detected MMR but not for 5' nick detected MMR (288). This is due to the activity of EXO1 that is capable of 5' mismatch excision in the presence of hMutSα or hMutSβ in complex with RPA (289) but requires the MutLα endonuclease activity that is activated by PCNA and replication factor C (RFC) (290). EXO1 removes bases from the point of the hMutLα incision beyond the mismatch in a 5'-3' direction (290). After excision of the mismatched bases, pol δ is recruited to resynthesise the removed bases. Finally, DNA ligase 1 reconnects the DNA strands. RPA appears to be involved at all stages of MMR, binding to the nicked DNA, stimulating DNA excision and facilitating DNA resynthesis (291).

DNA damage repair is not a perfect process. Damaged DNA can be repaired but the appropriate epigenetic markers may not be replaced, or inappropriate ones may be added which could result in inappropriate activation or inactivation of genes (292). If the DNA cannot be repaired, the cell

will most commonly undergo apoptosis, removing itself and the risk of cancer its DNA damage brings. Alternatively, the damaged cell may become senescent, exiting the cell cycle to prevent the spread of any mutations into daughter cells.

Throughout the cell cycle, there are a number of checkpoints. Among other things these allow the cell to check for DNA damage. When DNA damage is detected the cell cycle can be arrested and stopped at these points giving the cell chance to repair DNA damage and mutations before DNA replication which can result in mutations become permanent.

The detection, repair and overall cellular response to DNA damage require a large number of genes. In the relatively simple *Escherichia coli,* it is suggested that over 1,000 genes are involved in responding to DNA damage (293). A different response requires different genes, and so, by monitoring what genes are active in DNA damage-resistant organisms responding to DNA damage, we can glean information of how to resist DNA damage more effectively. However, with so many genes that could potentially be involved, a transcriptome-wide approach is required.

1.4 Functional genomics

In a cell, DNA stores information on how to create all the proteins a cell will create, and hence how the cell functions. This information is transcribed into RNA, and this RNA is in turn translated into a protein that will go on to perform its given function. Not all genes are active at once, however, and which genes are active depends on what the cell is doing. By analysing the cells transcribed RNA, also known as the transcriptome, we can identify what is happening in the cell. Doing this when the cell is responding to a DNA-damaging agent can tell us how the cell responses to DNA damage. There are two well-used methods for analysing the transcriptome: microarrays and RNA sequencing.

Microarrays are basically a solid surface with thousands of distinct spots. Each spot contains many copies of one specific strand of single-stranded DNA bound to the surface. These DNA strands known as probes are specifically designed to correspond to a section of a gene. All the RNA from a number of cells is extracted and reversed, transcribing it into cDNA (complementary DNA). The cDNA is then labelled with a fluorescent marker. Multiple samples can be labelled with a different coloured marker and pooled pair-wise together. This is then washed over the microarray allowing the cDNA to anneal to the corresponding probe. The microarray is then imaged to detect fluorescence; if RNA for a specific gene is present in the original sample and hence was being expressed in the cell, then the cDNA will be left bound to the spot(s) that corresponded to that gene and the fluorescent label will be visible. If the gene was present in both starting samples, then a combination of the fluorescence will be detected, and by detecting the ratio of fluorescence, we can say how much more a gene is

active in one sample than the other. Microarray analysis has successfully been applied to the study of ageing. For example, the use of microarrays analysis in long-lived *daf-16* mutant *C. elegans* identified a number of genes that were found to affect lifespan (294).

RNA sequencing (RNAseq) takes a different approach. There are various forms of RNAseq, and the field is still evolving. It is beyond the scope of this thesis to detail all methods and their merits, and so the basic method used in our analysis will be explained only (for further information the reader is directed to (295, 296)). As before, RNA is extracted from the chosen cells. The RNA sample will contain a large amount of ribosomal RNA (rRNA) (over 90%) which will saturate the results and so is removed. This RNA is amplified, and coding RNA is purified typically by targeting the poly-A tail. This is accomplished by passing the sample over magnetic beads coated with poly T oligonucleotides. The RNA is then fragmented and reverse transcribed to cDNA. Second generation sequencing is then employed to sequence these fragments. Computational analysis can detect which genes are present and in what quantities. RNAseq has been successfully implemented to monitor changes in the transcriptome of mouse brains at different ages and found previously unknown genes providing new candidates for further study (297). RNAseq has also been successfully used in analysing the NMR transcriptome in comparison to mouse and human cell lines. Such studies have identified increased expression of DNA damage, oxidoreduction and mitochondria-associated genes in NMR liver cells (192, 193).

Both technologies are widely used, and the appropriateness of each technology depends on the user's desired application. However, RNAseq offers a number of advantages over microarrays. RNAseq analyses the absolute amount of gene expression by counting the number of reads in a sample, but microarrays only analyse the relative amount of expression between different samples (298). RNAseq offers a greater dynamic range in expression values as microarrays rely on fluorescence, where high expression values can lead to signal saturation, and background noise can obscure lower expression values (295, 299, 300). Unlike RNAseq, microarrays do not analyse the whole transcriptome; they only analyse the presence of transcripts that have specific probes on the array and as such may miss non-coding RNA such as microRNAs (miRNA), which can be detected and are often discovered by RNAseq (300, 301). RNAseq can be used to identify mRNA (messenger RNA) complexities overlooked by microarrays such as SNPs and different splice isoforms including undiscovered isoforms (299, 300, 302). Finally, RNAseq can potentially be used on samples from any organism, unlike microarrays which require the organism to have a sequenced genome, microarrays made specifically for that genome and a high-quality annotation of the genome as any un-annotated genes will not be added to the microarray and hence would be missed by the analysis.

When studying ageing through gene expression data, three major caveats must be considered. First, RNA levels do not necessarily correlate with protein levels due to post-translational mechanisms such as suppression of mRNA by miRNA, and protein degradation (303-305). Additionally, the presence of a protein does not necessarily correlate with protein activity as post-translational modification may render the protein inactive. Second, genes that are being expressed may not be related to the underlying mechanism of ageing but instead to specific age-related diseases or be expressed in response to the ageing phenotype (306). Finally, complex multi-cellular organisms such as mammals have many different cell types that may not age in the same way or at the same rate, and it has already been indicated that different organs have different ageing-specific gene expression profiles (307). With these caveats in mind, these approaches still have the capacity to provide major insights into the ageing process (294, 297).

1.5 Aims

The overall aim of this thesis is to better understand successful ageing and avoidance of age-related morbidities, notably cancer. To this end we studied two models of successful ageing, caloric restriction in the nematode worm *C. elegans* and the naturally long-lived rodent *Heterocephalus glaber*.

Firstly, we analyse caloric restriction and candidate caloric restriction mimetic treatment in *C. elegans*. We performed a microarray on *eat-2* mutant worms, a caloric restriction model and worms treated with either rapamycin or allantoin that have been shown to extend lifespan in *C. elegans* (72). The aim of this experiment was to identify possible mechanisms and genes involved in these lifespan extensions. Additionally, we aimed to determine how similarly these caloric restriction mimetics acted to caloric restriction.

Next, building on previously published work (179) we examined the response of NMR cells exposed to the DNA damaging agents camptothecin and chromium (vi) oxide in comparison to that of mouse cells. These experiments serve to confirm the reproducibility of previous work and provide lethal dose 50 values with which to perform further experiments. Furthermore, these experiments provide a biological context for gene expression analysis.

To further our understanding of the processes taking place in the treated cells, RNAseq analysis was conducted on cells recovering from exposure to the genotoxic compounds. This analysis was designed to identify differences in how these species respond to such toxic stimuli in the hopes of identifying superior protective mechanisms in the NMR that may contribute to their increased

lifespan and cancer-resistant phenotype. We focused our analysis initially on DNA damage genes as previous findings (193) suggested an increased expression of such genes in NMR cells.

Finally, to test the results of the RNAseq analysis that suggested differences in cellular adhesion and cell cycle progression between the NMR and mouse, both flow cytometry and adhesion-based assays were conducted. These assays aimed to provide evidence that the observed differences in gene expression translated into observable differences in the cellular phenotype. Such differences, if observed, would confirm the initial findings and support the hypothesis that they are important in the NMR's long lifespan and/or cancer resistance.

Chapter 2: *Caenorhabditis elegans* microarray analysis

2.1 Introduction

In order to evaluate successful ageing, this chapter will examine the lifespan extending intervention, caloric restriction, in the nematode worm *C. elegans*. This examination will be at the functional genomics level to identify biological pathways or components important in caloric restriction-induced lifespan extension. We can consider organisms undergoing caloric restriction as a model of successful ageing. Any identified difference induced by this intervention may be essential for inducing successful ageing.

To achieve this goal, a microarray analysis was conducted on *C. elegans* undergoing caloric restriction or treatment with caloric restriction mimetics that have been shown to increase worm lifespan. A functional enrichment was performed on differentially-expressed genes to identify if genes involved in a particular process or pathway were enriched within the sample.

2.1.1 Caloric restriction in *C. elegans*

Caloric restriction is the most robust longevity intervention to date, capable of altering lifespan in a wide array of organisms including the nematode worm *C. elegans* (53-55). In addition to its capacity to increase lifespan, caloric restriction also reduces the risk of age-related morbidities such as cancer and can hence be considered a model of successful ageing (56). In reality, caloric restriction is thought to have a number of side effects and is difficult to maintain. Therefore, the use of caloric restriction mimetics, compounds that induce the beneficial effects of caloric restriction, are an attractive alternative through which humans could reap the benefits of longevity enhancement, without dealing with the difficult lifestyle and side effects (63, 308).

Caloric restriction mimetics were identified by us previously by using the gene expression profiles of rat cells exposed to sera from rats or rhesus monkeys undergoing caloric restriction and finding compounds that induce a similar profile in the Connectivity Map (version 2), a database of gene expression profiles in various human cells in response to different drugs (72, 309). In our previous study, wild-type worms and *eat-2* mutant worms that are long-lived and are deemed a caloric restricted model due to reduced feeding (61), were grown on nematode growth media that contained the candidate caloric restriction mimetics. The ligand-gated ion channel *eat-2* is located in the pharyngeal pump and is responsible for controlling the rate of pump contraction (162, 163). This pharyngeal pump facilitates food uptake by the worm; mutations of *eat-2* result in a decreased rate of pharyngeal pumping and hence decrease levels of food intake, inducing caloric restriction and

increasing lifespan (61, 163, 164). Allantoin and rapamycin increased the lifespan of wild-type worms (by 21.9 and 18.9%, respectively) but not the worms undergoing caloric restriction (72). If two different mechanisms were acting on lifespan, we would expect to see an additive effect on lifespan. Calorically restricted worms showed no additional lifespan increase when treated with these compounds, which suggests these two lifespan interventions act through similar mechanisms, and hence that these compounds are acting as caloric restriction mimetics. Additionally, worms treated with rapamycin and allantoin showed increased health-span, the period of an organism's lifespan during which they are considered healthy and free of major morbidity. This was detected as a slower rate of decline in pharyngeal pumping which is known to decline with age and is often used as a marker of ageing (72, 77). If the compounds of study acted in a manner distinct from caloric restriction, we would expect to see a synergistic increase in lifespan of *eat-2* worms treated with the compounds.

Rapamycin treatment has been shown to increase lifespan in different organisms from yeast to mammals (26, 310-312). Treatment with rapamycin has overlapping effects with caloric restriction in mice supporting the idea that it is a caloric restriction mimetic (107). Rapamycin inhibits TOR/let-363 (313), and manipulation of the TOR pathway is sufficient to induce the effects seen in rapamycin treatment. This indicates that TOR inhibition is the primary mode of action for rapamycin-induced lifespan extension (312, 314, 315). Treatment with rapamycin has been shown to delay the onset of age-related diseases in mice (316, 317) and *C. elegans* (72).

Allantoin is poorly studied in the context of ageing but has been shown to increase lifespan and prolong health-span in *C. elegans* (72). Allantoin has been shown to bind to the Imidazoline receptors I1R and I2R, inducing beneficial effects on energy regulation, lipid homeostasis and improving insulin resistance via the AMP kinase pathway (318-322). However, *C. elegans* does not appear to contain any Imidazoline receptors. It is possible that these receptors exist but they or their function as an Imidazoline receptor has not been discovered. Allantoin is thought to be produced naturally in *C. elegans* as a by-product of the reaction between uric acid and ROS (323). Hence allantoin may act as part of a feedback mechanism by which high levels of ROS result in high levels of allantoin which signals the presence of this high level of ROS to promote appropriate antioxidant and potentially life-extending pathways.

In 1998, *C. elegans* became the first multi-cellular organism to have its genome sequenced (324). This genome is now well annotated, and hence we now know the sequence of most if not all genes in the *C. elegans* genome. This allows for transcriptome-wide studies such as microarray analyses which require these sequences to make the probes on the array's surface. By hybridising

cDNA created from RNA extracted from *C. elegans* we can identify which genes are up or downregulated in response to a chosen stimuli, such as rapamycin and allantoin treatment.

2.2 Aims

Microarray analyses identify the relative gene expression between samples for nearly all genes in an organism's genome. To our knowledge, no such analysis has been conducted on the well-known caloric restriction mimetic rapamycin or the newly discovered caloric restriction mimetic allantoin. By studying microarray data from worms treated with allantoin or rapamycin, we hope to be able to identify how differently these two compounds act from each other and caloric restriction. Caloric restriction mimetics are unlikely to elicit the exact same response as caloric restriction itself, and hence by evaluating the overlap in responses, we can identify essential components that contribute to successful ageing. Additionally, caloric restriction mimetics may act through unique pathways opening up new potential mechanisms to exploit to prevent ageing. A better understanding of how caloric restriction mimetics work may aid in the discovery and development of new such compounds.

2.3 Materials and methods

2.3.1 Worm strains and cultures

N2 wild isolate and *eat-2* (DA465) strains were provided by the *Caenorhabditis Genetics Centre* (CGC), which is funded by NIH Office of Research Infrastructure Programs (P40 OD010440). The *eat-2* mutants have reduced neuronal signalling due to the loss of the *Eat-2* nicotinic acetylcholine receptor resulting in decreased pharyngeal pumping that induces a caloric restriction-like state by restricting feeding. All strains were grown at 20°C on standard nematode growth medium (NGM) as described in 'WormBook' (325) with *E. Coli* OP50 as a food source.

NGM plates were prepared up to 2 weeks in advance (stored at 4°C until use) and contained roughly 30ml of agar. OP50 streak plates were created from *E. coli* liquid culture already established in the lab on LB agar. This streak plate was used to seed all future liquid cultures and was stored at 4°C. LB broth (thermofisher ref:12780052) was inoculated by scraping a sterile pipette tip over a colony on the streak plate and placing this in the LB broth. This was incubated at 37°C overnight to create a stock solution. For live *E. coli* plates, 200µl of the overnight stock solution was pipetted to the centre of the plate and gently spread with a sterile glass spreader. These plates were left overnight at room temperature to allow *E. coli* growth before use or storage at 4°C. For killed *E. coli* plates stock solutions were made up to 20% ethanol and stored overnight at 4°C. This solution was irradiated with

UV radiation in a Bio-Rad GS gene linker set at 0–999mJ/cm^2 power 10 times to finalise the killing of the *E. coli*. This solution was centrifuged at 3,000g for 5 minutes and the supernatant replaced with LB broth at half the original volume. 1.5ml of killed stock was added to NGM plates and spread with a sterile spreader and allowed to dry in a sterile laminar flow hood to dry for 3 hours. Additional killed *E. coli* solution was added as needed. *C. elegans* stocks were maintained by cutting a 1 by 1cm square of agar from plates with low food and a high worm population to a fresh NGM plate with live *E. coli* using aseptic technique. This was performed as needed (approximately twice a week).

2.3.2 **Drug concentrations**

Rapamycin (ref. R0395), allantoin (ref. 93791) and FUDR (ref. F0503) were purchased from Sigma Aldrich, Dorset. The drug under study was added to 30ml NGM to give the final concentration of either 10µM rapamycin or 250µM allantoin. These concentrations were chosen as they have previously been shown to increase lifespan in *C. elegans* (72) and were originally determined by taking values seen in previous studies in worms, cells in the Connectivity Map and invertebrates (26, 309, 326). Another member of the lab group treated worms with variations of these doses and monitored for increased mortality. The highest concentration used in a preliminary experiment (not shown) that did not result in increased worm mortality was used for the study; however, it was later found that for some drugs the induced mortality was likely the result of increased levels of dimethyl sulfoxide (DMSO) which is known to be toxic in *C. elegans* at high concentrations (327) and hence the dosages used may be lower than the maximum non-lethal dose.

2.3.3 **Gene expression analysis**

Gene expression analysis was performed 72 hours after the worms were transferred to drug-containing NGM plates with killed *E. coli* to allow plenty of time for the compounds to induce changes in gene expression. Worms were treated with the drugs when in the L4 stage as this time point has been used for lifespan assays with the two drugs (72). Whole worms were washed from the plate with distilled water and spun down at 3,000rpm for 2 minutes. Afterwards, the worms were re-suspended in 400µl Trizol reagent (ThermoFisher, 15596026), and then transferred to 2ml screw cap tubes containing 1ml 0.1mm glass beads. Worms were lysed in a powerlyser at 4,000rpm for two 30 second runs, chilling the tubes on ice after each run. RNA was then extracted as per the manufacturer's instructions with a QIAGEN RNeasy extraction kit. Each condition was run in triplicate.

RNA samples were sent to the Liverpool Centre for Genomic Research, to be run on the microarrays in a manner outlined here. The samples were analysed in terms of quality and quantity using an Agilent 2100 Bioanalyser RNA 6,000 Nano Chip. Samples were labelled using the Affymetric GeneChip 3@ IVT Express labelling kit as per the manufacturer's instructions. 200ng of total RNA was input into the labelling reaction. Following amplification, 15ug of RNA was fragmented, and 12.5ug of fragmented, labelled RNA was hybridised onto Affymetrix GeneChip *C. elegans* Genome Arrays as per the manufacturer's instructions. These were hybridised for 16 hours at 45°C and 60rpm in an Affymetrix hybridisation oven 640. Hybridised arrays were washed using Affymetrix Hybridisation wash and stain kit on a GeneChip Fluidics station 450 and scanned using an Affymetrix GeneChip scanner 3,000 7G. Affymetrix GeneChip Command Console Software was used to generate .CEL files. This raw data was delivered to our lab group and has been submitted to Gene Expression Omnibus (GEO) under the accession GSE64336.

Analysis of gene expression data was initially completed by a member of our lab group with the Affymetrix® Transcriptome Analysis Console. Data pre-processing (using Robust Multi-array Average (RMA) normalisation) and quality control metrics were performed using Affymetrix® Expression Console™ and manually inspected afterwards. Finally, they performed expression analysis for each two pair-wise conditions.

The output of this analysis was received by myself, and Benjamini correction for multiple testing (328) ($P < 0.05$) was applied. This resulted in a slightly lower number of differentially expressed genes in most cases.

Comparisons involving N2 controls were an exception to this pattern as N2 controls appeared to be affected more by noise. This was likely due to higher variability in gene expression in the N2 control population compared to populations with pathological or drug-induced conditions. Surveying various worm datasets from experiments submitted to GEO revealed that in many cases there is a striking number of genes differentially expressed between N2 worm samples from different experiments (data not shown). In order to include differentially expressed genes that were only marginally significant in our subsequent analysis, we included all genes with a p-value of $p<0.05$, and fold change > 2.0. This was in line with our previous methods that focussed on finding pathways potentially associated with ageing and longevity (329).

Functional enrichment analysis was performed using DAVID 6.7 (330). The worm genome was used as the background with default settings for all analysis. Multiple hypothesis testing was carried out using Benjamini correction ($P < 0.05$).

2.4 **Results**

From the microarray, we found no or very few (less than 10) genes differentially expressed after FDR correction for a p-value of $p<0.05$ with a fold change of 1.5 or higher in any comparison with N2 control worms (Table 2.1). By performing a basic principle component analysis (Figure 2.1), we can see there was a large amount of variation between N2 control samples. This variation likely explains why so few genes were detected as differentially expressed. The other samples were much less varied which may be a result of the drug treatment itself that may be inducing the same specific gene expression profile in all the worms.

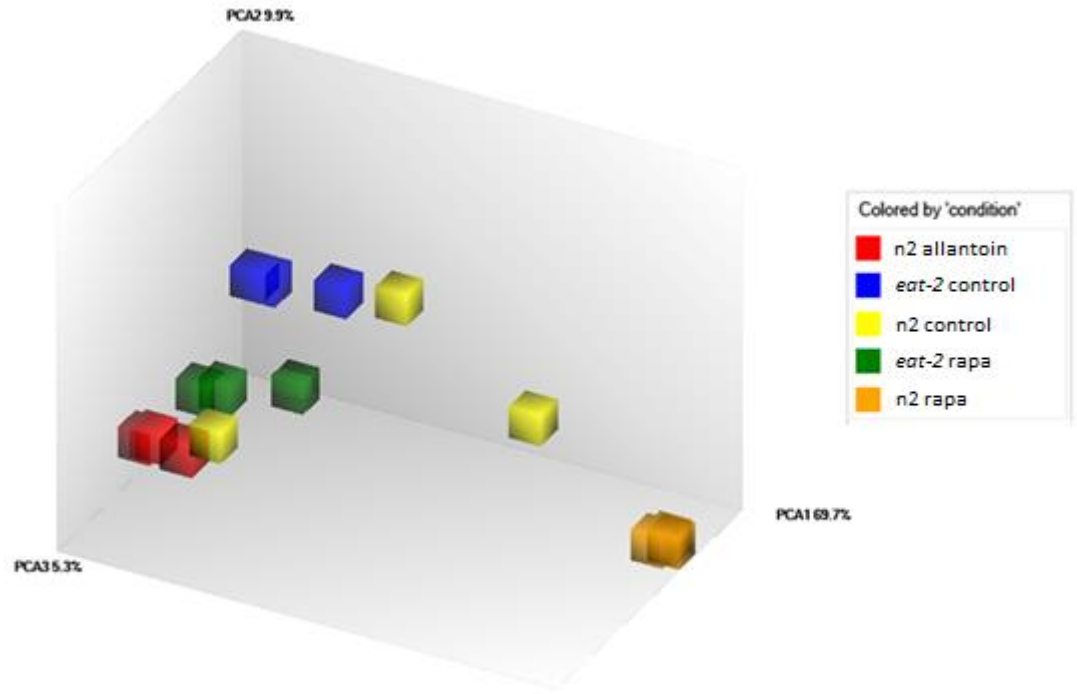

Figure 2.1. PCA plot of microarray data. Each cube represents an RNA sample used in the microarray analysis. N2 controls (yellow) show large amounts of variation which can be seen by the distance of each point from one another. Credit Robi Tacutu for this image.

Array-array correlation plots using Pearson's correlation (331) for all microarray comparisons were obtained using R (332) (Figure 2.2). The lowest correlation seen was between rapamycin treated N2 worms and all other treatments except untreated N2 worms with a score of ~0.92-0.96.

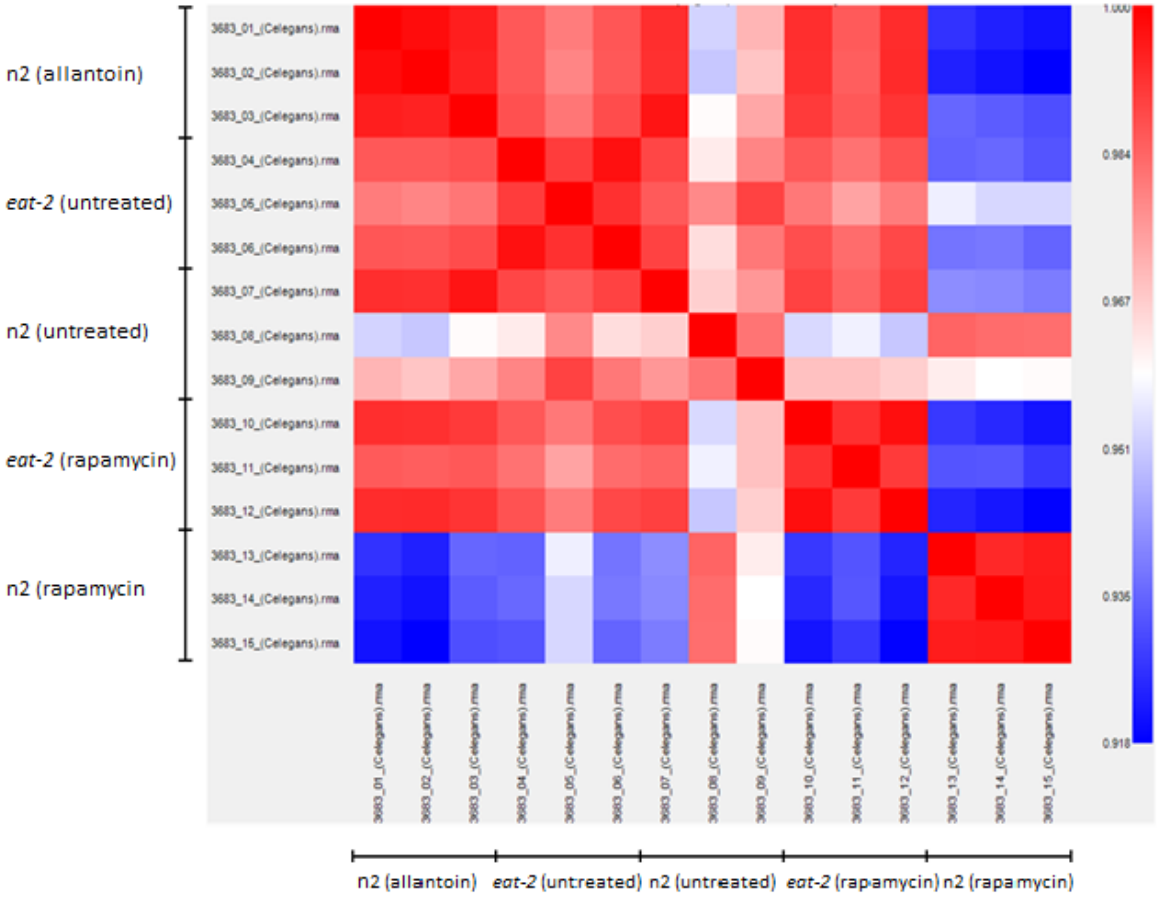

Figure 2.*2. Pearson's correlation of the signal (using RMA-normalised gene-level signals) between samples, obtained from the Affymetrix Expression Console. Credit Robi Tacutu for this image.*

Due to large variations in our N2 control samples, we cannot accurately comment on changes in gene expression from control samples. Treatment of *eat-2* mutants with rapamycin only resulted in 457 genes differentially expressed with a fold change of at least 1.5 and $p<0.05$ after FDR correction. This may in part be due to the reduced intake of rapamycin by the *eat-2* worms. *Eat-2* mutant worms have a pharyngeal pumping rate of 20% that of wild-type N2 worms, however *eat-2* food uptake is 60-80% that of N2 worms (333). Using a dose double that used in the microarray showed similar changes in lifespan indicating that the drug is taken up sufficiently to influence lifespan and hence should affect gene expression (72). Wild-type worms treated with rapamycin showed a large change in gene expression (6,378 genes) compared to *eat-2* controls indicating that rapamycin induces lifespan extension through pathways that are more distinct from those in caloric restriction**.** Perhaps the response to caloric restriction masks responses to rapamycin in *eat-2* worms. N2 worms treated with allantoin showed relatively low changes in gene expression (1,188 genes) indicating more overlap between allantoin and caloric restriction pathways. N2 worms treated with allantoin showed remarkably similar gene expression to *eat-2* worms treated with rapamycin (only 76 differentially

expressed genes). This may indicate a common response of the animals against substances they would not usually be exposed to at the high doses provided in this study. Allantoin and rapamycin seem to act distinctly as N2 worms treated with these compounds showed the largest number of differentially expressed (DE) genes (8,335 genes). Given the larger overlap of allantoin with caloric restriction and apparent difference of rapamycin and caloric restriction, it makes sense that there would be a large difference between the two compounds.

Table 2.1. Genes up (↑) or down (↓) regulated in the different comparisons with an FDR corrected p-value of p<0.05 and fold change of 1.5. Row vs. column.

vs	N2 control	*eat-2* control	N2 rapamycin	*eat-2* rapamycin	N2 allantoin
N2 control	-	1↑ 0↓	0↑ 7↓	0↑ 0↓	0↑ 0↓
eat-2 control	0↑ 1↓	-	3,099↑ 3,279↓	232↑ 225↓	598↑ 590↓
N2 rapamycin	7↑ 0↓	3,279↑ 3,099↓	-	3,920↑ 3,541↓	4,188↑ 4,147↓
eat-2 rapamycin	0↑ 0↓	225↑ 232↓	3,541↑ 3,920↓	-	67↑ 9↓
N2 allantoin	0↑ 0↓	590↑ 598↓	4,147↑ 4,188↓	9↑ 67↓	-

Table 2.2. Genes up (↑) or down (↓) regulated in the different comparisons with an FDR corrected p-value of p<0.05 and fold change of 1.5 that are present in DAVID. Row vs. column.

vs	N2 control	*eat-2* control	N2 rapamycin	*eat-2* rapamycin	N2 allantoin
N2 control	-	1↑ 0↓	0↑ 7↓	0↑ 0↓	0↑ 0↓
eat-2 control	0↑ 1↓	-	2,622↑ 2,881↓	207↑ 216↓	531↑ 559↓
N2 rapamycin	7↑ 0↓	2,881↑ 2,622↓	-	3,400↑ 2,992↓	3,613↑ 3,498↓
eat-2 rapamycin	0↑ 0↓	216↑ 207↓	2,992↑ 3,400↓	-	61↑ 9↓
N2 allantoin	0↑ 0↓	559↑ 531↓	3,498↑ 3,613↓	9↑ 61↓	-

Only one gene was significantly differentially expressed after FDR correction between untreated N2 and *eat-2* worms. This was the alpha catulin *ctn-1* which was up regulated in *eat-2* worms with a fold change of 6.45. *ctn-1* was also up regulated in allantoin treated N2 worms compared to rapamycin-treated *eat-2* worms, *eat-2* controls and N2 worms treated with rapamycin, and down

regulated in N2 worms treated with rapamycin compared to *eat-2*controls and *eat-2* worms treated with rapamycin. *ctn-1* is a poorly studied gene but its mammalian homologue, α-catulin, shares sequence homology to α-catenin, an adhesion molecule, which suggests a potential role of *ctn-1* in cell adhesion (334). CTN-1 localises to the cell membrane in various muscle tissues in *C. elegans* and has been shown to be required for localisation of proteins into dense bodies (335, 336). The dysfunction of one such protein the BK channel has been associated with a number of age-related conditions such as hypertension and erectile dysfunction (337, 338). A study using human cancer cells found that knocking out *ctn-1* induced senescence in these cells through both p53 dependent and independent mechanisms (339). Gene expression profiling through microarray analysis found this reduced *ctn-1* expression reduced the expression of genes associated with the cell cycle, DNA damage response and DNA damage repair. This could indicate increased DNA damage control in *eat-2*and allantoin treated worms which could contribute to their long lifespan. As such, *ctn-1* may be an important gene in ageing.

Rapamycin treatment of N2 worms only resulted in 7 differentially expressed genes, all of which were down regulated. The most down-regulated gene was*aff-1* (AF4/FMR2 family member) with a fold change of -5.54. *aff-1* is located on the plasma membrane but is associated with worm development in late L4 worms, and hence the difference in expression observed may simply be a result of a developmental delay in treated worms (340). The pseudogenes T20D4.17 and F39E9.1 were the most statistically significant genes and were thought to be regulated by the ageing-associated genes DAF-12 and DAF-2, respectively (341). This may indicate an ageing-associated function of these pseudogenes or may simply be indicative of DAF-12 and DAF-2 signalling.

Unfortunately, due to high levels of variation in the N2 control samples no genes were found to be differentially expressed significantly after correcting for multiple testing in Allantoin treatment. The most significantly differentially expressed gene was the downregulated gene *Asm-3* (acid sphingomyelinase). Inactivation of *Asm-3* has been shown to extend adult lifespan in *C. elegans* via the DAF-2/AGE-1 signalling pathway (342). Hence downregulation of this gene may contribute to increased lifespan, though this downregulation may only be detected by chance as it is not significant after FDR correction.

A functional enrichment of the comparisons with at least 100 genes was performed using DAVID 6.7 (Table 2.3-2.4) (330). In a number of comparisons, we observed terms related to development, such as 'GO:0003006~reproductive developmental process'. It could be that these drugs were inducing this expression, but they may be delaying the growth of the worms so that it appears to be the case. Both caloric restriction and rapamycin treatment delay development and if

allantoin is acting as a caloric restriction mimetic it may have similar developmental effects (315). The delay caused by these treatments may not be equal, and so the reproductive development of recently developed L4 worms entering adulthood may not progress equally between treatments. This developmental caveat could also explain a number of other enriched terms such as 'GO:0042302~structural constituent of cuticle' and 'GO:0002009~morphogenesis of an epithelium' which include collagen genes that change in expression throughout worm development (Figure 2.3).

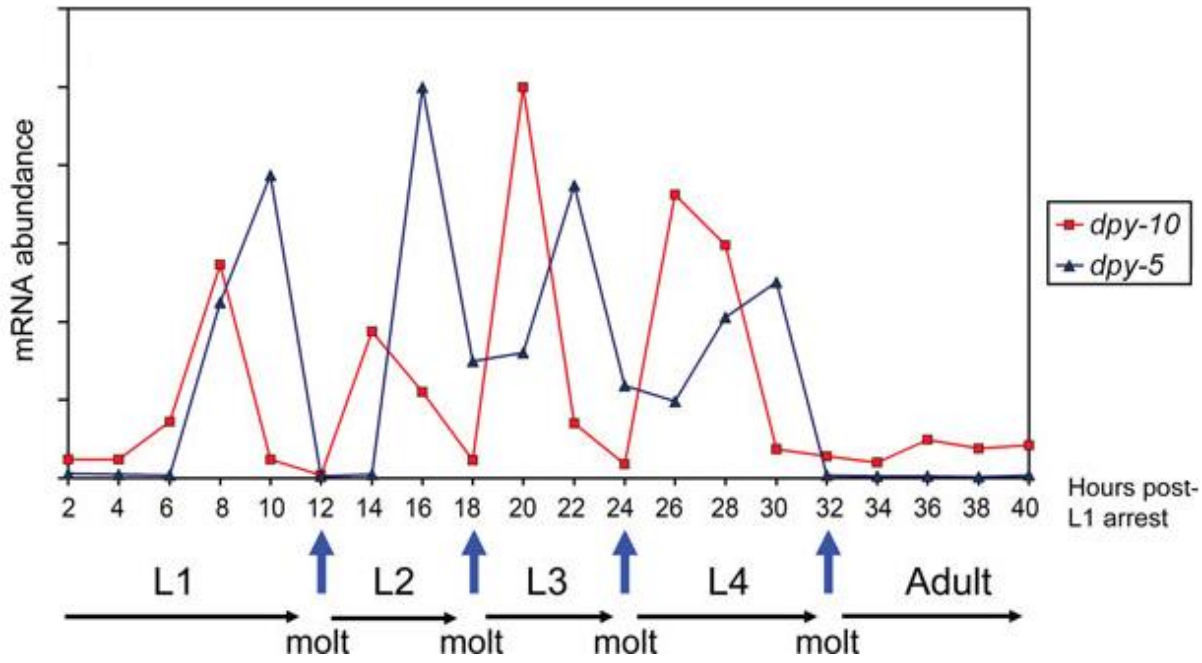

Figure 2.3. Representation of expression in two collagen genes (dpy-10 and dpy-5) through development. Messenger RNA from collagen genes fluctuate throughout worm development. There is a sharp change in expression of these genes in the three days following the L4 moult (third blue arrow), and hence any delay in development will result in different levels of collagen expression. Taken with permission from Wormbook (343). This representative image has no Y-axis values as this image serves only to indicate the time scale of expression fluctuations.

The *eat-2* control worms, compared to allantoin treated N2 worms, showed only two significantly enriched clusters for downregulated genes, 'GO:0042302~structural constituent of cuticle' as discussed above and 'IPR012885:F-box associated type 2' (Table 2.3). F-box proteins often bind SKP1 (S-phase kinase-associated protein 1) and other proteins to form SKP1-cullin-F-box protein ligases (SCFs). These SCFs are involved in an array of activities from nutrient sensing in yeast, to cell cycle regulation and developmental regulation in animals including *C. elegans* (344). This may tie in with differences in worm development. Upregulated genes produced more significantly enriched clusters (Table 2.4) including, 'GO:0010259~multicellular organismal ageing'. This term, including many heat shock proteins, likely encompasses other terms involving heat shock factors. This would

indicate these genes associated with ageing are more active in the allantoin treated worms indicating a deviation in life-extending pathways between the two treatments. Of these genes, only 4 were found in GenAge (14) (hsp-12.6, hsp-1, hsp-16.48, and hsp-49) and all were found to be pro-longevity. The remaining terms are more general. Saposin B domains are often involved in enzymatic activities. 'IPR009007:Peptidase aspartic, catalytic' could indicate turnover of proteins or could be a contributor to the change in collagen we see in the upregulated genes.

The N2 worms treated with allantoin compared to N2 worms treated with rapamycin had very broad terms for both upregulated and downregulated genes (Table 2.3-2.4) which are not helpful at identifying differences between the two treatments. Additionally, we saw terms that may indicate differences in the rate of development progression (e.g. 'IPR002486:Nematode cuticle collagen, N-terminal').

The *eat-2* worms treated with rapamycin compared to untreated *eat-2* worms had only 2 statistically significant clusters upregulated, but both terms refer to ageing (Table 2.3). The genes from these groups contain only 4 genes that are present in GenAge and are all considered pro-longevity genes. This indicates that rapamycin had an effect in these worms even if a change in lifespan is not observed. The only significantly downregulated cluster is 'IPR002486:Nematode cuticle collagen, N-terminal' which may indicate that rapamycin is affecting the rate of development in *eat-2* worms (Table 2.4).

The *eat-2* worms compared to N2 worms treated with rapamycin showed upregulated terms that may indicate a difference in developmental progression (Table 2.3). Terms regarding chromosomes and cell cycle may indicate that rapamycin treatment is altering the rate of cell division or this may be a result of differences in the progression of development. Downregulated terms included 'IPR000731:Sterol-sensing 5TM box', this sterol-sensing domain is involved in a variety of processes including cholesterol homeostasis, cytokinesis and cell signalling (Table 2.4). This may play into the cell division terms we saw upregulated.

The overlap between genes differentially expressed between *eat-2* control and rapamycin-treated worms and genes differentially expressed between *eat-2* control worms and rapamycin-treated N2 worms was examined (Figure 2.4). This may allow the identification distinctions between *eat-2* induce longevity and that induced from rapamycin treatment. There were 79 consistently upregulated and 51 consistently downregulated genes between the two comparisons. Functional enrichment analysis revealed that the upregulated genes were enriched for heat shock factors (enrichment score: 6.88). Enrichment scores were generated by DAVID. This score was derived from the p-values of the individual terms within the functional cluster. A score of 1.3 or higher is equivalent

to p≤0.05. Heat shock factors that often act as protein chaperones to prevent misfolding to maintain a stable proteome are associated with ageing in *C. elegans* (345, 346). Heat shock proteins have also been shown to be regulated by the IGF signalling pathway, a known caloric restriction pathway (discussed in Section 1.1.1) (345)). Downregulated genes were enriched for terms such as DNA binding, histone proteins, methylation and the nucleosome (enrichment score: 18.26). Histones control the density of the DNA structure, and the modification of these proteins facilitates access to the DNA by proteins necessary for transcription and DNA damage repair (reviewed in (347)). This may indicate that rapamycin treatment increases lifespan preferentially by increased heat shock protein activation whereas *eat-2* mutation increased lifespan through alteration of gene expression and or DNA damage responses.

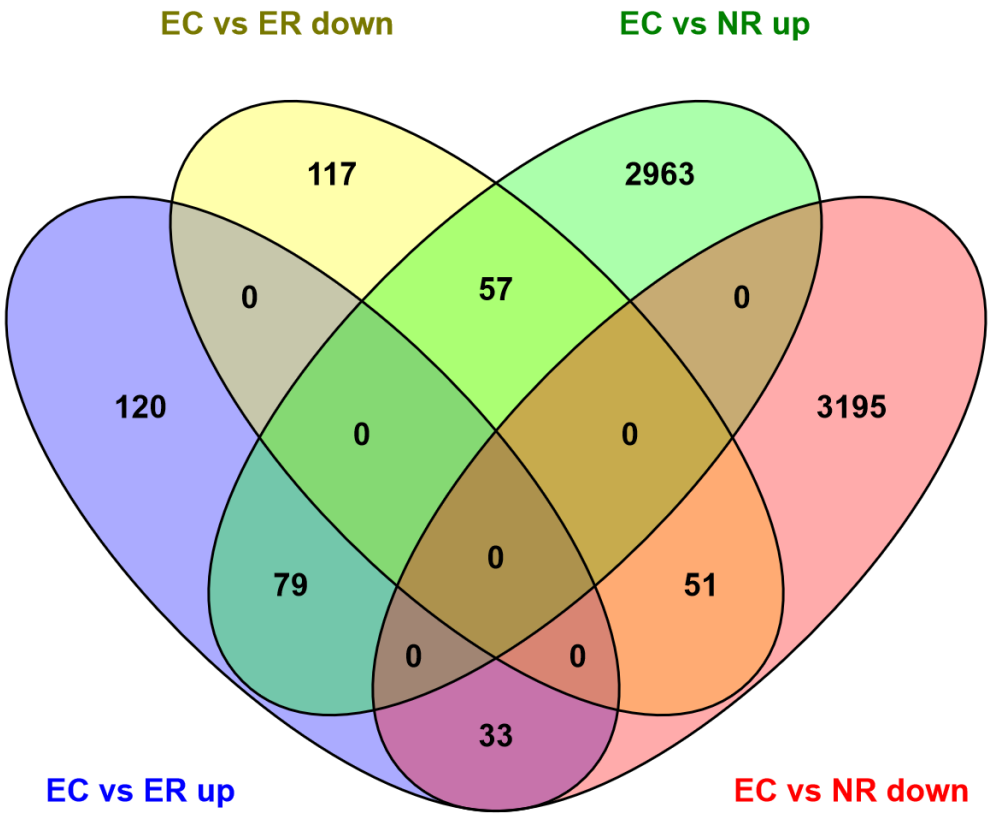

Figure 2.4. Venn diagram comparing up and downregulated genes between eat-2 *control and rapamycin-treated worms and between* eat-2 *control worms and rapamycin-treated N2 worms. Key EC* eat-2 *control, ER* eat-2 *treated with rapamycin, NR rapamycin treated N2 worms.*

When comparing *eat-2* worms treated with rapamycin and N2 worms treated with rapamycin we again saw changes in terms that may be attributed to changes in the rate of development, such as 'GO:0003006~reproductive developmental process' (upregulated) and 'IPR000535:Major sperm protein' (downregulated) (Table 2.3-2.4).

The overlap between genes differentially expressed between *eat-2* and N2 worms treated with rapamycin and genes differentially expressed between *eat-2* control worms and rapamycin-treated N2 worms was examined (Figure 2.5). There were 2,299 consistently upregulated and 2,806 consistently downregulated genes. Functional enrichment of upregulated genes revealed multiple functional clusters regarding cell cycle with clusters including terms such as cell cycle (enrichment score: 10.97), DNA replication (enrichment score: 8.88), and 'mitotic spindle midzone' (enrichment score: 3.80). This indicates increased cell cycle activity in N2 worms relative to *eat-2* worms without rapamycin treatment. Caloric restriction has been shown in mice to reduce cell proliferation rates (348). Downregulated genes were enriched for a number of enrichment clusters. These included clusters including terms referring to, the cytoskeleton (enrichment score: 17.49), protein phosphorylation (enrichment score: 11.89 and 6.08), collagen (enrichment score: 10.00), and histone proteins (enrichment score: 5.37). Changes in the cytoskeleton could indicate morphological changes, cell division or cell adhesion which may play into ageing (detailed in Section 5.1.1). As described earlier in this section histones may indicate alterations in DNA damage responses. This highlights potential differences in the two life-extending conditions *eat-2* mutation and rapamycin treatment.

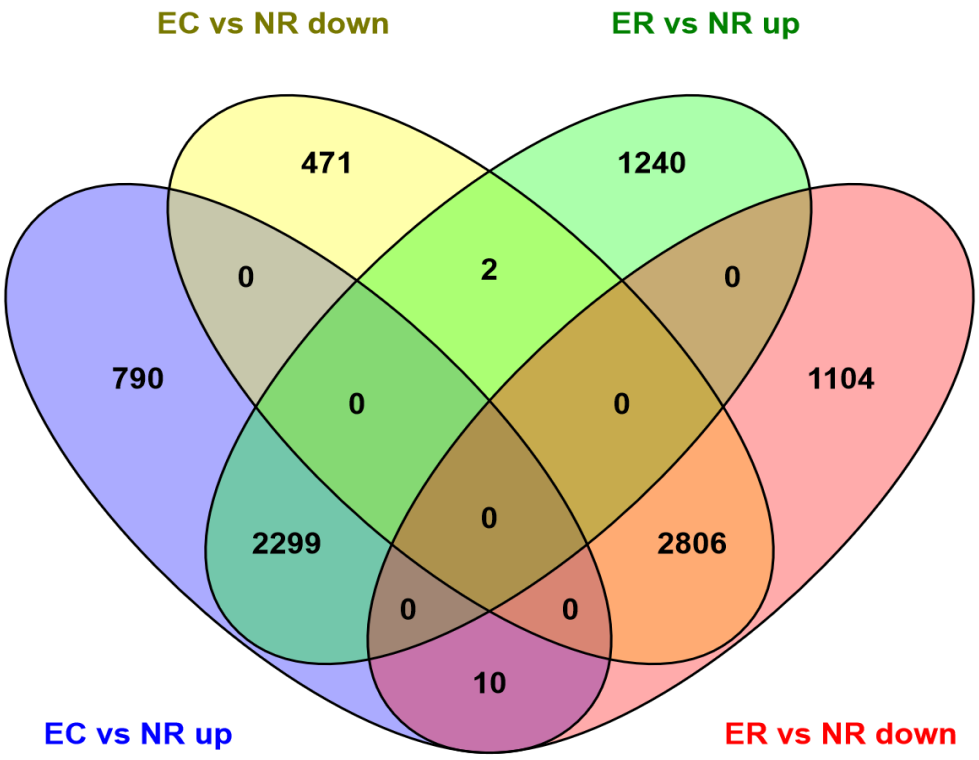

Figure 4.5. Venn diagram comparing up and downregulated genes between rapamycin-treated eat-2 *and N2 worms and between* eat-2 *control worms and rapamycin-treated N2 worms. Key EC* eat-2 *control, ER* eat-2 *treated with rapamycin, NR rapamycin-treated N2 worms.*

In these comparisons we saw a number of terms appearing multiple times; this is in part due to the broad nature of the terms which can encompass a wide range of activates but also may be due to a potential caveat in which the treatments may be causing changes in the rate of worm development.

*Table 2.3. Representative terms from the top five FE clusters, gene counts and the enrichment scores for the clusters from upregulated genes. Terms were selected that best represented all the terms in the cluster.*Enrichment score generated by DAVID. This score is derived from the p-values of the individual terms within the functional cluster. A score of 1.3 or higher is equivalent to p≤0.05.*

	Term	Count	Enrichment score*
eat-2 con vs. allantoin N2	GO:0005576~extracellular region	32	7.92
	IPR008139:Saposin B	11	7.05
	GO:0010259~multicellular organismal aging	19	3.66
	IPR009007:Peptidase aspartic, catalytic	7	3.56
	IPR001436:Alpha crystallin/Heat shock protein	8	3.35
N2 allantoin vs. N2 Rapa	IPR000242:Protein-tyrosine phosphatase, receptor/non-receptor type	48	12.5
	GO:0007218~neuropeptide signalling pathway	34	9.95
	GO:0005576~extracellular region	88	9.44
	IPR002486:Nematode cuticle collagen, N-terminal	56	8.42
	GO:0005856~cytoskeleton	61	6.17
eat-2 control vs. *eat-2* Rapa	IPR001436:Alpha crystallin/Heat shock protein	6	4.45
	GO:0007568~aging	12	3.88
	GO:0006732~coenzyme metabolic process	6	1.76
	GO:0003700~transcription factor activity	14	1.52
	GO:0040018~positive regulation of multicellular organism growth	9	1.35
eat-2 control vs. N2 Rapa	IPR012885:F-box associated type 2	92	20.7
	GO:0002009~morphogenesis of an epithelium	91	7.48
	GO:0003006~reproductive developmental process	192	7.14
	GO:0007049~cell cycle	108	6.85
	GO:0005694~chromosome	35	6.47
eat-2 Rapa vs. N2 Rapa	GO:0007049~cell cycle	148	17.0
	IPR012885:F-box associated type 2	83	12.0
	GO:0003006~reproductive developmental process	235	10.8
	GO:0002009~morphogenesis of an epithelium	109	9.41
	GO:0006260~DNA replication	33	8.61

*Table 2.4 Representative terms from the top five FE clusters, gene counts and the enrichment scores for the clusters from downregulated genes. Terms were selected that best represented all the terms in the cluster. *Enrichment score generated by DAVID. This score is derived from the p-values of the individual terms within the functional cluster. A score of 1.3 or higher is equivalent to p≤0.05.*

	Term	Count	Enrichment score*
eat-2 con vs. allantoin N2	IPR012885:F-box associated type 2	56	31.5
	GO:0042302~structural constituent of cuticle	18	4.40
	GO:0000279~M phase	16	2.32
	IPR016181:Acyl-CoA N-acyltransferase	5	1.59
	PIRSF038285:cuticle collagen	10	1.41
N2 allantoin vs. N2 Rapa	IPR012885:F-box associated type 2	105	23.8
	GO:0007049~cell cycle	163	21.5
	GO:0003006~reproductive developmental process	265	16.8
	GO:0002009~morphogenesis of an epithelium	124	14.3
	GO:0022402~cell cycle process	142	13.4
eat-2 control vs. *eat-2* Rapa	IPR002486:Nematode cuticle collagen, N-terminal	16	6.40
	IPR016638:Uncharacterised protein family UPF0376	4	2.14
	PIRSF038285:cuticle collagen	6	1.71
	cel00982:Drug metabolism	4	1.60
	IPR004045:Glutathione S-transferase, N-terminal	4	1.30
eat-2 control vs. N2 Rapa	IPR002486:Nematode cuticle collagen, N-terminal	80	19.0
	IPR000387:Dual-specific/protein-tyrosine phosphatase, conserved region	43	11.1
	GO:0005576~extracellular region	84	7.50
	IPR000731:Sterol-sensing 5TM box	17	5.41
	GO:0006793~phosphorus metabolic process	172	4.95
eat-2 Rapa vs. N2 Rapa	IPR000242:Protein-tyrosine phosphatase, receptor/non-receptor type	50	14.5
	IPR000535:Major sperm protein	44	7.18
	GO:0007218~neuropeptide signalling pathway	27	6.54
	GO:0005576~extracellular region	82	5.81
	IPR000731:Sterol-sensing 5TM box	17	5.56

GeneDR (349), a database of dietary restriction related genes lists 60 genes related to caloric restriction in *C. elegans*. The list of significantly differentially expressed genes was searched for these genes to identify changes in pathways important to caloric restriction. Allantoin treated worms had 17 caloric restriction-related genes upregulated compared to rapamycin-treated worms which only had 5 genes comparatively upregulated when compared to each other (Table 2.5). By looking at the level of overlap between genes differentially expressed in rapamycin-treated N2 worms relative to *eat-2* controls and to allantoin treated worms we saw a significant overlap of 16 caloric restriction related genes (up: p=0.005, down: p=4.61E-10) indicating high similarity between caloric restriction and allantoin treatment which can be seen from the low number of differentially expressed genes between *eat-2* controls and allantoin treated N2 worms. Notably, the gene*daf-16,* which is required for some forms of caloric restriction's lifespan extension, is upregulated in allantoin treated N2 worms and *eat-2* worms compared to rapamycin-treated N2 worms.

Table 2.5 Genes associated with caloric restriction in C. elegans *in GenDR that are up (↑) or down (↓) regulated in the different comparisons with an FDR corrected p-value of p<0.05. No genes were present in comparisons with N2 controls. Row vs. column.*

Vs	*eat-2* control	N2 rapamycin	*eat-2* rapamycin	N2 allantoin
eat-2 control	-	6↑ 13↓	2↑ 0↓	3↑ 0↓
N2 rapamycin	13↑ 6↓	-	16↑ 4↓	17↑ 5↓
eat-2 rapamycin	0↑ 2↓	4↑ 16↓	-	0↑ 0↓
N2 allantoin	0↑ 3↓	5↑ 17↓	0↑ 0↓	-

Due to the variation in our control samples, no genes were differentially expressed when comparing to N2 controls after FDR correction. If we discount this correction for multiple testing, we get considerably more genes marked as significantly differentially expressed; however, care must be taken when analysing such data as these genes may be significant purely by chance. This was done for all comparisons to N2 controls to give more useful numbers of genes (Table 2.6).

Table 2.6. Number of up (↑) or down (↓) regulated genes in each condition as compared to N2 control with an uncorrected p value of 0.05. Row vs. columns.

Vs	*eat-2* control	N2 rapamycin	*eat-2* rapamycin	N2 allantoin
N2 control	152↑ 273↓	1,594↑ 1,770↓	672↑ 428↓	525↑ 352↓

Rapamycin treatment of N2 worms resulted in a large number of differentially expressed genes (>3,000 genes), more than rapamycin treatment of *eat-2* worms relative to N2 controls (~1,000). By conducting a Fisher's exact test of independence, we found a significant overlap of 13 upregulated genes (p=2.20E-9) but not of downregulated genes. Additionally, there was a significant proportion of genes with opposite gene expression.

To determine if allantoin and rapamycin are acting similarly, the proportion of differentially expressed genes in both treatments relative to N2 controls was assessed. There were more genes that showed directionally similar changes in expression that we would expect by chance (15 genes, up: p=2.14E-10, down: p=4.61E-4). This would suggest similar action, but it was also found that the proportion of genes with opposite expression (156 genes) was also far greater than would be expected by chance, suggesting very different modes of action but perhaps with a similar underlying core mechanism.

Comparing *eat-2* worms to N2 worms showed relatively few differentially expressed genes (425 genes). By comparing the proportion of genes that overlap with either rapamycin or allantoin induced expression we can assess how similar these compounds are acting to caloric restriction. Allantoin treatment shows a significant number of genes with overlapping expression in the same direction (37 genes, up: p=1.01E-12, down: p=1.04E-4). There were a few genes with opposite expression but this was not more than we would expect by chance. This suggests similarity between allantoin treatment and caloric restriction. Rapamycin treatment, however, showed a significant proportion of overlapping gene expression for upregulated genes only (p=0.009) with a significant proportion of genes with opposite gene expression. This suggests rapamycin is acting in a fashion more removed from caloric restriction.

A functional enrichment was performed on these differentially expressed genes (Table 2.7-2.8). As before a number of developmental terms such as 'GO:0003006~reproductive developmental process' were differentially expressed indicating a delay in worm development.

Rapamycin treatment of N2 worms induced upregulation of DNA metabolic processes that includes DNA damage repair, suggesting rapamycin may improve this process. Additionally, terms

regarding the cell cycle were upregulated. Terms downregulated by rapamycin treatment included a number referring to the cell surface such as 'GO:0044421~extracellular region part' and 'glycoprotein'. Additionally, protein dephosphorylation was downregulated which may indicate cellular signalling as protein phosphorylation can control protein activity.

Eat-2 worms showed no significantly enriched terms for upregulated genes that do not relate to development. Downregulated terms again included those related to the extracellular component of the cell, such as 'glycoprotein' and 'IPR016186:C-type lectin-like'. Terms regarding lipase activity are also downregulated though this may be a direct consequence of decreased food uptake and hence lipid uptake. *Eat-2* worms treated with rapamycin showed almost exactly the same terms for downregulated genes which may reflect the low number of differentially expressed genes between these two conditions. Upregulated genes produced few significantly enriched clusters. Terms regarding the cytoskeleton may suggest cell motility or restructuring of the cell shape. Terms regarding major sperm protein affect sperm motility though the relevance of this is not clear.

Allantoin treatment showed upregulation of cell surface-related terms such as 'GO:0007166~cell surface receptor linked signal transduction'. No downregulated clusters are statistically significant but include terms referring to the cell cycle that are upregulated in rapamycin treatment.

*Table 2.7. Representative terms from the top five FE clusters, gene counts and the enrichment scores for the clusters from upregulated genes without FDR correction. Terms were selected that best represented all the terms in the cluster.*Enrichment score generated by DAVID. This score is derived from the p-values of the individual terms within the functional cluster. A score of 1.3 or higher is equivalent to p≤0.05.*

	Term	Count	Enrichment score*
N2 control vs. rapamycin up	GO:0051301~cell division	53	11.7
	GO:0007049~cell cycle	78	8.1
	GO:0003006~reproductive developmental process	130	6.9
	GO:0006259~DNA metabolic process	43	6.6
	GO:0060429~epithelium development	60	6.1
N2 control vs. *eat-2* up	GO:0042302~structural constituent of cuticle	35	32.7
	cuticle	10	6.4
	GO:0040002~collagen and cuticulin-based cuticle development	3	0.9
	GO:0008238~exopeptidase activity	3	0.4
	GO:0002119~nematode larval development	13	0.3
N2 control vs. *eat-2* rapamycin up	IPR000535:Major sperm protein	17	5.3
	cytoskeleton	13	3.8
	IPR008574:Protein of unknown function DUF856, Caenorhabditis species	5	3.8
	GO:0030968~endoplasmic reticulum unfolded protein response	5	2.5
	IPR001628:Zinc finger, nuclear hormone receptor-type	21	2
N2 control vs. N2 allantoin up	GO:0007166~cell surface receptor linked signal transduction	21	4.2
	IPR008574:Protein of unknown function DUF856, Caenorhabditis species	5	3.9
	GO:0005576~extracellular region	24	2.9
	IPR000535:Major sperm protein	10	2.4
	IPR002486:Nematode cuticle collagen, N-terminal	11	1.7

*Table 2.8. Representative terms from the top five FE clusters, gene counts and the enrichment scores for the clusters from downregulated genes without FDR correction. Terms were selected that best represented all the terms in the cluster.*Enrichment score generated by DAVID. This score is derived from the p-values of the individual terms within the functional cluster. A score of 1.3 or higher is equivalent to p≤0.05.*

	Term	Count	Enrichment score*
N2 control vs. N2 rapamycin down	GO:0006470~protein amino acid dephosphorylation	37	10.8
	IPR002486:Nematode cuticle collagen, N-terminal	44	10
	glycoprotein	67	7.9
	GO:0018996~molting cycle, collagen and cuticulin-based cuticle	43	5.9
	GO:0044421~extracellular region part	18	4.3
N2 control vs. *eat-2* down	glycoprotein	24	11.4
	IPR008139:Saposin B	9	7.3
	GO:0016298~lipase activity	10	5.4
	Secreted	17	4.7
	IPR016186:C-type lectin-like	12	3.8
N2 control vs. *eat-2* rapamycin down	glycoprotein	33	11
	IPR016186:C-type lectin-like	22	6.4
	GO:0016298~lipase activity	11	5.5
	Protease	17	5.4
	IPR008139:Saposin B	8	4.8
N2 control vs. N2 allantoin down	GO:0005777~peroxisome	5	1.9
	IPR001810:Cyclin-like F-box	15	1.7
	GO:0007530~sex determination	5	1.7
	GO:0007049~cell cycle	11	1.4
	GO:0034470~ncRNA processing	6	1.2

The Connectivity Map can be visualised using Mantra 2.0 (Figure 2.6) (350, 351). By doing so for all the compounds studied in depth in (72), we observed that rapamycin (also known as sirolimus) induced similar expression profiles to the other compounds in human cells. Allantoin, however, is more distant with no connections at the cut off used (0.75). This distance reflects the high number of differentially expressed genes between the two treatments. A cut off of 0.75 was used as lower cut-offs provided too many connections to glean useful information. The distance value between nodes was calculated by combining the output of a rank-aggregation analysis and gene set enrichment analysis; the lower the value, the more similar the gene expression profile with 0.8 being considered significant (350).

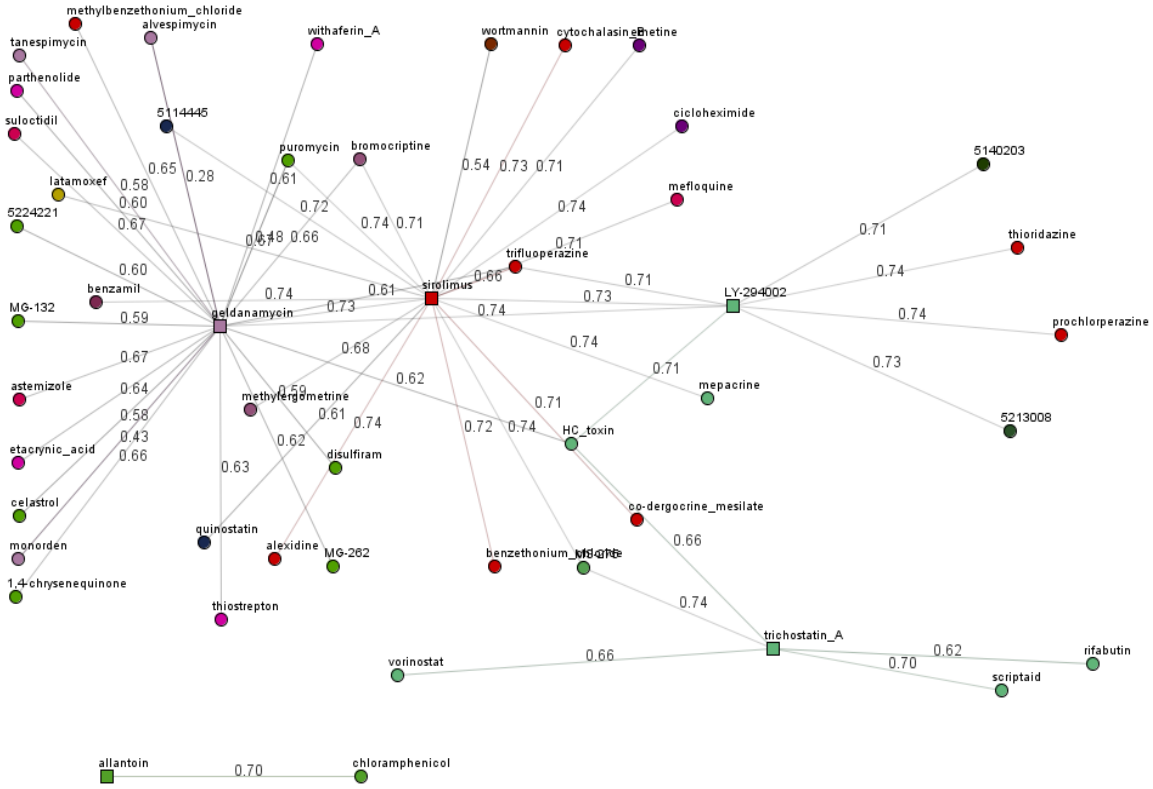

Figure 2.6. Mantra 2.0 analysis. Each square represents one of the drugs under investigation in (72). Each numbered line represents the similarity of induced gene expression profile in the Connectivity Map. Geldanamycin, rapamycin (sirolimus), and LY-294002 seem to be relatively similar in their induced gene expression profiles. Trichostatin A is more distinct with only an indirect connection to these drugs. The analysis used a 0.75 cut off due to larger cut-offs producing too many nodes to discern any useful information.

2.5 Discussion

Rapamycin is a well-documented caloric restriction mimetic; however, in this study, it appears to act comparatively less similar to caloric restriction than allantoin. There are a greater number of DE genes in rapamycin-treated N2 worms than allantoin treated N2 worms, compared to *eat-2* controls. This shows that allantoin has a more similar effect on gene expression to caloric restriction.

As discussed above, caloric restriction and caloric restriction mimetics have the potential to delay development (315), and a large portion of the change in gene expression seen in this study related to developmental processes. This may simply reflect treatment induced variation in organismal development. Alternatively, it could be that these genes affect lifespan as suggested by the developmental theory of ageing, by which genes acting to promote healthy growth and development in early life act to promote ageing in later life (13, 352). If the former is the case, then it is not clear if other differentially expressed terms are seen as a consequence of differences in developmental progression. To identify which of these scenarios is correct the experiment would need to be repeated in older worms that are no longer undergoing developmental changes.

In addition to terms clearly related to development, we see multiple terms regarding cell cycle and the cell surface or extracellular space. Changes in cell cycle progression between successfully ageing organisms such as those treated with the compounds in this study and wild-type animals may support the 'reproductive-*cell cycle* theory of ageing'. This theory states that hormones that control growth and reproduction early in life later induce ageing via cell cycle signalling (353). This theory is supported by clinical evidence suggesting a role of hormonal alterations in the cell cycle in a number of age-related diseases including cancer, heart disease and osteoporosis (354, 355). Changes regarding the cell surface have been seen in fibroblast in vitro ageing previously (356, 357) though it is not clear if the changes we see in this analysis are a cause or consequence of delayed ageing.

Both compounds have been shown to upregulate ageing and caloric restriction related genes as would be expected from two caloric restriction mimetics. Interestingly *daf-16* is upregulated in allantoin treated N2 worms compared to rapamycin-treated N2 worms but not *eat-2* worms, further supporting the similarity between allantoin treatment and caloric restriction. *daf-16* is required for lifespan extension via the IGF-1 signalling pathway (349). Interestingly *daf-16* is required for lifespan extension through some methods of caloric restriction but not through *eat-2* mutation (61, 164). In *eat-2* controls, *daf-16* is significantly more expressed than in rapamycin-treated N2 worms indicating that daf-16 is not involved in rapamycin-induced life extension which has been shown to be the case (72). This would also indicate a role for *daf-16* in *eat-2* lifespan, which may be the case as *daf-16*; *eat-2* double mutants have been shown to have a slight decrease in lifespan compared to *eat-2* mutant

worms, indicating a small non-essential contribution to this lifespan extension (164). Follow up work looking at *daf-16* mutants treated with allantoin showed similar results with *daf-16* not being essential for the lifespan extension but with a lower increase (19.7%) in *daf-16* mutant lifespan compared to N2 treated worms (21.9%) (72). Additionally, heat shock factors that are associated with ageing in *C. elegans* (346) were found to be differentially expressed in both allantoin and rapamycin treatment suggesting similarities in the core mechanism of these compounds.

Allantoin showed significant overlap with *eat-2* worms indicating similar modes of action. Rapamycin showed significant overlap of only upregulated genes and a significant number of genes with gene expression changes opposite that seen in *eat-2* worms.

There are a number of caveats that must be considered when reviewing this work. Firstly mRNA levels do not necessarily correlate with protein levels (303-305). Another potential caveat is that only one dosage has been investigated. Different doses may have different effects, as has been shown for the supposed caloric restriction mimetic metformin, in which some doses increased N2 lifespan, but decreased *eat-2* lifespan (358). The doses used in this assay have however been shown to be sufficient to increase lifespan in N2 worms and have no effect in *eat-2* worms. The use of *eat-2* worms as a model of caloric restriction may be limiting as other methods of caloric restriction induction show different levels of lifespan extension and gene expression (61) and worms are exposed to the caloric restriction effect of being eat-2 their entire life as opposed to the late-life treatment of the drugs in this study. Furthermore, only one time point (72 hours) post-treatment was studied. This time point is very short and does not allow the analysis of chronic treatment and how such treatment affects normal age-related changes in gene expression. This time point was chosen as the initial treatment provides the greatest exposure to the compounds of interest, while 72 hours provides the worms with time to appropriately respond to the treatment. Hence, we predicted that changes in gene expression would be at their most pronounced. Finally, pathways that affect ageing in *C. elegans* may not be conserved in mammals, and physiological differences could also affect drug activity (359). It would be interesting to run lifespan experiments in mice with allantoin to see if the lifespan extension is conserved. However, this is beyond the scope of this thesis. This study does hint towards these drugs having evolutionarily conserved mechanisms as the gene expression profile used as the input for the Connectivity Map was obtained from rodent cells exposed to sera from animals (rhesus monkeys or rats) undergoing caloric restriction. This was then compared with drug-induced gene expression profiles in various human cells. These drugs induced an extended longevity phenotype in worms, suggesting that their caloric restriction mimetic mechanism is evolutionary conserved.

This work supports the idea that these compounds are acting as caloric restriction mimetics. Due to large variations in gene expression in control wild-type worms, we cannot accurately detect how these compounds act on wild-type worms to increase lifespan. However, a number of candidate genes known to be important for caloric restriction and/or lifespan extension have been identified.

Chapter 3: Response to DNA damage in *Heterocephalus glaber* and *Mus musculus* skin fibroblasts

3.1 Introduction

In order to further our understanding of successful ageing, a microarray analysis of the nematode worm *C. elegans* undergoing caloric restriction or treatment with a caloric restriction mimetic was performed in the previous chapter. It was found that both caloric restriction and the mimetic compounds acted similarly but showed a large amount of differential gene expression between them. It was also observed that genes involved in the cell cycle and the surface chemistry of the cell were enriched within the differentially expressed genes suggesting a role in successful ageing for these cellular aspects.

In the present chapter, I will examine an alternative model of successful ageing, the naked mole rat (NMR), at the cellular level. The response of these cells to DNA damaging agents will be assessed and compared to cells derived from the short-lived mouse. As DNA damage is thought to be a major contributor to ageing we hypothesise that the NMR's previously reported high DNA damage resistance is integral to its long lifespan. By assessing how the cells respond to genotoxic stimuli we can infer broad mechanisms of DNA damage responses which may play into successful ageing. Additionally, evaluating how cells respond provides us with a context in which we can evaluate further experiments of cells responding to genotoxic stress. The study of differences in lifespan and health-span between these species is complementary to the previous chapter that studied these changes within a single species.

Firstly, a survival assay of NMR and mouse cells treated with two DNA-damaging compounds, camptothecin and chromium (vi) oxide was performed. These compounds were chosen as they will allow us to assess the response of these cells to both specific and broad-spectrum DNA damaging agents as camptothecin induces single-strand breaks specifically, whereas chromium (vi) oxide induces a broad spectrum of DNA lesions. From this assay, an LD50 or lethal dose 50 value, the dose at which half the cells die as a result of the treatment, was calculated for each species and compound. These values are used to evaluate the levels of resistance of the compounds in both species. A beta galactosidase assay was then performed to evaluate the number of cells that undergo irreversible senescence as a result of the genotoxic insult.

3.1.1 Cell culture

Maintaining live rodents for experiments is financially expensive, time-consuming and ethically challenging. A much more favourable approach is to take cells from the animal of study and grow them outside the body. These cells can then be experimented on quickly and cheaply without ethical concern.

Cells are grown in culture media such as minimum essential media (MEM) that contains amino acids, glucose, salts, vitamins and other nutrients the cells need to live. This alone is often not enough as cells also require survival signals. In the body, a cell receives constant signals from its local environment that allow it to detect where it is (360). In a culture flask without these signals, many cells will not grow or will undergo apoptosis. Growth factors and hormones can be added to the culture media to provide these signals and promote proliferation. This is typically done by the addition of foetal bovine serum (FBS) or similar animal derived sera. FBS is, as the name suggests, sera derived from bovine foetuses and is collected after the mother is slaughtered for meat. In addition to providing growth factors and hormones to promote growth, FBS also provides attachment and spreading factors, additional nutrients such as lipids and amino acids and protease inhibitors (361).

In addition to appropriate culture media, an appropriate culture surface is required for anchorage-dependent cells such as fibroblasts (362). Without such anchorage, the cell would not proliferate. In cell culture, this anchorage is to the culture vessel's surface. Culture vessels are typically made of polystyrene which is usually hydrophobic, so cells struggle to adhere to it. However, specialist treatment of the surface renders the surface hydrophilic allowing adhesion (363-365). Alternatively, coatings can be added to the culture surface, typically extracellular matrix components to increase cellular adhesion. Cells can only grow in a culture flask for a finite length of time. As the cell density increases toward 100% confluence (meaning 100% of the culture vessel surface is covered with cells), the rate of proliferation sharply decreases (186). This is due to contact between the cells allowing E-cadherin and α-catenin binding that results in inhibition of the pro-proliferation transcription factor Yes-associated protein (YAP)-1 via the hippo signalling pathway in a process known as contact inhibition (366-368). To continue proliferation, the cells must be passaged, which involves the detachment of the cells, typically by using trypsin to cleave the protein connections to the culture vessel surface, and then diluting the cell solution and transferring to a fresh culture vessel.

Cells can only proliferate for so long in cell culture. As the total number of cell divisions a cell has undergone increases, its proliferative potential decreases and eventually the cell will no longer proliferate (142). This limited number of divisions is known as the Hayflick limit. This limit is due to the repetitive sections of DNA at the end of chromosomes, called telomeres, shortening. Each round of

division fails to copy all of the telomere, and as a result, the telomeres become shorter. Eventually, this loss of material extends beyond the telomere into the rest of the chromosome, at which point the cell will stop proliferating and may undergo apoptosis (143, 369, 370). Cells that do continue to proliferate undergo crisis, a period of genomic instability during which most cells will die. In immortalised cell lines and cancer cells, telomerase, an enzyme that replaces the lost telomeres is thought to prevent this shortening (143). Cells taken directly from the organism of study, such as those used in this study, are called primary cells.

Such cell culture techniques have been successfully applied to the NMR and allowed the identification of a number of toxic compounds that NMR cells are more resistant to then mouse cells (175). As NMRs have a lower body temperature than mice, a lower incubation temperature was used (170, 175). Typically, mammalian cells are cultured at 37°C as this is the typical internal body temperature of mammals. However, NMR cells show poor replicative ability at 37°C because they have a lower body temperature and hence a lower temperature is used, typically ~33°C (371).

Typically, cells are cultured at atmospheric oxygen (~21% oxygen), however by using nitrogen to displace oxygen, cells can be maintained at lower concentrations (3% in this study) in part to mimic the low-oxygen environment of the NMR. The NMR lives in large colonies in subterranean burrows that have poor ventilation and hence result in low levels of oxygen (372). Additionally, cells are not exposed to atmospheric oxygen; they typically exist in 2-5% oxygen depending on the distance to the vasculature which contains a maximum of ~12% oxygen in arterial blood (373, 374). It has been shown that growing cells at lower oxygen concentrations improves growth, increases cellular lifespan and decreases the amount of cellular stress (375, 376). Hence the use of lower oxygen provides a more biologically relevant environment.

3.1.2 Naked mole rat cells

NMR skin fibroblasts have been shown previously to be more resistant to chromium (vi) oxide (5 fold increase in LD50) and camptothecin (15 fold increase in LD50) treatment than skin fibroblasts derived from mice (175). Additionally NMR fibroblasts were shown to have decreased proliferation post genotoxic stimuli than mouse fibroblasts, and this decreased proliferation lasted longer (179). This suggests these cells are less prone to proliferate while DNA damage is present and that more time is spent repairing this damage. Furthermore, NMR cells were less likely to become irreversibly senescent as a result of the treatment (179).

Skin fibroblast derived from NMR showed higher levels of the protein p53 compared to fibroblasts from mice (~50 fold higher) (179). Similarly, *Nrf2* has a 3-fold greater expression in NMR fibroblasts as compared to those from mice (179). Increased p53 and *Nrf2* expression may mean NMR cells are primed to stop proliferating in response to DNA damage.

3.1.3 Hexavalent chromium

Chromium is a naturally occurring transition metal typically found in one of two oxidative states, trivalent chromium or hexavalent chromium. Hexavalent chromium is classed as a group 1 carcinogen by the International Agency for Research on Cancer (IARC) (377), and professions with high exposure to chromium such as chromate pigment manufacture and chromium plating of metals have been associated with cancer (378). Hexavalent chromium enters the cell through non-specific sulphate/phosphate anionic transporters (379, 380). Once inside the cell hexavalent chromium undergoes metabolic reduction by a large number of potential cellular components but primarily ascorbic acid, glutathione and cysteine (381). If the amount of reductant in the cell is relatively low compared to the amount of chromium, then multiple one-electron reductions occur. However, if there is an abundance of reductant, then a two-electron reduction occurs followed by a one-electron reduction to create trivalent chromium (Figure 3.1). This reduction creates free radicals that may go on to damage DNA and other biological molecules (382).

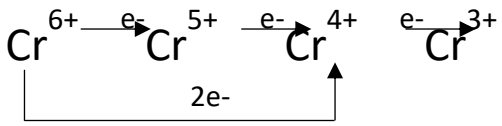

Figure 3.1. The reduction of hexavalent chromium (Cr^{6+}) in the cell. If there is a relative abundance of reductant, then a 2 electron reduction may take place. If there is relatively low reductant, then a series of one electron reductions will occur.

Hexavalent chromium does not interact with DNA but its reduction products can. Trivalent chromium is not considered toxic as it is unable to cross the cell membrane however it can accumulate when formed inside the cell as it is unable to leave (383). Trivalent chromium can form complexes with amino acids, proteins and nucleic acids (384-387). These interactions can result in DNA crosslinks to either proteins or other DNA strands (386-388). Additional types of DNA damage induced by the

reduction products of hexavalent chromium include DNA adducts, DNA single-strand break, oxidised bases, and abasic sites (389-392).

3.1.4 Camptothecin

Camptothecin is a prescribed anti-cancer drug. It acts by inducing single and double-strand breaks. Camptothecin does not interact with DNA specifically but binds the DNA - topoisomerase 1 complex (393, 394). Topoisomerase 1 is an enzyme that relaxes the tension of DNA by binding to double-stranded DNA and cleaving one of the strands. This allows the intact strand to pass through the cut strand. Topoisomerase 1 then promotes the religation of the cut strand and is released from the DNA (395). This reduction in DNA tension is essential for transcription and DNA replication. Binding of camptothecin prevents the religation step, thereby inducing a single-strand break (394, 396). During DNA replication the DNA and camptothecin-bound topoisomerase 1 causes arrest at the replication fork. If the single-strand break is on the leading strand of DNA synthesis, then a double-strand break can form. As the replication fork reaches the break the newly synthesised double-strand DNA will no longer be connected to the rest of the DNA beyond the single-strand break and hence becomes a double-strand break (Figure 3.2) (397, 398). This can result in cell death or G2 arrest (399). These double-strand breaks are considered the primary cause of camptothecin-induced cytotoxicity (400). As these double-strand breaks form during cell DNA synthesis, cells that are proliferating more are more susceptible to camptothecin cytotoxicity. This is why camptothecin is used to treat cancer, as the rapidly dividing tumour cells will be more likely to divide and form a double-strand break before the single-strand break is repaired.

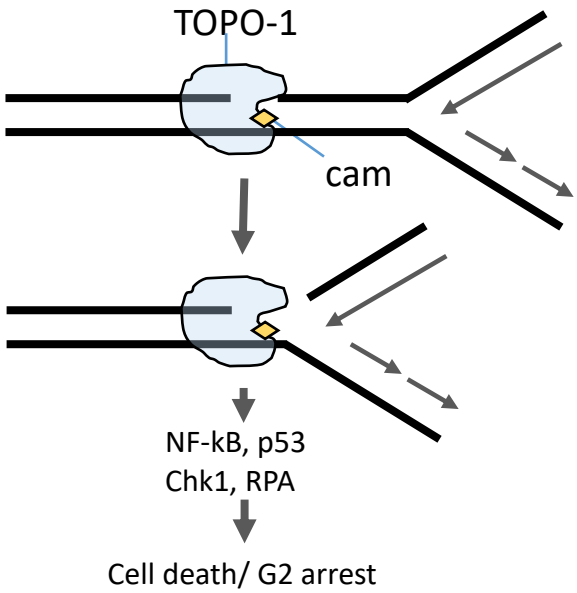

Figure 3.2. The collision model of topoisomerase 1 (TOPO-1) when bound to DNA and camptothecin (cam) at the replication fork. This will result in a double-strand break if the topo-1 induced cleavage occurs on the leading strand. As the replication fork reaches the break, the newly synthesised double-strand DNA will no longer be connected to the rest of the DNA beyond the single-strand break and hence becomes a double-strand break (397). The collision at the replication fork results in signalling via p53, NF-kB, Chk1 and RPA.

3.2 Aims

The naked mole rat is becoming increasingly popular as a model organism. However, it is still new and relatively poorly studied. For example, searching the term 'naked mole rat' in PubMed returns 299 items as opposed to the term 'mouse', which returns over 1.4 million results (as of October 2016). As such it is important to check that results seen in other labs can be reproduced both to ensure the validity of the data and the capability of the researcher repeating the experiment.

The dose of a drug that kills half the treated cells, known as the LD50, can be used as an indicator of how resistant a cell is to a drug; the higher the dose required, the more resistant the cell. Finding the LD50 in mouse and NMR cells will allow us to confirm previously reported genotoxin resistance in the NMR (175). Identifying these values will also facilitate further experiments by providing doses that elicit similar levels of stress between the two species. In addition to cell death, another key indicator of cellular stress is cellular senescence. Identifying levels of cellular senescence in mouse and NMR cells exposed to genotoxic stressors helps evaluate their tolerance to such treatment and provides further biological context by which to evaluate further experiments in these cells.

3.3 Materials and methods

3.3.1 Cell stock and cell culture

All primary cell cultures were grown on minimum essential medium (ThermoFisher 11095080) supplemented with 15% foetal bovine serum (ThermoFisher 10500064), 1% Penicillin Streptomycin (Lifetechnologies 15070-063), and 0.1% fungizone (ThermoFisher 15290026). Cells were grown in 75cm^2 culture flasks with 10ml of growth media unless otherwise stated, and were grown at 35°C with 3% oxygen and 5% carbon dioxide.

Initial primary skin fibroblasts from 3 naked mole rats and 3 C57BL/6 mice were kindly provided by Vera Gorbunova (referred to as alpha stocks). Due to contamination, these were replaced by C57BL/6 primary skin fibroblasts derived from 3 different specimens which were purchased from Caltag Medsystems Ltd and NMR primary skin fibroblasts derived from 3 NMRs provided by Vera Gorbunova (referred to as beta stock). Cells derived from Vera Gorbonova's group were taken from underarm skin and isolated as described by Seluanov *et al.* (401). Mice used were 4-6 months old, and NMRs were 2-5 months old. Skin was shaved and cleaned with 70% ethanol before harvesting. The tissue was minced and incubated in DMEM (Dulbecco's Modified Eagle's medium) F12 with 0.14 Wunsch U/mL collagenase at 37°C for 30-90 minutes with agitation. Disassociated cells were washed and added to culture dishes with DMEM F12 supplemented with 15% FBS and antibiotics/antimycotics. Cells were cultured at 5% CO_2 and 3% O_2. Mouse cells were cultured at 37°C, and NMR cells were cultured at 32°C. Cells were grown to confluency before passaging with trypsin and frozen using liquid nitrogen. Cells were not tested for identity as fibroblasts are more proliferative than other cell types and hence dominate the cell culture under the described conditions. Cells derived from Caltag Medsystems were extracted from underarm skin as described above from 6-week-old mice except only CO_2 was controlled (5%) and 'Cell Biologics Culture Complete Growth Medium' was used in place of DMEM F12. These cells were tested through immunofluorescent staining with anti-FSP1 (fibroblast specific protein1) (Millipore USA) a marker of fibroblast identify (402). Upon receipt, all cells were visually inspected and found to have a fibroblast morphology.

To passage cells, the growth media was aspirated, and the cells were rinsed with PBS. This was replaced with 5ml phenol red free trypsin (Lifetechnologies, 15090-046) and incubated at 37°C, 5% CO_2 for 5 minutes. The cells were checked under a microscope to confirm detachment and 5ml of growth media was added to quench the trypsin reaction. This was spun down at 1,000rpm for ten minutes and resuspended in the required volume of growth media.

Cells were periodically frozen to maintain cell stocks for later use. Confluent plates were trypsinised and spun down at 1,000rpm for ten minutes and resuspended in 1ml growth media (minimum essential medium, 15% FBS, 1% Penicillin Streptomycin 0.1% fungizone) with 10% DMSO. This was frozen in a cryovial stored in a polystyrene 15ml falcon tube holder at -80°C to facilitate slow freezing. To thaw, cryovials were placed in a 37°C water bath to defrost quickly. As soon as the vial had completely thawed, the contents were added to 10ml of growth media and mixed gently. This was spun down at 1,000rpm for ten minutes and resuspended in 10ml of fresh growth media to remove the DMSO. This was transferred to a fresh culture flask.

Cell images were taken of the alpha cell stock; however, due to a corrupted storage drive, these images were lost. All presented cell images are of the beta cell stock only.

3.3.2 LD50 assay

After 10 population doublings, cells were grown to near confluence and passaged using phenol red free trypsin (Lifetechnologies, 15090-046) and plated into T25 flasks ensuring an equal number of cells were transferred to each plate. Each was either treated with a serial dilution of chromium (vi) oxide (Sigma Aldrich 236470) (5, 10, 20, 40, 80, and 160µM) or camptothecin (Sigma Aldrich C9911) (3.75, 7.5, 15, 30, 60, 120µM) in 2% DMSO (Sigma Aldrich D4540) or 2% DMSO only in normal growth media for two hours. The plates were rinsed with PBS and media was replaced. After 24 hours post-stimuli, cells were removed from the plate surface with trypsin and diluted 1:0.5 with trypan blue to mark dead cells and counted using one half of a haemocytometer. This was done four times per sample. Dead cells were not counted. This was repeated twice per cell line on separate occasions. Mouse cell line 1 was run alongside NMR cell line 1. The same applies to cell line 2 and 3 for both species and cell stocks. One replicate of mouse cell line three from the beta stock treated with camptothecin was run alone. NMR cell line 2 samples were grown in twice the number of T25 culture flasks due to cell availability in stock samples. LD50 values were calculated using the method of Miller and Tainter (403). LD50 values for each species were compared by independent sample T test. The total number of cells from the alpha cell line in control conditions are as follows mouse 1 – 140,250, mouse 2 – 101,306, mouse 3 – 108,800, NMR 1 – 4,083, NMR 2 – 23,527 and NMR 3 4,888. The total number of cells from the beta cell line control conditions are as follows mouse 1 – 12,130, mouse 2 – 5,667, mouse 3 – 6,898 (chromium treatment) mouse 3 –21,556 (camptothecin treatment), NMR 1 – 678, NMR 2 – 9,630 and NMR 3 – 5,741. Mouse 3 cells treated with camptothecin and chromium were conducted at different times hence have a different number of cells. Comparisons between DMSO-treated controls and DMSO-free controls were conducted as described in Section 3.3.3.

3.3.2.1 LD50 assay optimisation

Initial chromium treatment was performed using sodium chromate. However, this proved ineffective at killing either mouse or NMR cells. This was only performed on the alpha cell stock. The following doses were administered to both species: 1.57, 3.13, 6.25, 12.5, 25, 50, 100, 200, 400 and 800um. This was performed once per cell line, (3 cell lines per species). A higher dose of 3,200µM was tested once per NMR cell line to assess the killing ability of this compound at an extreme dose.

Determining the LD50 proved technically challenging due to the high level of noise in the samples. Initial studies utilised a cell counter to speed up the assay and remove human error or bias from the analysis and used cells grown in a single well of a 24 well plate to allow large numbers of samples to be run simultaneously. However, the automated cell counter was communal and poorly maintained and was found to give irregular readings that persisted after replacing the inlet nozzle (which was found to contain mould) and flushing the system with water prior to analysis. As such, a haemocytometer was used instead and found to give more consistent readings. However, the cell counts were very low with control samples for NMR cells often including no cells at all. This was due to the low surface area in the 24 well plates combined with the volume of trypsin (0.5ml) required to coat the plate (lower volumes resulted in the centre of the plate often not being coated due to the meniscus of the liquid) and subsequent addition of culture media to neutralise the trypsin (0.5ml). To combat this the samples were spun down at 1,000rpm for 10 minutes and resuspended in 400µl however consistent removal of the supernatant without disturbing the pellet proved difficult and it was a concern that this would introduce variation within the samples. This was reflected in variation between technical replicates. Next, the level of starting material was increased instead using one well per 6-well plate for each sample, but these counts were still too low for NMRs that have a lower cell density due to early contact inhibition. Finally, the method described above was decided and provided sufficient cells to work with. However, due to the limited size of the incubator used and the slow-growing nature of the NMR cells, this proved very time-consuming.

Additionally, quantification of cell counts was also performed through the use of the abcam's WST-1 staining kit. WST-1 (Water-soluble Tetrazolium salt 1) is broken down by mitochondrial dehydrogenases into a formazan dye that can be detected by monitoring absorbance at 440nm. This level of absorbance indicates the number of cells in the well. This was run according to the manufacturer's specification. In short, ~1,000 cells were plated per well of a 96-well plate and allowed to attach overnight. These were then treated with genotoxic compounds as described in 3.3.2 for 2 hours and allowed to recover overnight. WST-1 was added and incubated for 4 hours. The plate was shaken to mix the contents and loaded onto a 96-well plate reader to monitor absorbance at 440nm.

This approach has been used successfully in NMR fibroblasts previously (175). This method had two major setbacks in that the available plate reader was very old and had high background noise, but also this was unavailable for use halfway through the initial experiments due to its use in the teaching laboratories. Due to the unreliability of this equipment and concerns regarding its reproducibility this assay was dropped in favour of the haemocytometer counting approach that was trialled at the same time.

3.3.3 Senescence assay

Beta galactosidase staining kit (9860S) was purchased from New England Biolabs and was used as specified by the manufacturer's instruction. In brief, cells that had undergone approximately 10 population doublings were plated into two 24-well plates (5,000 cells per well) per condition and time point. This cell density was chosen because higher cell densities resulted in high levels of overlap between cells reducing the accuracy of cell counts. Cells were either treated at LD50 (Mouse: camptothecin: 5.24µM, chromium (vi) oxide: 6.88µM, NMR: camptothecin: 30.93µM, chromium (vi) oxide: NMR1 24.68µM, NMR2 28.28µM, and NMR3 27.3µM) for alpha stocks or a logarithmic range of doses (camptothecin: 3.75-120µM, chromium (vi) oxide: 5-160µM) for beta stocks for each compound in 2% DMSO. Treatment lasted 2 hours; then wells were rinsed with PBS before replacing with fresh media. Additionally, alpha stocks were tested as above for control conditions with or without DMSO, 2 counts were made per well, and 2 wells were used per cell line however only NMR cell lines 2 and 3 were used in the analysis due to contamination of cell line 1. Alpha cells were analysed after 8 or 48 hours; beta cells were analysed after 24-hour post-treatment. Cells were fixed and incubated in beta galactosidase staining solution at pH6 for 3 days at 37°C at atmospheric CO_2 to ensure clear staining. This incubation time was selected because staining after the recommended 24 hours was too faint for accurate counting. The staining solution contains X-gal that is broken down by beta galactosidase and subsequently oxidised into 5,5'-dibromo-4,4'-dichloro-indigo, an insoluble blue compound. This reaction occurring at ph6 indicates senescence, and hence cells containing blue staining are presumed to be senescent. A random field of view was selected under the light microscope, and the percentage of stained cells was calculated twice per well resulting in six random fields of view per species per condition.

3.3.4 Population doubling time

Approximately 5,000 cells were plated into four wells of a six-well plate. These were allowed to grow for 24 hours or 48 hours. At these time points, half of the wells were trypsinised with 3ml of trypsin and the cells counted with a haemocytometer. Two counts were made per well. This was only performed on mouse cell lines one and two and NMR cell line two and three from the alpha cell stock.

3.4 Results

Initially primary skin fibroblast cell stocks derived from either 3 NMRs or mice were used in this project (referred to as the alpha cell stocks), however, due to a major contamination of cell stocks halfway through the project, these were replaced with new cell stocks (referred to as the beta cell stocks). Morphologically, untreated cells of each species appeared to look the same (Appendix Figure 1). The population doubling times for the alpha mouse 1 and 2 were calculated as 13.8 and 14.7 hours, respectively. NMR cell line 2 and 3 of the alpha cell stock was found to have a population doubling time of 33.5 and 31.3 hours, and hence these cells grow more than twice as slowly as the mouse cells.

Initial chromium treatment was performed using sodium chromate. However, this proved ineffective at killing either mouse or NMR cells (Appendix Figure 2) and treating NMR cells with an extreme dose of 3,200uM resulted in 20% survival. There was no significant difference between species or cell lines. Correspondence with the Buffenstein lab later indicated that these salts had been tested (unpublished data) and that a poor response was observed as these salts were taken up 'poorly' by the cells. Hence all further work was conducted using chromium (vi) oxide.

3.4.1 NMR cells show greater DNA damage resistance than cells derived from mice

We identified the LD50 of the two DNA damaging agents, chromium (vi) oxide (Figure 3.3-3.5, and 3.9-3.11) and camptothecin (Figure 3.6-3.8 and 3.12-3.14) for both primary NMR and mouse skin fibroblasts. In the alpha stocks, the cell survival of mouse cells (median 45%) was significantly lower than that in NMR cells (median 57%) when treated with 20µM chromium (vi) oxide (U_{25}=49, p=0.045). The mean LD50 was calculated in NMR as 25µM (+/- 14.65) and in mice as 6.88µM (+/- 0.06µM). The LD50 values for mice (Standard deviation (SD)=1.32) and NMR (SD=1.86) were significantly different (t(4)=-15.09 p>0.05). There was an approximate 4-fold increase of LD50 in NMR, which is similar to the previously reported 5-fold increase (175). There was a large standard error of the mean associated with the LD50 in NMR. This is due to variation seen in the three primary cell cultures, as such in future experiments the LD50 calculated for each primary cell culture would be used. These are as follows, NMR1 24.68µM (+/- 0.93µM), NMR2 28.28µM (+/- 3.09µM), and NMR3 27.3µM (+/- 12.42µM).

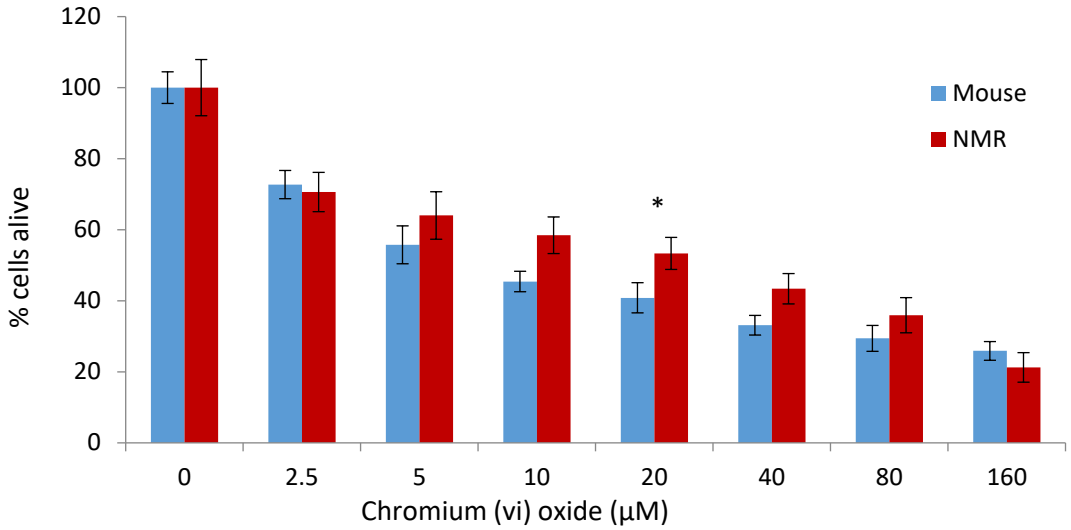

Figure 3.3. Percentage survival of primary skin fibroblasts from either mouse (blue) or NMR (red) from the alpha cell stocks after treatment with chromium (vi) oxide for 2 hours in media with 2% DMSO. A clear increase in resistance to chromium (vi) oxide is seen in the NMR with an LD50 in NMR at 25µM (+/- 14.65) and in mice at 6.88µM (+/- 0.06µM). Error bars indicate +/- one standard error of the mean between each cell line (3 cell lines per species, each cell line value is the average of two independent experiments which each consist of four individual counts). Star (*) indicates significance at the p<0.05 level between the percentage of cells alive in mouse and NMR cell cultures by Mann Whitney U test. The total number of cells under control conditions for each species is 350,356 cells for mice and 32,498 cells for NMR. The total number of cells counted in control conditions was greater than or equal to 300 cells. In the treated samples this was greater than or equal to 150 cells.

To assess the variability between alpha cell lines treated with chromium (vi) oxide within each species an ANOVA (analysis of variants) was performed. There was no statistical difference observed between mouse cells treated with chromium (vi) oxide ($F(2, 18)= 1.201$, $p=0.324$). NMR cells, however, were significantly different ($F(2, 18)= 9.116$, $p=0.002$). A post hoc Turkey test showed that NMR cell line 1 was significantly lower than the other cell lines ($p>0.05$), but that there was no significant difference between the other two cell lines (Figure 3.4).

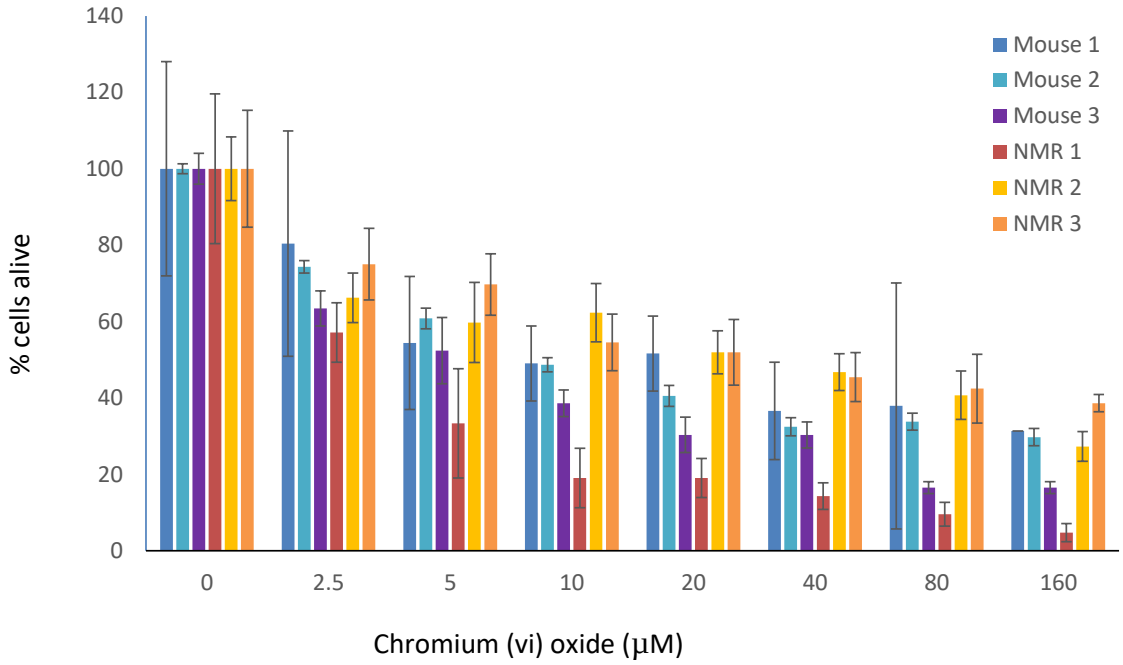

Figure 3.4 *Percentage survival of primary skin fibroblasts in each of the primary skin fibroblast cell lines from 3 mice and NMRs that form the alpha cell stocks after treatment with chromium (vi) oxide for 2 hours in media with 2% DMSO. Error bars indicate ± one standard error of the mean between two independent experiments which each consist of four individual counts. The total number of cells under control conditions for each cell line is as follows mouse 1 – 140,250, mouse 2 –101,306, mouse 3 – 108,800, NMR 1– 4,083, NMR 2 – 23,527 and NMR 3 4,888. Each cell line was analysed twice. The total number of cells counted in control conditions was greater than or equal to 100 cells. In the treated samples this was greater than or equal to 50 cells.*

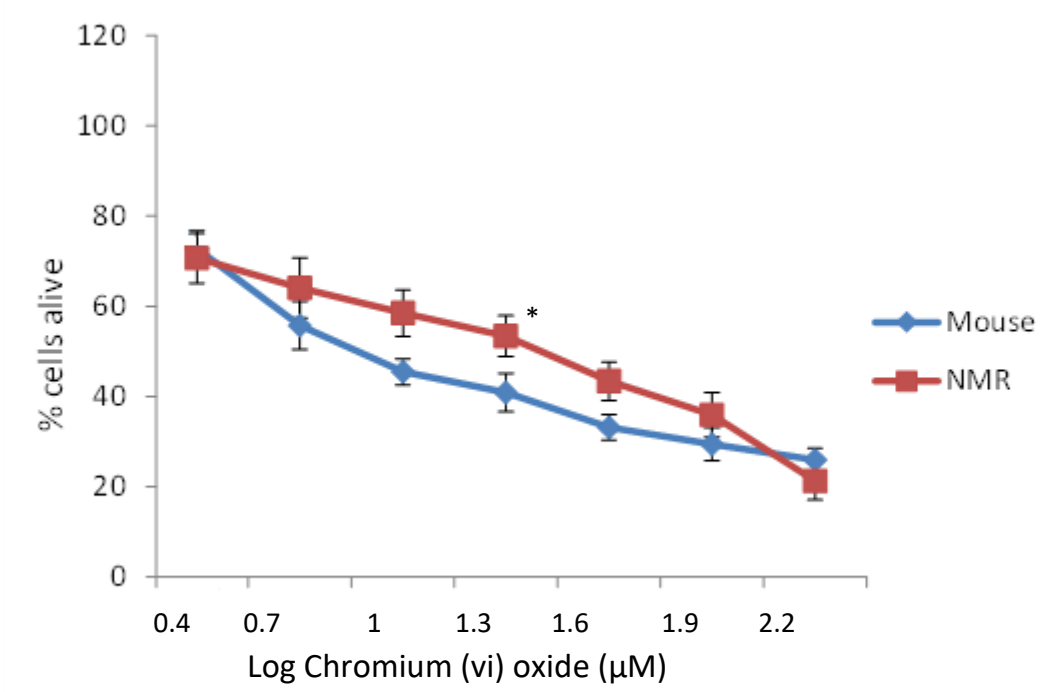

Figure 3.5. Percentage survival of primary skin fibroblasts from either mouse (blue) or NMR (red) from the alpha cell stocks after treatment with chromium (vi) oxide for 2 hours in media with 2% DMSO. A clear increase in resistance to chromium (vi) oxide is seen in the NMR with an LD50 in NMR at 25µM (+/- 14.65µM) and in mice at 6.88µM (+/- 0.06µM). Error bars indicate +/- one standard error of the mean between each cell line (3 cell lines per species, each cell line value is the average of two independent experiments which each consist of four individual counts). Star (*) indicates significance at the p<0.05 level between the percentage of cells alive in mouse and NMR cell cultures by Mann Whitney U test. The total number of cells under control conditions for mice was 350,356 and NMRs was 32,498. The total number of cells counted in control conditions was greater than or equal to 300 cells. In the treated samples this was greater than or equal to 150 cells.

When treated with 3.75uM, 7.5uM, 15µM or 30µM of camptothecin, cell survival of mouse cells (median 83%, 54%, 49% and 48%, respectively) was significantly lower than that in NMR cells (median 90%, 74%, 59% and 57%, respectively) (U_{28}=11, p=0; U_{22}=4, p=0; U_{22}=32, p=0.021; U_{22}=24, p=0.006, respectively) in alpha cell stocks. The LD50 was calculated in NMR as 30.93µM (+/- 5.3µM) and in mice as 5.24µM (+/- 0.03µM). The LD50 values for mice (SD=0.43) and NMR (SD=1.28) were significantly different (t(4)=-32.82 p>0.05). This is an approximate 6-fold increase of LD50 in NMR, which is lower than the 15-fold increase that has been previously reported (175).

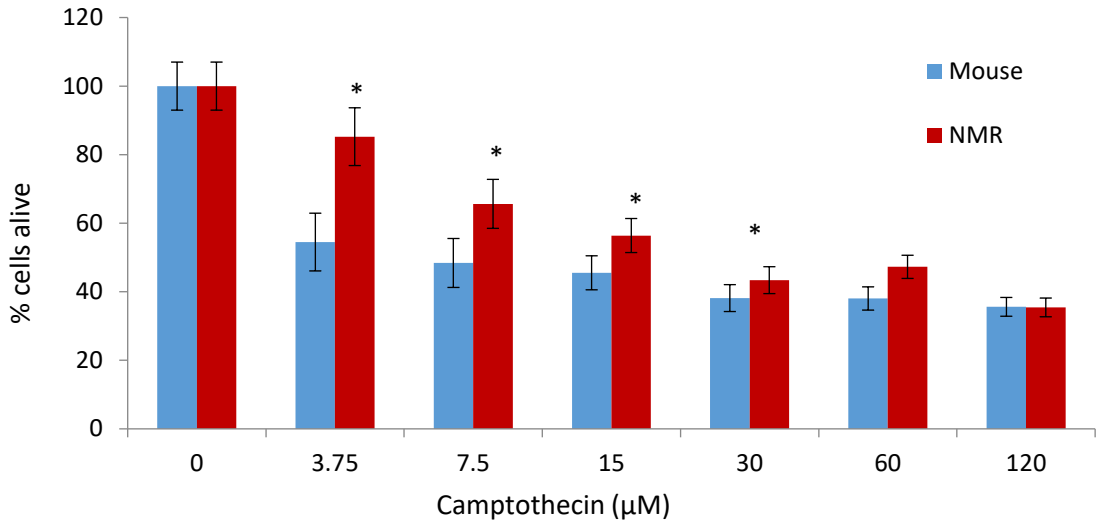

Figure 3.6. Percentage survival of primary skin fibroblasts from either mice (blue) or NMR (red) from the alpha cell stocks after treatment with camptothecin for 2 hours in media with 2% DMSO. A clear increase in resistance to camptothecin was seen with an LD50 in NMR at 30.93µM (+/- 5.3µM) and in mice at 5.24µM (+/- 0.03µM). Error bars indicate +/- one standard error of the mean between each cell line (3 cell lines per species, each cell line value is the average of two independent experiments which each consist of four individual counts). Star (*) indicates significance at the p<0.05 level between the percentage of cells alive in mouse and NMR cell cultures by Mann Whitney U test. The total number of cells under control conditions for mice was 350,356 and NMRs was 32,498. The total number of cells counted in control conditions was greater than or equal to 300 cells. In the treated samples this was greater than or equal to 150 cells.

To assess the variability between alpha cell lines treated with camptothecin within each species an ANOVA was performed. There was no statistical difference observed between mouse or NMR cell lines treated with camptothecin (mouse: $F(2, 18)=0.595$, $p=0.562$, NMR: $F(2, 18)= 0.023$, $p=0.977$) (Figure 3.7).

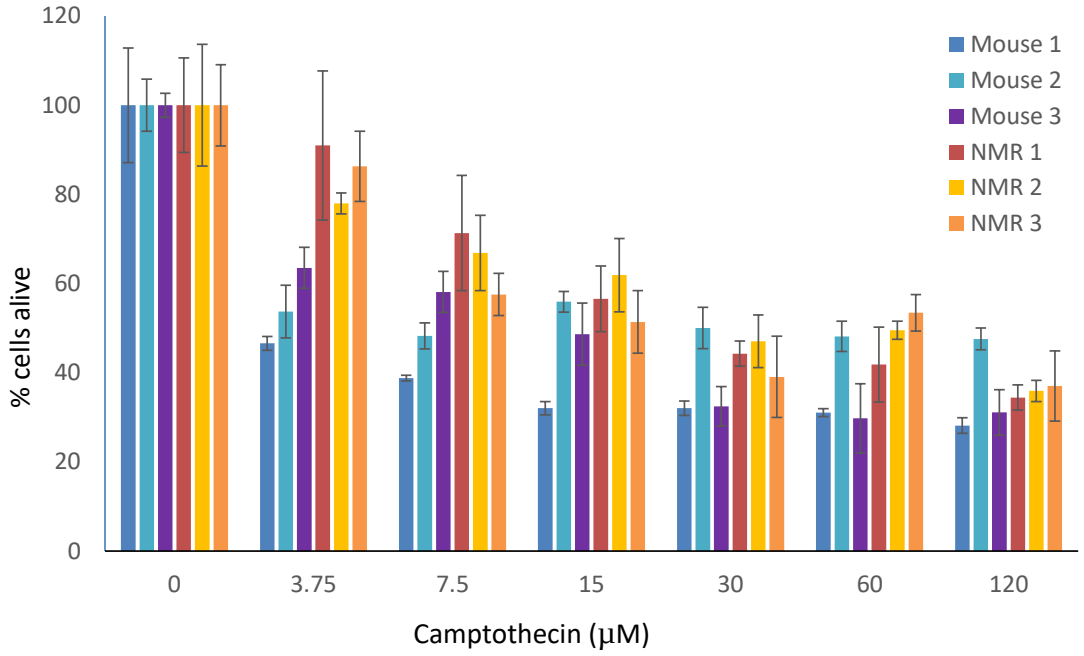

Figure 3.7 *Percentage survival of primary skin fibroblasts in each of the primary skin fibroblast cell lines from 3 mice and NMRs that form the alpha cell stocks after treatment with camptothecin for 2 hours in media with 2% DMSO. Error bars equal ± one standard error of the mean between two independent experiments which each consist of four individual counts. The total number of cells under control conditions for mice was 350,356 and NMRs was 32,498. The total number of cells under control conditions for each cell line was as follows mouse 1 – 140,250, mouse 2 – 101,306, mouse 3 – 108,800, NMR 1 – 4,083, NMR 2 – 23,527 and NMR 3 4,888. Each cell line was analysed twice. The total number of cells counted in control conditions was greater than or equal to 100 cells. In the treated samples this was greater than or equal to 50 cells.*

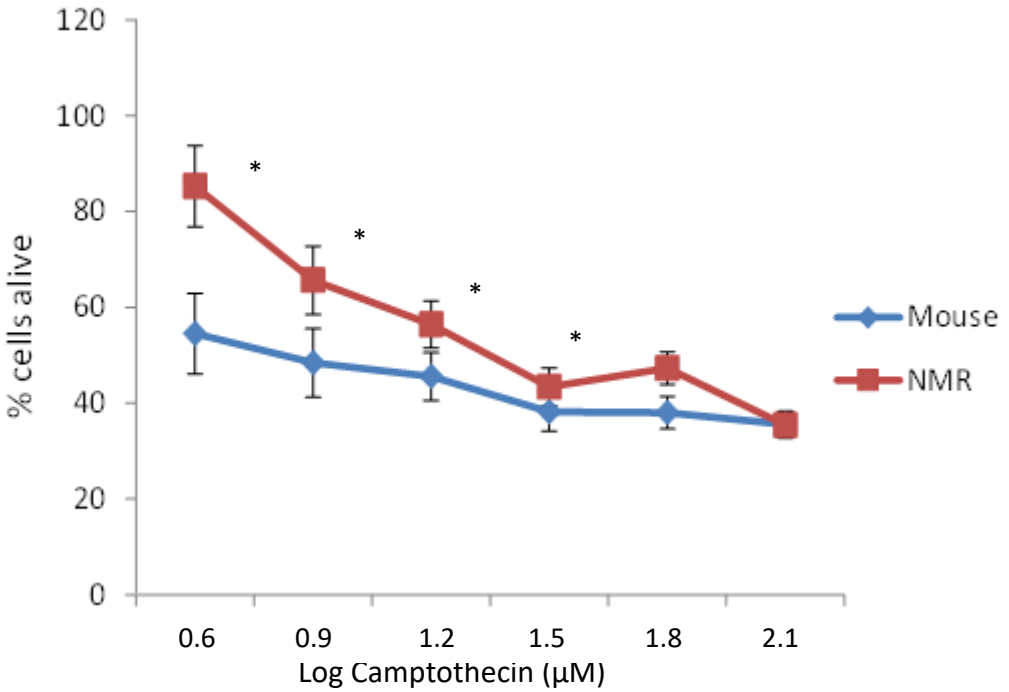

Figure 3.8. Percentage survival of primary skin fibroblasts from either mice (blue) or NMR (red) from the alpha cell stocks after treatment with camptothecin for 2 hours in media with 2% DMSO. A clear increase in resistance to camptothecin is seen with an LD50 in NMR at 30.93µM (+/- 5.3µM) and in mice at 5.24µM (+/- 0.03µM). Error bars equal ± one standard error of the mean between each cell line (3 cell lines per species, each cell line value is the average of two independent experiments which each consist of four individual counts). Star (*) indicates significance at the p<0.05 level between the percentage of cells alive in mouse and NMR cell cultures by Mann Whitney U test. The total number of cells under control conditions for mice was 350,356 and NMRs was 32,498. The total number of cells counted in control conditions was greater than or equal to 300 cells. In the treated samples this was greater than or equal to 150 cells.

When this analysis was repeated on the beta primary cell cultures, the difference between NMR and mouse resistance was less pronounced. In chromium treatment, there were no individual doses that are significantly different though 40µM shows near significance ($t(4)=-2.73$, $p=0.052$) between NMR (68%) and mouse (52%) (Figure 3.9). The average LD50 was calculated as 48.4µM (±1.2) for mouse cells and 92.2µM (±18.1) and was significantly different ($U_4=0$, $p=0.05$). These values are much higher than were found in the alpha primary cell cultures which may be due to variation between the cells or variations in the equipment used to weigh the compounds out. There was ~2 fold greater LD50 in NMR than mice; this is lower than the 4 fold seen previously.

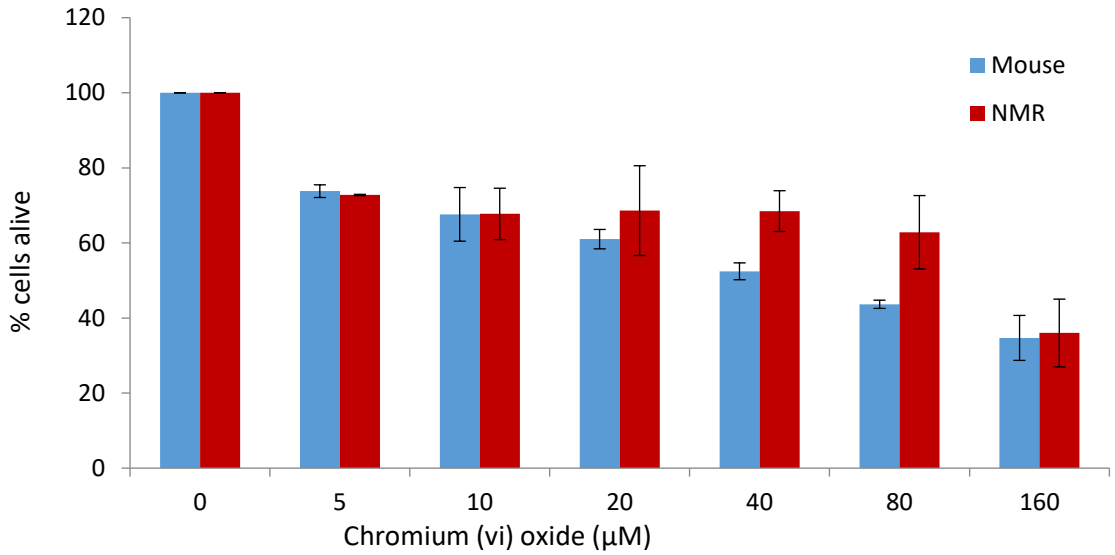

Figure 3.9. Percentage survival of primary skin fibroblasts from either mice (blue) or NMR (red) from the beta cell stocks after treatment with chromium (vi) oxide for 2 hours in media with 2% DMSO. Error bars equal ± one standard error of the mean between each cell line (3 cell lines per species, each cell line value is the average of two independent experiments which each consist of four individual counts). The total number of cells under control conditions for mice was 24,695 and NMRs was 2,469. The total number of cells counted in control conditions was greater than or equal to 300 cells. In the treated samples this was greater than or equal to 150 cells.

To assess the variability between beta cell lines treated with chromium (vi) oxide within each species an ANOVA was performed. There was no statistical difference observed between mouse or NMR cell lines treated with chromium (vi) oxide (mouse: $F(2, 18)= 0.096$, $p=0.909$, NMR: $F(2, 18)= 0.24$, $p=0.789$) (Figure 3.10).

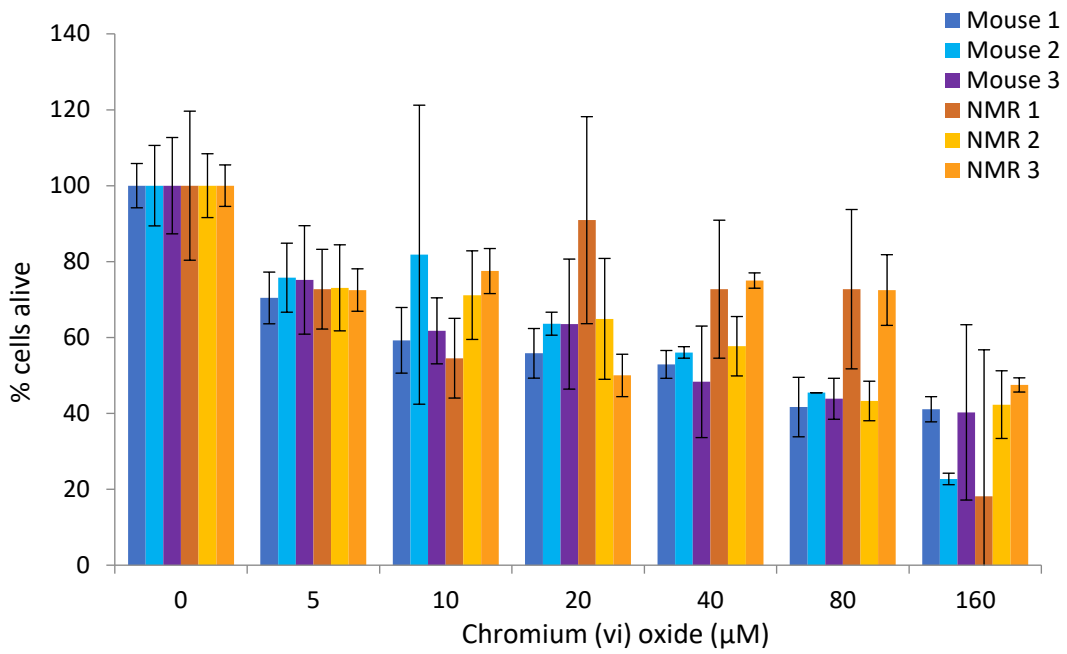

Figure 3.10 Percentage survival of primary skin fibroblasts in each of the primary skin fibroblast cell lines from 3 mice and NMRs that form the beta cell stocks after treatment with chromium (vi) oxide for 2 hours in media with 2% DMSO. Error bars equal ± one standard error of the mean between two independent experiments which each consist of four individual counts. The total number of cells under control conditions for each cell line was as follows mouse 1 – 12,130, mouse 2 –5,667, mouse 3 – 6,898, NMR 1 –678, NMR 2 –9,630 and NMR 3 – 5,741. Each cell line was analysed twice. The total number of cells counted in control conditions was greater than or equal to 100 cells. In the treated samples this was greater than or equal to 50 cells.

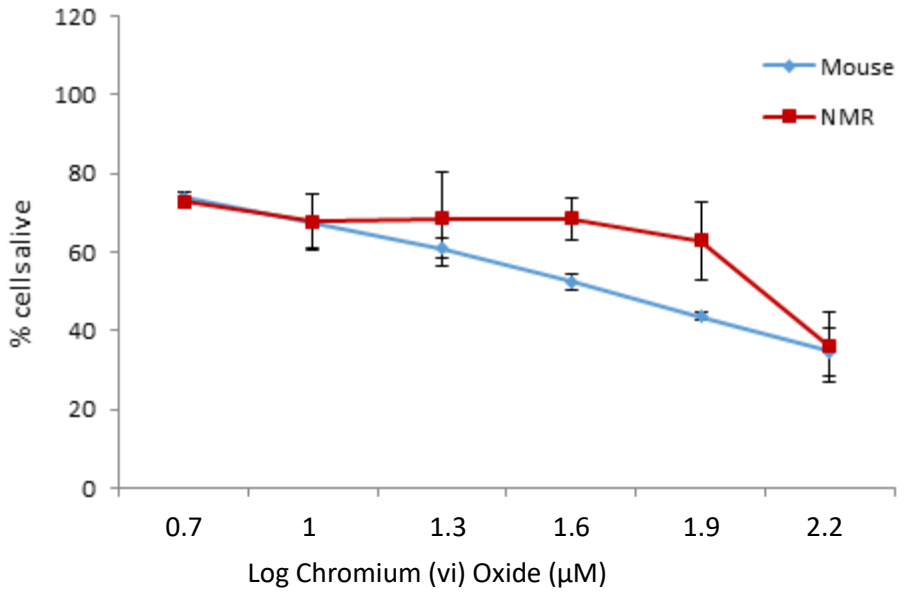

Figure 3.11 Percentage survival of primary skin fibroblasts from either mice (blue) or NMR (red) from the beta cell stocks after treatment with camptothecin for 2 hours in media with 2% DMSO. Error bars equal ± one standard error of the mean between each cell line (3 cell lines per species, each cell line value is the average of two independent experiments which each consist of four individual counts). The total number of cells under control conditions for mice was 24,695 and NMRs was 15,648. The total number of cells counted in control conditions was greater than or equal to 300 cells. In the treated samples this was greater than or equal to 150 cells.

As seen in the alpha primary cell culture, camptothecin treatment showed a greater difference between species in terms of survival. However only one dose (30µM) was significantly different between mouse (53%) and NMR (73%) ($t(4)= -10.7$, $p=0.00$). The average LD50 was calculated as 44.4µM (5.9±) for mouse and 128.1µM (21.0±) for NMR which was significantly different ($U_4=0$, $p=0.05$). Again, these values are greater than those seen in the alpha primary cell cultures. This was a ~3 fold increase in NMR relative to mouse cells, which is half of what was seen in the alpha primary cell cultures.

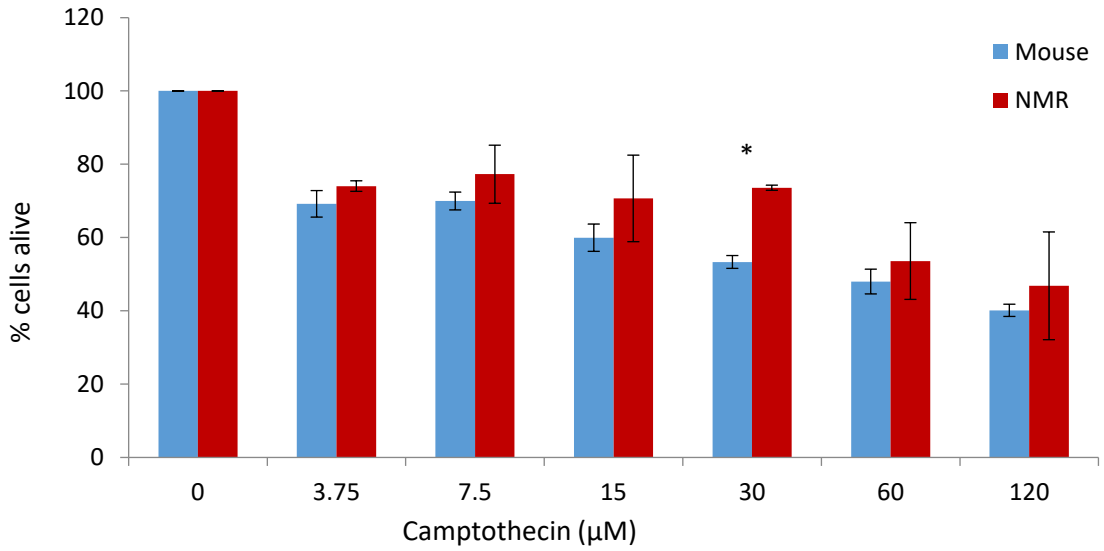

Figure 3.12. Percentage survival of primary skin fibroblasts from either mice (blue) or NMR (red) from the beta cell stocks after treatment with camptothecin for 2 hours in media with 2% DMSO. Star (*) indicates significance at the p<0.05 level between the percentage of cells alive in mouse and NMR cell cultures by student T test. Error bars equal ± one standard error of the mean between each cell line (3 cell lines per species, each cell line value is the average of two independent experiments which each consist of four individual counts). The total number of cells under control conditions for mice was 39,353 and NMRs was 15,648. The total number of cells counted in control conditions was greater than or equal to 300 cells. In the treated samples this was greater than or equal to 150 cells.

To assess the variability between beta cell lines treated with camptothecin within each species an ANOVA was performed. There was no statistical difference observed between mouse or NMR cell lines treated with camptothecin (mouse: $F(2, 18)= 0.192$, $p=0.827$, NMR: $F(2, 18)= 0.942$, $p=0.412$) (Figure 3.13).

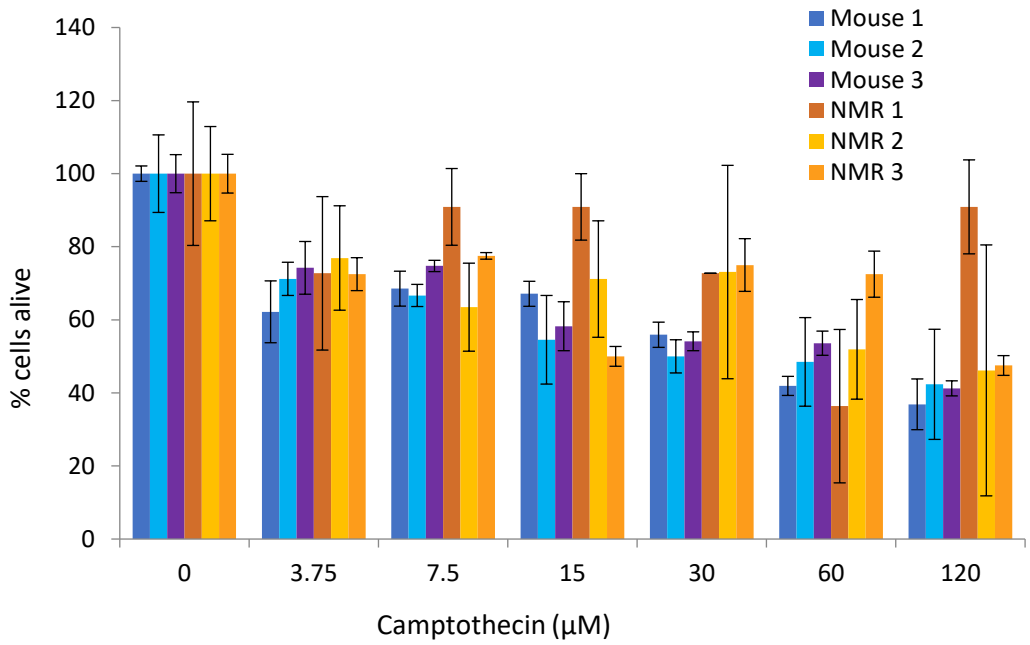

Figure 3.13. Percentage survival of primary skin fibroblasts in each of the primary skin fibroblast cell lines from 3 mice and NMRs that form the beta cell stocks after treatment with camptothecin for 2 hours in media with 2% DMSO. Error bars equal ± one standard error of the mean between two independent experiments which each consist of four individual counts. The total number of cells under control conditions for each cell line was as follows mouse 1 – 12,130, mouse 2 – 5,667, mouse 3 – 21,556, NMR 1 – 678, NMR 2 – 9,630 and NMR 3 – 5,741. Each cell line was analysed twice. The total number of cells counted in control conditions was greater than or equal to 100 cells. In the treated samples this was greater than or equal to 50 cells.

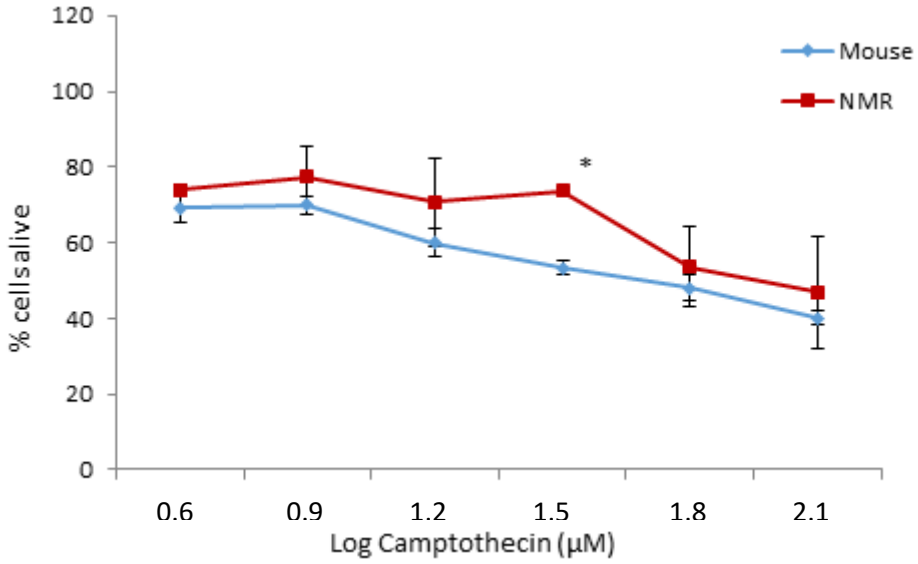

Figure 3.14. Percentage survival of primary skin fibroblasts from either mice (blue) or NMR (red) from the beta cell stocks after treatment with camptothecin for 2 hours in media with 2% DMSO. Star (*) indicates significance at the p<0.05 level between the percentage of cells alive in mouse and NMR cell cultures by student T test. Error bars equal ± one standard error of the mean between each cell line (3 cell lines per species, each cell line value is the average of two independent experiments which each consist of four individual counts). The total number of cells under control conditions for mice was 39,353 and NMRs was 15,648. The total number of cells counted in control conditions was greater than or equal to 300 cells. In the treated samples this was greater than or equal to 150 cells.

To assess the effect of DMSO on cell mortality, cell counts from an assay looking at how DMSO affects senescence was analysed. This count data is less accurate than the above analyses as the cells were counted while still attached to the plate, and cell densities vary across the plate. No significant difference was observed between the DMSO treated and untreated samples. There was found to be no significant difference between the number of cells in counts from samples treated (mouse: 67 SD: 57, NMR: 71 SD: 50) or untreated (mouse: 80 SD: 66, NMR: 69.3 SD: 66) with DMSO (mouse: t(22):0.50, p=0.623, NMR: t(14): -0.07, p=0.943) (Figure 3.16).

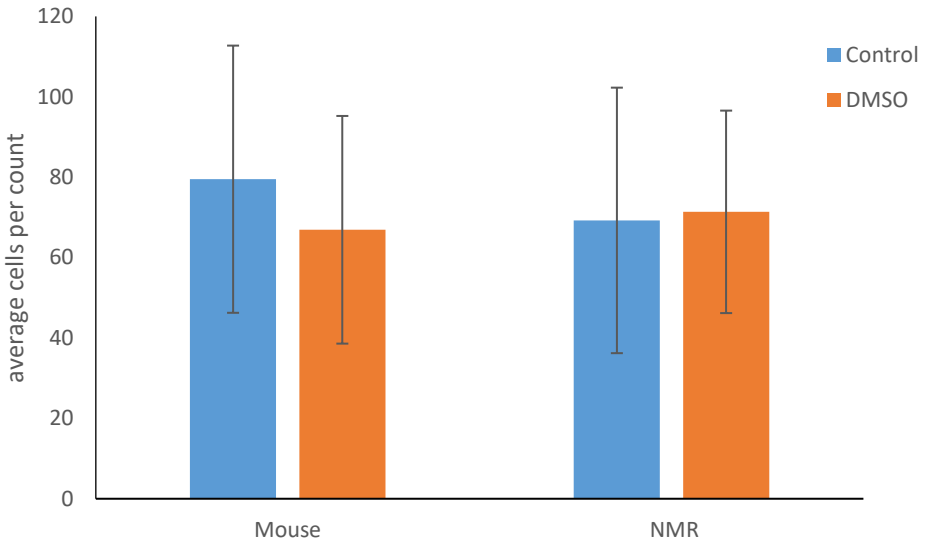

Figure 3.15. Cell counts of samples treated or untreated with 2% DMSO for 2 hours. There was found to be no significant difference between the number of cells in counts from samples treated (mouse: 67 SD: 57, NMR: 71 SD: 50) or untreated (mouse: 80 SD: 66, NMR: 69.3 SD: 66) with DMSO (mouse: t(22): 0.50, p=0.623, NMR: t(14): -0.07, p=0.943). Error bars indicate +/- one standard error of the mean between three cell lines in mouse and two cell lines in NMR (cell line 1 was not included) each cell line value is the average of two replicates performed as part of one experiment.

3.4.2 Naked mole rat cells are less prone to enter senescence in response to genotoxic stressors than mouse cells

To better characterise the cellular response to genotoxic stimuli in mouse and NMR a preliminary beta galactosidase staining assay was performed on the alpha stocks to visualise the levels of senescence in these cells after treatment with the DNA damaging agents; camptothecin and chromium (vi) oxide (Figure 3.16-3.17). The proportion of senescent cells in the NMR cell cultures did not significantly increase between control treated or DNA damaging agent treated samples after 8 hours or 48 hours. However, mouse cells showed a significantly higher level of senescence both in response to the DNA damage stimuli at both 8 and 48-hour time points compared to controls, and also showed increased senescence over time with all treatments showing greater levels of senescence at 48 hours compared to 8-hour time points. The increase in senescence was greatest in the DNA damaged samples indicating that this increase was in part in response to the received DNA damage. After 48 hours mouse cells showed significantly more senescence in all treatments than the NMR cells. At 8 hours control treated NMR cells showed greater senescence then control treated mouse cells.

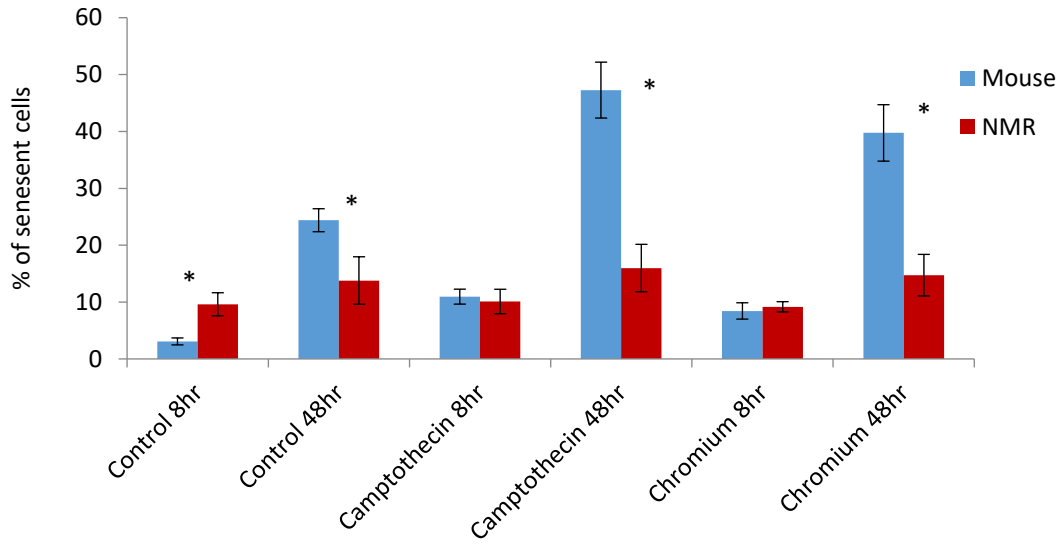

Figure 3.16. Beta Galactosidase assay of mouse and NMR cells treated with chromium (vi) oxide (green), camptothecin (red) or control media (blue) with 2% DMSO at LD50 for each species. Star (*) indicates a significance between NMR and mouse at the p<0.05 level between the percentage of senescent cells in mouse and NMR cell cultures by one way ANOVA. Treated mouse cells upon either 8 or 48 hours had significantly greater senescence than comparative controls. At 48hours mouse cells showed significantly more senescence than NMR cells and this difference was greatest in the treated cells. Error bars indicate +/- one standard error of the mean between the three cell lines within each species; each cell line value is the average of two replicates performed as part of one experiment. The number of cells counted for each sample were >600 cells per sample.

To assess the variability between alpha cell lines treated with camptothecin or chromium within each species an ANOVA was performed. There was no statistical difference observed between mouse cell lines on control, camptothecin or chromium (vi) oxide treatment after 8 or 48-hour treatment ($F(2, 9)<1.5$, $p>0.05$). All NMR samples showed a significant difference ($F(2,9)>8$, $p<0.05$). Post hoc turkey analysis of 48-hour samples showed this is due to NMR cell line 2 being significantly higher than both other samples. Post hoc turkey analysis of 8-hour samples indicated that each of the cell lines showed significantly different levels of senescence in control samples, NMR cell line 2 was significantly greater than cell line 3 in camptothecin-treated samples and NMR cell line 2 is significantly greater than the other cell lines in chromium treatment (Figure 3.17).

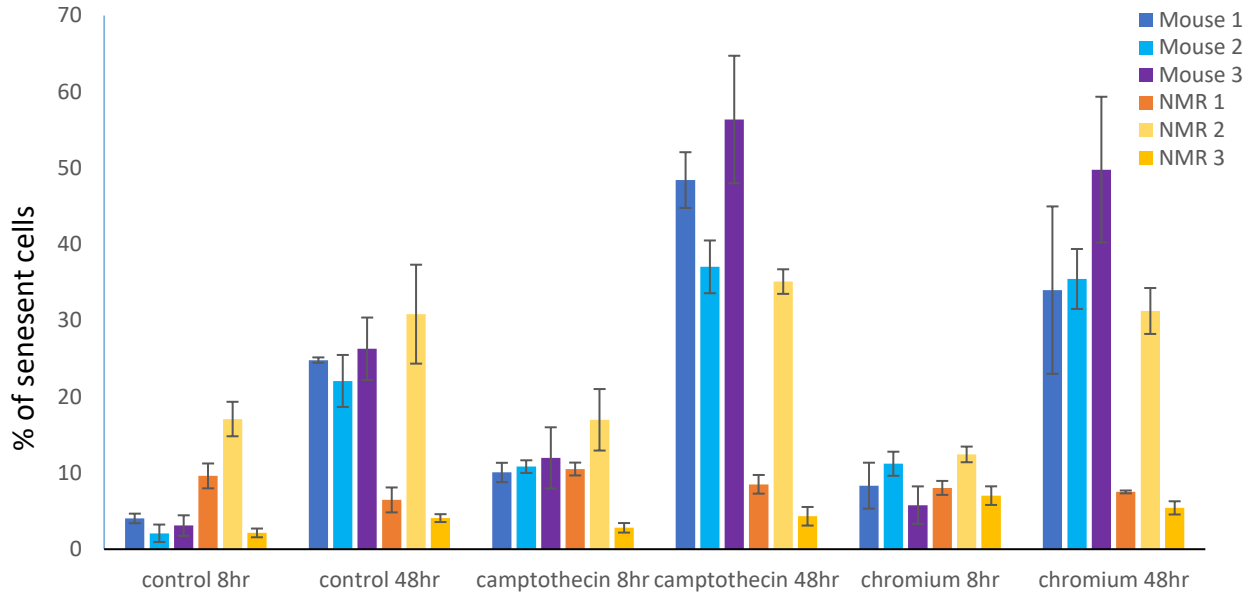

Figure 3.17. Percentage senescent cells in each of the primary skin fibroblast cell lines from 3 mice and NMRs that form the alpha cell stocks after treatment with camptothecin, chromium, or control conditions for 2 hours in media with 2% DMSO. Error bars equal ± one standard error of the mean between two replicates performed as part of one experiment. The number of cells counted for each sample were >200 cells per sample.

This analysis was repeated in the beta stocks (Appendix Figure 3). Due to limited time only one time point was studied, 24 hours post stimuli as a compromise between 8 and 48 hours. Additionally, instead of looking at LD50 which is limiting, a logarithmic range of doses for both compounds was analysed (Figure 3.18-3.20). Control treated NMR cells showed significantly more senescent cells (46%) than mouse cells (17%) under the same treatment ($t(4)=-12.2$, $p<0.01$). However, as the dose of either compound was increased the percentage of senescent cells increased in mouse cells, but only increased in the highest doses in NMR (Figure 3.7-3.8). This can be seen clearly from the maximum increase in senescence observed; only a total increase of 7% in NMR cells after either treatment, however camptothecin and chromium treatment resulted in a maximum increase of 44% and 46%, respectively in mouse cells. For camptothecin treatment the only doses that differed significantly were 60µM (NMR: 42%, Mouse: 54%) and 120µM (NMR: 53%, Mouse: 61%) with mice showing significantly more senescence (60µM: $t(4)= 2.9$, $p=0.043$, 120µM: $t(4)= 3.3$, $p=0.029$) (Figure 3.7). For chromium treatment, the only significantly different dose was 10µM (NMR: 44%±11, Mouse: 34%±3) with mouse showing significantly less senescence ($t(4)=-4.7$, $p=0.01$). Two-way ANOVAs of the data set and the data set minus control data showed a statistically significant interaction between

dose and species indicating the two species were responding differently to the stimuli (camptothecin: $F(5,24)= 2.9$, $p=0.035$, chromium: $F(5,24)= 4.7$, $p<0.01$).

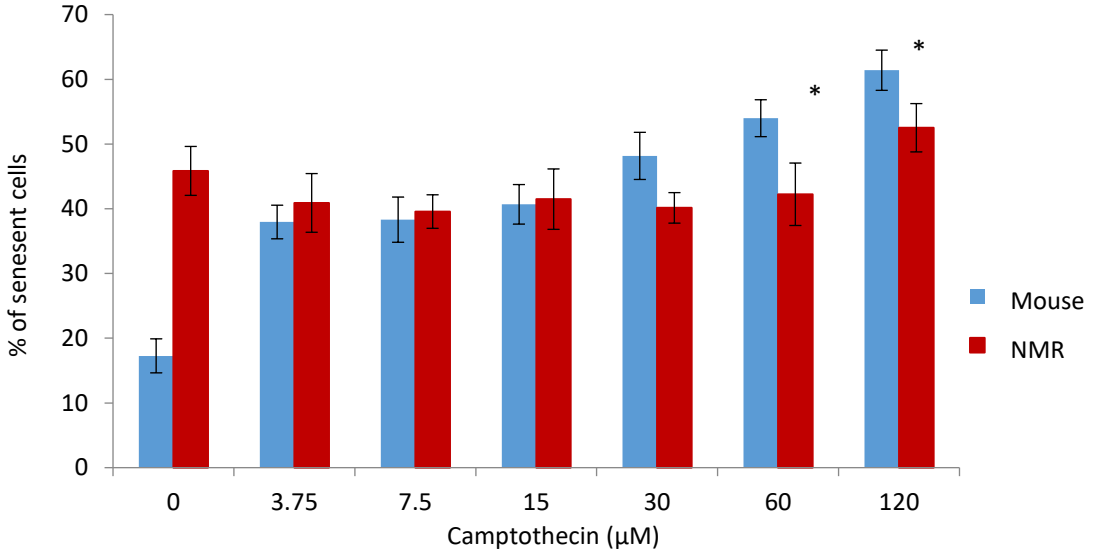

Figure 3.18. The percentage of senescent cells 24 hours after treatment with camptothecin at various doses. NMR cells show higher senescence in control samples than mice however there is very little increase in senescence at higher doses in NMR. Mouse cells show a large increase in senescence with increased dose. Large doses (30-120µM) show more senescence in mice than in NMR cells. Error bars represent +/- one standard error of the mean between 3 cell lines each cell line value was the average of two replicates performed as part of one experiment. Star (*) indicates significance at the 0.05 level between the percentage of senescent cells in mouse and NMR cell cultures by student T test. Each count consists of over 300 cells per point.

To assess the variability between beta cell lines treated with camptothecin within each species an ANOVA was performed. There was no statistical difference observed between mouse or NMR cells treated with camptothecin (mouse: $F(2, 18)= 0.27$, $p=0.766$, NMR: $F(2, 18)= 1.137$, $p=0.343$) (Figure 3.19).

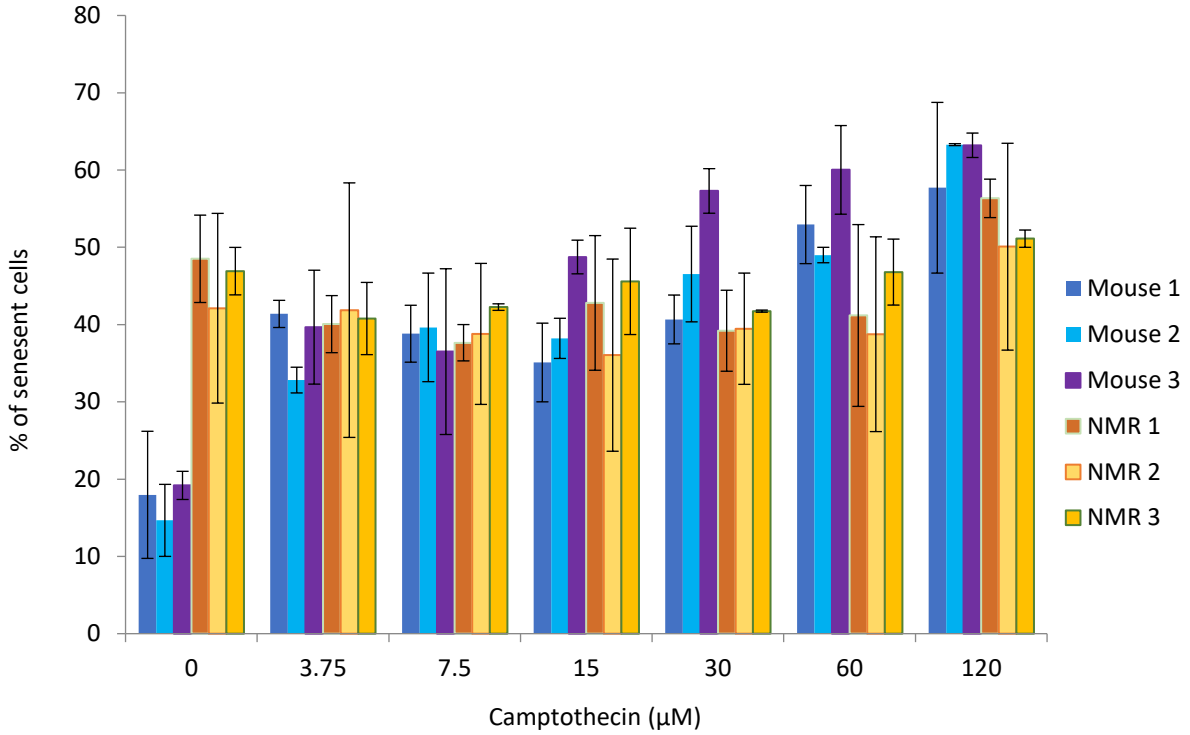

Figure 3.19. Percentage senescent cells in each of the primary skin fibroblast cell lines from 3 mice and NMRs that form the alpha cell stocks after treatment with camptothecin, or control conditions for 2 hours in media with 2% DMSO. Each data point is the mean between 3 cell lines each cell line value was the average of two replicates performed as part of one experiment. Each count consists of over 100 cells per point. Error bars represent +/- one standard error of the mean between two replicates performed as part of one experiment.

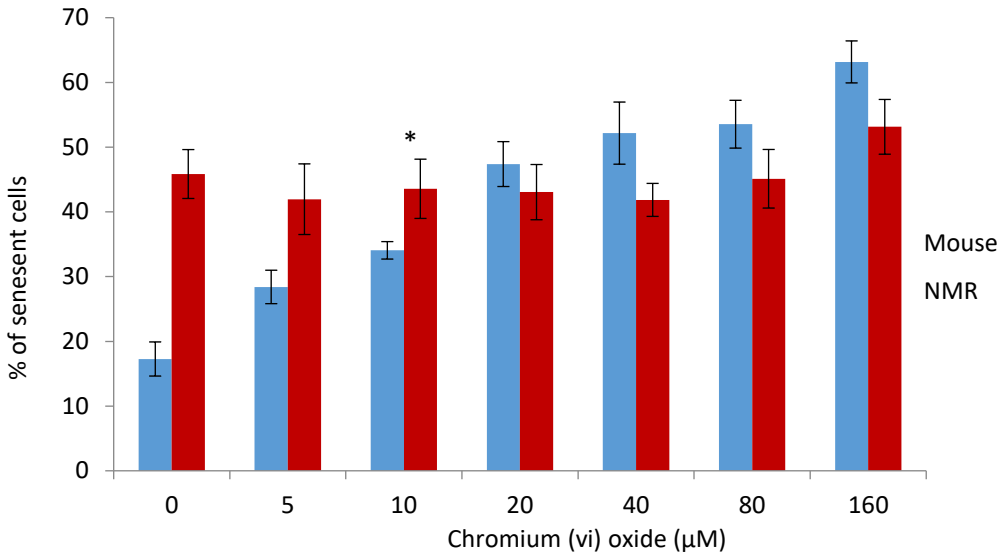

Figure 3.20. The percentage of senescent cells 24 hours after treatment with chromium (vi) oxide at various doses. NMR cells show higher senescence in control and low dose samples than mice, however, there is very little increase in senescence at higher doses in NMR. Mouse cells show a large increase in senescence with increased dose. Large doses (40-160µM) show more senescence mice in than NMR cells. Error bars represent +/- one standard error of the mean between 3 cell lines each cell line value was the average of two replicates performed as part of one experiment. Star (*) indicates significance at the 0.05 level between the percentage of senescent cells in mouse and NMR cell cultures by student T test. Each count consists of over 300 cells per point.

To assess the variability between beta cell lines treated with chromium (vi) oxide within each species an ANOVA was performed. There was no statistical difference observed between mouse or NMR cell lines treated with chromium (vi) oxide (mouse: $F(2, 18)= 0.075$, $p=0.928$, NMR: $F(2, 18)= 1.422$, $p=0.267$) (Figure 3.21).

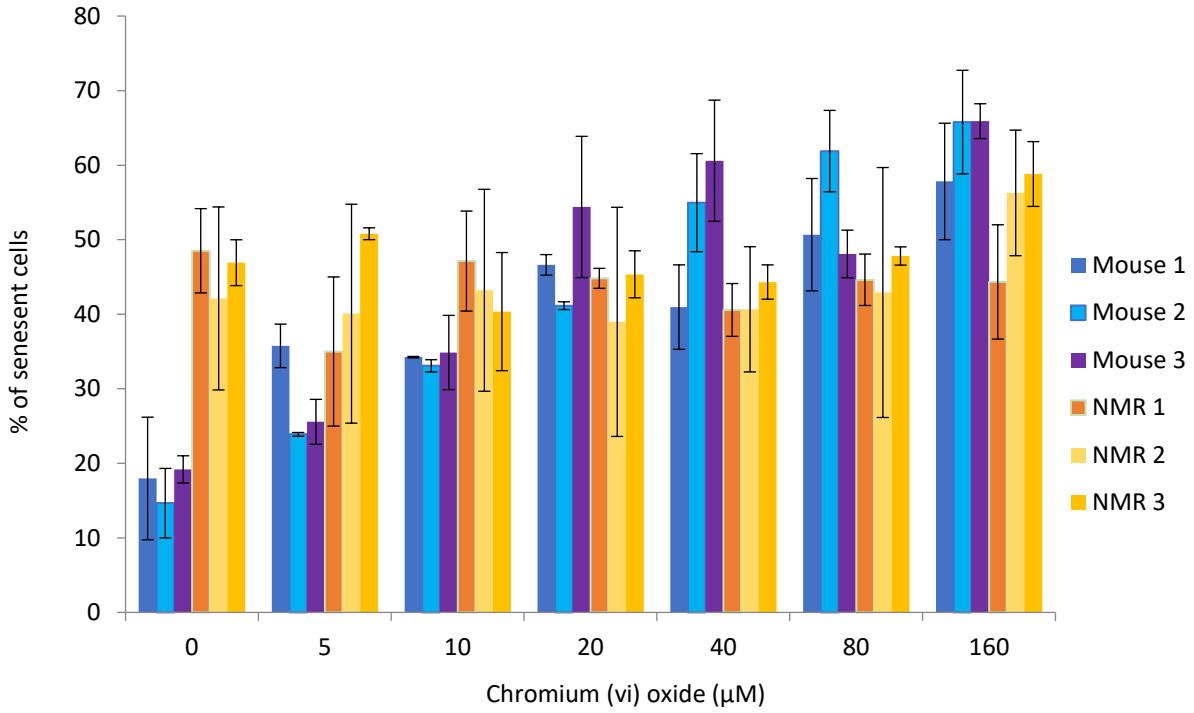

Figure 3.21. Percentage senescent cells in each of the primary skin fibroblast cell lines from 3 mice and NMRs that form the alpha cell stocks after treatment with chromium (vi) oxide, or control conditions for 2 hours in media with 2% DMSO. Error bars have not been included due to large overlap. Each data point is the mean between 3 cell lines each cell line value was the average of two replicates performed as part of one experiment. Each count consists of over 100 cells per point. Error bars represent +/- one standard error of the mean between two replicates performed as part of one experiment.

In order to conduct accurate comparisons between control and treated cells, the control samples were treated with 2% DMSO for 2 hours, removing this as a source of variation between the treatments. However, this exposure to DMSO was suspected of being the cause of the high level of senescence seen in control cells. Hence this analysis was repeated for control conditions with and without DMSO. There was found to be no significant difference between the number of senescent cells in samples treated (mouse: 1.9% SD: 0.02, NMR: 2.8% SD: 0.03) or untreated (mouse: 2.5% SD: 0.02, NMR: 2.9% SD: 0.05) with DMSO (mouse: $t(22)$: 0.644, $p=0.526$, NMR: $t(14)$: 0.003, $p=0.998$) (Figure 3.22).

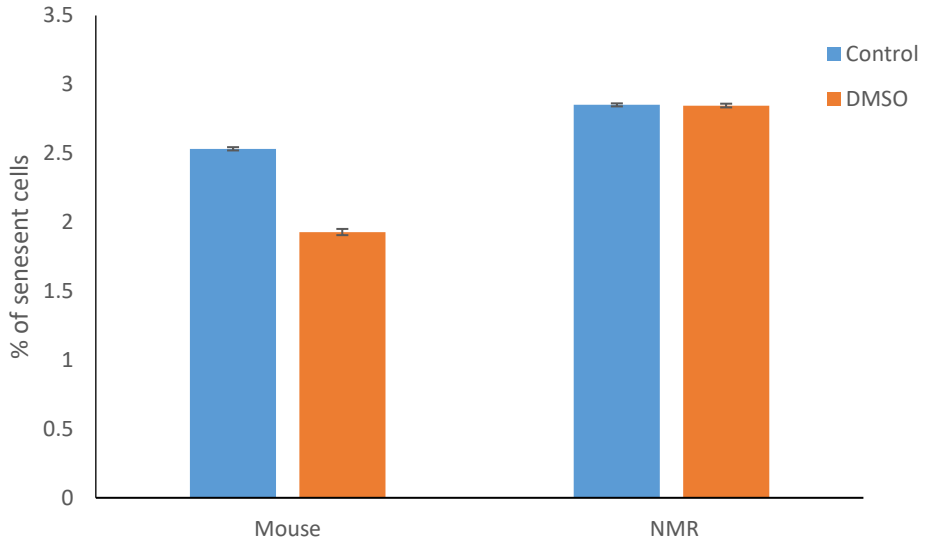

Figure 3.22. The percentage of senescent skin fibroblasts from mouse and NMR that were either untreated or treated with 2% DMSO for 2 hours. There was found to be no significant difference between the number of senescent cells in samples treated after 24 hours (mouse: 1.9% SD: 0.02, NMR: 2.8% SD: 0.03) or untreated (mouse: 2.5% SD: 0.02, NMR: 2.9% SD: 0.05) with DMSO (mouse: t(22): 0.644, p=0.526, NMR: t(14): 0.003, p=0.998). Error bars indicate +/- one standard error of the mean between the 3 mouse cell lines and NMR cell line 2 and 3. Each cell line value was the average of two replicates performed as part of one experiment. Total number of cells counted are as follows: mouse control – 975 cells, mouse DMSO treated – 791 cells, NMR control – 480 cells and NMR DMSO treated – 594 cells.

3.5 Discussion

The NMR has a lower resting body temperature (~32°C) than mice (37°C) (170). NMR cells grow poorly at 37°C (175, 371) and hence a lower temperature than standard is required. NMR cells have been successfully grown at 33°C (175), but this is several degrees lower than the optimal mouse growing conditions. As only one incubator is available and consistency between primary cell cultures is essential for reliable and comparable results a compromise of 35°C was selected. Both primary cell cultures appear to grow under these conditions. As has been discussed previously, low oxygen (3%) was used in this study to represent the native environment of a cell. Conditions for cell culture were optimised by Vera Gorbunova's lab at 3% oxygen (176).

3.5.1 Resistance of NMR to DNA damage stimuli

NMR skin fibroblasts show greater resistance to DNA damaging stimuli than those derived from mice. This is seen in the approximately 3-6 fold and 2-4 fold increases in LD50 of the cells for camptothecin and chromium (vi) oxide, respectively. This is a small difference in resistance and less than the previously reported 15 and 5 fold resistances (175) and is likely due to the difference in growth conditions and variation between cells. When looking at each dose in the survival assay, we see more doses of camptothecin that result in a significant difference between the mouse and NMR survival than with chromium (vi) oxide. These differences are relatively small. Still, this indicates that the sensitivity of these primary cell cultures to chromium is more similar than with camptothecin. These compounds cause different kinds of DNA damage with chromium inducing a broad array of damage types and camptothecin specifically inducing single and double-strand breaks. This suggests NMR cells may have mechanisms to enhance their ability to prevent and repair DNA strand breaks specifically. The increased resistance to camptothecin observed in this assay may be down to camptothecin's mode of action. Camptothecin acts by binding topoisomerase 1 and preventing the religation of DNA after topoisomerase 1 induced single-strand cleavage. However, if the level of topoisomerase was lower in the NMR, then less single-strand breaks would occur as a result of camptothecin treatment. Additionally, single-strand breaks become more hazardous double-strand breaks if unrepaired before DNA replication. As NMR cells divide more slowly than mouse cells (175, 187, 188) they may be less likely to have unrepaired single-strand breaks during DNA replication. Were more time available we would assess if this is the case by analysing a compound that induces single-strand breaks independently of topoisomerases such as bleomycin in place of camptothecin.

There was a large amount of variation in the NMR alpha cell line between NMR cell line 1 and the others. Cell line 1 was significantly lower and if considered an outlier would not affect our conclusion, however, if this cell line was representative, then we would have to conclude that there was little difference between NMR and mouse cells in terms of survival. It is not clear why such variation is observed. This could be due to intrinsic variations within the cell or variations in the environment that the cells were maintained.

An unknown factor in this experiment is the effect of DMSO on the cells as this was never tested directly in our lab. The preliminary data utilised from the senescence assay indicates no difference in cell mortality between cells treated or untreated with 2% DMSO for 2 hours. This data shows a large amount of variability likely due to variability in cell density on the culture plate surface in the area of the count. Studies using transformed mouse cells have indicated that treatment with

2% DMSO can result in ~50-70% cell viability (404, 405). However, both analyses use a 24-hour treatment which will likely have a much more amplified effect than the 2 hours used in this study. As both control and treatments contain DMSO, the effects seen in this study will be down to the compounds under study. However, it is possible that DMSO may act synergistically or antagonistically with these compounds enhancing the damaging effects or protecting against it which would impair our ability to assess the compounds of study. This would not affect our analysis of the species of study unless one organism reacted differently to DMSO treatment than the other which our preliminary data indicates is not the case.

3.5.2 Reduced senescence in response to DNA damage in the NMR

When treated with the LD50 of either compound under study NMR skin fibroblasts showed lower beta galactosidase staining in response to DNA damage than cells derived from mice. At 8 hours post initial DNA damage stimuli, there is a significantly greater level of senescent mouse cells in the treated condition than the untreated control. This increase is not seen between NMR treatments indicating that these cells do not enter senescence in response to this DNA damage. However, NMR cells under control conditions have a significantly higher proportion of senescent cells than control mouse cells. This may be a caveat of NMR cells' slower growth rate as the less frequent passaging would allow the accumulation of such cells that would otherwise be diluted out of the population in faster-growing cell lines. Alternatively, this could indicate suboptimal growth conditions for the NMR cells. Were this project to continue, these growth conditions would be optimised for these cells. This could easily be done by taking a design of experiments (DoE) approach that uses statistical modelling to predict responses under study from fewer experiments (discussed in more detail in Chapter 6). A design could be implemented varying the oxygen content, temperature and FBS media content. The level of senescence and growth rates would be used to assess how well the cells grow. After 48 hours the level of senescence-associated staining increased in mouse cells under all treatments. The increase was larger for the cells treated with the DNA damaging agent, and these cells showed significantly more staining than the 48-hour mouse control cells. This increase over time for treated cells could mean that these cells take longer than 8 hours to undergo senescence or that the increased level of senescent cells is having a negative effect and creating unfavourable conditions that further promote senescence in these cells that only appear senescent at the later time point (as discussed in Section 5.1.2). For untreated cells, this increase could again be caused by senescent cells already present in the sample or could indicate an effect of the DMSO in the control treatment, however as discussed below this is unlikely as DMSO treatment did not increase levels of senescence relative to untreated cells. NMR cells did not increase in levels of senescence from 8 to 48 hours. When treated with a logarithmic range of doses, the same trend is observed. NMR cells have a higher starting senescence

level which only increases a little at high doses of the compounds and mouse cells have very little starting senescence that dramatically increases as the dose increases. Camptothecin-treated mouse cells showed similar or significantly more senescence than NMR cells, however, statistically, the opposite was true for chromium treatment. This may be because the difference in perceived resistance to chromium is smaller between these two species. The alpha and beta cell lines responded similarly with NMR having large levels of starting senescence that did not increase with treatment and mice having a lower starting level of senescence that increased with increased treatment. The beta cell stocks showed consistently higher levels of senescence than the alpha cell stock. This was much greater in NMR (40-50% vs. 10-20%) than in mice (20-60% vs. 20-50%). This could in part be explained by the fact the beta cell line experiments were carried out at 24 hours post stimuli as opposed to 8 and 48 hours. Differences in the cells themselves may explain this difference as well with the alpha cell line simply being more resistant to senescence induction than the beta cell lines.

Interestingly the levels of senescence in NMR cells vary dramatically between the two experiments. This will likely be in part due to differences between primary cell cultures, but may also be due to experimental variation or variation in the assay kit as a new kit was used for the later assay.

It was found that exposure to DMSO has no significant effect on levels of senescence. Hence this data indicates that DMSO has no effect on the incidence of senescence in these cell lines; however, it is possible that DMSO can act synergistically and or antagonistically to alter the levels of senescence induced by the compounds of study. In this experiment similar levels of senescence between mice and NMR cells was observed with only a ~1% difference between the samples, which is in contrast to previous results; additionally, lower levels were observed in this experiment (~2.5% vs. 10% in NMR). Again, this could be due to variation in the assay kit used or because this experiment was carried out after 24 hours as opposed to 8 and 48 hours.

The alpha cell line showed a large level of variation between the cell lines for NMR cells, particularly NMR cell line 2 which frequently had more senescent cells than the other cell lines. If this cell line was taken as an outlier, it would not affect our present conclusion that NMR cells show lower incidence of senescence in response to the toxic stimuli studied. However, it could be that this cell line is representative of NMR skin fibroblasts and the other cell lines are unusual in which case we would conclude that there is no difference between mouse and NMR cells. It is not clear why such variation is present but may indicate some intrinsic difference in these cells, such as a genetic variation, or differences in the treatment such as variation in temperature or culture media.

Taken together these results show that in response to DNA damaging agents the NMR cells are less prone to enter senescence than those from mice which show an immediate increase in

senescence which increases over time. The reduced tendency to enter senescence in response to genotoxic insults in the NMR would result in such exposed tissues being healthier as senescent cells have been associated with accelerated ageing and age-related pathologies (406). As such the NMR's tendency to avoid induced senescence may contribute to its long-lived status but may also be a consequence of this status.

Chapter 4: RNAseq analysis of *H. glaber* and *M. musculus* skin fibroblasts

4.1 Introduction

In the previous chapter, it was shown that NMR skin fibroblasts appear more resistant than mouse cells to the DNA damaging agents, camptothecin and chromium (vi) oxide. This confirms what was previously shown in other studies (175). Additionally, we indicated that the NMR cells responded differently to these genotoxic compounds showing less induced senescence than mouse cells.

In this chapter, the ways by which these skin fibroblasts differ in their response to DNA damaging agents will be examined at the molecular level. How gene expression changes in response to treatment with DNA damaging compounds indicates how the cells deal with this genotoxic insult. By looking at how these responses differ between the NMR and mouse cells, genetic explanations for the variation in lifespan, cancer susceptibility and DNA damage resistance between these two species can be inferred.

To this end, an RNAseq experiment was run to identify the levels of gene expression in mouse and NMR cells responding to DNA damaging agents in the short term (8 hours after initial exposure) or long term (48 hours after initial exposure). A functional enrichment was performed on the data to identify if differentially expressed genes were enriched for particular pathways or processes. Genes involved in DNA damage repair and cellular adhesion were specifically studied to determine if these cancer-associated components vary between the two species.

4.1.1 RNAseq analysis

Cells respond to stimuli such as genotoxic insults through either changes in protein activity directly or changes in gene expression that ultimately affect protein activity. The purpose of RNAseq analysis is to detect these changes in gene expression at the mRNA level. The process (detailed in Chapter 1.4) essentially quantifies the amount of mRNA from each sample. The read count is the number of sequenced pieces of cDNA (derived from the sample mRNA) that correspond to a given gene. These read counts have been shown to be linearly related to the amount of the target transcript (298). However, these counts need to be normalised to remove technical bias between samples. A number of methods can be employed to normalise RNAseq data, but for our analysis, we used the statistical program, DEseq's, inbuilt method (407). In short, the normalised value is calculated by dividing the read count of a given gene in a given sample by the geometric mean of these values across the samples (407). Whether a gene is significantly differentially expressed is determined by a test that is initially analogous to Fisher's exact test but is based on the assumption that the number of reads in a sample assigned to a given gene fits a modified negative binomial distribution as detailed in (407).

The final output of an RNAseq analysis is essentially a list of genes with expression values of each gene in the compared samples, the fold change between these values and a p-value. This p-value tells us the probability of these expression values being as they are by chance if the null hypothesis of equality between the expression values was correct. These lists of genes are often too large to yield useful information on their own and as such further analysis must be conducted. Typically, this is done by grouping genes by function by either selecting for certain types of gene and seeing if collectively these are more expressed in one sample.

Functional enrichment is a statistical method to identify types of genes (classified by GO (gene ontology) terms for example) that are over represented in a dataset. By looking at the total number of genes that fall into a particular group in the entire sample and comparing that to the number genes differentially expressed through a modified Fisher's exact test we can determine the probability of observing these values and hence whether a particular type of gene is significantly enriched in the sample (330). This analysis essentially takes a list of genes and outputs a list of enriched biological terms which is often easier to interpret.

4.1.2 Quantitative polymerase chain reaction

Polymerase chain reaction (PCR) is a commonly used technique for amplifying DNA. The reaction requires the following ingredients: the target DNA that the reaction is aiming to amplify, an abundant supply of nucleotides that the newly synthesised DNA will be made of, a DNA polymerase to synthesise the new DNA and a pair of primers specifically designed to match the target gene. These primers are short nucleotide sequences (~ 20 nucleotides long in this assay) that are complementary to the DNA that flanks the region of the target DNA to be amplified. The reaction is controlled by changes in temperature; hence a thermocycler that repeatedly induces the required temperatures is required. To begin the reaction, the solution of the above ingredients is heated to 95°C. This results in the double-strand DNA melting into single-strand DNA. Additionally, hot start polymerase (as used in this assay) are activated as the high temperature denatures the attached antibodies that otherwise block their activity. The mixture is then cooled to 60°C. At this temperature, the primers anneal to the target DNA sequence. The DNA polymerase binds to this primer and begins synthesising new DNA on the end of the primer using the target DNA as a template. This can happen at 60°C in a two-step process as used in this assay. Alternatively, a three-step process can be used in which the sample is heated to ~72°C to facilitate the synthesis of DNA. This synthesis continues until the DNA polymerase falls off the chain. The mixture is then heated to 95°C again to melt the newly formed double-stranded DNA. When the sample is cooled to 60°C, both the original sample DNA and the newly synthesised

DNA strands can be used as templates for synthesising new DNA. As such, the amount of the target DNA increases exponentially.

Quantitative PCR (qPCR) is a version of PCR that allows quantification of the DNA that is amplified. It works as described above except that the amount of DNA in the sample is recorded at each thermal cycle. This is done by the use of specialist fluorescent dyes such as SYBR Green that, when bound to double-stranded DNA has a >1,000 fold increase in fluorescence (408). The fluorescence emitted is measured, and hence the relative amount of DNA can be determined. To calculate the fold change of the target DNA between samples, the number of cycles required for the level of fluorescence in the sample to hit a pre-determined threshold, known as a cycle threshold (ct) value, must be obtained. The threshold used is largely arbitrary but must fall within the linear phase of the amplification plots to allow for accurate comparison. This method can be used to validate RNAseq data, by checking a small selection of genes to ensure that the fold change observed for these genes in the RNAseq data can also be observed through qPCR.

A major source of error in qPCR is the amplification of contaminating genomic DNA in the sample instead of cDNA. To minimise this DNase can be used to digest the genomic DNA during RNA extraction as has been performed in this analysis. Another measure that can be taken is to use primers that span exons either directly (the primer encodes the ends of two exons) or indirectly (the amplified region between primers span over multiple exons). As genomic DNA will contain introns, it will not be amplified. Exon spanning was not factored into the primer design in this analysis.

Another source of error is due to sample and run variation. Ideally, we would extract the same amount of mRNA from the same number of cells for each sample and the level of degradation and/or contamination of these samples would be the same and minimal. However, variation in these factors may result in differences in the observed ct values obtained. Similarly, each run will likely vary due to variations in the running of the machine, and sample preparation between days among other possible factors. To account for this reference or housekeeping genes are used. These are genes that are presumed to have consistent expression over all conditions, i.e. that they are unaffected by the treatment. As their expression should be consistent, the ct values observed for this gene, if amplified with appropriate primers, should be the same for both control and treated samples. Variation in these ct values indicates other sources of variation during the harvesting, purification, reverse transcription and qPCR of the mRNA. We can use the ct values of the housekeeping genes to normalise the ct values of our genes of interest to remove this source of error. There are many commonly used reference genes, including the two used in this study, *Tbp* (TATA-Box Binding Protein) and *Hprt1* (Hypoxanthine Phosphoribosyltransferase 1). The TATA-box binding protein *Tbp* is a general transcription factor that

binds specifically to TATA-box DNA sequence. It is involved in the transcriptional initiation of RNA polymerase 1, 2 and 3 (409). This gene has been found to have stable expression in various treatments, particularly *Tbp* has been shown to be one of the most stably expressed genes in skin fibroblasts in mice as part of studies into skin wound healing (410). *Hprt1* is a transferase that plays a key role in the generation of purine nucleotides. Its expression has been shown to be stable in skin fibroblasts in humans (411).

4.2 Aims

RNAseq analysis identifies the level of expression of all genes in an organism. As discussed in Chapter 1.4, RNAseq is a powerful technique that has been employed successfully in the NMR to help elucidate the mechanisms behind their remarkable cancer resistant and long-lived phenotype. However, no RNAseq studies have been performed on cells responding to genotoxic stress to date. By performing RNAseq on mouse and NMR cells exposed to DNA damaging agents, we can identify how changes in gene expression in response to DNA damage differ between the two organisms. A dose predicted to be sufficient to kill half the cells was used to ensure similar levels of stress in the surviving cells of both species. This LD50 was calculated in Section 3. In NMR cells senescence does not appear to increase at these doses, and hence we can be sure the reduction in cell numbers is due to half the cells being killed and not by the induction of senescence. The mouse cells used in this assay (alpha stock) showed up to 8% and 22% more senescent cells at 8 and 48 hours post-treatment with the designated LD50 dose, respectively. An intermediate value is likely to represent the level of senescence at 24 hours (the time the LD50 value was derived from). As such the majority of the decrease in cell count will be due to cells dying however such senescence may result in underestimation of the LD50 in mice. By identifying differences between the NMR and mouse, it may be possible to identify mechanisms by which the NMR cells elicit their apparent DNA damage resistance and potentially why they are more resistant to cancer and are longer lived than mice.

4.3 Materials and methods

4.3.1 RNA sequencing

Cells from mouse and naked mole rat (NMR) were grown to near confluence in 100mm culture dishes with media and under the conditions described in Section 3.3.1. These were treated with camptothecin or chromium (vi) oxide (Sigma Alderich) at LD50 (found in this study to be 5.24 µM camptothecin and 6.88µM chromium (vi) oxide for all mouse primary cell cultures, 26.93µM camptothecin for all NMR primary cell cultures and 24.68uM, 28.28µM and 27.3µM chromium (vi) oxide for NMR primary cell cultures 1, 2 and 3, respectively). The compounds were dissolved in media with 2% DMSO that was also present in control treatments. Treatment lasted 2 hours, and RNA was collected using RNeasy RNA extraction kit as per manufacturer's instructions, 8 or 48 hours after the start of the treatment. Only cells from the alpha cell stock were used in this assay. Prior to RNA extraction, the cells were examined, and no change in morphology was observed. The cells in 48-hour post-treatment samples were counted prior to RNA extraction to check that the treatment had killed approximately 50% of the cells. Only the 48-hour samples were counted as the 8-hour time point was deemed not long enough to see differences in cell count. Only one count per sample was performed as a 'quick check'.

RNA samples were sent to the Centre for Genomic research at the University of Liverpool to run the RNAseq experiment as follows. The total RNA was depleted with the Ribo-Zero Low Input Gold Kit (Human/Mouse/Rat) from Epicentre using 500-1,000ng of starting material. The success of the depletions was assessed using Qubit and Bioanalyzer for each sample. RNA–Seq libraries were prepared from the enriched material using the Epicentre ScriptSeq v2 RNA-Seq Library Preparation Kit. The rRNA depleted RNA was used as input, and following 15 cycles of amplification, libraries were purified using AMPure XP beads. Each library was quantified using Qubit and the size distribution assessed using the Agilent 2100 Bioanalyzer. These final libraries were pooled in equimolar amounts into 6 pools using the Qubit and Bioanalyzer data. The quantity and quality of each pool was assessed by Bioanalyzer and subsequently by qPCR using the Illumina Library Quantification Kit from Kapa on a Roche Light Cycler LC480II according to manufacturer's instructions. The average read length over all the pools was 386bp with an average concentration of 26.9ng/µl. Each pool of libraries was sequenced on one lane of the HiSeq 2,500 at 2x50bp paired-end sequencing in the rapid run mode.

The data received from the Centre for Genomic research was analysed through our lab's pipeline that consists of STAR (412) and readcounter (413). The mouse genome used to map mouse data was the GRCm38 from Ensembl release 76. The NMR genome used to map NMR samples was the

NCBI (National Centre for Biotechnology Information) annotation of HetGla_female_1.0 NMR assembly. A combination of the NMR database (414), NCBI gene database (http://www.ncbi.nlm.nih.gov/gene) and Ensembl (415) were used to name each gene.

The genes *Cdkn2a* (Cyclin-Dependent Kinase Inhibitor 2A) and *Cdkn2b* (Cyclin-Dependent Kinase Inhibitor 2B) do not appear in the current NMR annotation, for *Cdkn2a* this is likely due to a premature stop codon in the NMR (described in Section 1.2.2) (175, 414). To make sure these genes were included in our analysis we BLAST the known NMR *Cdkn2a* sequence from the NMR database (414) and the mouse sequence of *Cdkn2b* (GI:3075496) against the nr database from NCBI. The top matches in NMR were taken as the homologues. These were LOC101701430 and LOC101701062, respectively.

Deseq (407) was used to analyse the RNAseq data using default settings. Deseq2 (416) was also used with default settings as this is thought to be less stringent and hence have a reduced type two error. Deseq was also used to normalise the data as described in 4.1.1. and to calculate fold change values as the normalised value of one condition divided by the normalised value for the other condition.

4.3.2 Quantitative PCR

RNA was extracted using an RNAeasy mini kit as per the manufacturer's specification including the use of DNase to remove DNA contaminant (which could otherwise be amplified instead of our target cDNA) and hence remove the need for exon spanning primers. The tetro cDNA synthesis kit by Bioline was used to generate cDNA as per the manufacturer's instructions for Oligo $(dT)_{18}$ and incubated for an additional 30 minutes to ensure a complete reaction. Primers (Table 4.1) were designed using OligoPerfect™ Designer (Invitrogen Corp. Carlsbad, CA) using the following parameters: Primer size: Min 18, Opt 20, Max 27, Primer Tm: Min 57, Opt, 60, Max 63, Primer GC percentage: Min 40, Opt, 50, Max 60, Product size: Min 100, Max 150, Salt Conc: 50 and Primer Conc: 50. The output primers were checked for specificity using the NCBI's primer blast tool (417). Primers for *Hprt1* and *Tbp* in NMR were taken from (192), and primers for *Hprt1* in mice were taken from (418) as these have been extensively tested. No product length for the NMR *Tbp* primers was provided as this primer was designed to the mouse ortholog and hence the product length provided here was predicted from gels run on control RNA (Figure 4.20).

To test the specificity of the primers control sample cDNA was diluted 1 in 50 and 5µl of this was added per required well with 10µl Maxima SYBR Green/ROX qPCR master mix (x2) (Invitrogen

Corp. Carlsbad, CA), 4µl nuclease-free water and 0.5µl of 10µM forward and reverse to give a final volume of 20ul. This was done for each primer pair in triplicate. The plate was immediately placed in a StepOnePlus Real-Time PCR System by Applied Biosystems. Each cycle consisted of 15 seconds at 95°C and 60 seconds 60°C period and was repeated 40 times. To assess the specificity of the primers the PCR product was mixed with 5µl loading buffer and 10µl of this solution was run on a 3% agarose gel. The gel was prepared by mixing 6µl of Midori Green to 100ml of molten 3% agarose before pouring the gel. The gel was run at 110 volts for 1.5 hours. This was then imaged using UV light.

Due to limited amounts of RNA remaining after the RNAseq analysis only the following mouse samples could be analysed, mouse primary cell culture 1, (8 hours post stimuli all samples, and 48-hour post stimuli control, and camptothecin samples) and mouse primary cell culture 2 (8-hour post stimuli control and camptothecin-treated samples and 48-hour post stimuli control and chromium treated samples). Each sample was run in triplicate. For each sample, a standard curve was created using a five-fold serial dilution of the control cDNA with each sample being amplified and analysed in triplicate (Appendix Figure 4 to 7). Only samples with an efficiency of 95-105% (efficiency calculated as: $10^{(-1/slope)}$ -1 where 'slope' refers to the slope of the standard curve (Appendix Table 1)) and an R^2 value of ≥0.98 were used for the quantification analysis initially. For mouse cell line 1, *Foxo1* in 8-hour post-treatment samples, *R3hcc1* (R3H Domain And Coiled-Coil Containing 1) in 48-hour post-treatment sample and p21 from both 8 and 48-hour post-treatment samples was included in this assay despite high efficiency (106-113%) and hence care should be taken when interpreting data from these samples. Due to limited starting volumes of RNA, only a subset of the target genes could be tested, and those that failed to meet the required efficiency and R^2 could not be re-tested. To assess that DNA contamination was not being amplified in the PCR reaction, RNA samples that had not undergone reverse transcription were used as the input to the qPCR reaction. However, due to limited remaining RNA, this was only performed on primary mouse cell culture 2 8-hour and 48-hour control samples using the primer pair designed for p21. No amplification was observed suggesting nuclear DNA contamination is not an issue in these samples.

Fold change was calculated by taking the ct value of *Tbp* from the target gene ct value to give delta ct (Δct). As *Tbp* expression should remain consistent between treatment, this normalises for differences in starting RNA and cDNA concentrations. Fold change in a sample was then calculated by the following: $2^{-(\Delta ct\ control\ (untreated)\ -\ \Delta ct\ treatment)}$. Upon analysis of ct values for the housekeeping genes *Tbp* and *Hprt1* (Appendix Table2) it was found that there was little variation between them with the coefficient of variation (calculated as the standard deviation of the ct divided by the average ct within a run (control and treated cells) multiplied by 100 to be expressed as a percentage) between control and treated samples in each qPCR run being less than 4%. The coefficient of variation is a statistic for

assessing the variation in expression of a gene that allows for comparisons between genes with large differences in base expression. There is no agreed value that the coefficient of variation needs to be, but the lower, the better. The ct values were input into a one way ANOVA using the statistical package SPSS to assess if there was significant variation between samples.

Table 4.1. All primers created for this experiment. With the exception of Hprt1 and Tbp targeting primers, all primers were designed especially for this study. Star (*) value derived from the gel image as no predicted size was available.

Gene	Forward 5' – 4'	Reverse 5' – 4'	Product Size
P21 nmr p1	ATAGTGGCTCAGGAGGACCA	TTTTCGGCTCTGAGAGGTTC	114
P21 nmr p2	ACCTCTCAGAGCCGAAAACG	TAGGCCGTGGATTCTGTGGG	101
P21 mouse p1	TTGCACTCTGGTGTCTGAGC	TCTGCGCTTGGAGTGATAGA	112
P21 mouse p2	ACCACCAAGCCATTCCATAG	ACACTATCCTGGGCATTTCG	111
Sox5 NMR p1	GGAAGGTGGCTGTTGTGAAT	TCCATCATTGCATGGCTAAA	136
Sox5 NMR p2	TGACCCTTACCCTGTTCAGC	GCTTCCCTCCTGGAGATACC	137
Sox5 Mouse p1	CCGTGTCTCCTACCAGCATT	GGTGATTTGCCATCAGAGGT	124
Sox5 Mouse p2	AACTGTGCCCAGACAAAACC	CCCCTAGGGAAAACTCTTGG	113
Grik2 NMR p1	CATCAAGGCTCCATCAAGGT	TTGCCTCGCTTCATTTCTTT	102
Grik2 NMR p2	CTCATGCAGCAAGGTTCTGA	ACTGTCAGAAAGGCGGCTAA	128
Grik2 Mouse p1	GCAATGAGGAAGGGATTCAA	GTGCCAACACCATAGCCTTT	145
Grik2 Mouse p2	TCGACTTTTCAAAGCCGTTT	GCAAGCCAGCAGAACATACA	134
R3hcc1 NMR p1	CTGGCCACGTTCTCTGAGTT	TTGGTCAGAGCCTCAGTAGC	113
R3hcc1 NMR p2	GGCTCAAGATCCAGTGGGTA	GCTCTGAGCTTCGACTGCTT	145
R3hcc1 Mouse p1	AAGGATTTCTCCGTGCTCAA	CCTTCGATAGTCGCAGGAAC	100
R3hcc1 Mouse p2	TACTCCCCCAAGTGTTCTGC	AAGGGGCTGTCCTGGTATCT	103
Serpinb2 NMR p1	ATGAGGCAACCAAGATGGTC	CCTGTTCACACGGAAAGGAT	107
Serpinb2 NMR p2	TGTTGATGAGGCAACCAAGA	CCTGTTCACACGGAAAGGAT	112
Serpinb2 Mouse p1	ACCTGCTACCCGAAGGTTCT	CGAGTTCACACGGAAAGGAT	131
Serpinb2 Mouse p2	AAATCCCAAACCTGCTACCC	CGAGTTCACACGGAAAGGAT	140
Dpp10 NMR p1	CCCAAAGCAAAGCAGTATCC	GGTGGCATGAGTTCCAAAGT	110
Dpp10 NMR p2	TACCGTGCGTCATCTGACAT	TGGGAGATAACTCGGTGCTC	104
Dpp10 Mouse p1	GCGAACCCATCAGTGAAGTT	ACCACCTGACCACTGTCCTC	148
Dpp10 Mouse p2	TGGCATACGACGTTAAGCAG	CTCAACTTCTGGGGGATTCA	107
FOXO NMR p1	GGCTATTCTTCCGTGAGCAG	GTCACAGTCCAAACGCTCAA	111
FOXO NMR p2	TGCCTCTTTCCCATCCTATG	GTCACAGTCCAAACGCTCAA	146
FOXO Mouse p1	CCGGAGTTTAACCAGTCCAA	TGCTCATAAAGTCGGTGCTG	124
FOXO Mouse p2	ACATTTCGTCCTCGAACCAG	GGTGGATACACCAGGGAATG	116
P57 NMR p1	GTGGAAACGTCCCTGTGATG	AGTTGAAGTCCCAGCGGTTC	141
P57 NMR p2	TGGAAACGTCCCTGTGATGG	AAGTTGAAGTCCCAGCGGTT	141
P57 Mouse p1	AGAGAACTGCGCAGGAGAAC	TCTGGCCGTTAGCCTCTAAA	141
P57 Mouse p2	GGAGCAGGACGAGAATCAAG	GTTCTCCTGCGCAGTTCTCT	145
Hprt1NMR p1	GCTTCCTTCTCCGCAGACT	CTTCATCACGTCTCGAGCAA	215
Hprt1 Mouse p1	GGACTAATTATGGACAGGACTG	GCTCTTCAGTCTGATAAAATCTAC	195
Tbp NMR p1	GAGAGGAGCTGCTTCGGATT	GCTCATGCCAGAGAATAGGC	208*
Tbp Mouse p1	TGTCTGCCATGTTCTCTTGC	TGCTGCCACCTGTAACTGAG	109

4.4 Results and discussion

4.4.1 Quality control

Prior to RNA extraction, the cells from the 48-hour post-treatment samples were counted to check that ~50% of the cells had been killed by the treatment (Figure 4.1). On average, there were almost exactly 50% fewer cells in treated samples compared to untreated controls for mouse cells (50.5% and 50.6% for camptothecin and chromium treatment, respectively) with very little variation between the cell lines (Appendix Figure 8). However, NMR cells varied more with camptothecin-treated samples having an average of 45.7% the number of cells from untreated control samples and chromium (vi) oxide treated cells having 58.8% the number of cells in control samples. This chromium treated samples showed much more variation between cell lines (43.1-68.8%) (Appendix Figure 8). Despite the variation, these numbers suggest that the compounds of study are in fact killing or otherwise reducing the number of cells in the sample by approximately 50%. The deviations from this value may be due to the fact the cells had an extra 24 hours to grow and or die. Given the data previously collected that showed mouse cells had significantly more senescent cells in treated samples compared to control cells and that NMR cells showed no increase after 48 hours post-treatment (Figure 3.16), it is surprising that the deviation from 50% is not the reverse of what we observe. Mouse cells should deviate more due to the accumulation of non-dividing cells reducing the cell count relative to the dividing control cells. Perhaps the accumulation of senescent cells occurs slowly and so the number of senescent cells observed at 48 hours only recently arriving at such levels. Given the suggestion that senescent cells can promote further senescence (discussed in Section 5.1.2) we would expect a non-linear accumulation of senescent cells over time with the rate of accumulation of senescent cells increasing with time. This means that some of the senescent cells observed at 48 hours would not have been around long enough to affect the population growth. Alternatively, the dose provided may have not quite killed 50% of the cells so that the difference was made up by the senescent cells in the population.

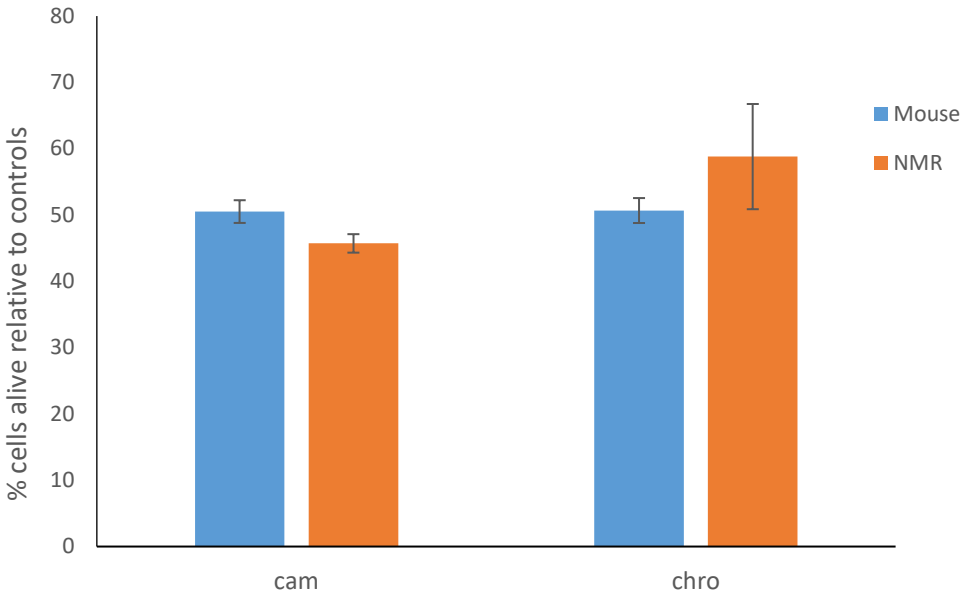

Figure 4.1 Average proportion of mouse or NMR cells from the alpha cell stock alive after genotoxic treatment prior to RNA extraction for 48hour post-treatment samples. Error bar indicates ± one standard error of the mean between three cell lines; each cell line is a single sample (no replicates). Key, cam - camptothecin, chro - chromium (vi) oxide, con - control. Each cell line count consisted of ~100 cells, hence the average displayed above consists of ~300 cells counted.

In order to detect changes in gene expression in response to DNA damage, RNA was extracted from primary skin fibroblasts from both C57BL/6 mice, and NMRs treated with camptothecin, chromium (vi) oxide or control conditions after 8 and 48 hours. These time points were selected to allow detection of changes in the response over time.

Due to low cell numbers (due to early contact inhibition and slow growth) lower amounts of RNA were obtained from NMR samples (Table 4.2). Additionally, variation was seen between different cell cultures and treatments. This may reflect variations between the cell lines, variations in conditions within the incubator or variations in the RNA extraction. Lower levels of starting material mean that genes with very low levels of expression may be lost and hence the assay becomes less sensitive. We proceeded with these lower amounts of RNA as we wished to use primary cells that had undergone as few cell passages as possible to ensure the cells represented their *in vivo* counterparts as best as possible. Dilution of the RNA to equal concentrations was performed prior to the analysis to minimise this as a source of variation within the data. In future work, this variation in RNA could be avoided by counting the number of cells before RNA extraction and using the same number for each extraction. Any differences in RNA yield observed under these conditions would indicate species variation in either RNA content of the cells or the cells' ability to be purified by the method used. Furthermore, if

work were to be repeated the incubator used would be heat mapped when empty and at varying levels of full. This would assess possible sources of variation and a maximum safe-fill level in which air circulation is still possible to facilitate consistent temperatures.

Table 4.2. The total RNA extracted from each primary cell culture and condition (ng).
Key, cam-camptothecin, chro-chromium (vi) oxide, con-control.

		Mouse			NMR		
		Culture 1	Culture 2	Culture 3	Culture 1	Culture 2	Culture 3
8hr	cam	5,314	2,898	1,385	1,361	1,666.8	493
	chro	3,924	1,783	3,580	1,692	1,890	718
	con	5,171	5,035	9,044	1,208	1,070	472
48hr	cam	9,698	10,639	2,040	1,741	1,828	276
	chro	5,656	9,264	1,175	1,559	1,280	453
	con	14,414	15,163	2,848	1,841	986	511

To assess the quality of the RNA, samples were input into a 2100 Bioanalyzer (Agilent technologies). The Bioanalyzer assesses RNA quality by analysing the ratio of small to large RNA products as well as the ratio of ribosomal subunits RNA (28S:18S) and assigns an RNA integrity number (RIN score). A large proportion of small RNA molecules indicate sample degradation which is reflected by a lower RIN score. Sample degradation affects measurements of gene expression and can reduce library complexity (419). The RNA samples can be displayed graphically by plotting the size of the RNA in nucleotides (nt) against fluorescence units (FU); the greater the FU, the greater the volume present (Figure 4.2). By doing this, we can see that the samples are dominated by RNA fragments of a given length. This is the ribosomal RNA. This RNA is visibly different between NMR and mouse. In mouse, there were two clear peaks representing the 18s and 28s ribosomal subunits (Figure 4.2). However, in NMR we saw at least 3 peaks (Figure 4.3). In the NMR the 28s ribosomal subunit is divided into two unequal sized fragments reported to be 2,500nt and 3,000nt (177). The software incorrectly identifies the peaks in all NMR samples resulting in inaccurate RIN scores. As such RIN scores (Table 4.3) were only used as an indicator of RNA integrity for NMR samples and the Bioanalyzer traces were used to decide which samples were intact. The peak representing the 18s subunit was likely the peak to the left of the one mislabelled as 18s (labelled with #) (Figure 4.3). The peak labelled at 18s is likely a component of the 28s subunit as well as the peak to the right of this (labelled with *).

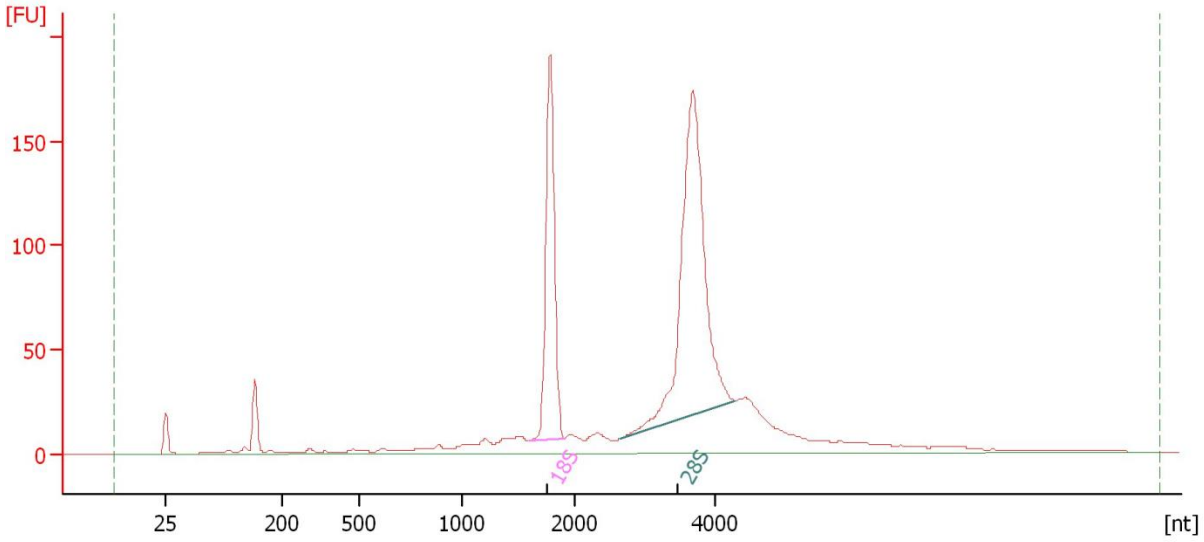

Figure 4.2. Fragment size plot by 2100 Bioanalyzer of mouse RNA samples. Fragment size in nucleotides (nt) plot against fluorescent units (FU). Representative graph of control samples of the Mouse 2 primary cell culture (alpha cell stock).

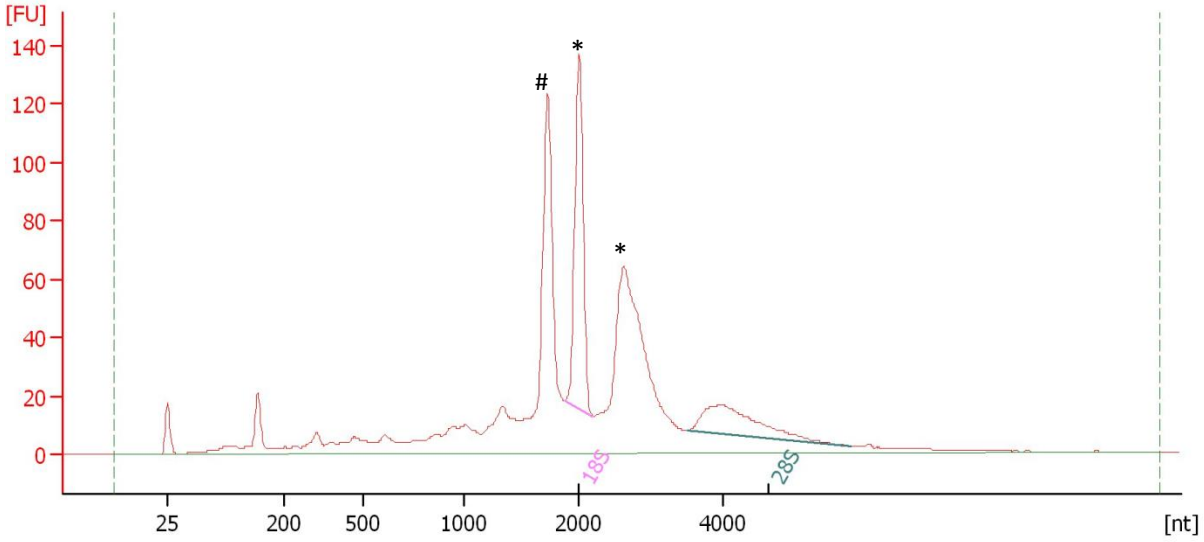

Figure 4.3. Fragment size plot by 2100 Bioanalyzer of NMR RNA samples. Fragment size in nucleotides (nt) plot against fluorescent units (FU). Representative graph of control samples of the NMR 2 primary cell culture (alpha cell stock). The peaks are mislabelled in the graph; stars (*) indicates peaks representing the two 28s ribosomal subunits, hash (#) indicates the peak representing the 18s ribosomal subunit.

Table 4.3. RIN scores calculated by the 2100 Bioanalyzer. All NMR scores are inaccurate due to misidentification of the peaks representing the 18S and 28S ribosomal subunits due to NMR 28S being divided in two. Key, cam-camptothecin, chro-chromium (vi) oxide, con-control, dash (-) indicates no score was generated.

		Mouse			NMR		
		Culture 1	Culture 2	Culture 3	Culture 1	Culture 2	Culture 3
8hr	cam	8.6	9	9.6	7	-	7.7
	chro	8.2	8.2	9.2	6.8	-	3.9
	con	8.5	8.2	9.5	8	-	6
48hr	cam	8.3	9.3	8.8	7	-	5
	chro	9.1	8.1	9.6	8.9	7.9	6.7
	con	7.8	9.4	9.2	7.2	7.3	5.8

In mammalian cells rRNA accounts for 90% of the total cellular RNA (420). As we aimed to look at changes in gene expression, rRNA was removed from the samples to enrich them for mRNA. As NMR's 28S is naturally fragmented into two species and due to low starting amounts of RNA a RiboZero™ Gold Kit (illumina) was used. To determine the effectiveness of this removal the samples were analysed in a 2100 Bioanalyzer again (Figure 4.4-4.5). From these graphs, we can see both the 18s and all 28s peaks are greatly reduced meaning the samples are enriched for mRNA.

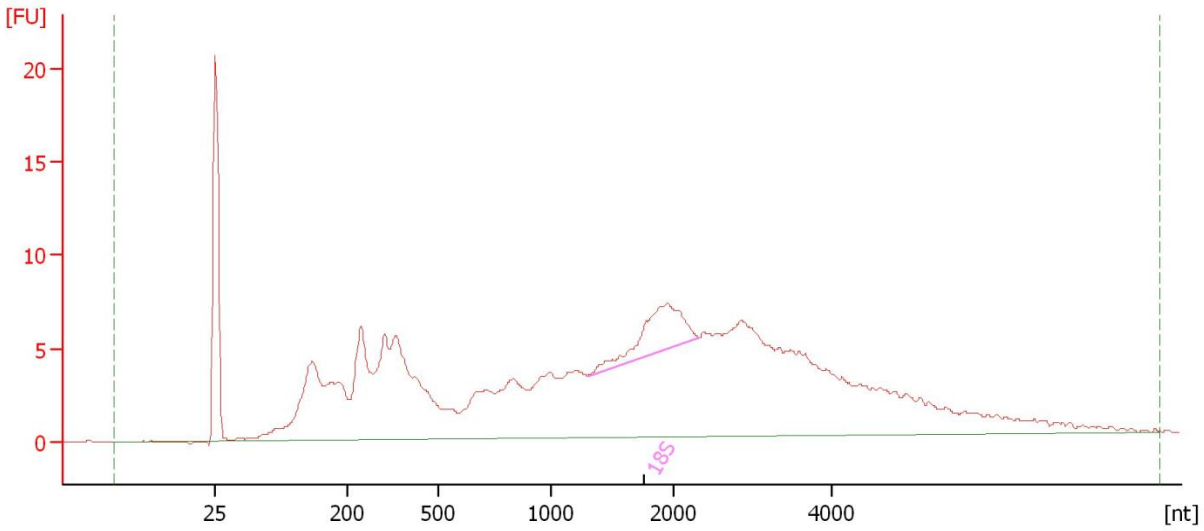

Figure 4.4. Fragment size plot by 2100 Bioanalyzer of mouse RNA samples post-ribo depletion. Fragment size in nucleotides (nt) plot against fluorescent units (FU). Representative graph of control samples of the Mouse 2 primary cell culture (alpha cell stock).

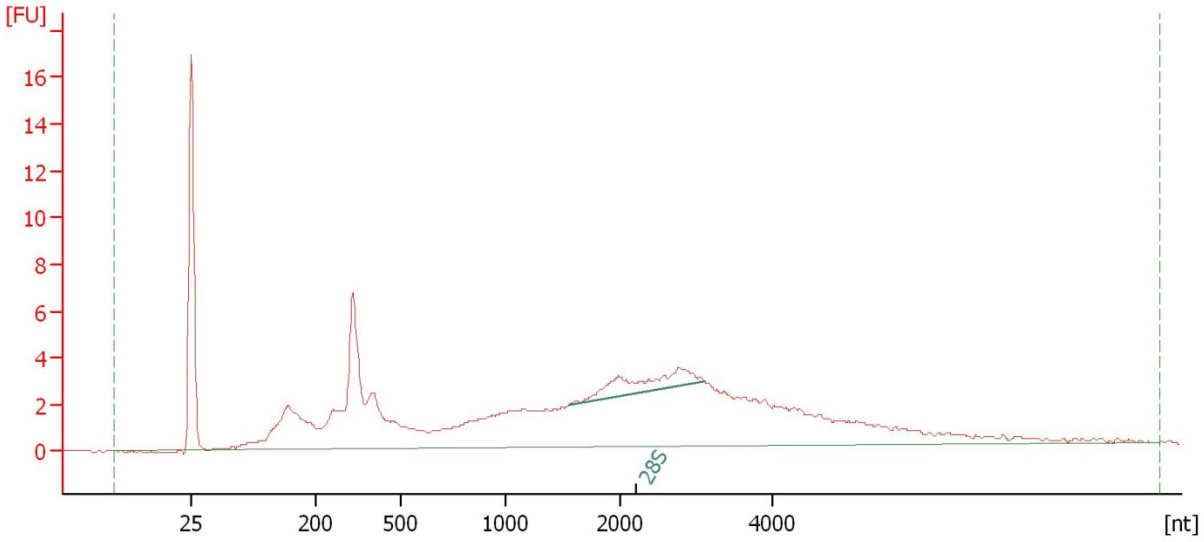

Figure 4.5. Fragment size plot by 2100 Bioanalyzer of NMR RNA samples post-ribo depletion. Fragment size in nucleotides (nt) plot against fluorescent units (FU). Representative graph of control samples of the NMR 2 primary cell culture (alpha cell stock).

4.4.2 Data analysis

A total of 41,234 mouse genes and 30,556 NMR genes were sequenced as part of the RNAseq analysis, of these 12,508 homologous genes were found between NMR and mouse. The total number of reads sequenced for each sample is given in Table 4.4. The predicted coverage calculated by the formula 'average read length multiplied by the number of reads divided by the haploid genome length' is given in Table 4.5. The percentage of reads mapped to the appropriate genome is given in Table 4.6.

Table 4.4. The number of reads sequenced on a HiSeq 2,500 at 2x50bp paired-end sequencing in the rapid run mode as part of the RNAseq analysis for each condition and cell culture. The average read length over all samples was 386bp with an average concentration of 26.9ng/µl. Key, con – control, cam – camptothecin, chro – chromium.

		Mouse			NMR		
		Culture 1	Culture 2	Culture 3	Culture 1	Culture 2	Culture 3
8hr	cam	23,254,806	18,275,002	23,017,315	27,269,161	22,194,735	21,348,897
	chro	21,108,723	24,156,943	22,954,573	25,561,563	22,330,800	22,787,996
	con	25,150,051	19,292,317	19,714,514	26,709,122	22,014,809	20,170,712
48hr	cam	27,212,040	18,304,740	22,043,113	22,154,439	25,051,295	22,416,515
	chro	20,766,259	18,149,393	25,431,317	23,090,066	24,870,279	18,705,381
	con	26,912,903	21,664,828	25,936,412	23,457,149	25,308,882	16,437,557

Table 4.5. The predicted coverage for each sample. This was calculated by the formula: average read length multiplied by the number of reads (Table 4.4) divided by the haploid genome length (Mouse (GRCm38): 2,730,855,475bp, NMR (HetGla_female_1.0): 2,314,771,103bp). Key, con – control, cam – camptothecin, chro – chromium.

		Mouse			NMR		
		Culture 1	Culture 2	Culture 3	Culture 1	Culture 2	Culture 3
8hr	cam	3.2	2.5	3.2	4.0	3.3	3.2
	chro	2.9	3.3	3.2	3.8	3.3	3.4
	con	3.5	2.7	2.7	4.0	3.3	3.0
48hr	cam	3.8	2.5	3.0	3.3	3.7	3.3
	chro	2.9	2.5	3.5	3.4	3.7	2.8
	con	3.7	3.0	3.6	3.5	3.8	2.4

Table 4.6. The percentage of reads sequenced on a HiSeq 2,500 at 2x50bp paired-end sequencing in the rapid run mode as part of the RNAseq analysis that successfully mapped to either the mouse (GRCm38) or NMR (HetGla_female_1.0) genome. Total number of reads given in Table 4.4. Key, con – control, cam – camptothecin, chro – chromium.

		Mouse			NMR		
		Culture 1	Culture 2	Culture 3	Culture 1	Culture 2	Culture 3
8hr	cam	86.0%	86.8%	88.9%	92.7%	92.1%	86.2%
	chro	86.7%	88.6%	89.1%	92.4%	92.8%	85.6%
	con	86.2%	88.4%	89.8%	92.6%	93.4%	87.0 %
48hr	cam	87.5%	87.8%	89.1%	92.5%	92.5%	87.1%
	chro	87.8%	88.2%	87.7%	92.5%	92.1%	85.4%
	con	87.6%	87.5%	88.9%	93.0 %	92.5%	85.5%

The variation between primary cell cultures of the same species appeared greater than the variation between treatments, particularly in the naked mole rat. This is shown more clearly in a PCA plot (Figure 4.6-4.8). When all samples were considered, we saw a large separation between NMR and mouse samples as expected for two distanced species (Figure 4.6). However, even at this scale, we saw two distinct clusters for NMR samples (Figure 4.6) one made up of NMR cell line 1 and 3 and the other made up of NMR cell line 2 samples (Appendix Figure 9). By looking at each species separately, we saw three clusters, each one representing an individual primary cell culture (Figures 4.6-4.7). This would seem to suggest that variation between individuals of the same species is greater than the variation induced by treatment. This is unexpected as B6 mice, like most inbred mouse strains, are

almost completely genetically homogeneous (421). Similarly, NMRs from the same colony (as our cell donors were) are highly similar genetically due to inbreeding and colonies being predominantly made up of siblings (422, 423). Additionally, animals of the same species were likely housed in very similar conditions and so environmental effects on the epigenetics of the cell would likely be similar. NMRs do show variations within colonies with their position in the colony hierarchy which correlates with both body mass and testosterone levels, varying between animals which may account for some variation seen in the gene expression (424). If this is the case then based on these plots the NMR from which NMR cell line 2 was derived may have had a different position in the hierarchy, may have been mis-aged or potentially undergoing some stress such as injuries caused by bites which are common within NMR colonies which may explain its apparent dissimilarity from the other cell lines. However, the remaining cell lines also showed dissimilarity and so all cell lines will be kept within the analysis as no one cell line can be considered 'wrong' or unusual.

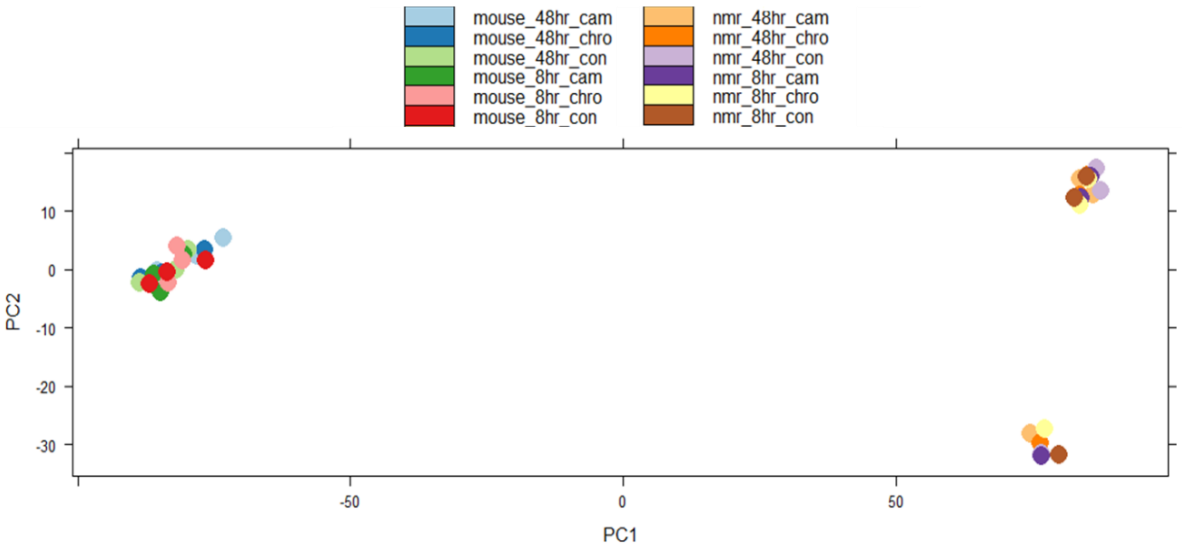

Figure 4.6. PCA plot of RNAseq data for all samples. Each dot represents a single RNA sample used in the analysis. Mouse samples seem to form one large cluster on the left and NMR samples from two distanced clusters on the far right with NMR cell lines 1 and 3 making up the top cluster and NMR cell line 2 making up the bottom cluster (alpha cell stock). Key con - control, cam - camptothecin treatment, chro – chromium (vi) oxide treatment. PCA plot generated in R (332).

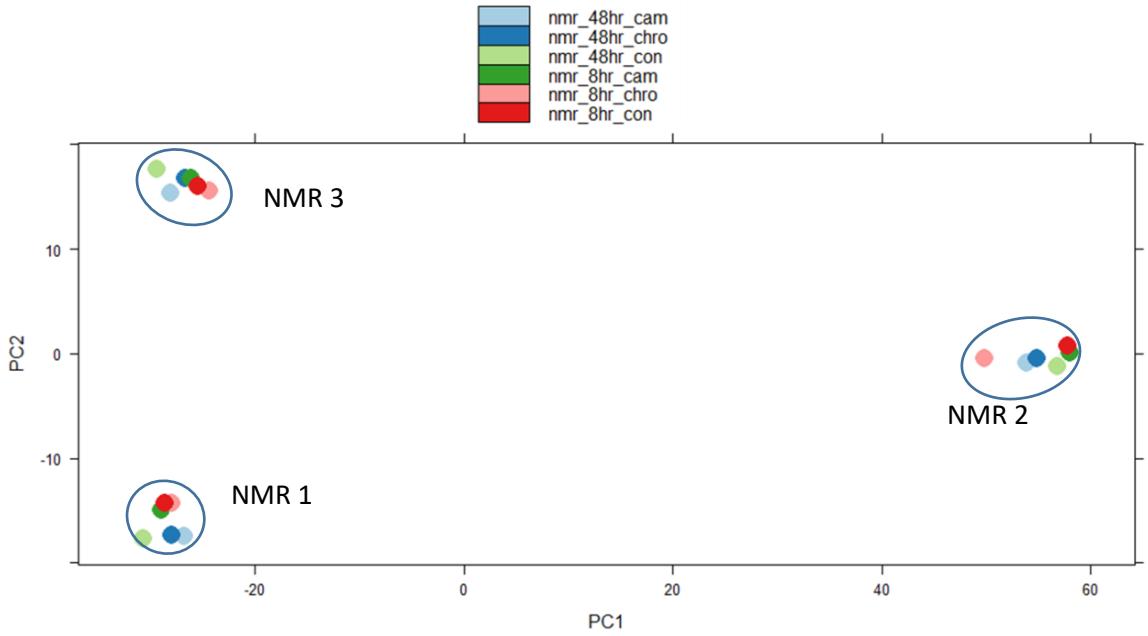

Figure 4.7. PCA plot of RNAseq data for NMR samples (alpha cell stock). Each dot represents a single RNA sample used in the analysis. There are three tight clusters which each represent a different primary cell culture (circled). They are labelled with which cell line they represent (NMR 1, 2 and 3). This shows far greater variation between primary cell cultures than treatments. Key con - control, cam - camptothecin treatment, chro – chromium (vi) oxide treatment. PCA plot generated in R (332).

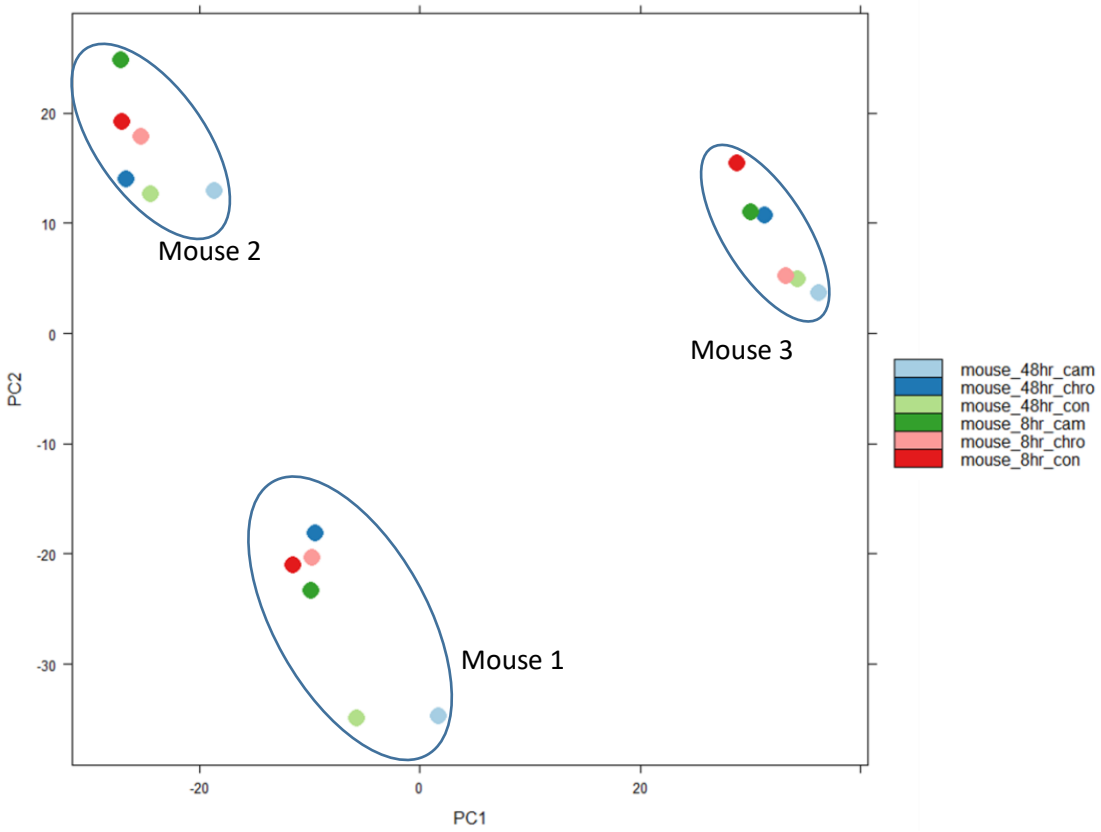

Figure 4.8. PCA plot of RNAseq data for mouse samples (alpha cell stock). Each dot represents a single RNA sample used in the analysis. There are three loose clusters which each represent a different primary cell culture (circled). They are labelled with which cell line they represent (mouse 1, 2 and 3). This shows greater variation between primary cell cultures than treatments. Key con - control, cam – camptothecin treatment, chro – chromium (vi) oxide treatment. PCA plot generated in R (332).

4.4.2.1 Differential expression between treatments

Deseq (407) was initially used to analyse the RNAseq data. As the variation in gene expression between primary cell cultures of the same species was greater than the variation caused by treatment with the DNA-damaging compounds, conventional methods of analysis indicated that only one gene was near significantly different ($p<0.8$ after multiple testing correction) between treatments. This was *Ifit1* (Interferon-Induced Protein with Tetratricopeptide Repeats 1) in mouse cells after 48 hours post camptothecin treatment. Comparisons between species, however, yielded many significant genes (on average 6,635 genes between all treatments with a p-value less than $p=0.05$ after correcting for multiple testing). Deseq2 (416) was also used as this is thought to be less stringent and hence have a reduced type two error. This seemed to be the case as we find more genes with p-values of $p<0.1$ after multiple testing correction. In NMR cells there was only one gene significantly downregulated at the 0.1 level, and that was *R3hcc1* at 48 hours post camptothecin treatment. The only other gene that

nears this level of significance in NMR was the extracellular matrix protein TNC (Tenascin C) with an adjusted p-value of p<0.5, which was also downregulated. In mouse cells, three genes were significant at the 0.1 level. *Ifit1* and *Pmaip1* (Phorbol-12-Myristate-13-Acetate-Induced Protein 1) were both upregulated at 48 hours post camptothecin treatment, and *Cenpf* (Centromere Protein F) was downregulated at 8 hours post camptothecin treatment.

R3hcc1 is a poorly studied gene. GO annotations related to this gene include nucleotide binding and nucleic acid binding suggesting a role in the nucleus. These terms are derived from the presence of an R3H motif in the protein; this motif is thought to bind nucleic acids (425).

To overcome the issue of variability and extract useful information from the data, the fold change between control and treated samples were analysed for each primary cell culture separately. Genes were then selected as DE if they showed a fold change of at least 1.5 in at least two of the three primary cell cultures providing that the third did not show a fold change of 1.5 or more in the opposite direction.

We saw a much larger difference in gene expression in all mouse comparisons compared to those in NMR (Table 4.7-4.8). This may be in part due to the lower amounts of RNA obtained from NMR samples (Table 4.2).

Table 4.7. Genes up (↑) or down (↓) regulated in NMR between the listed conditions (left) and the number of these genes present in DAVID (right). Comparisons are in the form row vs. column.

NMR	Camptothecin 8hr	Chromium 8hr	Control 48hr	Camptothecin 48hr	Chromium 48hr
Control 8hr	262/150↑ 321/210↓	259/157↑ 212/97↓	434/267↑ 442/308↓		
Camptothecin 8hr		365/239↑ 286/149↓		988/690↑ 616/414↓	
Chromium 8hr					590/313↑ 752/534↓
Control 48hr				565/373↑ 537/376↓	214/102↑ 236/130↓
Camptothecin 48hr					284/160↑ 527/361↓

Table 4.8. Genes up (↑) or down (↓) regulated in mouse between the listed conditions (left) and the number of these genes present in DAVID (right). Comparisons are in the form row vs. column.

Mouse Up	Camptothecin 8hr	Chromium 8hr	Control 48hr	Camptothecin 48hr	Chromium 48hr
Control 8hr	514/421↑ 710/599↓	656/546↑ 664/568↓	1,164/1,042↑ 1,114 /958↓		
Camptothecin 8hr		744/638↑ 549/470↓		1,749/1,571↑ 791/665↓	
Chromium 8hr					559/491↑ 490/394↓
Control 48hr				973/854↑ 422/362↓	454/371↑ 518/471↓
Camptothecin 48hr					687/556↑ 1,349/1,208↓

To get an overview of how the cells respond, a functional enrichment (FE) analysis was performed on differentially expressed genes between control and treated cells using DAVID 6.7 with all homologous genes as the background and otherwise default parameters (330, 426). This tool groups similar genes into clusters based on factors such as Gene Ontology (GO) terms. These clusters are assigned a score based on the significance of the terms within the group. The greater the score, the more enriched the group. A score of 1.3 is equivalent to a p-value of p=0.05 (330).

The functional enrichment reflected these lower number of genes as each NMR comparison had fewer enriched terms with some conditions having no terms enriched at all. The number of genes was further reduced as many NMR genes have not been annotated and hence have no mouse homologues. Additionally, not all known mouse genes are within the DAVID database. The final number of genes analysed by DAVID is given in Tables 4.7-4.8.

When comparing control to camptothecin or chromium (vi) oxide treated NMR cells after 8 hours there were no individual terms enriched to a statistically significant degree except for downregulated genes in camptothecin-treated cells (Table 4.9).

Mouse cells treated with either camptothecin or chromium (vi) oxide showed a clear stress response at the 8-hour time point in upregulated genes (Table 4.10). We saw terms regarding the mitochondrial envelope being upregulated which hints at an apoptotic response in both treatments with chromium treatment also showing the term ‘xenobiotic metabolic process’, clearly indicating a response to the xenobiotic hexavalent chromium. Additionally, both conditions show a cluster referring to the ribosome with camptothecin also showing terms for transcription indicating that new proteins are being generated to either replace damaged ones or to facilitate changes in cellular activity.

In 8-hour camptothecin treatment of mouse cells, all of the top 5 downregulated FE clusters appear to be related to cell cycle progression, specifically mitosis, either directly referring to the process, or indirectly referring to specific aspects of mitosis such as spindle formation or the motor proteins involved in chromosome segregation. In chromium treatment at the 8-hour time point, we saw a cluster of terms regarding the downregulation of transcription which matches the upregulation of transcription we see in camptothecin. We do not, however, see any terms related to cell cycle or cell division directly, with terms regarding cytoskeleton appearing but not in the top 5 terms. What we did see was the terms Pleckstrin homology and SH3. These protein domains are found in many proteins involved in signal transduction or the cytoskeleton (427, 428). Additionally, a number of terms regarding GTPase activity were seen which tie in with one of the top five enriched terms GO:0030695~GTPase regulator activity. GTPases are involved in a wide array of signalling pathways.

At 48 hours the similarity between treatments breaks down. Camptothecin-treated cells appear to still be under stress from the treatment with upregulation of a term regarding apoptosis and downregulation of terms regarding cell cycle and DNA replication. Strangely the term 'DNA repair' was also downregulated suggesting that a DNA damage response is winding down. Both treatments showed upregulation of the term glycoprotein and cell adhesion indicating changes at the cell surface. Chromium treatment otherwise appears to have elicited a somewhat different response as we did not see any downregulation of terms regarding the cell cycle but instead saw a term regarding the immune system indicating that the stress response was turning down.

In NMR we saw a very different response after 8 hours. No terms from upregulated genes in either camptothecin or chromium treated cells were statistically significant after FDR correction, but some still had high enrichment scores (≥1.3) (330). There were no terms related to apoptosis as in mouse, but chromium treated cells did show a term regarding transcription similar to what we saw in mouse cells. However, the enrichment score was very low (<1.3) (Table 4.9). In camptothecin treatment, we saw a number of terms regarding the cell membrane which may suggest an alternative method of cellular protection from harsh external stimuli. The term 'glycoproteins' appeared in both treatments; glycoproteins are typically located at the cell surface supporting the idea for changes at the cell membrane. Chromium treatment showed the term 'GO:0007188~G-protein signalling, coupled to cAMP nucleotide second messenger' which may indicate cell signalling. Additionally, chromium showed the term 'DNA-binding region:T-box' at 8 hours post-treatment, however, this entire cluster only contained 3 genes. Camptothecin treatment resulted in the downregulation of terms regarding the cell membrane which taken with the upregulated terms indicating the same, suggest a major remodelling at the membrane. Chromium treatment seemed to have a similar effect with one term for the cell membrane. Both treatments show the term 'IPR007110:Immunoglobulin-

like' as downregulated. This may indicate that an immediate stress response is ending at this early time point as these genes are downregulated to compensate for earlier high expression or that these cells are decreasing these genes as part of the initial stress response.

At 48 hours in NMR cells, we saw something of a continuation of the response seen at 8 hours. Terms regarding the cell membrane were both up and downregulated in camptothecin-treated cells, and a downregulation of terms regarding the immune system was still seen. There was increased evidence of a stress response with the term 'GO:0006955~immune response' upregulated in camptothecin treatment and 'GO:0009611~response to wounding' upregulated in chromium treatment. This could suggest there was a delayed stress response that appears only later on, or that there was a prolonged stress response that was simply not detected at the earlier time point. Chromium treatment resulted in changes of expression of terms which may indicate cell membrane changes such as 'GO:0060350~endochondral bone morphogenesis' and 'cognition'. Additionally, the term 'GO:0005509~calcium ion binding' may indicate changes in signalling as calcium ions often serve as cellular messengers.

Clusters of terms involving glycoproteins and cell membrane frequently appeared in many of the conditions under study. This is similar to what is seen in Cordeiro et al.'s study (429) that exposed endothelial cells to ethylene glycol and performed a microarray analysis. The similarity in these profiles indicates a generalised stress response. As glycoproteins are frequently components of the plasma membrane, these terms indicate a focus at the cells' surface. This could indicate a cellular response of preventing entry or removing the damaging agents. This was observed more prevalently in NMR cells.

We can see from Table 4.7 and 4.8 that simply allowing cells to grow under control conditions for an additional 40 hours resulted in changes in gene expression. Functional enrichment was applied to these differentially expressed genes (Table 4.11).

NMR cells showed no significantly enriched terms after 48 hours culture for upregulated genes. However, several functional enrichment clusters showed scores greater than 1.3. These included the term glycoprotein and terms relating to the plasma membrane that we saw for downregulated genes also. These terms were seen frequently enriched in response to the genotoxic treatments. This could suggest that this extended culture time could be harmful to the cells, possibly due to some depletion of nutrients in the media or build-up of toxic by-products. The fact that these terms are still enriched in the treatments at 48 hours would suggest further changes in such gene expression. It also suggests that such changes in gene expression require very little in term of stimulus to occur as the change in condition between 8 and 48 hours is likely to be very small relative to

treatment at an apparent LD50 dose of genotoxin. In addition, we saw upregulated terms enriched for the innate immune response including 'Toll-like receptor signalling pathway' and 'innate immune response' which may suggest a general stress response. The most upregulated gene was *Efna5* (Ephrin A5) with an average fold change of 7.4 (upregulated in cell line 2 and 3). *Efna5* encodes a surface-bound protein that has been shown to be involved in bidirectional communication between cells and cell adhesion (430), likely contributing to the cell adhesion associated transcription profile discussed above. The most downregulated gene was *Fam135b* (family with sequence similarity 135 member B) with an average fold change of 0.08 (downregulated in cell line 1 and 3). *Fam135b* encodes a protein with no known function that has been associated with Oesophageal cancer in one study (431). It is not clear what role this gene has in the present study.

Mouse cells showed enrichment for cell-surface-related genes in both up and downregulated genes. This enrichment of cell surface and adhesion genes was similar to what we saw in NMR cells exposed to the genotoxic treatment and a stark contrast to the profile we saw in mouse cells exposed to such stress, which showed terms more focused around apoptosis and DNA damage. This may indicate that the treatment is too stressful so that we go beyond this cell surface response and see more internal responses such as apoptosis and that the stress encountered from the increased culture time was less harmful and hence only this cell surface response is seen. Alternatively, the cells may just act differently over time, secreting extracellular proteins to make their environment more like they would experience naturally within an animal, particularly as a later time point may mean a higher cell density and hence more interaction and contact between the cells within the population. Terms relating to DNA damage repair and DNA replication being upregulated may indicate a stress response (the repair and replacement of damaged DNA) or may relate to DNA replication to produce new cells and may indicate that at the 8-hour time point the cells are still adjusting to their relatively new surrounding and hence are not yet dividing at as fast a rate. The most upregulated gene between these samples was *Gas1* (Growth arrest-specific protein 1) with an average fold change of 21.9 (upregulated in all cell lines). *Gas1* prevents cellular proliferation to keep cells in G0 (432), indicating growth arrest in these cells which suggests that the observed gene expression profile was a result of stress. The most downregulated gene was *Ostn* (Osteocrin) with an average fold change of 0.04 (cell line 2 and 3). *Ostn* is a poorly studied gene that has been shown to act as a secreted signalling molecule in both the brain to regulate neuronal activity and in bones to regulate bone formation (433, 434). This may play into the idea that there are more cells to communicate with, though without knowing what role this gene plays in fibroblasts, it is difficult to speculate on its function here.

As a follow up to these findings, an additional gene expression analysis could be performed over a simple time course, following the cells to assess how this gene expression changes. I would

hypothesis that three distinguishable profiles would be observed: an early profile associated with the cells adapting to the new surroundings, an intermediate profile in which the cells are growing optimally in the environment and an end profile in which overcrowding, depletion of nutrients and/or build-up of toxins results in a decline in growth and a shift towards senescence and apoptosis. Such a time course would help to identify time periods of stable gene expression and allow for more accurate evaluation of gene variation over time in response to our stimulus of study. As comparisons are between the controls at each time point and the treated cells at that time point, differences over time in untreated cells should be accounted for.

A Venn diagram of homologous genes that are differentially expressed between 8 and 48 hours of control treatment was generated (Figure 4.9). There is some commonality with 33 genes upregulated and 46 genes downregulated in both NMR and mice. Interestingly there were 28 genes upregulated and 11 genes downregulated in mice that show the opposite change in gene expression in NMRs. Performing a functional enrichment on these genes did not give statistically significant results due to the small sample size but did allow us to see that these genes downregulated in NMR but upregulated in mice were related to the terms such as 'Glycoprotein' and 'cell membrane'. The genes upregulated in NMR but downregulated in mice relate to terms including 'glycoprotein', 'cell membrane' and 'DNA binding'. This further supports the idea of differences at the cell membrane between these two species.

In summary, mouse cells appeared to undergo changes in biological activity that changed between treatments over time as can be seen by differences in enriched terms between 8 and 48 hours post stimuli between the two treatments. NMR cells, however, seemed more consistent with their response over time. Overall, the predominant activity in mouse cells seemed to indicate that initially the cells were becoming apoptotic and eliciting a stress response while exiting the cell cycle. Though this appeared to continue, we also saw a remodelling of the cell surface and a reduction in repair and immune terms indicating that the response to the stressors was ending. NMR cells however primarily showed remodelling of the cell membrane that continued through the observed time points. This response includes terms and genes involved in both cell adhesion and cell signalling. As this response was seen to a lesser extent at the later time point in mouse it may be that this membrane response being elicited greater and faster helps to protect the cell more readily from incoming damage.

Table 4.9. Functional enrichment (FE) results for NMR data. Representative terms from the top five FE clusters, with corresponding gene counts and FDR-corrected probability values and the enrichment score for the cluster. Terms were selected that best represented all the terms in the cluster, of these the term with the highest gene count and lowest FDR score was reported.

NMR	Term	Count	FDR	Enrichment Score
Control vs. Camptothecin up 8hr	glycoprotein	44	4.45	2.25
	GO:0044459~plasma membrane part	26	3.86	2.14
	GO:0016021~integral to membrane	50	20.85	1.54
	GO:0008146~sulfotransferase activity	4	10.47	1.48
	GO:0044459~plasma membrane part	26	3.86	1.39
Control vs. Camptothecin down 8hr	GO:0031224~intrinsic to membrane	88	<0.001	5.87
	topological domain:Extracellular	56	<0.001	5.33
	GO:0044456~synapse part	15	0.0028	3.51
	IPR007110:Immunoglobulin-like	17	0.011	3.04
	GO:0045202~synapse	18	0.0044	2.77
Control vs. Chromium (vi) oxide up 8hr	DNA-binding region:T-box	3	14.94	1.87
	GO:0007188~G-protein signalling, coupled to cAMP nucleotide second messenger	5	2.09	1.57
	Glycoprotein	44	10.49	1.47
	GO:0003700~transcription factor activity	15	9.57	1.22
	GO:0044459~plasma membrane part	22	22.81	1.21
Control vs. Chromium (vi) oxide down 8hr	PIRSF001630:serpin	3	9.19	1.42
	GO:0031224~intrinsic to membrane	32	5.83	1.35
	IPR007110:Immunoglobulin-like	7	14.43	1.27
	GO:0006821~chloride transport	3	43.17	1.15
	Glycoprotein	29	12.31	1.10
Control vs. Camptothecin up 48hr	Glycoprotein	121	<0.001	4.92
	cell membrane (including 'glycoprotein')	64	0.01	4.16
	GO:0031226~intrinsic to plasma membrane	22	<0.001	2.03
	IPR000859:CUB	7	2.81	1.83
	GO:0006955~immune response	21	0.39	1.68
Control vs. Camptothecin down 48hr	GO:0007155~cell adhesion	49	<0.001	10.45
	signal peptide	117	<0.001	8.75
	Glycoprotein	136	<0.001	6.55
	IPR003961:Fibronectin, type III	20	<0.001	4.32
	IPR007110:Immunoglobulin-like	27	<0.001	3.79
Control vs. Chromium (vi) oxide up 48hr	Glycoprotein	33	5.67	2.42
	GO:0009611~response to wounding	7	23.19	1.65
	GO:0050877~neurological system process	11	3.90	1.62
	Cognition	8	8.21	1.55
	GO:0044421~extracellular region part	13	1.27	1.49
Control vs. Chromium (vi) oxide down 48hr	disulfide bond	32	<0.001	2.35
	IPR006026:Peptidase, metallopeptidases	4	<0.001	1.44
	GO:0005509~calcium ion binding	16	2.41	1.26
	GO:0060350~endochondral bone morphogenesis	3	16.92	1.17
	GO:0050890~cognition	6	86.43	1.05

Table 4.10 Functional enrichment (FE) results for mouse data. Representative terms from the top five FE clusters, with corresponding gene counts and FDR-corrected probability values and the enrichment score for the cluster. Terms were selected that best represented all the terms in the cluster, of these the term with the highest gene count and lowest FDR score was reported.

Mouse	Term	Count	FDR	Enrichment Score
Control vs. Camptothecin up 8hr	GO:0005740~mitochondrial envelope	19	0.16	2.66
	mmu03010:Ribosome	10	0.07	2.5
	growth factor	10	1.10	2.26
	GO:0006350~transcription	54	0.45	2.11
	GO:0008270~zinc ion binding	59	1.29	1.84
Control vs. Camptothecin down 8hr	GO:0000279~M phase	42	<0.001	15.96
	GO:0005856~cytoskeleton	67	<0.001	8.00
	mmu04110:Cell cycle	15	0.005	4.46
	IPR001752:Kinesin, motor region	10	0.004	4.28
	GO:0005694~chromosome	28	0.005	3.80
Control vs. Chromium (vi) oxide up 8hr	mmu03010:Ribosome	22	<0.001	9.72
	GO:0005198~structural molecule activity	30	0.002	3.27
	GO:0044455~mitochondrial membrane part	9	0.04	2.98
	GO:0044455~mitochondrial membrane part	9	0.04	2.78
	GO:0006805~xenobiotic metabolic process	4	5.68	1.88
Control vs. Chromium (vi) oxide down 8hr	GO:0005925~focal adhesion	13	<0.001	5.16
	IPR001849:Pleckstrin homology	20	0.12	3.54
	domain:SH3	15	0.48	3.14
	GO:0030695~GTPase regulator activity	28	0.001	3.01
	GO:0016481~negative regulation of transcription	23	0.50	3.00
Control vs. Camptothecin up 48hr	Glycoprotein	202	<0.001	5.49
	GO:0044421~extracellular region part	62	<0.001	4.52
	IPR011993:Pleckstrin homology-type	28	0.057	3.96
	GO:0007155~cell adhesion	40	0.27	3.08
	GO:0043068~positive regulation of programmed cell death	25	0.04	2.82
Control vs. Camptothecin down 48hr	GO:0005694~chromosome	61	<0.001	18.79
	GO:0007049~cell cycle	55	<0.001	14.76
	GO:0006260~DNA replication	27	<0.001	14.45
	GO:0006281~DNA repair	26	<0.001	11.61
	GO:0000775~chromosome, centromeric region	19	<0.001	6.89
Control vs. Chromium (vi) oxide up 48hr	cell adhesion	16	2.85	2.15
	Glycoprotein	88	0.25	1.76
	IPR005816:Secreted growth factor Wnt protein	4	5.54	1.72
	lipid synthesis	7	8.65	1.67
	GO:0051781~positive regulation of cell division	5	5.56	1.54
Control vs. Chromium (vi) oxide down 48hr	Glycoprotein	139	<0.001	8.57
	GO:0044421~extracellular region part	53	<0.001	8.55
	GO:0030247~polysaccharide binding	13	0.05	3.56
	GO:0044420~extracellular matrix part	11	0.05	3.05
	GO:0006955~immune response	27	0.02	2.65

Table 4.11 Functional enrichment (FE) results for NMR and Mouse data for 8-hour vs. 48-hour control samples. Representative terms from the top five FE clusters, with corresponding gene counts and FDR-corrected probability values and the enrichment score for the cluster. Terms were selected that best represented all the terms in the cluster, of these the term with the highest gene count and lowest FDR score was reported.

Species	Comparison	Term	Count	FDR	Enrichment score
NMR	8hr control vs. 48hr control up	mmu04620:Toll-like receptor signalling pathway	8	0.12	2.09
		GO:0005886~plasma membrane	67	0.58	1.75
		Glycoprotein	63	3.34	1.57
		mmu04380:Osteoclast differentiation	8	0.86	1.56
		GO:0045087~innate immune response	10	12.61	1.45
	8hr control vs. 48hr control down	Glycoprotein	101	<0.001	5.85
		Cell membrane	71	<0.01	3.59
		GO:0030054~cell junction	27	1.25	2.62
		GO:0045211~postsynaptic membrane	13	1.19	2.52
		GO:0006811~ion transport	22	2.61	1.93
Mouse	8hr control vs. 48hr control up	Glycoprotein	223	<0.001	7.41
		GO:0005578~proteinaceous extracellular matrix	45	<0.001	6.83
		GO:0006260~DNA replication	22	<0.01	4.9
		DNA repair	33	0.04	3.91
		Copper	10	0.56	2.73
	8hr control vs. 48hr control down	IPR011993:Pleckstrin homology-like domain	41	0.04	3.02
		SH2 domain	16	0.18	2.99
		GO:0030054~cell junction	56	0.16	2.68
		domain:SH3	18	2.16	2.24
		GO:0007275~multicellular organism development	64	6.11	2.21

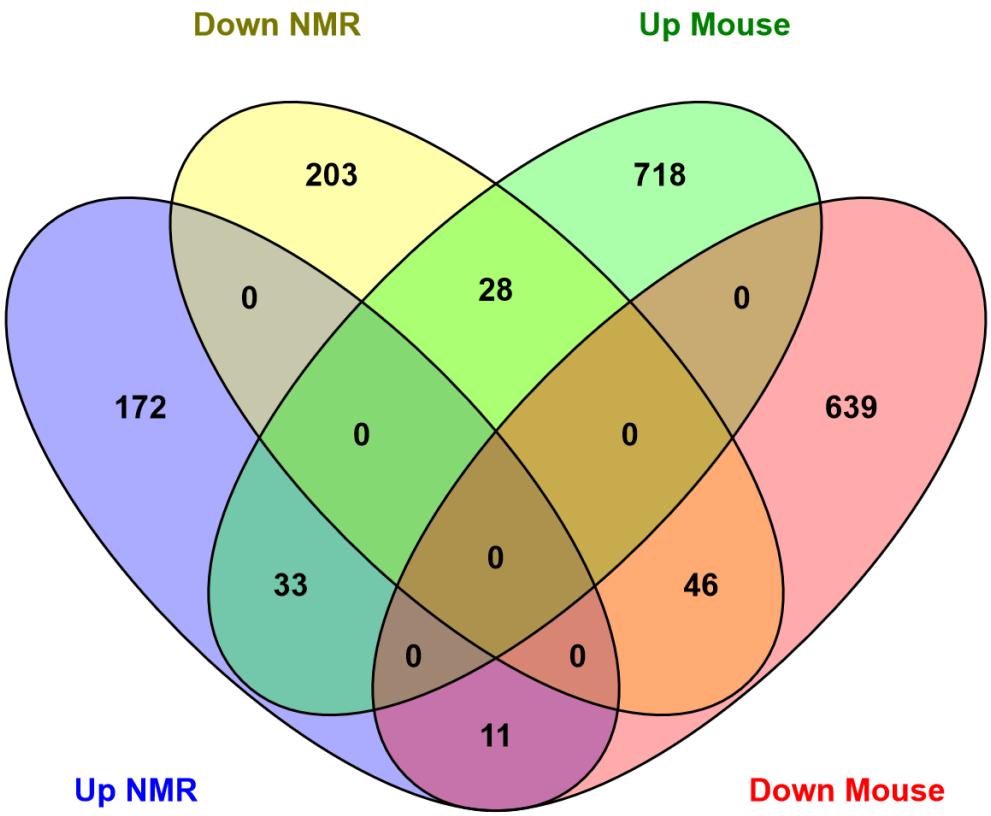

Figure 4.9 Venn diagram of differentially expressed homologous genes for 8-hour vs. 48-hour control comparisons in mouse and NMR (alpha stock).

4.4.2.2 Differential expression between genes with the greatest fold change

To identify genes with the largest fold change which may have an important role in responding to DNA damaging agents, the average fold change was calculated. This was done by averaging the fold change for each gene in which 2 or more of the primary cell cultures had at least 10 reads. The 10 genes with the highest and lowest fold change were selected (Table 4.12). Genes present in the top 10 genes from more than one condition particularly stand out for further analysis. These were *Hoxc10* (Homeoprotein C10), *Pik3r6* (Phosphoinositide-3-Kinase Regulatory Subunit 6), and *Muc5ac (*Mucin-5 Subtype AC, Tracheobronchial).

Table 4.12. The top 10 up and downregulated NMR genes and the average fold change. Star (*) indicates presence in more than one condition. Fold change calculated from normalised treated NMR sample read count over normalised untreated NMR sample read count.[o] indicates genes selected based off fold changes from 2 out of 3 cell lines.

Condition	Up	Fold change	Down	Fold change
cam 8hr	Pcdh10	10.42	Srrm4	-9.09
	Yjefn3	5.59	Nlgn4x	-7.69
	Ptchd2	5.40	St8sia1[o]	-6.67
	Hoxc10*	5.11	Fam5c	-6.67
	Tlr9[o]	4.20	Hnf4g	-5.88
	Slc16a5	4.13	Ksr2	-5.00
	Rpl3l	3.90	Adarb2	-4.76
	Gimd1[o]	3.47	Grm1[o]	-4.76
	Pou2af1	3.26	Pik3r6*[o]	-4.55
	Psd2	2.81	Arhgap20[o]	-4.55
chro 8hr	Zbtb16	11.68	Pik3r6*[o]	-4.17
	Znf536[o]	9.08	Kcna3	-3.70
	Efna5[o]	7.55	Rgs1[o]	-3.13
	Nme5[o]	6.20	Cntn3	-2.78
	Pax3[o]	5.92	Gltpd2	-2.70
	Prph	5.77	Clca2[o]	-2.70
	Hoxc10*	5.32	Sh3tc2[o]	-2.50
	Tbx22	5.28	Slc35f2[o]	-2.50
	Il3ra	5.09	Tek[o]	-2.38
	Syngap1[o]	4.95	Serpini1[o]	-2.33
cam 48hr	Grhl3	10.74	Tmem179[o]	-3.33
	Chst9	9.38	Tjp3	-2.94
	Itgbl1	8.92	Sox5	-2.86
	Clca2	8.75	Lpp	-2.78
	Kctd8	8.34	Muc5ac*[o]	-2.70
	Arhgef15[o]	7.10	Naaladl2	-2.56
	Rab3c	6.89	Glyat	-2.56
	Ppp1r1c	6.84	Dpp10	-2.50
	Ddx4[o]	6.81	Ca2[o]	-2.44
	Fpr1	6.72	Kcnip4	-2.38
chro 48hr	Nrk[o]	7.18	Muc5ac*[o]	-4.17
	Kiaa0226l[o]	3.62	Gpr128	-3.23
	Nol4[o]	3.59	Figf	-3.23
	Qrfp[o]	3.34	Pygm[o]	-3.13
	Gsg1	3.31	Slc9c2[o]	-3.13
	Ubap1l[o]	3.21	Zic4[o]	-2.94
	Trim55	3.07	Rd3[o]	-2.94
	Serpinb5[o]	2.95	Cd80	-2.78
	Il36g[o]	2.93	Scn3b[o]	-2.78
	Sbk2	2.81	Frzb	-2.78

Hoxc10 encodes one of the hox proteins that are transcription factors involved in the development of body axis in the embryo (435). It has been shown in HeLa cells that *Hoxc10* undergoes changes in expression that correlate with the cell cycle, accumulating in S phase, matching the expression of cyclin A (436). *Hoxc10* levels are subsequently reduced through ubiquitination and proteolysis at the proteasome. If this destruction failed to occur, the transition between metaphase and anaphase was delayed indicating that *Hoxc10* can act as a cell cycle regulator (436). As *Hoxc10* was upregulated at 8 hours in both treatments, it may be acting to halt the progression of the cell cycle to facilitate DNA damage repair (Table 4.12). *Hoxc10* only appeared upregulated in mouse cells 8 hours after camptothecin treatment. It is noteworthy that in Gabellini et al.'s study (436), northern blots were also undertaken that showed levels of *Hoxc10* mRNA was present at constant levels. Perhaps the change in expression seen here allows for fine tuning of this response.

Pik3r6 was downregulated in both treatments after 8 hours in NMR (Table 4.12). *Pik3r6* is a PI3K regulator protein thought to particularly regulate the $PI3K_{\gamma}$ (gamma) form. $PI3K_{\gamma}$ is thought to act on the immune system with $PI3K_{\gamma}$ mutants and drugs that target $PI3K_{\gamma}$ reducing inflammatory responses in mice (437). PI3K positively regulates cell cycle progression from G1 to S phase and G2 to M phase (438). Inhibition of PI3K results in G1 arrest or G2 arrest in synchronised cells when treated with the PI3K inhibitor LY294002 at S phase (439, 440). This may mean cell cycle progression is being blocked at either G1 or G2 and hence provide more time for accurate DNA damage repair. PI3K is involved in a wide array of signalling pathways that affect cell cycle progression, apoptosis, autophagy and DNA damage such as the FOXO or mTOR signalling pathways (441, 442). The downregulation of *Pik3r6* which is required for $PI3K_{\gamma}$ signalling may alter the activity of these processes in response to genotoxic stress in NMR. *Pik3r6* only appeared downregulated in mouse cells 8 hours after camptothecin treatment.

The upregulation of *Hoxc10* and downregulation of *Pik3r6* and hence potentially *Pi3k* both occurred after 8 hours post stimuli and indicate the cells may have been arresting at either G1 or G2.

Muc5ac is a major airway mucin that has been shown to be overexpressed in response to oxidative stress in human airway epithelial and fibroblasts as a result of ERK*1/2* signalling (443). *Muc5ac* is expressed in mouse embryonic fibroblasts (MEFs) in response to a number of toxic stimuli (444). This indicates that *Muc5ac* production is a typical stress response, but what the function of this protein would be for skin fibroblasts is not clear. *Muc5ac* was seen to be downregulated in both treatments after 48 hours (Table 4.12). This may indicate that the gene was upregulated at an earlier time point other than at 8 hours and hence was then downregulated to compensate for the high

protein levels. Alternatively, *Muc5ac* is constantly expressed and is specifically downregulated at 48 hours as part of the long-term cellular response.

To identify genes that may contribute to the NMR's DNA damage resistance the genes with the largest fold change were looked at more thoroughly in the established literature. In addition to these genes, any gene that is present in multiple conditions was also assessed. The DE genes between control and treated cells were input into venny (445) to produce Venn diagrams of overlapping gene expression (Figure 4.10-4.14). This allows us to pick out changes in expression that were specific to each treatment and time point and which changes occur as a general stress response in both treatments. In NMR cells, there were significantly more DE genes in common between treatments at the same time point (median of 9% of the total genes compared) than there were between time points under the same treatment (median of 2% of the total genes compared) ($U=0.00$, $p=0.029$, $N_1=N_2=4$). This indicates that the time post-treatment determines the cell's response more than the difference in genotoxic insult received. The presence of such common genes suggests a core response mechanism that changes over time. This does not appear to be the case in mouse cells, as no significant difference is observed in the proportion of genes in common between treatments at the same time point (median of 9% of the total genes compared) than there were between time points under the same treatment (median of 3% of the total genes compared) ($U=2$, $p=0.114$, $N_1=N_2=4$). However, it should be noted that the small sample size reduces the accuracy of this analysis.

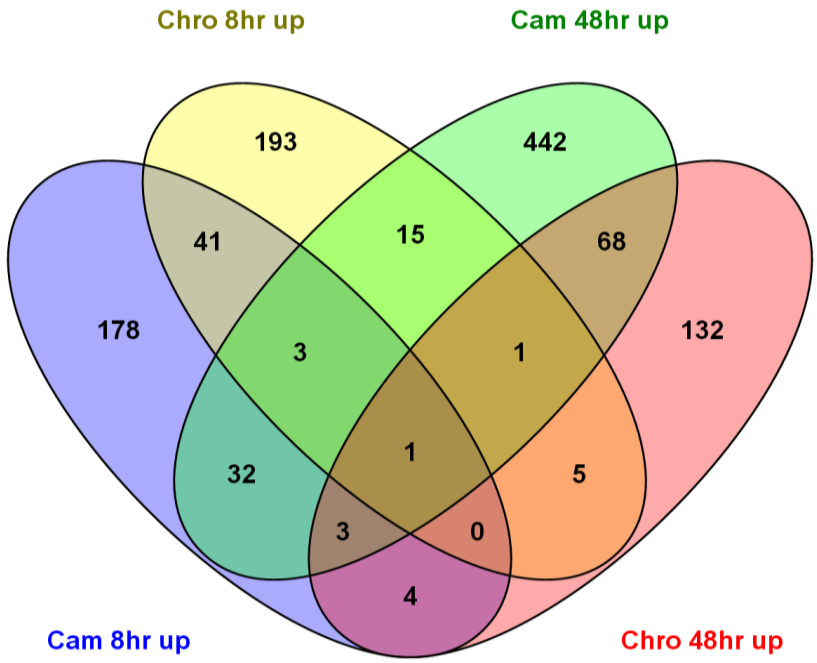

Figure 4.10. Number of genes that are upregulated between all treatments and time points as compared to controls in NMR skin fibroblasts (alpha stock). *Abbreviations: cam – camptothecin, chro – chromium (vi) oxide, hr – hours.*

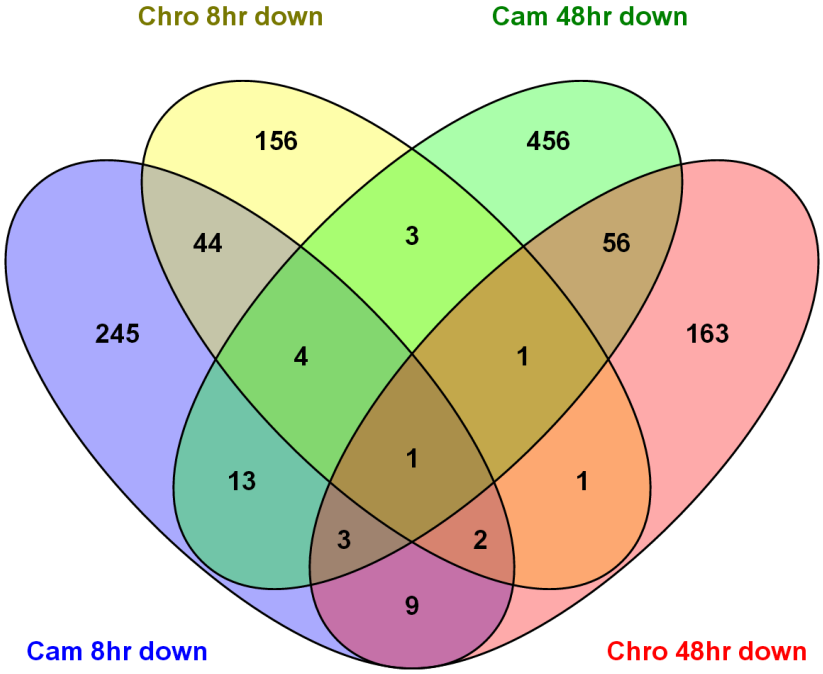

Figure 4.11. Number of genes that are downregulated between all treatments and time points as compared to controls in NMR skin fibroblasts (alpha stock). *Abbreviations: cam – camptothecin, chro – chromium (vi) oxide, hr – hours.*

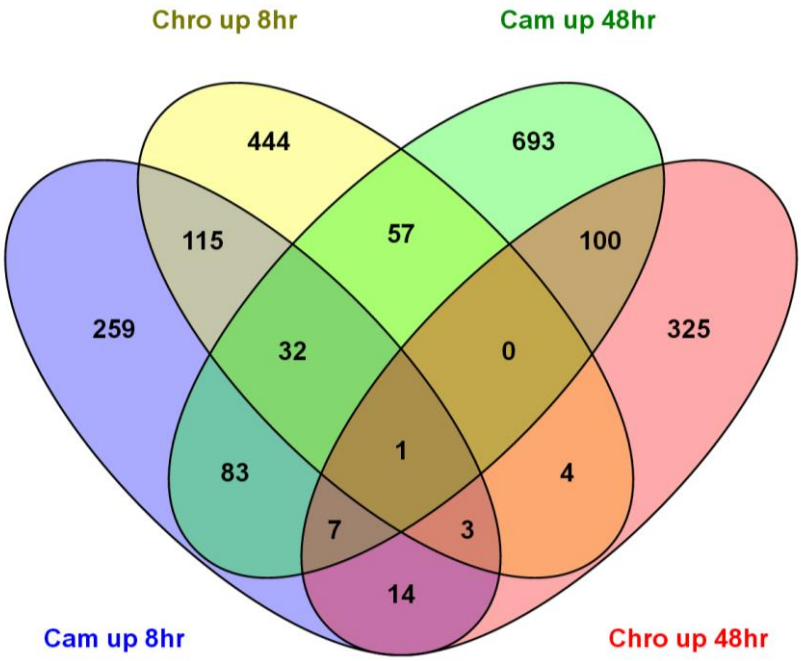

Figure 4.12. Number of genes that are upregulated between all treatments and time points as compared to controls in Mouse skin fibroblasts (alpha stock). *Abbreviations: cam – camptothecin, chro – chromium (vi) oxide, hr – hours.*

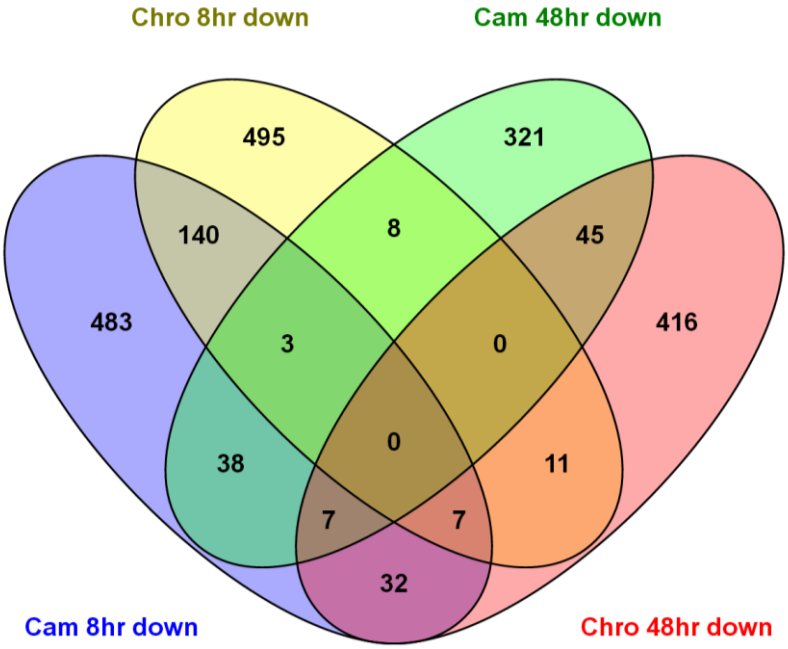

Figure 4.13. Number of genes that are downregulated between all treatments and time points as compared to controls in Mouse skin fibroblasts (alpha stock). *Abbreviations: cam – camptothecin, chro – chromium (vi) oxide, hr – hours.*

To identify genes that are important in a general response to genotoxic stress, genes that are either up or downregulated in three or more of the conditions and time points were selected (Table 4.13- 4.14).

Table 4.13. Upregulated NMR genes present in three or more conditions. Abbreviations: cam – camptothecin, chro – chromium (iv) oxide, hr – hours.

Conditions	Symbol	Gene name
cam 8hr, chro 8hr, cam 48hr and chro 48hr	Gpr19	G protein-coupled receptor 19
cam 8hr, chro 8hr and cam 48hr	Ptchd2	patched domain containing 2
	Liph	lipase, member H
	Cdkn1a	cyclin-dependent kinase inhibitor 1A (P21)
chro 8hr, cam 48hr and chro 48hr	Sag	S-antigen, retina and pineal gland (arrestin)
cam 8hr, cam 48hr and chro 48hr	Slc16a5	solute carrier family 16, member 5
	Rspo1	R-spondin homolog (Xenopus laevis)
	Crabp1	cellular retinoic acid binding protein I

Table 4.14. Downregulated NMR genes present in three or more conditions. Abbreviations: cam – camptothecin, chro – chromium (iv) oxide, hr – hours.

Conditions	Symbol	Gene name
cam 8hr, chro 8hr, cam 48hr and Chro 48hr	LOC101708733	
cam 8hr, chro 8hr and cam 48hr	LOC101726662	
	Sox5	SRY (sex determining region Y)-box 5
	Htr2c	5-hydroxytryptamine (serotonin) receptor 2C
	Grik2	glutamate receptor, ionotropic, kainate 2 (beta 2)
chro 8hr, cam 48hr and chro 48hr	LOC101711364	
cam 8hr, cam 48hr and chro 48hr	Oc90	otoconin 90
	LOC101719188	
	LOC101703905	
cam 8hr, chro 8hr and chro 48hr	Vstm2b	V- containing 2B
	Sox18	SRY (sex determining region Y)-box 18

Gpr19 (G protein-coupled receptor 19) was the only gene upregulated in all treatments in NMR cells (based on 2 out of 3 cell lines in 8-hour chromium treatment). *Gpr19* mRNA levels have been found to be high in both the germ cell layer of the developing embryo and in some lung cancers (446). Additionally, knockdown of *Gpr19* mRNA levels depressed cell growth indicating a pro proliferation activity (446). However, this knockdown caused cell death in lung cancer cells and resulted in polylobed cells which may indicate premature entry into mitosis and hence mitotic catastrophe (446, 447). This may indicate that *Gpr19* may serve as a checkpoint protein prior to mitosis; this is also supported by an increase in homologous repair when this gene is knocked down in human cells (448). High mRNA levels do not necessarily indicate high activity, and as *Gpr19* mRNA levels are regulated by the cell cycle, the high levels seen in all treatments may be a result of cell cycle arrest at a point when *Gpr19* mRNA levels are highly expressed. *Gpr19* mRNA expression peaks at s-phase but remains high through G2. Taken together these results indicate that NMR cells may be arresting at G2, potentially as an effect of Grp19 activity itself. There is also the possibility that high levels of *Gpr19* are priming the cell to proceed through mitosis if *Gpr19* is indeed a pro proliferation gene. Grp19 did not appear differentially expressed in any mouse comparisons.

Cdkn1a (p21) was upregulated after 8 hours in both treatments and after 48 hours in camptothecin-treated NMR cells (based on 3 out of 3 cell lines for all samples). Camptothecin treatment is known to upregulate p21 and upregulation of p21 provides resistance to camptothecin treatment in rat cells (449). It has been shown that p21-/- HCT116 cells have reduced viability when treated with hexavalent chromium (450) and BJ-hTERT fibroblasts show increased p21 expression after 8 hours post chromium treatment as seen in this study and levels are still elevated after 18 hours (451). p21 is a known cell cycle regulator and can induce cell cycle arrest at G1 through interactions with CDK1, CDK2, cyclin E and cyclin A (452, 453). Additionally, p21 null MEFs were significantly deficient in their ability to arrest growth at G1 in response to DNA damage (454). Arrest at G2 is also mediated by p21 by interactions with CDK-activating kinase and cyclin B1 (455, 456). Cyclins A2 and B1 degradation is promoted by p21 in response to DNA damage to maintain G2 arrest (457, 458). This indicates that NMR may be undergoing cell cycle arrest at either G1 or G2. Additionally, p21 is thought to contribute to DNA damage repair directly through interactions with PCNA to control base excision repair (BER), nucleotide excision repair (NER) and homologous recombination (459). The localisation of p21 in these cells would be interesting to identify, as cytoplasmic p21 protects against apoptosis and nuclear p21 may promote apoptosis, temporary cell cycle arrest or irreversible senescence (460, 461). In mouse cells, upregulation of p21 was only seen in camptothecin treatment at 48 hours (based on 2 out of 3 cell lines).

Grik2 (glutamate receptor, ionotropic, kainate 2) was downregulated in NMR cells 8 hours post-treatment with either compound and at 48 hours post camptothecin treatment (based on 2 out of 3 cell lines in 48-hour camptothecin treatment). In mouse cells, it was only downregulated at 48 hours post camptothecin treatment (based on 3 out of 3 cell lines). *Grik2* encodes a subunit of a kainate glutamate receptor. *Grik2* has been shown to be upregulated in p53 -/- mice (462) suggesting that p53 downregulates *Grik2*. *Grik2* has also been shown to be upregulated in old human skin fibroblasts when undergoing cellular stress, more so than younger fibroblasts exposed to the same stress (463). If we assume the cellular response of older cells is less effective than that of younger cells, this may suggest that decreasing *Grik2* levels may be advantageous. Levels of l-glutamate are increased in inflamed skin, and hence glutamate signalling may be important for mediating an inflammatory response (464). Chronic inflammation has been linked to premature ageing in part through the stabilisation of DNA damage (465), and hence alterations in inflammatory responses could be at play in the NMR's long lifespan. *Grik2* is predicted to be regulated by various miRNAs which are upregulated in ionising radiation and Resveratrol treatment in human cancer cells (466, 467).

Sox5 (SRY (sex determining region Y)-box 5) was downregulated in NMR cells 8 hours post either treatment and 48 hours post camptothecin treatment (based on 3 out of 3 cell lines for all samples). *Sox5* is active during mammalian development where it is thought to regulate proliferation through opposing the Wntβ-catenin pathway (468). Downregulation of *Sox5* reduced proliferation rates in human cancer cells (469). Taken together, these observations indicate that *Sox5* can act as a pro-proliferation gene, which may explain why it would be downregulated in response to the harmful stimuli. *Sox5* was also downregulated in mouse cells after 8 hours with either treatment (based on 2 out of 3 cell lines in 8-hour camptothecin treatment).

4.4.2.3 Rank product analysis

An alternative method to identify which genes are important was to find the rank product of each gene, essentially ranking the genes in order of fold change size, taking into account the fold change of each gene in each primary cell culture. The top 10 genes identified by this ranking are given in Table 4.15. These results were similar to the top 10 genes sorted by average fold change as would be expected. However, the results do vary, which may highlight important DE genes. One such gene was *Cdkn1c* (Cyclin-Dependent Kinase Inhibitor 1C also known as p57) which was upregulated at 8 hours in NMR under both treatments. P57 is a multifunctional protein that in part acts as a tumour suppressor inhibiting cyclin D1 and CDK2 (470) and hence acts similarly to p21. Of the genes present in the top ten genes from both methods *Hoxc10* stands out as it is present in the top ten upregulated genes at 8 hours in both treatments under both analysis methods.

Table 4.14. The top 10 up and downregulated NMR genes identified by rank product analysis. Estimated E-values are given. Star (*) indicates presence in more than one condition. Hash (#) indicates presence in the top 10 genes based on average fold change counts. Fold changed calculated from normalised treated NMR sample read count over normalised untreated NMR sample read count. o indicates averages based off fold changes from 2 out of 3 cell lines.

Condition	up	E-value	down	E-value
cam 8hr	Pcdh10#	0	Adarb2#	0
	Yjefn3#	0	Grip1	0
	Rpl3l#	0	Zfpm2	0
	Psd2#	0	Kcnh8	0
	Gimd1#	0.1	Fam71e2	0.1
	Cdkn1c	0.4	Pou6f2	0.1
	Ptchd2#	0.5	Sox5*#	0.1
	Onecut2	0.5	Klhl1	0.1
	Hoxc10*#	0.8	Eya1	0.1
	Ckm	1	Erbb4	0.2
chro 8hr	Tmem150c	2	Cntn3#	0.2
	Stap1	2.2	Nlgn4x#	0.4
	Fcrla	2.9	Cdh12	1.6
	Panx2	3.7	Ptprr	2.2
	Hoxc10*#	4	Grm1#	2.3
	Fam83e	4.6	Srrm4#	2.9
	Rfx4	4.6	Nell1	3.1
	Tlcd2	4.6	Reln	3.3
	Evpl	6	Sh3gl3	3.9
	Syngap1#	6	Dach1	4.9
cam 48hr	Grhl3#	0	Sox5*#	0.1
	Clca2#	0	Lpp#	0.1
	Ascl2	0.1	Dpp10#	0.3
	Col17a1	0.1	Naaladl2#	0.3
	Slc16a5	0.2	Kcnv2	0.3
	Itgbl1#	0.3	Kcnip4#	0.4
	Kcnma1	0.3	Cacna1c	1
	Chst9#	0.4	Adam12	1.1
	Cacna2d4	0.4	Kcnmb2	1
	Ehf	0.4	Kif26b	1.1
chro 48hr	Gsg1#o	0.1	Arr3	0.1
	Adcy8	0.4	Cldn6	0.4
	Trim55#	0.4	St6galnac5	0.4
	Gpr19	0.6	Lmx1a	0.6
	Luzp2	1.3	Hdc	0.8
	Masp1	1.4	Mmp25	4.5
	Ptpro	2.6	Lrrc3	4.5
	Znf385b	2.9	Dnhd1	4.7
	Serpinb2	3.1	Coch	4.8
	Cspg5	3.7	Kcnh3	5.4

4.4.2.4 Differential expression between genes with high read counts

Though these genes stand out for their presence in multiple groups, it is important to consider the reliability of the data. Small changes in gene expression may well have large and important effects but the smaller the number of reads the more likely the difference is simply down to chance. If we employed an arbitrary cut off of 500 reads, we found only p21 remains from our selected genes with around 1,000-3,000 reads depending on the sample. *Sox5*, *R3hcc1* and *Grik2* can also be considered as they had only slightly less than 500 with around 100-400 reads in the samples.

By applying the arbitrary cut off of 500 reads to the whole data set, we can select for genes that we are more confident are undergoing the fold change the data suggests (Figure 4.14-4.17). For NMR we found a total of 34 genes upregulated and 262 genes downregulated from all conditions. With at least 500 reads and in mice we find 399 genes upregulated and 467 downregulated. NMR genes DE in more than one treatment were selected (Table 4.16-4.17). Two of these genes, *Dpp10 (*Dipeptidyl Peptidase Like 10) and *Serpinb2* (Serpin Family B Member 2), were also present in the top ten genes selected by the rank product analysis (Table 4.15).

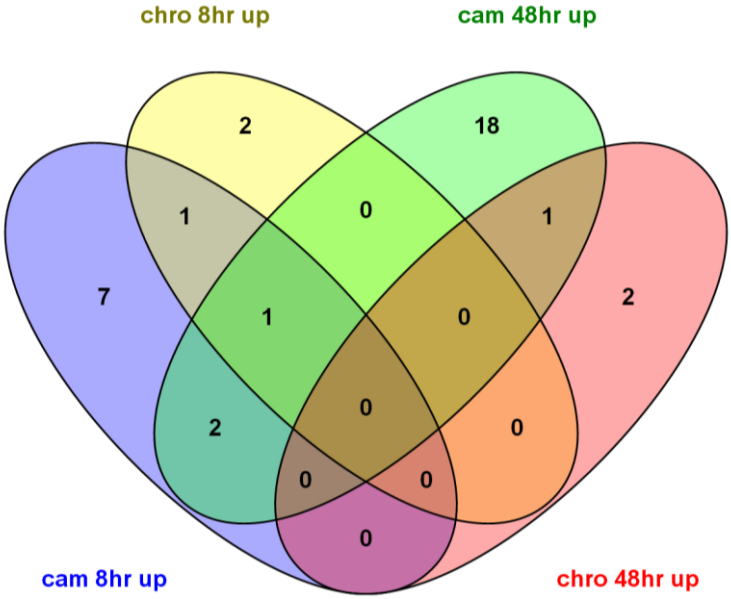

Figure 4.14. Number of genes that are upregulated between all treatments and time points as compared to controls and have at least 500 reads in NMR skin fibroblasts (alpha stock). Abbreviations: cam – camptothecin, chro – chromium (vi) oxide, hr – hours.

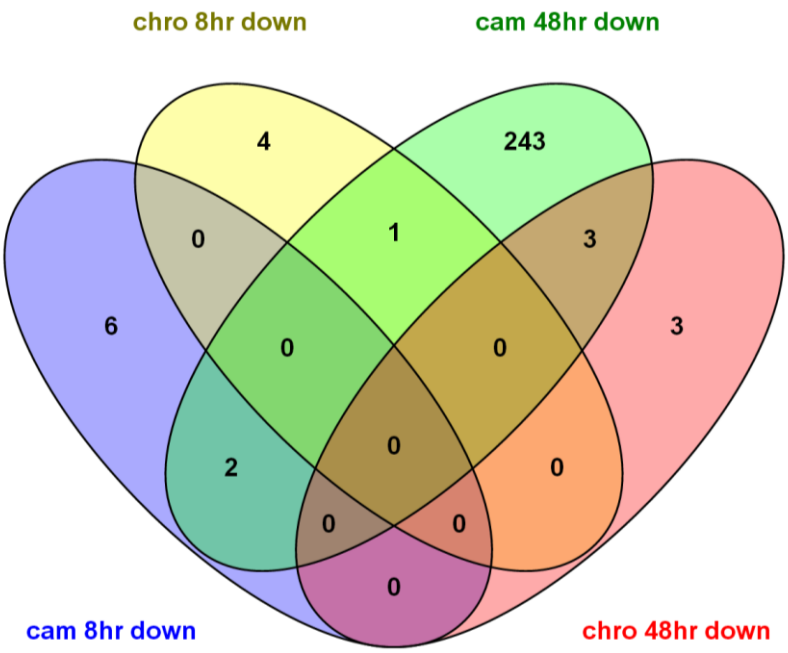

Figure 4.15. Number of genes that are downregulated between all treatments and time points as compared to controls and have at least 500 reads in NMR skin fibroblasts (alpha stock). Abbreviations: cam – camptothecin, chro – chromium (vi) oxide, hr – hours.

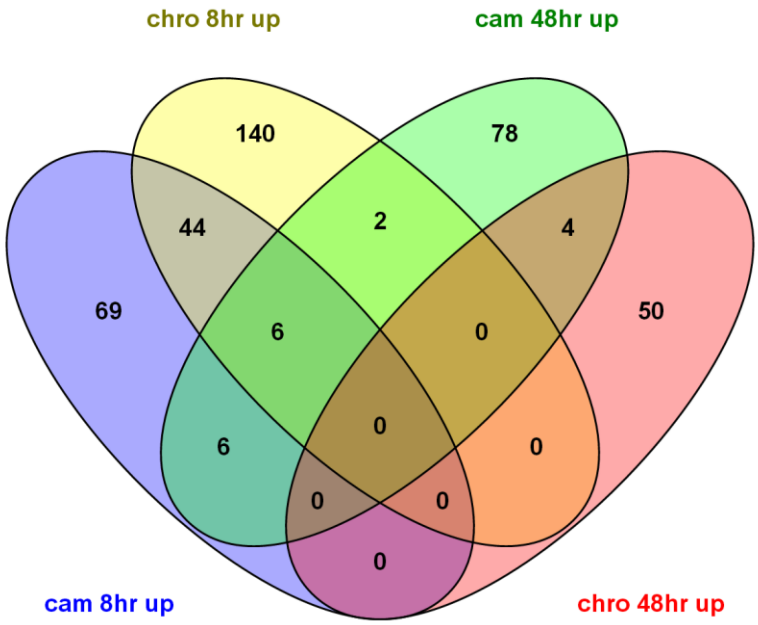

Figure 4.16. Number of genes that are upregulated between all treatments and time points as compared to controls and have at least 500 reads in mouse skin fibroblasts (alpha stock). Abbreviations: cam – camptothecin, chro – chromium (vi) oxide, hr – hours.

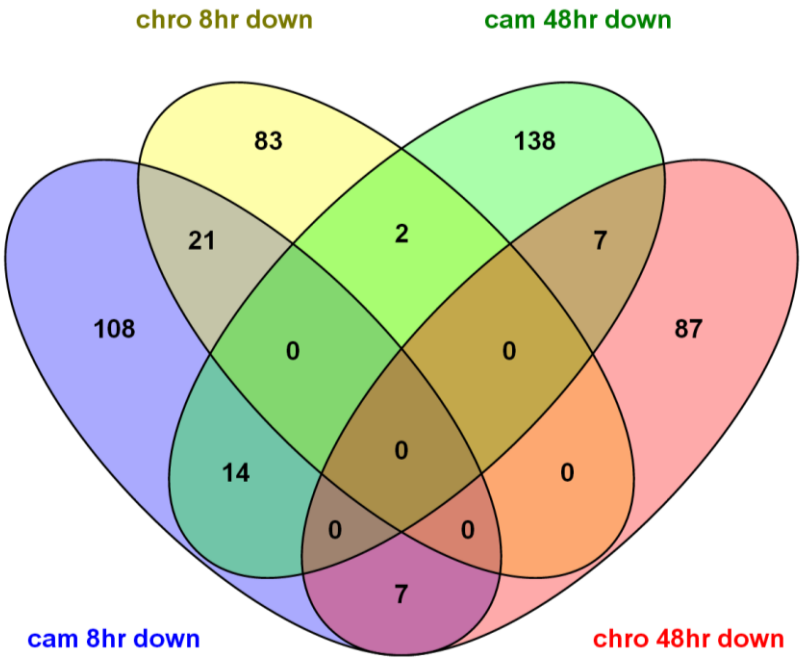

Figure 4.17. Number of genes that are downregulated between all treatments and time points as compared to controls and have at least 500 reads in mouse skin fibroblasts (alpha stock). Abbreviations: cam – camptothecin, chro – chromium (vi) oxide, hr – hours.

Table 4.16. Upregulated NMR genes present in two or more conditions with at least 500 reads. Abbreviations: cam – camptothecin, chro – chromium (iv) oxide, hr – hours.

Conditions	Symbol	Gene name
cam 8hr, chro 8hr, cam 48hr	Cdkn1a	cyclin-dependent kinase inhibitor 1A (P21)
cam 8hr, chro 8hr	Phlda1	pleckstrin homology-like domain, family A, member 1
cam 8hr, cam 48hr	Il8	chemokine (C-X-C motif) ligand 15
	Rrm2	ribonucleotide reductase M2
cam 48hr, chro 48hr	Serpinb2	serine (or cysteine) peptidase inhibitor, clade B, member 2

Table 4.17. Downregulated NMR genes present in two or more conditions with at least 500 reads. Abbreviations: cam – camptothecin, chro – chromium (iv) oxide, hr – hours.

Conditions	Symbol	Gene name
cam 8hr, cam 48hr	Mbnl1	muscleblind-like 1 (Drosophila)
	Smurf2	SMAD specific E3 ubiquitin protein ligase 2
cam 48hr, chro 48hr	Dpp10	dipeptidylpeptidase 10
	Foxo1	forkhead box O1
	Hspg2	perlecan (heparan sulfate proteoglycan 2)
chro 8hr, cam 48hr	Cadm2	cell adhesion molecule 2

Dpp10 was downregulated 48 hours post-treatment with either camptothecin or chromium (vi) oxide in NMR cells only (based off 3 out of 3 cell lines). *Dpp10*, the Dipeptidyl peptidase 10 lacks peptidase enzymatic active and modulates the activity of the potassium channel Kv4.2, increasing its ability to transport potassium ions without changes in protein level (471). Kv4.2 has been associated with youthful skin ageing through a genome-wide association study. However, this expression was suggested to be in Langerhans cells as opposed to skin fibroblasts (472). Cells' permeability to potassium changes throughout the cell cycle being lowest at g2-m phase (473, 474). A decrease in *Dpp10* and hence Kv4.2 permeability may be indicative of cell cycle arrest at G2. *Dpp10* was not differentially expressed in mouse cells.

Serpinb2 was upregulated 48 hours post-treatment with either camptothecin or chromium (VI) oxide in NMR cells only (based off 3 out of 3 cell lines). *Serpinb2* is a member of the clade B family of serine protease inhibitors. It is one of the most upregulated genes in response to cellular stress and required for effective autophagy (475). *Serpinb2* may aid the maintenance of the cell's proteome which may help confer resistance to the DNA damaging stimuli used in this study. *Serpinb2* may also reduce cancer metastasis (476) which may contribute to the NMR's cancer resistant phenotype. *Serpinb2* was not differentially expressed in mouse cells.

Interestingly, *Foxo1* also appeared downregulated 48 hours after treatment with either camptothecin or chromium (vi) oxide (based off 2 out of 3 cell lines for 48-hour chromium sample). *Foxo1* has been shown to increase p21 expression when *Foxo1* expression is increased either through fasting or experimental overexpression (477, 478). This is the opposite of our results that indicate that p21 is upregulated even after 48 hours post camptothecin treatment at which point *Foxo1* appears downregulated. *Foxo1* can act as a pro-apoptotic gene regulated by cyclin-dependent kinase 1 and 2 (479, 480) and can promote cell cycle arrest at G1/S through interactions with smad proteins (481). *Foxo1* has been implicated in the antineoplastic effect of caloric restriction in mice and is required for the lifespan extension of daf-2 and AGE-1 mutant in *C. elegans* (85, 92). *Foxo1* was downregulated in mouse cells after 8 hours post camptothecin treatment (based off 2 out of 3 cell lines).

The genes examined in more detail are only a small subset of the total gene expression profiles. However, when taken together, they do show a similar theme of cell cycle regulation that was not detected by the FE analysis. This cell cycle regulation was seen in genes from 8 and 48 hours post stimuli. Additionally, we saw some genes known to be upregulated in cellular stress either in general or as has been specifically seen in camptothecin and/or chromium (vi) oxide treatment. This

would suggest that NMR cells undergo cell cycle arrest to a greater extent or for a longer period than mouse cells. It is not clear at what point of the cell cycle the cells are arresting as genes involved in G1 and G2 arrest were differentially expressed.

4.4.2.5 Differential expression between species

Deseq (407) was used to analyse the RNAseq data between species. There was a large number of differentially expressed genes between the two species as we would expect (on average 6,635 genes between all treatments) however there was very little variation between the number of differentially expressed genes in each treatment (total range of 199 genes) (Table 4.18). This may be a result of the high variation seen between primary cell cultures as discussed above. A large number of the differentially expressed genes were found to be consistently differentially expressed across treatments (Figure 4.18). There were 2,719 genes consistently upregulated, and 2,357 genes consistently downregulated in all 8hour samples. In the 48-hour samples, there were 2,713 genes consistently upregulated, and 2,428 genes consistently downregulated. The differentially expressed genes in the control sample can be thought to represent the base transcriptomic difference between the two species.

Table 4.18. The number genes up (↑) or down (↓) regulated in NMR cells compared to mouse cells for different treatments and time points. Genes significant at the 0.05 level after correcting for multiple testing.

	Control	Camptothecin	Chromium (vi) oxide
8hr	3,437↑ 3,107↓	3,630↑ 3,074↓	3,570↑ 3,103↓
48hr	3,618↑ 3,077↓	3,564↑ 3,122↓	3,328↑ 3,177↓

To better identify biological activity, a functional enrichment was performed using David (Table 4.19-4.20) (330, 426). As there were too many genes to allow for the generation of functional clusters, enriched GO terms were analysed instead.

Enriched GO terms for upregulated genes showed a large amount of similarity for all 8-hour treatments and 48-hour control samples (Table 4.19). This may indicate that 8 hours after the stimulus was not long enough for cells to show a significant transcriptional response, that the two species initially responded similarly, or that variations in cellular response were obscured by the large differences in gene expression already present between the two species. These samples showed upregulation of genes involved in the membrane. Terms such as ‘GO:0044459~plasma membrane

part' and 'GO:0016021~integral to membrane' are significantly enriched in all of these conditions indicating significant variations between species in terms of the cell membrane. Downregulated terms for these conditions (Table 4.20), with the exception of 8-hour post chromium treatment, also showed a large similarity. Terms such as 'GO:0007049~cell cycle' and 'GO:0000278~mitotic cell cycle' repeatedly appeared indicating changes within the cell cycle between the two species. This may be a result of the different growth rates of the two species. Samples of 8-hour post chromium treatment were more distinct from the above but did show some overlap in terms with 'GO:0031974~membrane-enclosed lumen' in this sample and both the control samples.

Samples analysed 48 hours after treatment with camptothecin showed terms regarding DNA replication and cell cycle progression enriched for both up and downregulated genes (Table 4.19-4.20). This may be indicative of a DNA damage response resulting in different progression through the cell cycle and may indicate cell cycle arrest preventing mitosis. Differences in such processes may underlie the NMR's increased survival.

Samples analysed 48 hours after treatment with chromium (vi) oxide showed few terms enriched for up or downregulated genes that are statistically significant (Table 4.19-4.20). The only term that is significant 'GO:0019898~extrinsic to membrane' was enriched in downregulated genes. Other not statistically significant terms also refer to the membrane. Taken together, this indicates differences between the two species in terms of their cellular surface.

Table 4.19. The top 5 most significant GO terms from the functional enrichment of upregulated genes for each treatment. Comparisons of mouse vs. NMR. NMR – Naked mole rat.

Treatment	GO term	Count	FDR
8hr Control Mouse vs. NMR up	GO:0005509~calcium ion binding	224	1.49E-03
	GO:0030054~cell junction	142	8.32E-03
	GO:0044459~plasma membrane part	374	9.44E-03
	GO:0044456~synapse part	76	1.10E-02
	GO:0016021~integral to membrane	912	1.99E-02
8hr camptothecin Mouse vs. NMR up	GO:0031224~intrinsic to membrane	1,037	2.48E-5
	GO:0016021~integral to membrane	992	4.44E-5
	GO:0005509~calcium ion binding	238	1.13E-4
	GO:0044456~synapse part	83	9.00E-4
	GO:0044459~plasma membrane part	401	0.002
8hr chromium Mouse vs. NMR up	GO:0031224~intrinsic to membrane	1,021	4.07E-06
	GO:0016021~integral to membrane	979	4.13E-06
	GO:0005509~calcium ion binding	228	0.004458
	GO:0044456~synapse part	78	0.012723
	GO:0044459~plasma membrane part	386	0.014098
48hr Control Mouse vs. NMR up	GO:0005509~calcium ion binding	239	7.17E-05
	GO:0016021~integral to membrane	980	1.04E-04
	GO:0031224~intrinsic to membrane	1,016	5.46E-04
	GO:0044459~plasma membrane part	389	2.35E-02
	GO:0007155~cell adhesion	155	4.49E-02
48hr camptothecin Mouse vs. NMR up	GO:0006260~DNA replication	65	6.82E-09
	GO:0007049~cell cycle	191	1.95E-08
	GO:0006259~DNA metabolic process	136	8.35E-08
	GO:0031974~membrane-enclosed lumen	305	2.51E-06
	GO:0043233~organelle lumen	292	2.66E-05
48hr chromium Mouse vs. NMR up	GO:0044456~synapse part	71	0.114035
	GO:0005509~calcium ion binding	206	0.146838
	GO:0016021~integral to membrane	878	0.198614
	GO:0008066~glutamate receptor activity	17	0.238145
	GO:0005261~cation channel activity	76	0.358067

Table 4.20. The top 5 most significant GO terms from the functional enrichment of downregulated genes for each treatment. Comparisons of mouse vs. NMR. NMR – Naked mole rat.

Treatment	GO term	Count	FDR
8hr Control Mouse vs. NMR down	GO:0007049~cell cycle	179	8.77E-06
	GO:0031974~membrane-enclosed lumen	302	3.23E-05
	GO:0000278~mitotic cell cycle	85	3.98E-04
	GO:0005739~mitochondrion	286	8.87E-04
	GO:0043233~organelle lumen	286	9.69E-04
8hr camptothecin Mouse vs. NMR down	GO:0007049~cell cycle	195	1.30E-10
	GO:0006259~DNA metabolic process	134	7.46E-08
	GO:0000278~mitotic cell cycle	94	1.27E-07
	GO:0006260~DNA replication	61	3.68E-07
	GO:0051301~cell division	99	5.03E-07
8hr chromium Mouse vs. NMR down	GO:0000166~nucleotide binding	499	2.60E-17
	GO:0031974~membrane-enclosed lumen	302	3.08E-16
	GO:0043232~intracellular non-membrane-bounded organelle	439	9.72E-15
	GO:0043228~non-membrane-bounded organelle	439	9.72E-15
	GO:0043233~organelle lumen	288	2.10E-14
48hr Control Mouse vs. NMR down	GO:0007049~cell cycle	193	4.99E-10
	GO:0000278~mitotic cell cycle	90	4.54E-06
	GO:0031974~membrane-enclosed lumen	301	7.29E-06
	GO:0043232~intracellular non-membrane-bounded organelle	420	1.50E-05
	GO:0043228~non-membrane-bounded organelle	420	1.50E-05
48hr camptothecin Mouse vs. NMR down	GO:0006260~DNA replication	65	6.82E-09
	GO:0007049~cell cycle	191	1.95E-08
	GO:0006259~DNA metabolic process	136	8.35E-08
	GO:0031974~membrane-enclosed lumen	305	2.51E-06
	GO:0043233~organelle lumen	292	2.66E-05
48hr chromium Mouse vs. NMR down	GO:0019898~extrinsic to membrane	234	4.08E-04
	GO:0005794~Golgi apparatus	328	0.166067
	GO:0016192~vesicle-mediated transport	231	0.43551
	GO:0042995~cell projection	274	0.369391
	GO:0044459~plasma membrane part	667	0.779626

There was a large overlap in gene expression between control and treated samples with an average of 5,670 genes (~77%) shared between each treatment and its appropriate control (Figure 4.18). These overlapping genes were excluded, and the functional enrichment analysis was repeated in the hope of identifying important differences in responses to DNA damaging stimuli between mouse and NMRs. There were very few significantly enriched go terms and due to the lower number of genes a functional clustering analysis could be performed (Table 4.21). Additionally, a Venn diagram of genes differentially expressed under control conditions at 8 or 48 hours between the species was produced

(Figure 4.19). Here we saw the majority of the differentially expressed genes were conserved over time with no genes switching between being over or underexpressed.

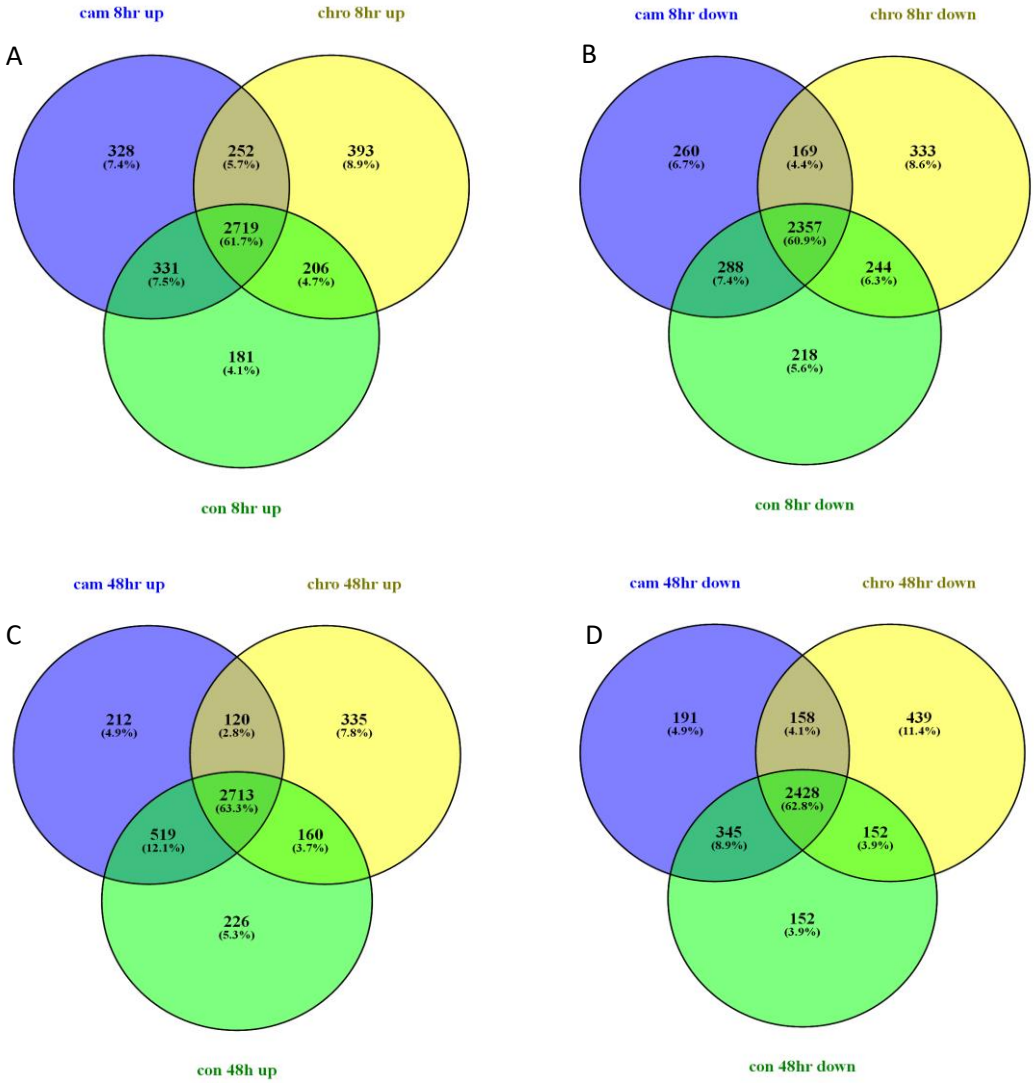

Figure 4.18. Venn diagrams of significantly (p<0.05) differentially expressed genes derived from comparisons between mouse and NMR in each of the labelled conditions. A) Upregulated genes in each treatment after 8 hours post-treatment. B) Downregulated genes in each treatment after 8 hours post-treatment. C) Upregulated genes in each treatment after 48 hours post-treatment. D) Downregulated genes in each treatment after 48 hours post-treatment.

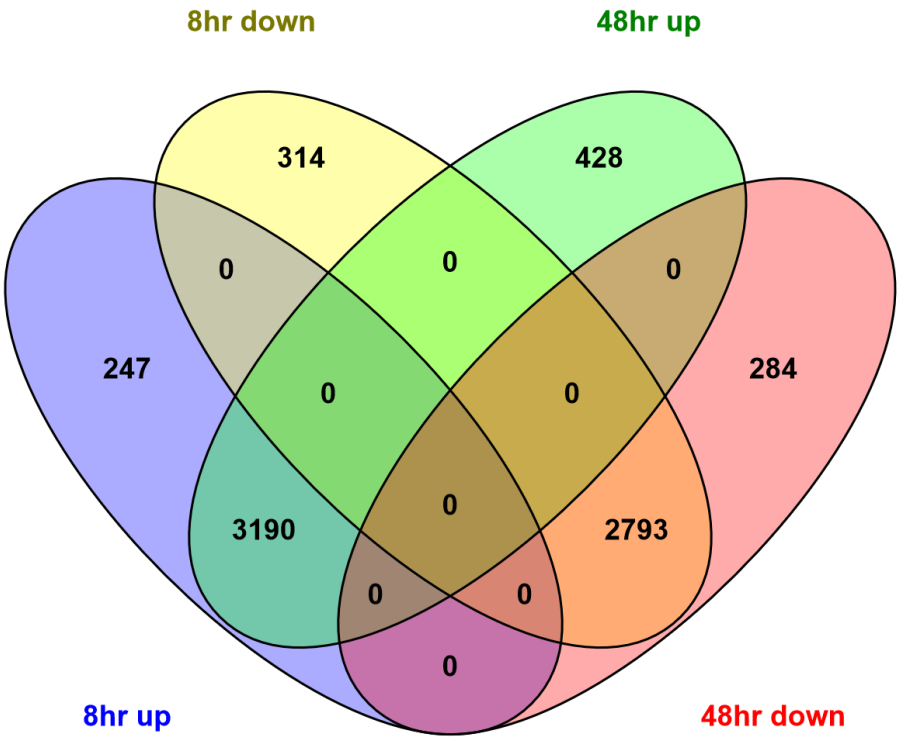

Figure 4.19. Venn diagram of genes up and downregulated between NMR and mice under control conditions after 8 and 48 hours.

Table 4.21. Functional enrichment (FE) results for either up or downregulated genes between mouse and NMR under the stated treatments. Genes found to be differentially expressed in control samples were removed from the gene lists used in this assay. Representative terms from the top five FE clusters, with corresponding gene counts and FDR-corrected probability values and the enrichment score for the cluster. Terms were selected that best represented all the terms in the cluster, of these the term with the highest gene count and lowest FDR score was reported.

Treatment	Term	Count	FDR	Enrichment Score
cam 8hr up	GO:0015031~protein transport	43	0.20	2.48
	GO:0006811~ion transport	39	0.46	1.56
	GO:0008092~cytoskeletal protein binding	25	10.72	1.29
	GO:0007267~cell-cell signalling	16	78.91	1.22
	GO:0050804~regulation of synaptic transmission	8	63.74	1.19
cam 8hr down	GO:0007049~cell cycle	34	0.38	2.91
	GO:0005694~chromosome	19	1.59	2.74
	domain:SH3	13	2.97	1.98
	GO:0015630~microtubule cytoskeleton	21	4.40	1.8
	IPR001849:Pleckstrin homology	15	18.17	1.69
chro 8hr up	GO:0031224~intrinsic to membrane	206	0.04	4.01
	Glycoprotein	158	0.41	2.09
	GO:0005887~integral to plasma membrane	30	5.61	1.89
	IPR000306:Zinc finger, FYVE-type	5	42.94	1.35
	IPR002110:Ankyrin	15	53.22	1.34
chro 8hr down	IPR001849:Pleckstrin homology	22	0.21	3.61
	sh3 domain	16	3.68	2.17
	GO:0030705~cytoskeleton-dependent intracellular transport	6	9.22	2.13
	domain:Ras-associating	6	6.31	2.02
	GO:0005856~cytoskeleton	47	3.36	2
cam 48hr up	GO:0005794~Golgi apparatus	26	3.53	2.49
	GO:0005773~vacuole	10	18.44	1.9
	GO:0042995~cell projection	17	1.84	1.62
	GO:0008092~cytoskeletal protein binding	16	29.75	1.4
	GO:0044463~cell projection part	7	70.12	1.38
cam 48hr down	sh3 domain	14	0.81	3.03
	GO:0031981~nuclear lumen	30	5.73	1.67
	IPR001715:Calponin-like actin-binding	6	16.55	1.55
	GO:0046872~metal ion binding	88	35.47	1.53
	GO:0002520~immune system development	14	22.00	1.42
chro 48hr up	GO:0043228~non-membrane-bounded organelle	68	6.37	2.11
	GO:0000502~proteasome complex	7	9.72	1.9
	GO:0005739~mitochondrion	43	48.51	1.63
	repeat:BNR 4	3	25.44	1.54
	GO:0006260~DNA replication	8	80.81	1.21
chro 48hr down	cell adhesion	31	0.04	3.58
	IPR001849:Pleckstrin homology	22	2.70	2.65
	sh3 domain	18	3.51	2.18
	GO:0032403~protein complex binding	9	12.90	1.99
	GO:0019838~growth factor binding	10	3.88	1.96

Though the enrichment scores for the clusters were still high (>1.3) few or no terms within the clusters were individually significant (Table 4.21).

Camptothecin-treated cells analysed after 8 hours contained a number of upregulated clusters that together suggest the release of signalling molecules from the cell. These terms either relate directly to transport of ions or protein (e.g. 'GO:0015031~protein transport'), the process by which they are moved (e.g. 'GO:0008092~cytoskeletal protein binding') or the process by which they are released or detected (e.g. 'GO:0007267~cell-cell signalling'). Downregulated genes form clusters that refer to the cell cycle either directly or indirectly, suggesting NMR cells decrease proliferation after genotoxic insult, in agreement with previously reported data (179). Downregulated terms also included terms regarding Pleckstrin homology and SH3 protein domains. These protein domains are found in many proteins involved in signal transduction or the cytoskeleton (427, 428).

Chromium treated cells analysed after 8 hours showed upregulated genes that produce functional clusters regarding the cell membrane including 'GO:0031224~intrinsic to membrane', the only term that was statistically significant in this treatment. As with camptothecin treatment, we saw terms regarding Pleckstrin homology and SH3 protein domains. Additionally, clusters regarding cellular transport via the cytoskeleton were differentially expressed.

At 48 hours post camptothecin treatment, terms such as 'GO:0005794~Golgi apparatus' and 'GO:0005773~vacuole' were upregulated suggesting increased protein synthesis and degradation. Terms regarding cellular projections and the cytoskeleton were also upregulated. These clusters included genes such as *Myo1c* (Myosin IC), a molecular motor protein involved in intracellular transport, and *Ezr* (Ezrin), a protein-tyrosine kinase substrate that acts as an intermediate between the plasma membrane and cytoskeleton and may be important for cell adhesion (482). Downregulated clusters again contained terms regarding the cytoskeleton such as 'sh3 domain' and 'IPR001715:Calponin-like actin-binding' but also terms regarding the nuclear lumen and ion transport. Terms regarding the immune system potentially indicating a general stress response were also downregulated.

At 48 hours post chromium treatment, a variety of terms are upregulated. The cluster with the highest score that contained the term 'GO:0043228~non-membrane-bounded organelle' also contained the term 'GO:0005856~cytoskeleton', indicating that these genes are primarily related to the cytoskeleton. Terms such as 'GO:0000502~proteasome complex' may indicate protein turn over and the terms such as 'GO:0005739~mitochondrion' may indicate changes in energy homeostasis or may relate to apoptosis. Downregulated genes produced clusters regarding the outside of the cell,

such as cell adhesion, and growth factor binding, as well as terms regarding Pleckstrin homology and SH3 protein domains which are downregulated in most conditions.

In summary, this analysis seemed to suggest that mice and NMR under control conditions differ greatly in terms of the cell membrane with many up and downregulated terms regarding the cell surface. When we factored out genes seen as differentially expressed in control conditions we see that initially (8 hours) after treatment NMR cells show further increases in membrane-associated terms further supporting the significance of the membrane. These membrane terms seem to be more related to cellular signalling but include genes involved in cell adhesion. Proliferation was downregulated in NMRs, and so were aspects of the cytoskeleton which may have been a result of reduced mitosis. These differences in the membrane may have served to protect the NMR cells by increasing harmful compound efflux or decrease its uptake. This has been shown to be the most common reason for drug resistance in tumours (483) through changes in transporter activity or expression of uptake inhibiting glycoproteins (484). Alternatively, it has been suggested that membrane alterations can induce stress signalling and accumulation of heat shock proteins in or on cell membranes to correct misfolded proteins and alter the membrane structure (485, 486). Reduced proliferation may provide NMR cells more time to repair and respond to the treatment. Later (48 hours post stimuli), there seems to be an increase in protein synthesis and turnover in NMRs compared to mice. This may be to replace damaged proteins or may be indicative of a wider response. Downregulation of cytoskeleton components may also suggest reduced proliferation or motility in these cells. Taken together the results suggest activity at the membrane as a major component concerning observed differences between the NMR and mouse with potential importance of increased protein synthesis and turnover as part of the long-term response or recovery of these cells.

4.4.2.6 Differences in DNA damage associated genes

To identify if genes involved in DNA repair are more expressed in NMR than mouse a list of 136 genes involved in DNA repair were compiled from (193) and REPAIRtoire, a database of DNA repair pathways (487). More of these genes appeared upregulated in mice (Table 4.22). By performing a Wilcoxon paired sample signed-rank test (performed in SPSS version 22.0) on these genes that were differentially expressed (Appendix Table 3), we find that they were expressed significantly higher in 48-hour control and in both 8 and 48-hour camptothecin-treated mouse samples (Figure 4.20).

Table 4.22. The number of DNA repair genes up (↑) or down (↓) regulated in NMR cells compared to mouse cells for different treatments and time points. Genes significant at the 0.05 level, after correcting for multiple testing.

	Control	Camptothecin	Chromium (vi) oxide
8hr	35↑ 46↓	32↑ 56↓	39↑ 47↓
48hr	36↑ 51↓	33↑ 55↓	40↑ 42↓

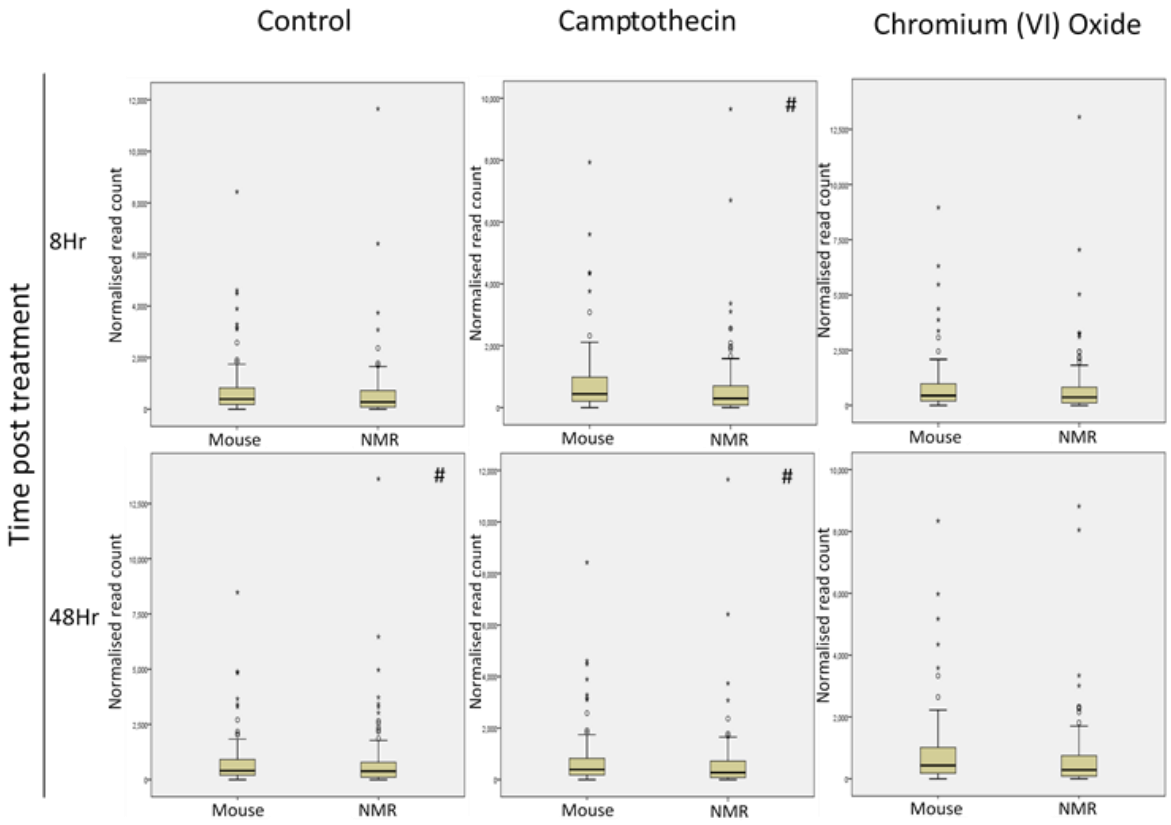

Figure 4.20. Normalised gene expression of 136 genes involved in DNA repair. These genes were identified from (193) and REPAIRtoire (487). Circles indicate outliers (1.5 to 3 times the interquartile range out) and stars indicate far outliers (greater than 3 times the interquartile range out). Hash (#) indicates statistically significant levels of gene expression between mouse and NMR as determined by Wilcoxon paired sample signed-rank test (performed in SPSS version 22.0). Controls after 48 hours post-treatment and both camptothecin-treated show significantly greater expression in mouse cells then NMR ((Z score: -2.019, p=0.044), (Z score: -3.004, p=0.003), (Z score: -3.104, p=0.002), respectively). The gene Ddb1 has been excluded from these figures. Abbreviation Hr – hour.

Ddb1 in mouse had the highest expression of all the DNA damage-related genes studied with an average read count of approximately 28,150 (average fold change of 7.91). DDB1 in conjunction with DDB2 detects UV induced DNA damage and acts to promote the degradation of p21 in response to a low dose of UV radiation to mediate appropriate DNA repair (488). Perhaps the lower levels of Ddb1 in NMR facilitate a more p21 based repair mechanism and perhaps this low level reflects the NMR's susceptibility to UV induced DNA damage (175).

To identify if particular DNA repair mechanisms are expressed differently, genes involved in non-homologous end join, homologous recombination, nucleotide excision repair, base excision repair and mismatch repair (discussed in Section 1.3) (as defined in REPAIRtoire) were analysed by Wilcoxon paired sample signed-rank test (performed in SPSS version 22.0) (Appendix Table 4). The only statistically significant difference was found for nucleotide excision repair genes in both (8 and 48-hour) control samples and camptothecin samples after 48 hours ((Z score: -2.068, p=0.039), (Z score: -2.138, p=0.033), (Z score: -2.103, p=0.035), respectively). In addition to these samples, all samples showed reduced expression of NER associated genes in NMRs.

Though the overall levels of expression of BER genes were similar, there was still a total of 14 differentially expressed genes over all the conditions, which could reflect important changes in this pathway. Of the 7 upregulated genes, 6 were glycosylases or associated with glycosylases whereas only 3 of the 7 downregulated genes were glycosylases. Only 1 polymerase, POLL (DNA Polymerase Lambda), was upregulated, but 4 are downregulated. The role of glycosylases in BER is to is to detect and remove DNA legions whereas polymerases act later to replace the removed DNA (discussed in Section 1.3). This may indicate that the NMR is more primed to detect and remove legions due to this increased glycosylase expression. It is of note that POLL is thought to act principally in NHEJ (489, 490) and hence its upregulation may have related to its role in this DNA damage repair pathway and not BER. Increased glycosylase activity has been observed previously (491) providing consistency to this finding.

In addition to POLL which was upregulated in chromium treated samples and 8hour control samples, the only other NHEJ associated gene upregulated was*Nhej1* (Non-homologous end-joining factor 1). *Nhej1* had increased expression in all NMR samples relative to those from mice. *Nhej1* has been shown to affect hematopoietic stem cell ageing with knock out mice showing reduced stem cell renewal and decreased functional capacity in transplantation assays (492). Additionally, studies in human induced pluripotent stem cell model of *Nhej1* deficiency confirm this reduced stem cell

renewal (493). This may suggest stem cell maintenance is improved in NMRs. The only downregulated NHEJ associated gene was *Lig4* (DNA Ligase 4) which was downregulated in NMRs relative to mice in all samples. *Lig4* religates the broken strand in NHEJ, and it is not clear what this lower expression would mean in this context, but might suggest that homologous recombination is prioritised.

Similar to BER genes, homologous recombination genes did not show significant differences, but still had a total of 11 genes differentially expressed across all treatments. There was no clear trend of function within up and downregulated genes as we saw in BER genes. However of note is the gene *Brca1*. *Brca1* is involved in both checkpoint control and repair and is seen upregulated in chromium treatment after 48 hours. It was one of only two checkpoint genes seen to be upregulated in this assay, and it was not clear if it is its role as a checkpoint or a homologous recombination protein or both that explains its upregulation here.

Genes associated with DNA damage signalling, also termed checkpoint control genes (as defined by REPAIRtoire) were also analysed by Wilcoxon paired sample signed-rank test (performed in SPSS version 22.0) (Appendix Table 4). NMRs showed significantly lower expression in these genes in all samples (Z score: <-1.6, $p<0.05$). This is counter-intuitive, as we would expect cells that appear more resistant to DNA damage to be primed to respond to such damage with increased expression on genes involved in detecting such damage and altering cell cycle activity in response to such damage. This finding suggests that in this instance, resistance to DNA damaging agents is likely down to mechanisms other than DNA damage repair and may indicate more preventative measures for DNA damage.

There appeared to be little variation in DNA damage gene expression between each treatment suggesting the variation between species is masking the variation due to the treatment or that the treatment itself is having a low impact on this gene expression.

These results are a stark contrast to previous work (193) in NMR liver cells. It was shown that in liver cells from NMRs had significantly greater expression in DNA damage signalling and MMR and non-significantly more expression of homologous recombination and NHEJ genes (193). An increase in double-strand break repair would have explained an increased resistance to camptothecin that specifically causes single and double-strand breaks, though the lack of difference may reflect the small difference in observed resistance. Elevated levels of oxidative stress characterize chronic liver disease, and the liver is a target for a number of DNA damaging compounds which may particularly be the case

in the NMR which feeds on toxic tubers (494, 495). This may explain the observed differences, as skin fibroblasts are less exposed to DNA damaging agents and hence do not require such high levels of DNA repair gene expression. As NMR are subterranean, they have little exposure to sunlight. Mice on the other hand, though nocturnal and covered in fur may experience higher light exposure. This is supported by studies showing that NMR cells are susceptible to UV radiation (175). UV induced DNA damage is primarily repaired by nucleotide excision repair (496). Lower levels of such genes in the NMR may reflect the difference in UV susceptibility of the organisms under study and likely reflect evolutionary redundancy of such repair in subterranean living.

The tumour-related protein p53 was significantly upregulated between all conditions that matched what has previously been reported. However *Nrf2*, which has also been reported as being highly expressed in NMR, only had significantly higher expression in NMR cells after chromium treatment or 48 hours post control treatment (179). One explanation for p53's higher expression is that it primes the cell to respond to stress. The protein would simply need to be activated as opposed to transcribed in order to elicit a response. However, if we consider the results of our senescence assay which showed high base levels of senescence in NMR cells, the high p53 expression may simply be indicative of this. If this is the case, then it may be due to accumulation of senescent cells due to the low frequency of cellular passaging in the slow-growing NMR cells, or it may indicate that the cells are undergoing chronic stress due to improper culture conditions. As NMRs are a relatively new model, culture conditions may still need further optimisation.

These results indicate that the total expression of DNA repair genes is either less relevant than the specific profile with an appropriate combination of a few genes being more effective than high activity of a less appropriate combination. Alternatively, it would suggest that NMRs are not repairing DNA damage in a fashion greater than in mice, but are instead taking a longer time to repair the damage, an idea supported by the presence of differentially expressed cell cycle-associated genes. Another potential explanation is that NMRs could be negating the effect of DNA damaging compounds through alternative means such as preventing the damage occurring.

4.4.2.7 Differences in cell adhesion associated genes

Our functional enrichment analyses indicated pronounced differences in the membrane proteome between NMR and mice. A key aspect of a cell's surface chemistry that affects cancer susceptibility is the presence of cell adhesion molecules (466, 497, 498). To determine if there are significant differences in cell adhesion molecule expression, a list of 176 genes listed as 'cell adhesion molecules' were taken from the KEGG (Kyoto Encyclopedia of Genes and Genomes) database (Release 78.2) (441, 499). Of these genes, 94 were present in our dataset (appendix Table 5). A higher proportion of these genes were upregulated in NMR cells relative to mouse cells (Table 4.23). The number of differentially expressed genes was similar between treatments with a range of 6 upregulated genes and 9 downregulated genes. There was a large amount of overlap between control and treated cells with an average of 40 genes (73%) present in both the treatment and the appropriate control indicating this difference in cell adhesion was not induced by the treatment. A paired Wilcoxon signed rank analysis was performed on the expression of these genes that were found to be differentially expressed. Control (8-hour: Z score: -2.1, p=0.035, 48-hour: Z score: -2.4, p=0.018) and camptothecin (8-hour: Z score: -3, p=0.002, 48-hour: Z score: -2.1, p=0.031) treated NMR cells showed significantly more expression than cells from mouse under these conditions 8 and 48 hours post-treatment. Chromium treatment did not show significant differences in adhesion molecule expression. However, 8-hour post-treatment did show near significance (Z score: -2, p=0.051).

Table 4.23. The number of cell adhesion genes up (↑) or down (↓) regulated in NMR cells compared to mouse cells for different treatments and time points. Genes significant at the 0.05 level after correcting for multiple testing.

	Control	Camptothecin	Chromium (vi) oxide
8hr	35↑ 18↓	35↑ 13↓	33↑ 14↓
48hr	32↑ 14↓	33↑ 18↓	29↑ 22↓

The biggest difference in expression was consistently in the gene *Selplg* (Selectin P Ligand) with an average fold change of 14 between all conditions (range: 3.1). *Selplg* is the ligand of P-selectin, though it can be bound by other selectins (500-502). *Selplg* is present on endothelial cells and allows tethering and extravasation of circulating immune cells (501, 502). As such, this may be an indicator that the cells are trying to recruit immune cells as part of a general stress response. P-selectin and its

ligand have been implicated in cancer with knockouts resulting in decreased growth and metastasis (503). This is in part due to immunoregulatory effects of *Selplg* present on the surface of T cells (504). However, p-selectin has been shown to contribute to metastasis (505). As such it is surprising that a cancer-resistant model such as the NMR would have such high expression levels compared to the cancer-susceptible mouse. Fibroblasts expressing *Selplg* may make themselves too sticky for metastasising cells to pass through, preventing them from spreading, or may help recruit an appropriate immune response.

Significant differences in cell adhesion may be essential in the NMR's cancer resistance. As we will discuss in Chapter 5.1, cell adhesion is thought to affect cancer by regulating proliferation and both facilitating and preventing metastasis. As such, increased expression of cell adhesion genes may either limit cellular proliferation and possibly facilitate the early contact inhibition observed in NMR or could make cells too sticky for metastasising cancer cells to escape local tissues, preventing the spread of tumours.

4.4.3 Quantitative PCR validation

To validate our data the expression of 9 genes of interest were quantified through qPCR.

Primer dimer, whereby the PCR primers anneal to each other, results in amplification of the primers. This would generate an amplification signal (increased CYBR green fluorescence) in the absence of their target making accurate detection of the target impossible. Similarly, amplification of multiple genes also made it impossible to determine whether or not changes in the signal you detect is due to changes in your target gene's expression level or that of the unspecific target. To test if our primers (Table 4.1) are specific to our target and do not form primer dimers, control RNA was converted into cDNA and amplified by qPCR, and the product was analysed by gel electrophoresis on a 3% agarose gel. The majority of primers produced a single clear band indicating successful amplification of the specific target. However, primer pair 2, designed to target *p57* in mouse, gave two distinct bands (Figure 4.21). Due to the size of these bands (both >100bp) which are too large for amplification of primer dimers (typically no longer than 50bp) these primers were likely amplifying a non-specific target such as another gene, or potentially a variation of *p57*. Fortunately, primer pair 1 designed to target *p57* gave a single band and will be used for future assays.

A number of the primer pairs produced faint or apparently absent bands or conversely in the case of the primer designed to detect mouse*Hprt1,* a very bright and broad band that could represent multiple overlapping species (Figure 4.21-4.22). To test these primers, the PCR product was loaded onto another gel with a higher load (25ul) and wider narrower wells (Figure 4.23). From this assay,

four primers were found not to produce any bands and hence no amplification. These were both primer pairs that targeted *Dpp10* in mouse and *Grik2* in NMR. The absence of any amplification indicates that either the primers simply didn't work, or that the gene target was expressed very poorly or not at all. By looking into the RNAseq data, we see that for both genes there is very low expression. *Dpp10* in mouse shows 0 to 0.9 reads, and *Grik2* in NMR has 45 to 535 reads after normalisation under control conditions, varying between primary cell cultures, which would explain the absence of bands here. The primer pair targeting mouse *Hprt1* still appears very bright but on closer inspection appears to be a single band. The predicted product size (Table 4.1) matches the size present on the gel, further supporting that these bands represent the desired amplification product. For this study primers listed as 'p1' were used with the exception of mouse *p21*, NMR *R3hcc1* and NMR *Sox5* which used the primer listed as 'p2' (Table 4.1).

	3% Agarose, 6µl Midori Green			
Lane	Sample	Predicted size (bp)	Load	
1	Ladder	100-1,000	5µl	
2	M p21 p1	112	10µl	
3	M p21 p2	111	10µl	
4	M Sox5 p1	124	10µl	
5	M Sox5 p2	113	10µl	
6	M Grik2 p1	145	10µl	
7	M Grik2 p2	134	10µl	
8	M R3hcc1 p1	100	10µl	
9	M R3hcc1 p2	103	10µl	
10	M Serpinb2 p1	131	10µl	
11	M Serpinb2 p2	140	10µl	
12	M Dpp10 p1	148	10µl	
13	M Dpp10 p2	107	10µl	
14	M FOXO p1	124	10µl	
15	M FOXO p2	116	10µl	
16	M P57 p1	141	10µl	
17	M P57 p2	145	10µl	
18	M Hprt1 p1	195	10µl	
19	M Tbp p1	109	10µl	

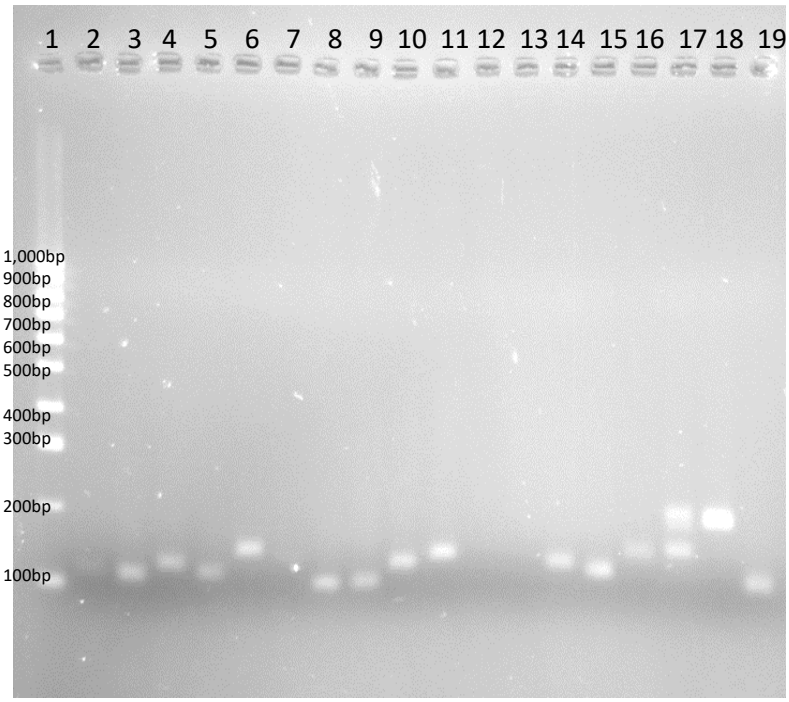

Figure 4.21. PCR products produced with different primers in control mouse cDNA samples. These were run on a 3% agarose gel containing 0.006% Midori Green. The size of each band on the ladder is given to the left of the image. RNA derived from mouse cell line 1 from the beta cell stock.

	3% Agarose, 6µl Midori Green		
Lane	Sample	Predicted size (bp)	Load
1	Ladder	100-1,000	5µl
2	N p21 p1	114	10µl
3	N p21 p2	101	10µl
4	N Sox5 p1	136	10µl
5	N Sox5 p2	137	10µl
6	N Grik2 p1	102	10µl
7	N Grik2 p2	128	10µl
8	N R3hcc1 p1	113	10µl
9	N R3hcc1 p2	145	10µl
10	N Serpinb2 p1	107	10µl
11	N Serpinb2 p2	112	10µl
12	N Dpp10 p1	110	10µl
13	N Dpp10 p2	104	10µl
14	N FOXO p1	111	10µl
15	N FOXO p2	146	10µl
16	N P57 p1	141	10µl
17	N P57 p2	141	10µl
18	N Hprt1 p1	215	10µl
19	N Tbp p1	208	10µl
20	Ladder	100-1000	5µl

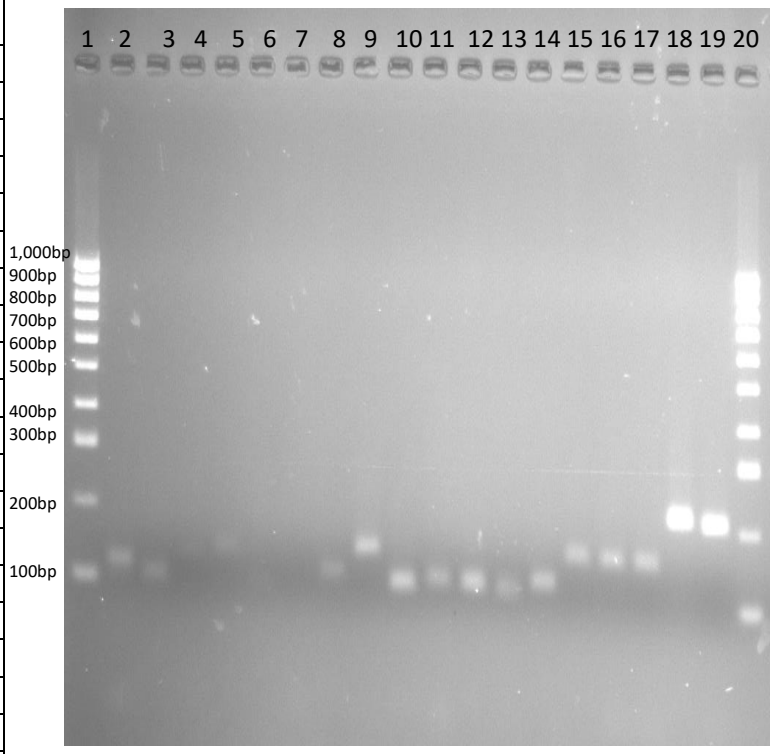

Figure 4.22. PCR products produced with different primers in control NMR cDNA samples. These were run on a 3% agarose gel containing 0.006%m Midori Green. The size of each band on the ladder is given to the left of the image. RNA derived from NMR cell line 2 from the beta cell stock.

	3% Agarose, 6µl Midori Green		
Lane	Sample	Predicted size (bp)	Load
1	Ladder	100-1,000	5µl
2	M p21 p1	112	10µl
3	M Grik2 p2	134	10µl
4	M Dpp10 p1	148	10µl
5	M Dpp10 p2	107	10µl
6	M Hprt1 p1	195	10µl
7	N Sox5 p1	136	10µl
8	N Sox5 p2	137	10µl
9	N Grik2 p1	102	10µl
10	N Grik2 p2	128	10µl

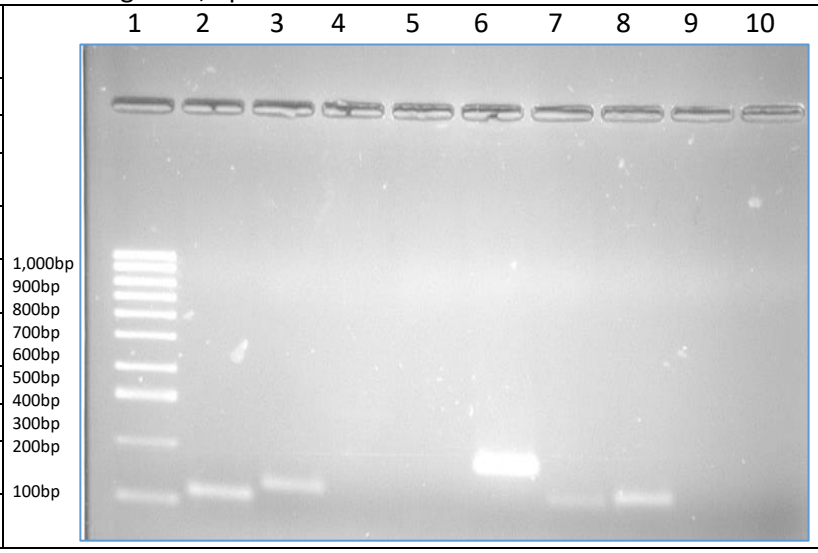

Figure 4.23. PCR products produced with different primers in control mouse cDNA samples. These were run on a 3% agarose gel containing 0.006% Midori Green. The size of each band on the ladder is given to the left of the image. RNA derived from mouse cell line 1 and NMR cell line 2 from the beta cell stock.

To validate the results of the RNAseq experiment, qPCR was employed (Figure 4.24). Genes of interest were chosen to be tested (Table 4.1). Due to limited volumes of leftover RNA, only mouse RNA samples used for the RNAseq could be used for this validation. For most samples, the change in gene expression is the same in both RNAseq and qPCR. However, *R3hcc1* after 8-hour chromium treatment and *Foxo1* after 48-hour camptothecin treatment in mouse primary cell culture one showed a decrease fold change in the qPCR dataset and increase fold change in the RNAseq dataset. Additionally, P21 in 8-hour post chromium treated mouse 1 cells showed a much larger increase in expression than in the RNAseq. All samples that failed to reach the 95-105% efficiency cut off (appendix Figure 10) showed similar expression between RNAseq and qPCR. Overall the direction of change was largely similar between the two methods. However, when interpreting the RNAseq data caution must be taken as variation between the two techniques is observed.

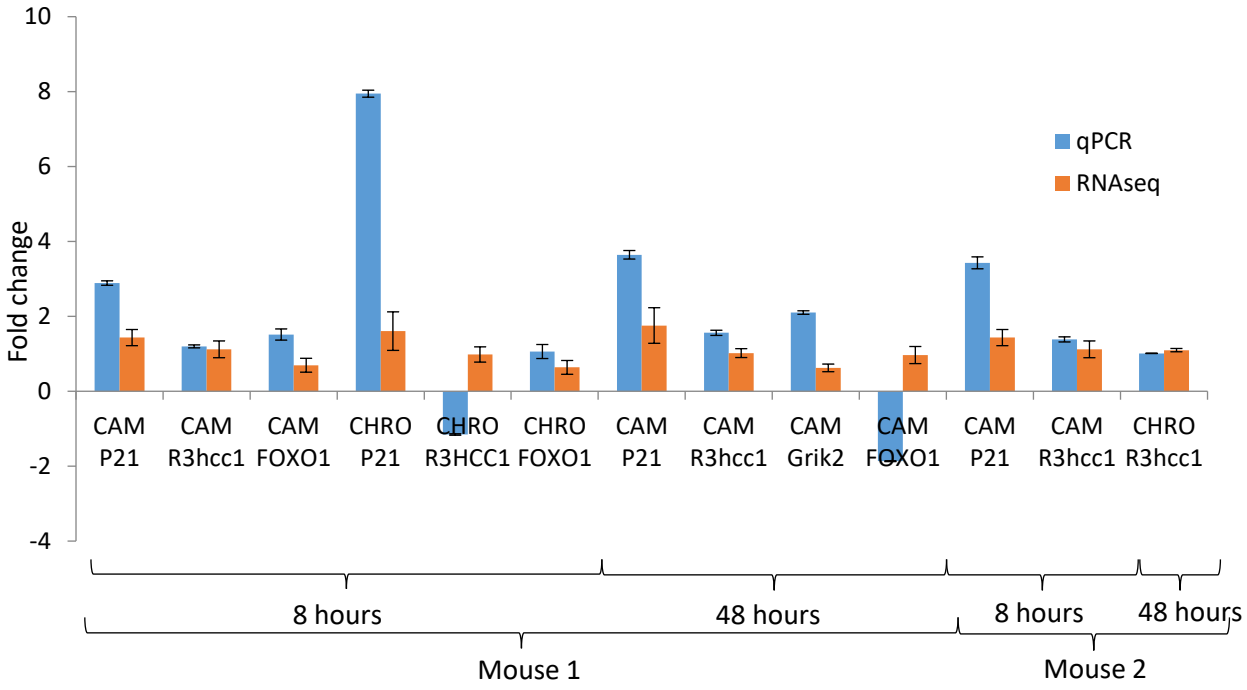

Figure 4.24. The fold change in gene expression between control and treated samples as determined by RNAseq (red) and qPCR (blue). For most samples the change in gene expression is the same in both RNAseq and qPCR. However, R3hcc1 after 8-hour chromium treatment and Foxo1 after 48-hour camptothecin treatment in mouse primary cell culture *one, show a decrease fold change in the qPCR dataset and increase fold change in the RNAseq dataset. Samples from the alpha cell stock. Tbp was used as the housekeeping gene for this analysis.*

Melt curves were produced and examined for multiple peaks. No cases of multiple peaks were detected indicating specific amplification (Figure 4.25). The PCR products from these reactions were loaded onto a 3% gel and examined for multiple bands (Figure 4.26-4.27). No double bands were detected confirming specific amplification; additionally, each gene produced the same size band regardless of the sample used indicating consistency of the primers (Figure 4.26-4.27). Control wells, which contain all components except the cDNA, test for contamination of the reagents. As amplification was detected in several of these wells; these samples were also loaded onto a gel as before (Figure 4.28). Bands can be seen for both *p57* and *Hprt1* indicating contamination. These samples among others were run again at a higher load (25ul) to check this (Figure 4.29). The faint band previously seen for p57 is not present. However, the band for *Hprt1* is (Figure 4.29). This indicates contamination in the reagent that may confound data using *Hprt1* as such *Tbp* will be used as the only housekeeping gene for these samples. Gels of the m2 mouse primary cell culture pcr products were also analysed by gel electrophoreses and produced no double bands (Appendix Table 6 and 7). Some contamination of 8-hour *Tbp* was detected which may mean inaccuracies in the 8-hour post-treatment m2 samples as *Tbp* was used to normalise the data (Appendix Table 6). The ct values of the housekeeping genes (Appendix Table 2) were input into a one way ANOVA using SPSS to assess if there was significant variation between samples. In all cases except control vs. chromium in m1 and m2 at 8 hours post-treatment, there was a statistically significant difference suggesting these genes are not suitable housekeeping genes. However, the actual observed differences were small, and these differences are likely due to between-sample-and-run variation, particularly samples within each run that had less than a 2 ct range. The biggest variation was seen between 8 and 48 hours of both cell lines. This could indicate differences in expression over time or may reflect that 8-hour and 48-hour samples were run and originally harvested on different days. Were this study to be repeated a collection of at least 5 candidate housekeeping genes would be selected, and qPCR would be run using primers designed for these genes in control and treated conditions. These genes could then be assessed with publicly available software such as 'NormFinder' and 'RefFinder' to select the most appropriate and most stably expressed reference gene (506, 507). This approach has the benefit that all the genes should be stable in theory, and so the external variation should be consistent within these genes, and hence unstable genes should stand out even in a variable experimental background. *Hprt1* and *Tbp* were chosen as housekeeping genes as they have been used as such in NMR cells studied previously (192).

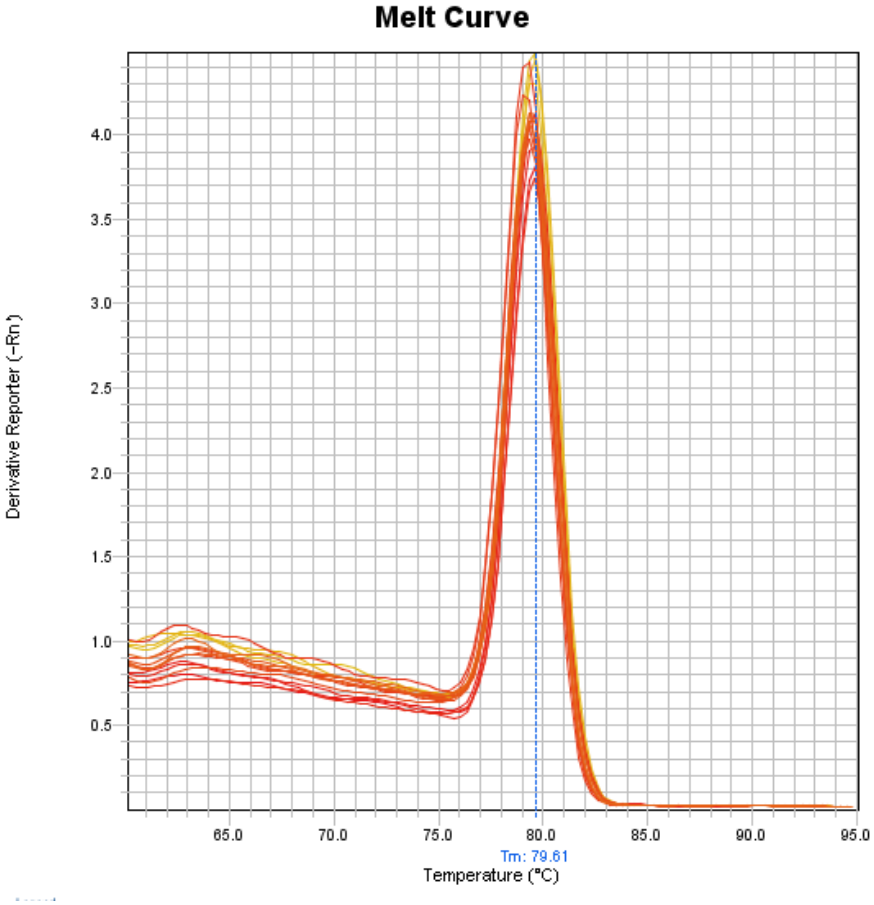

Figure 4.25. Representative Melt curve plot. Melt curve plot of mouse 1 (alpha stock) p21, 48 hours post-treatment. Red lines represent control samples; orange lines represent camptothecin-treated samples and yellow indicate chromium (vi) oxide treated samples. All these samples show a single clear peak indicating only one amplification product.

	3% Agarose, 6µl Midori Green			
Lane	Sample	Predicted size (bp)	Load	
1	Ladder	100-1,000	5µl	
2	p21 control	111	8µl	
3	p21 cam	111	8µl	
4	p21 chro	111	8µl	
5	p57 control	141	8µl	
6	p57 cam	141	8µl	
7	p57 chro	141	8µl	
8	Hprt1 control	195	8µl	
9	Hprt1 cam	195	8µl	
10	Hprt1 chro	195	8µl	
11	Tbp control	109	8µl	
12	Tbp cam	109	8µl	
13	Tbp chro	109	8µl	
14	R3hcc1 control	100	8µl	
15	R3hcc1 cam	100	8µl	
16	R3hcc1 chro	100	8µl	
17	Sox5 control	124	8µl	
18	Sox5 cam	124	8µl	
19	Sox5 chro	124	8µl	
20	Grik2 control	145	8µl	
21	Grik2 cam	145	8µl	
22	Grik2 chro	145	8µl	
23	FOXO1 control	124	8µl	
24	FOXO1 cam	124	8µl	
25	FOXO1 chro	124	8µl	

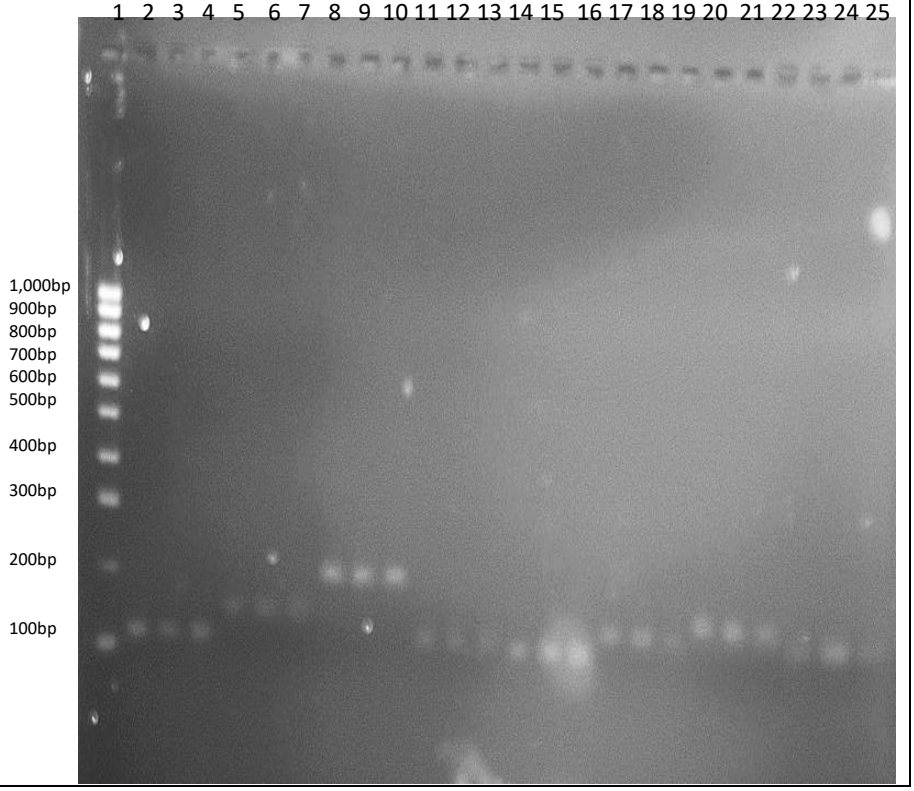

Figure 4.26. PCR products produced with different primers in cDNA samples from the m1 mouse primary cells (alpha stock) after 8 hours post-treatment with either camptothecin (cam) or chromium (vi) oxide (chro) in media with 2% DMSO or media with 2% DMSO as control. These were run on a 3% agarose gel containing 0.006% Midori Green. The size of each band on the ladder is given to the left of the image.

	3% Agarose, 6µl Midori Green			
Lane	Sample	Predicted size (bp)	Load	
1	Ladder	100-1,000	5µl	
2	p21 control	111	8µl	
3	p21 cam	111	8µl	
4	p57 control	141	8µl	
5	p57 cam	141	8µl	
6	Hprt1 control	195	8µl	
7	Hprt1 cam	195	8µl	
8	Tbp control	109	8µl	
9	Tbp cam	109	8µl	
10	R3hcc1 control	100	8µl	
11	R3hcc1 cam	100	8µl	
12	Sox5 control	124	8µl	
13	Sox5 cam	124	8µl	
14	Grik2 control	145	8µl	
15	Grik2 cam	145	8µl	
16	FOXO1 control	124	8µl	
17	FOXO1 cam	124	8µl	

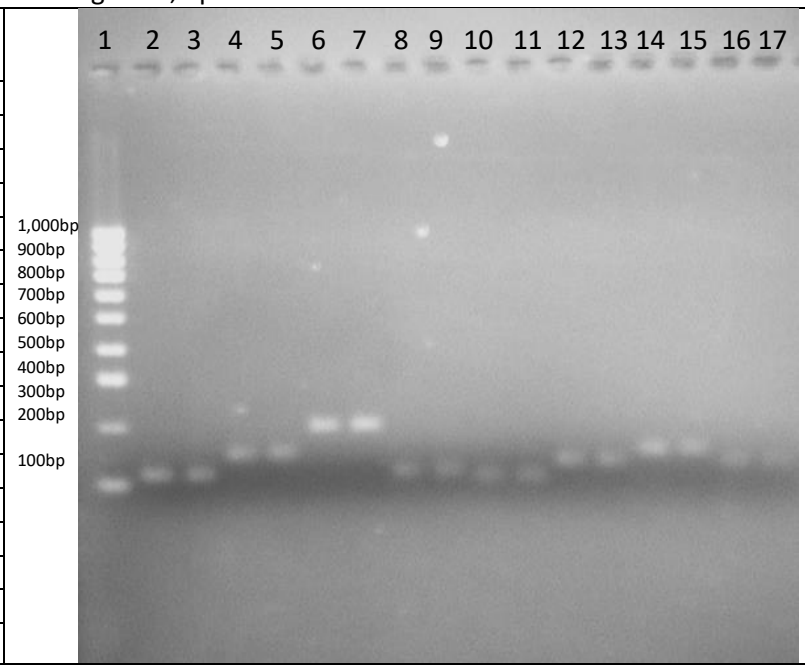

Figure 4.27. PCR products produced with different primers in cDNA samples from the m1 mouse primary cells (alpha stock) after 48 hours post-treatment with camptothecin (cam) in media with 2% DMSO or media with 2% DMSO as control. These were run on a 3% agarose gel containing 0.006% Midori Green. The size of each band on the ladder is given to the left of the image.

	3% Agarose, 6µl Midori Green			
Lane	Sample	Predicted size (bp)	Load	
1	Ladder	100-1,000	5µl	
2	p21 8hr	111	8µl	
3	p57 8hr	141	8µl	
4	Hprt1 8hr	195	8µl	
5	Tbp 8hr	109	8µl	
6	R3hcc1 8hr	100	8µl	
7	Sox5 8hr	124	8µl	
8	Grik2 8hr	145	8µl	
9	FOXO1 8hr	124	8µl	
10	p21 48hr	111	8µl	
11	p57 48hr	141	8µl	
12	Hprt1 48hr	195	8µl	
13	Tbp 48hr	109	8µl	
14	R3hcc1 48hr	100	8µl	
15	Sox5 48hr	124	8µl	
16	Grik2 48hr	145	8µl	
17	FOXO1 48hr	124	8µl	

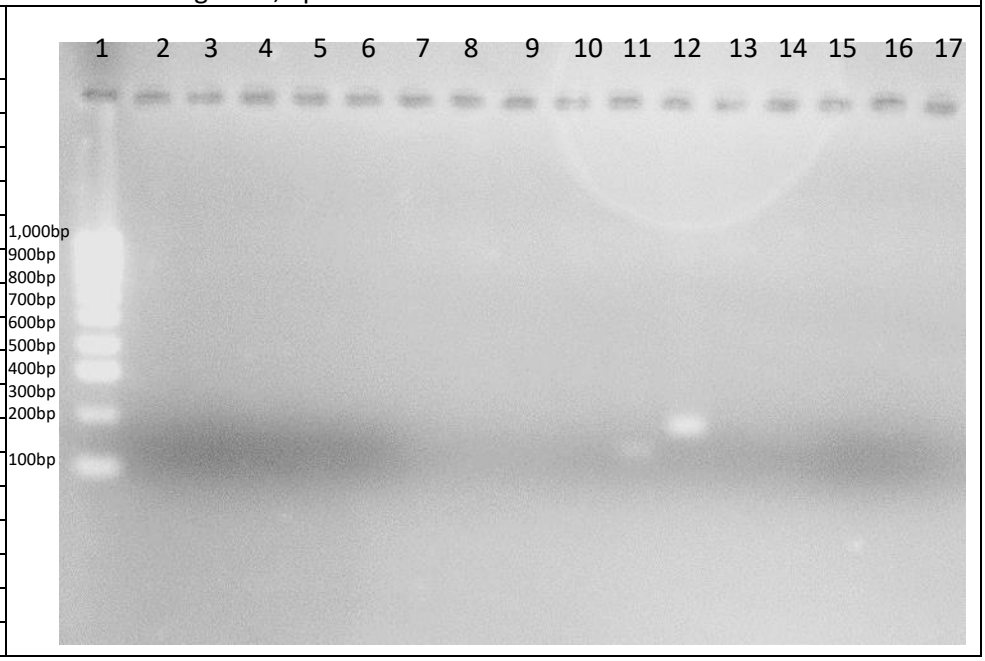

Figure 4.28. PCR products produced in blank samples that lack cDNA. These were run on a 3% agarose gel containing 0.006% Midori Green. The size of each band on the ladder is given to the left of the image.

	3% Agarose, 6µl Midori Green		
Lane	Sample	Predicted size (bp)	Load
1	Ladder	100-1,000	5µl
2	p21 48hr	111	25µl
3	p21 48hr	111	25µl
4	p57 48hr	141	25µl
5	p57 48hr	141	25µl
6	Hprt1 48hr	195	25µl
7	Hprt1 48hr	195	25µl
8	Tbp4 48hr	109	25µl
9	Tbp 48hr	109	25µl

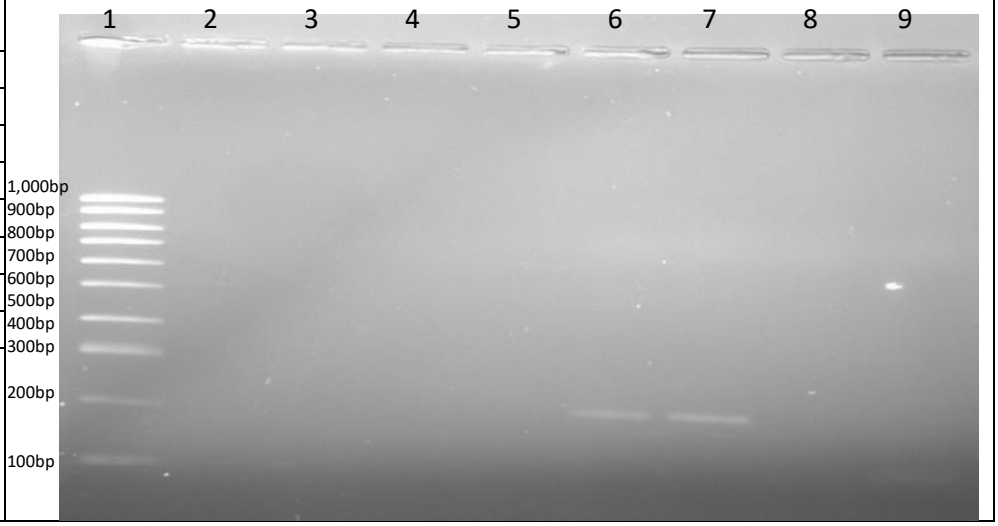

Figure 4.29. PCR products produced in blank samples that lack cDNA. These were run on a 3% agarose gel containing 0.006% Midori Green. The size of each band on the ladder is given to the left of the image.

4.5 Summary

Previous work on the NMR has suggested that their resistance to cancer is in part down to constitutively high expression of p53 and *Nrf2* as well as increased expression of DNA damage repair genes (179). Our study shows that while p53 is expressed at a higher level in NMR compared to mice, *Nrf2* does not seem to be, and DNA damage repair genes seem to be expressed at similar or lower levels than in mice. The most prominent difference observed between these species is the expression of cell adhesion genes which were significantly higher in the NMR. It has been shown that cell adhesion can promote p53 expression (508) and that this expression is required for the early contact inhibition seen in NMR (184). Additionally, pRB was also shown to be required for this early contact inhibition (184). In addition to being a cell cycle regulator pRB may also act to promote cell adhesion through focal adhesions (509) and hence pRB's essential function in early contact inhibition may be through its effect on adhesion molecules and not its effect on the cell cycle. Hence the high expression of cell adhesion molecules detected in this analysis may facilitate the observed early contact inhibition in NMRs. Alternatively, differences in cell adhesion may affect cancer more directly by inhibiting the movement of metastasising cancer cells.

Additionally, differences in cell cycle progression were detected. A previous study has shown that NMR cells show prolonged growth arrest after genotoxic insult, and our results seem indicative of this (179). Though it is not clear how this change in cell cycle progression is achieved, it likely involves the cell cycle regulator p53 which shows consistently high expression in NMR. Additionally,

p21 is also upregulated in response to the DNA damaging stimuli and often shows significantly higher expression in NMR than mice. Genes related to checkpoint control seem significantly downregulated in NMRs which is surprising as we would expect decreased proliferation to go hand in hand with increased checkpoint control. The relatively smaller checkpoint response may simply mean this response requires less transcriptional activity in NMR. It is of note that some such genes showed increased transcriptional activity in chromium treatment hence showing some checkpoint based response.

This RNAseq analysis provides not only useful information used in this analysis but also provides raw data that can be later 'mined' for additional information by future researchers. This is particularly useful in relatively poorly studied organisms such as the NMR.

A number of caveats must be considered when analysing this data. RNAseq analyses the level of mRNA but changes in RNA abundance do not necessarily mean changes in protein abundance, due to post-translational mechanisms such as miRNA suppression of mRNA, and protein degradation (303-305). Furthermore, even if the expression does reflect the protein level, the presence of a protein does not necessarily correlate with protein activity as post-translational modification may render the protein inactive. RNAseq works under the assumption that in general mRNA reflects protein activity, but to truly understand the system under study further work looking at the protein level (e.g. western blot analysis) is required.

In RNAseq, there is a bias for longer transcripts to be detected as the longer the sequence, the more likely a given read will encompass part of that transcript and hence be detected. For our analysis, this means that short transcripts may be missed and hence differences in such gene's expression could also be missed. Lower numbers of reads would reduce the statistical power of our analysis, for example, the difference between 10 and 30 reads is a less convincing example of differential expression than 1,000 and 3,000 reads. This could be rectified by increasing the coverage or sequencing 'depth' of the analysis by sequencing more reads. This would increase the cost of the analysis but also the statistical power of the assay and increase the likelihood of reads mapping to short transcripts. The coverage used in this analysis was fairly low at 2.4-4 (Table 4.5) meaning that theoretically the genome should be sequenced 2.4-4 times in our analysis. This low coverage was used principally to minimise costs. As we are comparing the same transcripts between samples, this bias should not affect our differential expression analysis beyond the potential loss of short transcripts from our data set and the reduction in statistical power previously mentioned.

A further limitation of this study is that only one cell type was studied in cell culture. Different cell types are not only exposed to different environmental cues but are epigenetically programmed to express a different subset of genes and undertake different functions. Cells grown in culture experience a vastly different environment to cells in *vivo,* particularly cells grown in 2D cell culture which poorly represents the complex 3D niche cells would normally occupy. Different cell types and cells derived directly from the organism as opposed to cells grown in cell culture can show different gene expression profiles. This can be seen in a previous study looking at liver cells taken directly from sacrificed NMRs which showed a markedly different gene expression profile resulting in the author concluding that NMRs show significantly higher expression of DNA damage genes which was not seen in the present study (193).

These limitations must be considered when assigning biological significance to observations of the generated data. However, RNAseq still possesses the ability to provide meaningful insights into the transcriptome that can be built upon and validated through further analysis.

Chapter 5: Phenotypic evaluation of cell cycle and adhesion in fibroblasts

5.1 Introduction

The RNAseq analysis in the previous chapter indicated that cell adhesion molecules (CAM) showed greater expression in skin fibroblasts derived from NMRs than those from mice. This was determined through functional enrichment which showed that CAMs were over-represented in the data sets and through analysing expression levels of CAMs which showed significantly higher expression in NMRs. Additionally, genes involved in cell cycle progression were also differentially expressed as identified from the functional enrichment analysis.

The aim of this chapter is to determine whether or not the differences in gene expression reflect differences in the cellular phenotype. Detecting differences in cellular adhesion or cell cycle progression post cellular stress in these primary cell cultures would provide phenotypic confirmation of our results. Additionally, cell adhesion has been associated with a wide arrange of biological processes and may influence the NMR's cancer-resistant phenotype.

To determine if differences in cell adhesion can be detected a trypsin-based detachment assay was conducted to identify how long it takes to remove each cell type from a culture plate using trypsin and EDTA. To complement that assay an attachment assay was performed to determine how quickly the cells would attach to a culture plate. Finally to evaluate the rate of cell cycle progression flow cytometry was performed.

5.1.1 Cell adhesion

Cell adhesion is important in cell growth, migration and differentiation. CAMs are proteins at the cell surface that mediate cell-cell interactions and interactions between the cell and the extracellular matrix. CAMs are thought to be integral to a wide variety of cellular processes including inflammation, cellular communication, and apoptosis (510). There are many different types of CAM, but these mostly fall into one of several superfamilies. These can be calcium dependent such as the integrins, cadherins and selectins (511-513) or calcium independent such as the immunoglobulin superfamily. The CAMs claudins and occludins may be dependent on intracellular but not extracellular calcium (514).

CAMs play a central role in metastasis. Metastasis is the process by which cancer cells leave their tumour of origin and relocate to another part of the body where they can proliferate to form a secondary tumour. This process can be divided into three key stages: invasion, intravasation and

extravasation. Invasion is when the cells become motile, passing through the extracellular matrix. Loss of cell adhesion in cancer cells facilitates this by allowing the cells to leave the primary tumour and move to other areas of the body. Motility of the cell also requires CAM activity. Intravasation is the process of entry into the vasculature by cells. Once inside the circulatory system cancer cells can be transported great distances. In order to leave the vasculature through the process of extravasation, CAMs need to adhere to the endothelium.

Tight junctions are connections made by claudins and occludins between two cells. These junctions close the intracellular space essentially creating an intracellular fence between the two cells (515). This barrier can serve to physically block metastasising cells from entering tissues (516). Additionally, these junctions stick cells together and can prevent their release and spread by metastasis (517). Studies have shown decreased activity of tight junction proteins in breast cancer cells and background tissues indicating their clinical relevance (498).

Adherens junctions are another cell-to-cell adhesion structure. Cadherins are the primary component of these junctions with E-cadherin being the most abundant of these. The structure of these junctions varies between cell types, but in fibroblasts, they seem to form distinct spots on the cell surface (518). E-cadherin is downregulated in most epithelial cancers (497) and generating these E-cadherin adhesion sites has been shown to prevent the invasion of cancer cells (519, 520).

Disruption of adhesion to the extracellular matrix has been shown to be able to induce apoptosis through integrin-mediated signalling (521, 522). Similarly, the Deleted in Colorectal Cancer (*Dcc*) gene encodes a cell surface adhesion molecule in the Ig superfamily. Inactivation of this gene has been associated with cancer progression in humans, and its activity promotes apoptosis or cell cycle arrest (523). Hence such CAMs could prevent cancer by preventing growth or inducing apoptosis of cancer cells with abnormal interactions to the extracellular matrix or other cells, particularly in cells undergoing metastasis which would have no such interactions while traversing the vasculature. Coxsackie and adenovirus receptor (CAR) is an Ig-like molecule with cell adhesion properties that has been shown to inhibit tumour cell proliferation and induce accumulation of p21 (524).

CAMs may also act to promote cancer. Studies of integrin αv show increased expression in cancer cells that were more prone to metastasis (525) and knock down of integrin αv decreased cancer cells' capacity for metastasis (526). These studies propose that integrin αv acts during motility and extravasation. E-selectin has also been shown to be capable of facilitating extravasation (527).

Collectively the above studies clearly show a strong role for CAMs in cancer formation and progression. It is interesting that our RNAseq analysis showed a large amount of differential expression

of genes at the cell surface including CAMs between mouse and NMRs. It is tempting to speculate that this may be a contributing factor to the NMR's apparent cancer resistance. To determine if changes in cell adhesion between the two species could be detected a simple trypsinisation assay was performed.

In cell culture, cells attach to the culture vessel initially through electrostatic interactions between the cell and the culture vessel surface. This interaction facilitates integrin binding. The cells which were spherical in suspension become flatter due to both natural deformation and active reorganisation of the cellular structure providing a greater surface for attachment. Re-organisation of the actin cytoskeleton takes place and focal adhesions form (528, 529). Focal adhesions are highly organised structures that connect the binding substrate to the cytoskeleton and are important in cell signalling and proliferation among other cellular functions (530, 531). The longer the cell remains attached to the surface the more adhesion molecules can bind and the greater the strength of attachment up to a point presumably when there is no room for additional adhesion molecules to act (529).

To detach a cell that has adhered to a culture flask, trypsin is typically added. Trypsin is a serine protease that cleaves peptide chains primarily at the carboxyl side of either arginine or lysine residues (532). This results in the CAMs (and any other susceptible protein on the cell surface) being cleaved, cutting the connection to the plate's surface and hence detaching them. An alternative method to remove the cells is to use a calcium chelating agent such as EDTA or sodium citrate. This works because integrins (and various other CAMs) are calcium dependent in their binding activity and the removal of available calcium results in the bonds being broken without damaging the surface proteins (533). Typically a combination approach is used in which trypsin and EDTA are added together. The more CAMs connecting the cell to the culture plate surface, the stronger the connection and presumably the longer it will take to detach the cell with trypsin or EDTA. By monitoring how long it takes cells from both species to be detached in response to trypsin and EDTA differences in CAM abundance can be inferred.

5.1.2 Cell cycle

The cell cycle is essentially the life cycle of the cell. It is comprised of multiple different stages that a cell may undergo. Interphase, a period of cellular growth and DNA synthesis makes up the majority of the cell cycle and is comprised of 3 distinct phases (Figure 5.1).

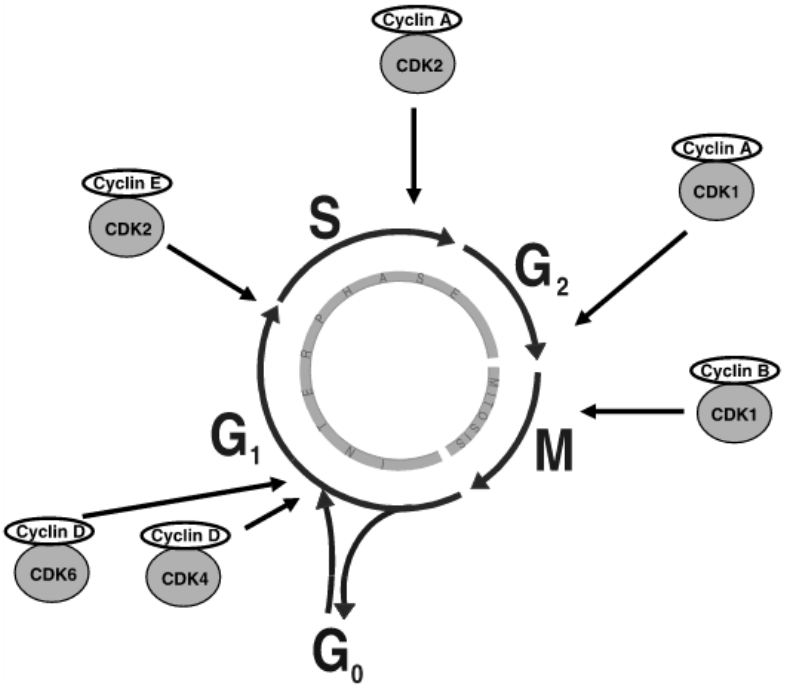

Figure 5.1. Stages of the cell cycle. Points of Cyclin/CDK activity have been indicated. Taken with permission from (534).

G1 or Gap 1 is the primary growth phase. During this phase, the cell synthesises new proteins and organelles (such as mitochondria) and increases in size. As these are divided between the two new daughter cells, this phase allows these components to be replaced. This phase also contains the G1 checkpoint that ensures that everything is ready for DNA synthesis, arresting the cell cycle if this is not the case. Cell cycle checkpoints are principally controlled by cyclins and cyclin-dependent kinases (CDKs). These CDKs are highly functionally conserved between species (535). At the G1 checkpoint, cyclin D is essential (536). Cyclin D binds to CDK 4 or 6 and once activated by CDK-activating-kinase, it phosphorylates Rb in the nucleus. Phosphorylation of Rb prevents its usual inhibitory activity on the E2F transcription factors that in turn promote the transcription of a variety of genes that promote transition into S phase. These include cyclin E and CDK2 which phosphorylates Rb, forming a positive feedback loop (536, 537). Upon detection of DNA damage or other defects, this process can be disrupted to result in cell cycle arrest and prevent entry into S phase. ATM (ataxia telangiectasia mutated) and ATR (ataxia telangiectasia and rad3-related protein) are activated in response to DNA damage and in turn, activate checkpoint kinase 1 and 2 (CHK1 and 2). These ultimately inhibit cyclin E/CDK2 to prevent cell cycle progression. Additionally, CHK1 and 2 stabilise and activate p53 which in turn promotes transcriptional activation of p21 which inhibits cyclin E/CDK2 and hence inhibits entry into S phase. Alternatively, p21 may be activated by accumulation of p16 (538).

Providing no inhibitory signals are detected the cell will continue into S phase, the synthesis phase during which all the DNA in the cell is duplicated. This stage is in part regulated by cyclin A which

binds CDK 2, replacing cyclin E. This complex regulates DNA synthesis through phosphorylation of components of the DNA replication machinery (539). While the DNA undergoes replication, it is vulnerable. Single-strand DNA is more susceptible to chemical modification, and replication forks are prone to stall or collapse if blocked. Defects in DNA synthesis during this phase (and also DNA defects in the other stages) can be detected through the detection of long strands of ssDNA coated in RPA that serves as a warning signal (540). This process acts via ATR and results in a temporary halt in S phase progression (540). It is thought that ATR can act at the replication fork to stabilise it and prevent further unwinding of the DNA until replication has completed (541, 542). Should the replication fork stall due to defects in the DNA strand, ATR acts through phosphorylation of CHK1 to protect the replication fork (540).

Once the cell's DNA has successfully been replicated, the cell enters the G2 or Gap 2 phase. G2 is another period of protein synthesis and cellular growth, however, it appears not to be essential as some cell types and cancers bypass G2 and transition from S phase directly into mitosis (543, 544). Through G2, cyclin B accumulates, binding to and activating CDK1 (545). CDK1 is phosphorylated and inactivated by WEE1 (WEE1 G2 checkpoint kinase), but activated CDK1 inactivates WEE1 and activates CDC25 (cell division cycle 25A) which dephosphorylates and hence activates CDK1 forming positive feedback loops (546). Such positive feedback loops ensure commitment of cells transitioning between stages of the cell cycle. Once the required concentration of activated cyclin B/CDK1 has been reached, it translocates to the nucleus and phosphorylates a number of targets including histone proteins and centrosomal proteins to facilitate mitosis (545). DNA damage results in activation of the transcription factor p53 that promotes the expression of p21, *Gadd45* (growth arrest and DNA damage inducible alpha) and 14-3-3σ which inhibit the activity of cyclin B/CDK1 by preventing cyclin B and CDK1 binding (*Gadd45*), sequestering inactive cyclin B/CDK1 in the nucleus (p21), or sequestering active cyclin B/CDK1 in the cytoplasm (14-3-3σ) (547). Additionally, p53 transcriptionally inhibits CDK1 (547). ATR and ATM also act in response to DNA damage and act through CHK1 which promotes the degradation of CDC25 and hence inactivation of CDK1 (548). ATR and ATM also activate p53 (547). These pathways that inactivate cyclin B/CDK1 result in cell cycle arrest at G2.

Once cells pass through G2, they enter M phase, which is mitosis. Mitosis consists of 4 key stages, prophase, metaphase, anaphase and telophase. Prophase is dominated by chromatin condensation, a process that condenses the DNA into tightly bound chromosomes. Additionally, the nucleolus disperses, and the centrosomes separate, moving to the poles of the cell. An intermediate phase referred to as prometaphase is the period in which the nuclear membrane breaks apart and newly synthesised microtubules attach to the kinetochores of each chromosome. In metaphase, the chromosomes align at the metaphase plate, a line equidistant to each of the centrosomes. This

alignment is due to the counterbalance of each microtubule's polling force. This tension indicates appropriate spindle attachment, without which the cell would not progress into anaphase, and hence serves as a checkpoint. Detection of this results in activation of anaphase-promoting complex which degrades securin, which functions to inhibit seperase (549). Seperase is an enzyme that breaks down cohesins, the proteins responsible for binding the two sister chromatins together (550). The enzymatic cleavage of this bond releases the two sister chromatids which then move to opposite ends of the cell, towards the centrosomes. Anaphase consists of this chromatid movement. Additionally, the non-kinetochore bound spindle fibres push against each other to elongate the cell.

The final stage of mitosis is telophase. The nuclear membrane reforms, chromatids unwind into chromatin and nucleoli reform. Additionally, the remaining microtubules de-polymerise and the cell splits in two through cytokinesis. In animals, cytokinesis acts through a contractile ring of myosin II and actin filaments that forms equatorially. This ring contracts, pulling the cell membrane with it to divide the cell. The process of abscission finalises this process by cleaving the cell in two at the contracted point.

In addition to G1, S, G2 and M phase the cell can exit the cell cycle and enter G0. Cells in G0 are either quiescent or senescent. Quiescent cells are not dividing nor preparing to divide; this may be a temporary delay or a permanent exit from the cell cycle. Senescence is considered an alternative to apoptosis as it removes damaged cells that may produce defective progeny from the cell cycle permanently. An important concept that is often overlooked is that senescent cells, though no longer dividing, are still performing their cellular function, and communicating with other cells. In the case of senescent cells, this can have negative consequences (406).

5.1.2.1 Flow cytometry

A flow cytometer can simply be considered a liquid pump that takes cell solutions and passes them through a small channel with a sensor that detects the cell. This sensor can detect changes in electrical opposition, known as electrical impedance or changes in fluorescence. The flow cytometer then counts the number of 'events' or times a signal is detected to infer the number of cells to pass the sensor. The sensor can also monitor the level of fluorescence detected. By staining DNA with a fluorescent dye, we can not only count the number of cells but also assess the DNA content of the cell. Different stages of the cell cycle have different DNA contents. G1 has the normal DNA content for a species; G2 will have double this amount, and hence the fluorescence of such cells would be twice as bright. Cells in S phase will have an intermediate amount of DNA and hence fluorescence as only a part of the DNA will be synthesised. Cells in G0 are typically indistinguishable from those in G1 as they typically have the same DNA content. Apoptotic cells have a lower DNA content as they undergo DNA

fragmentation. Additionally, senescent cells may lose DNA content, and hence these cells will have lower fluorescence (551-553).

5.2 Aims

Cell cycle checkpoint controls are important factors in DNA damage repair. As discussed previously these checkpoints allow the cell to check for DNA damage and respond appropriately. The position of a cell in the cell cycle can affect damage repair. For example, homologous recombination can only occur if an extra copy of the cell's DNA is present, namely during G2. By identifying differences in cell cycle progression between NMR and mouse we can speculate about differences in DNA damage responses and repair.

Cell adhesion genes have been shown to influence cancer, both inhibiting and facilitating its development. By identifying differences in cell adhesion between the NMR and mouse we aim to confirm the results of the RNAseq analysis that suggested such differences and identify a potential causal factor in the NMR's cancer-resistant phenotype.

5.3 Materials and methods

5.3.1 Culture conditions

Cells were cultured as described in Chapter 3.3.1. In short, cells were cultured at 35°C, 3% oxygen and 5% carbon dioxide in MEM supplemented with 15% FBS, 1% Penicillin streptomycin, and 0.1% fungizone. Only the beta cell stocks were used in this assay.

5.3.2 Detachment and attachment assays

Cells were plated in t25 culture flasks. Low cell numbers were used (mouse ~10,000, NMR ~4,000) to ensure normal growth and no overlap between the cells that may affect trypsin activity. Fewer NMR cells were used due to limited availability. Cells were given 24 hours to attach before being treated with either LD50 camptothecin (NMR: 128µM mouse: 57µM), chromium (NMR: 94µM mouse: 49µM) or control conditions for 2 hours. Cells were allowed to recover for 24 hours. The plates were visually inspected to ensure there was no significant overlap or contact between cells.

The detachment assay was run as described in (554). In short, each dish was rinsed with PBS then 0.5% trypsin 2.21mM EDTA (Sigma Aldrich: 03620). This was collected and replaced after 1, 2, 3 and 5 minutes. Care was taken to minimise agitation and trypsin was pipetted gently to prevent the cells being washed off. After 5 minutes the plates were inspected to ensure all cells had detached. The

cells were spun down at 1,000rpm for 10 minutes and resuspended in 200µl fresh media and counted using a haemocytometer. This was performed twice per cell line in one experiment.

For attachment assay, the cells were trypsinised with 0.5% trypsin 2.21mM EDTA. These were spun down at 1,000rpm for 10 minutes and resuspended in fresh media. Each condition was plated in duplicate into a well of 4 96-well plates (one per time point of analysis). Approximately 200 cells were added per well. After 1, 2, 4, or 6 hours the media containing unattached cells was removed and replaced with 70% ethanol (Sigma Aldrich: E7023) to fix the attached cells for at least 10 minutes at 4°C. The ethanol was aspirated and replaced by Hematoxylin Solution (sigmaMHS80). This was allowed to stain for 1 minute to aid cell counting. The cells were then rinsed twice with 200µl PBS, and cells in each well were counted manually. This was performed twice per cell line in one experiment.

5.3.3 Initial cell surface area prediction

Images were taken of at least 3 cells per primary cell culture for each treatment. The radius of each cell was measured twice (horizontally and vertically) to calculate an average value. These values were averaged across each primary cell culture of the same species for each treatment (total of 9 cells). The species average radius was used to predict the species average surface area using the equation, $4\pi r^2$ (r=radius). For the purpose of this estimation, cells were assumed to be perfect spheres.

5.3.4 Flow cytometry

Initially, 24 and 6 well plates were used to grow the sample cells but provided too few cells for the analysis and hence T25 culture flasks were used. Cells for flow cytometry were treated for 2 hours at LD50 while at near confluency and allowed to recover for 24 hours. These were then removed from the plate with trypsin. Cells were centrifuged at 1,000g for 10minutes, resuspended in 1ml PBS to rinse, and then centrifuged again at 1,000g for 4 minutes. The cells were then resuspended in 70% ice cold ethanol and left for 1 hour at 4°C to fix before transfer to -18°C freezer for storage until use. Cells were centrifuged at 1,000g for 4 minutes and resuspended in 200µl fresh PBS and transferred to a 96 well plate. To each well, 25µl Triton X 0.9% (Sigma Alderich T8787), RNase A 0.9mg/ml (Sigma Alderich R4875), Propidium Iodine (Sigma Alderich P4170) 0.1mg/ml in PBS was added. The plate was immediately transferred to the flow cytometer and analysed using Guava Cell Cycle Analysis software. The total number of cells analysed for each cell line and treatment is given in Appendix Table 8. This was performed twice per cell line in two independent experiments.

Median forward scatter (FSC) values were calculated by manually changing the gating with the guava cell cycle software until only half the cells were included. Cells that fell into G0 were not included in this assay to prevent changes in cell size due to cell death affecting the analysis. FSC was

found to be consistent through all other cell stages, and hence these were not differentiated within the analysis.

5.4 Results

5.4.1 Cell adhesion assays

To assess adhesion strength the time taken to detach cells with trypsin and EDTA was determined (Figure 5.2). Mouse cells appeared to detach faster, though this was only statistically significant in stressed cells after 3 hours and this difference was very small. Chromium and camptothecin-treated NMR cells (chromium: 91.2%, camptothecin: 97.5%) showed a significantly lower percentage of detached cells at three hours compared to mouse cells (chromium: 99.4%, camptothecin: 99.6%) under the same treatment (chromium: $t(4)= 4.2$ $p=0.014$, camptothecin: $t(4)= 8.3$ $p=0.001$). Similarly, stressed cells also appeared to detach more slowly particularly in NMR cells however this is not statistically significant.

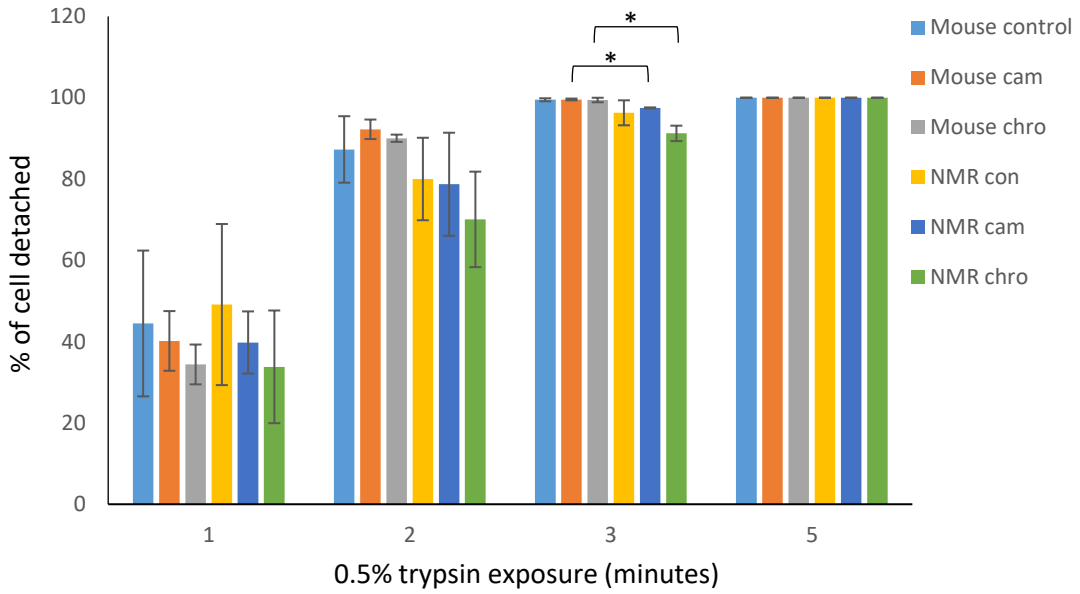

Figure 5.2. Percentage of cells (beta stock) that detach after varying levels of trypsin exposure after 24 hours of cell culture post-treatment for 2 hours with genotoxic insult or control conditions. Cells were exposed to 0.5% trypsin 2.21mM EDTA. After 3 hours exposure to trypsin, genotoxin treated NMR cells show a significantly lower percentage of cells as some cells remained attached while complete detachment was seen in mouse cells (camptothecin: t(4)=8.28 p=0.001, chromium: t(4)= 4.16 p=0.014). No other significant differences in detachment patterns between times or species were observed. However genotoxic treatment seemed to delay the rate of initial cell detachment in both species (after 1 minute of trypsin exposure) though this delay is not significant. Abbreviations, con – control, cam – camptothecin, and chro – chromium. Error bars indicate ± one standard error of the mean between three different cell lines (each cell line value is the average of 2 replicates in one experiment). Star (*) indicates significance at the p<0.05 level. All counts consisted of ~100 cells for samples with less than 100% detachment. 100% indicates the following total number of cells per sample, mouse control – 112,888 cells, mouse camptothecin-treated – 94,667 cells, mouse chromium (vi) oxide treated – 90,778 cells, NMR control –16,333 cells, NMR camptothecin-treated – 13,444 cells, and NMR chromium (vi) oxide treated – 14,666 cells.

In addition to detachment, the time for trypsinised cells to re-attach to a standard 96 well culture plate was determined (Figure 5.3). NMR cells under control conditions appeared to adhere slower than mouse control cells though this was not statistically significant. Treatment with either genotoxic compound decreased the rate of attachment in NMR cells though not significantly. Similarly, treatment with either compound appeared to increase the rate of cellular attachment in mouse cells thought this was only statistically significant at 2 hours for chromium treatment (control: 55.5% chromium: 94.3%, t(3)=-3.3 p=0.047) though camptothecin showed near significance after 2

hours (p=0.066). A two-way analysis of variants (ANOVA), taking time point as one factor and treatment and species as another showed significant variation between the treatment and species condition (f(5, 35)=18.4, p=0). Post hoc Turkey test showed NMR cells treated with either compound had significantly lower attachment than all mouse conditions (p<0.05) and mouse cells treated with either compound had significantly higher attachment than all NMR conditions (p<0.05).

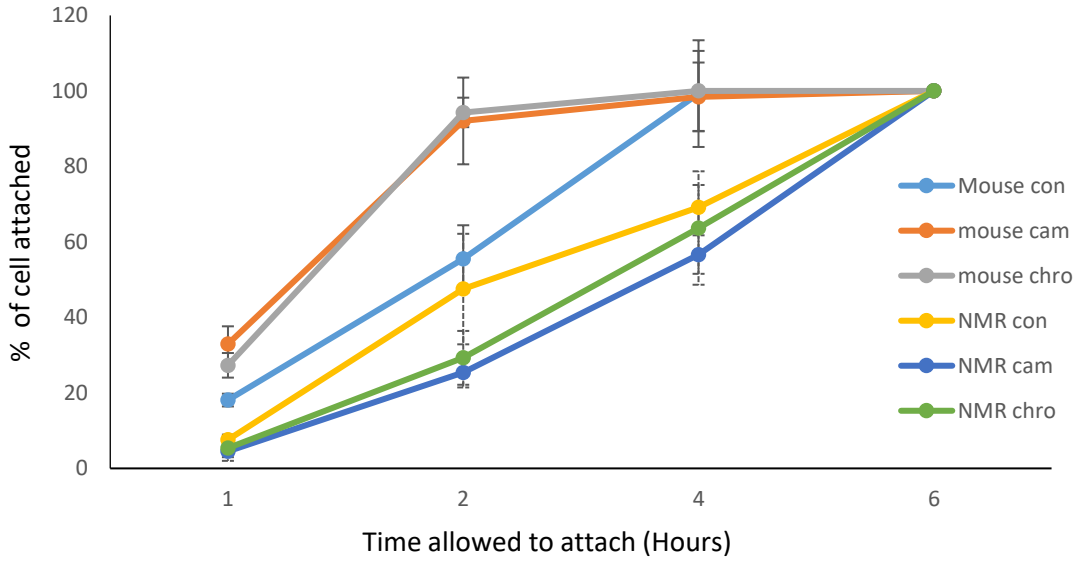

Figure 5.3. Attachment rate of mouse and NMR cells (beta stock) exposed to genotoxic insult. Treated cells from each species were significantly different from cells of the other species regardless of treatment. Mouse cells appear to attach faster than NMR cells, especially after genotoxic treatment. Mouse cells treated with control conditions showed significantly lower attachment to chromium treated cells (t(3)=-3.3 p=0.047) and near significance to camptothecin-treated cells (t(4)=-2.5 p=0.066) after 2 hours. NMR cells appear to attach slower after genotoxic treatment though this is not statistically significant. Abbreviations, con – control, cam – camptothecin, and chro – chromium. Error bars indicate ± one standard error of the mean between the three cell lines within each species (each cell line value is the average of two replicates in one experiment). Solid error bars indicate mouse samples and dashed error bars indicate NMR samples. 100% indicates the following total number of cells and cells counted for each of the following, mouse control – 796 cells, mouse camptothecin-treated – 603 cells, mouse chromium (vi) oxide treated – 411 cells, NMR control – 502 cells, NMR camptothecin-treated – 375 cells, and NMR chromium (vi) oxide treated – 355 cells.

To assess whether differences in cell surface associated gene expression are due to variations in cell size between NMRs and mice, the average surface area was initially predicted for each species under each condition by measuring the diameter of a small sample of imaged cells (Appendix Figure

11) as a preliminary indicator of cell size (Table 5.1). NMR fibroblasts (1,082.0um^2) have a significantly smaller surface area than those derived from mice (1,610.8um^2) (t(16)=3.8, p=0.001) (Figure 5.4) based on this data. There was no significant difference between treatments in either species.

Table 5.1. The average surface area of mouse and NMR skin fibroblasts in µm^2.

	Mouse	NMR
con	1,489.0	1,101.7
cam	1,422.6	1,061.9
chro	1,920.7	1,082.4

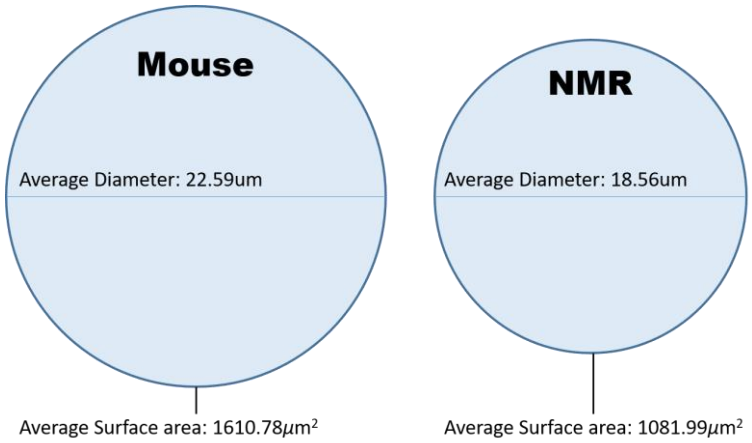

Figure 5.4. Visual representation of predicted cell size of fibroblasts derived from mice and NMRs.

As a follow-up analysis, the flow cytometry data presented in Section 5.4.2 was utilised. When the laser in the flow cytometer shines onto a cell passing through the detector, the light is scattered. Light that passes through the cell and is scattered less than ~2^o relative to the original path of the laser is called forward scatter (FSC). The scattering of light by a cell is a result of the cells size, shape, structure and the refractive index (and absorption) of the contents of the cell (491). FSC is closely related to the size of the cell as this light passes through the entirety of the cell, the greater the FSC, the greater the size of the cell providing no other factors that affect light scattering change. As such for this analysis we assume that all the cells vary only in size and not their reflective index. This is a reasonable assumption as these are cells of the same type, though variation between species may exist. Median FSC (Table 5.2) did not vary significantly between treatments within species. This matches our preliminary analysis of cell size. However, though no statistically significant difference exists it is of note that camptothecin-treated cells consistently showed slightly higher FSC and chromium treated cells showed slightly lower FSC. This may suggest these cells are reacting differently. This difference was greater in mice with NMRs showing less variation between

treatments. NMR cells showed significantly lower FSC than mouse cells (t(13)=-4.40, p=0.001) and a one way ANOVA with turkey post hoc analysis showed significant differences (F(5, 9)= 7.81, p=0.004) between camptothecin-treated mouse cells and any NMR sample (p<0.05) and near significance between control cells of both species (p=0.06). Again, this confirms the preliminary analysis that suggests that NMR cells are smaller than mouse cells.

Table 5.2. The median forward scattering (FSC) of Mouse or NMR cells treated with camptothecin (cam), chromium (vi) oxide (chro) or under control conditions (con).

	Median FSC	Total cell count	Std dev
Mouse con	1,730.67	1,8567	40.67
Mouse cam	1,855.17	1,6142	106.50
Mouse chro	1,635.33	1,0283	59.07
NMR con	1,464.00	552	125.87
NMR cam	1,523.00	318	80.61
NMR chro	1,504.50	1,015	106.77

5.4.2 Flow cytometry

To assess the progression of the cells through the cell cycle, flow cytometry was performed (Appendix Figure 12 - 14). There were no significant differences between species or treatment. NMR cells treated with camptothecin appeared to show increased arrest at G2 (control: 14.5% camptothecin: 25.3%), however, this was not statistically significant (Figure 5.5). It is of note that a large increase in cells arresting at G2 (97.7%) was seen in one replicate. This was not reproduced in subsequent assays. However, all subsequent assays used a lower number of cells (Appendix Table 8) that may reduce the accuracy of these results. ANOVA analysis indicated that each component of the cell cycle differed significantly (F(2, 36)=55.4 p=0) with G2 showing the greatest accumulation, and S phase the smallest.

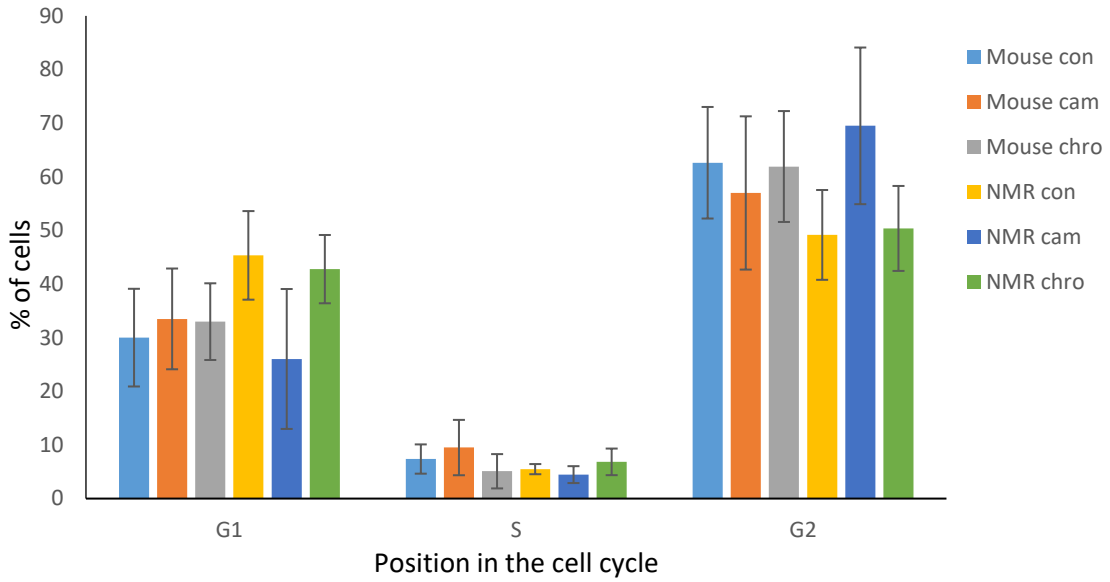

Figure 5.5. The percentage of living cells at each position in the cell cycle for mouse and NMR cells (beta stock) after 24-hour post-treated with genotoxic compounds after 24 hours of cell culture. Each position of the cell cycle showed significant variation from each other stage for both species ($F(2, 36)=55.4$ $p=0$). There was no significant variation between species or treatment, however, NMR cells treated with camptothecin seemed to show greater arrest in G2, however, this was not statistically significant. Abbreviations, con – control, cam – camptothecin, and chro – chromium. Error bars indicate ± one standard error of the mean between three cell lines (each composed of two average of two independent experiments). Total number of cells examined is given in Appendix Table 8.

Additionally, the proportion of cells that did not fall within G1, S or G2 was assessed (Figure 5.6). These cells that had a lower DNA content than at G1 comprised primarily apoptotic cells, though they may also include senescent cells. Camptothecin treatment in NMR cells appears to have resulted in an increase in such cells however this is not significant (control: 62.4%, camptothecin: 74.2%). The proportion of these cells was the same for both species after treatment which we would expect as both species were treated with LD50. There was no significant increase in these cells after treatment relative to controls indicating a similar number of apoptotic or potentially senescent cells.

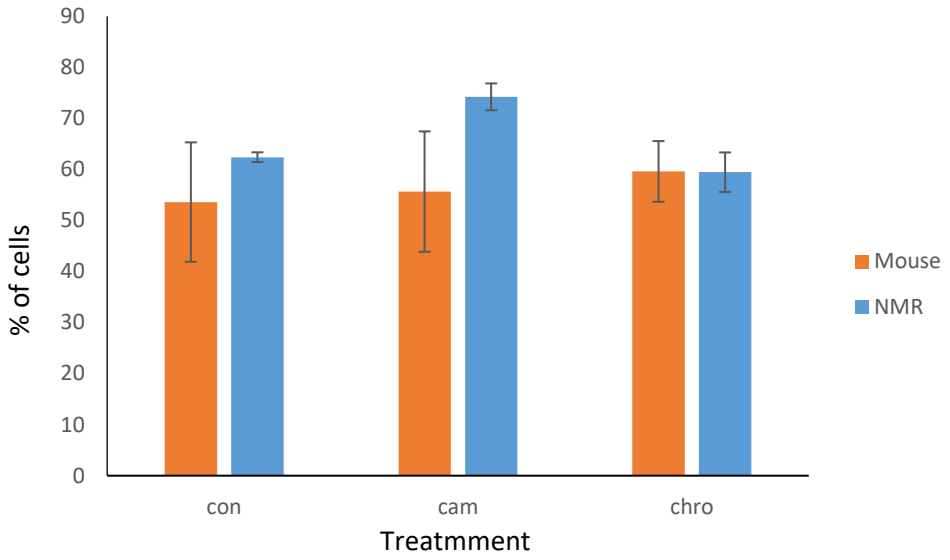

Figure 5.6. The percentage of senescent and/or apoptotic mouse or NMR cells (beta stock) 24 hours after genotoxic treatment. Statistically, there was no significant difference between any of the samples or treatments. However, NMR cells appear to show more senescence and/or apoptotic cells than mouse cell after camptothecin treatment. Abbreviations, con – control, cam – camptothecin, and chro – chromium. Error bars indicate ± one standard error of the mean between three cell lines (each are the average of two independent experiments). Total number of cells examined is given in Appendix Table 8.

5.5 Discussion

In the previous chapter, it was demonstrated that NMRs' fibroblasts have greater levels of gene expression of cell adhesion genes than fibroblasts derived from mice. Here we demonstrate phenotypic variations in cell adhesion. NMR cells appear to show slower attachment than mouse cells. This difference was not significant in control condition but was in cells treated with genotoxic compounds. Both NMR and mouse cells showed opposite responses with NMR cells showing slower attachment and mouse cells having accelerated attachment in response to the stress. This observation disproves our initial hypothesis that NMR cells are too 'sticky' to metastasise or develop into tumours. However such differences in adhesion may influence the differences in cancer incidence observed in mouse and NMRs. Cancer cells rely on cellular adhesion to facilitate motility and extravasation during metastasis. Cells that bind to surfaces less readily would be slower or less capable of metastasising. A lack of metastasis would limit any cancerous cells to the primary tumour and hence would be considered benign and would be more difficult to detect. Once the cells have attached to a substrate, there does not appear to be any difference in cell attachment strength as both NMR and mouse cells took similar times to detach in response to trypsin treatment. NMR cells did seem to take a little longer

to detach though this was only significant at 3 minutes in treated cells and only a very small difference was observed (a difference of 2% (camptothecin), and 8% (chromium) difference between species) and hence is likely not biologically significant. NMR cells appear smaller than mouse cells, hence these cells will have a smaller surface area in contact with the attachment surface, and there for the increased expression of cell adhesion genes may simply compensate for this to give similar levels of cell adhesion between differently sized cells. As our data suggests similarities in cell cycle progression, the observed difference in cell size should not be due to cells being in different parts of the cell cycle.

Statistically, there was no difference in cell cycle progression between species or treatments. This is unusual considering the differences in expression of a number of cell cycle regulating genes such as p53 and p21 observed in the RNAseq data. One replicate did, however, show a large accumulation of NMR cells in G2 after treatment with camptothecin. This observation would match the gene expression profile observed in the previous chapter that showed a number of genes known to induce arrest at G2 were differentially expressed. Increased arrest in G2 may facilitate superior repair of double-strand breaks due to the presence of two sets of genomic DNA that allows for homologous recombination. Were more time available the results of this assay would be checked by repeating the assay with a greater number of cells. As no difference in cell cycle progression is observed, we must conclude that after 24 hours post-treatment there is no remaining growth arrest. Perhaps a sooner time point after treatment would provide more insight into any differences in cell cycle progression. Were more time available more time points post stimulus would be studied to ensure differences in cell cycle progression were not being missed. The proportion of cells in G0 is the same both between treatments and species. These cells in G0 represent cells undergoing cellular senescence and apoptosis. We would expect the treatment at LD50 to drastically increase the proportion of apoptotic cells. However, this is not observed indicating that the cells killed by the genotoxic treatment have already died and been removed from our test population. Similar levels of G0 match the previously observed amount of cellular senescence after 24 hours post-stress between species in Chapter 3.4. However, we would expect to see an increase in stressed mouse cells relative to mouse controls as a drastic increase in cellular senescence was observed in Chapter 3.4 between untreated and LD50 treated cells. This indicates that cells in G0 are not representative of levels of total cellular senescence.

Chapter 6: General discussion

6.1 Discussion

In this study, we have used a transcriptomic approach to guide research into successful ageing. Two opposite approaches were taken to gain a broad overview of life-extending processes. Firstly, the examination of whole organisms experiencing a lifespan and health-span extending intervention in the form of *C. elegans* undergoing caloric restriction or treatment with caloric restriction mimetics. Secondly, we studied in detail differences at the cellular level between a long (*H. glaber*) and short (*M. musculus*) lived organism through cell culture studies. These two approaches looking between and within species to study changes of health-span and lifespan provide a complementary view of these aspects.

Firstly, microarray analysis of *C. elegans* undergoing caloric restriction or treatment with the caloric restriction mimetics rapamycin and allantoin was conducted in Chapter 2. This analysis showed that the newly discovered caloric restriction mimetic allantoin induced a similar gene expression profile to caloric restriction, helping to confirm its status as a caloric restriction mimetic. This similarity was greater than was seen in the well-established caloric restriction mimetic, rapamycin. Functional enrichment analysis of these caloric restriction mimetic treated worms showed enrichment of differentially expressed genes related to development. Genes that act early on in development to promote rapid growth and survival may continue to act inappropriately in later life and result in ageing. Hence alterations in such activity may promote successful ageing. Rapamycin treatment and caloric restriction are known to inhibit cellular growth (555, 556) and delay development in a variety of model organisms including *C. elegans* (557-561). These changes in development are not equal between treatments showing different levels of lifespan extension pathways activity despite similar changes in lifespan (72). It is not clear if these developmental factors are a cause or consequence of the anti-ageing activity of these treatments. Allantoin and rapamycin treatment produced different transcriptional profiles with a large number of differentially expressed genes being identified between these two treatments. This suggests that these compounds act differently.

Additionally, differentially expressed genes relating to the cell surface and the cell cycle were also enriched. Differences in cell cycle progression could prolong lifespan in accordance with the 'reproductive-*cell cycle* theory of ageing'. As has been discussed in Chapter 2.5, this theory states that early processes that promote required cellular growth early in life continue to act in later life when such growth is not required. This inappropriate growth is considered a driving force in ageing. More appropriate cell growth may allow for conserving of resources, and more rigorous checking of cellular damage to prevent propagation of cellular defects. Changes in cell cycle may act to prolong ageing in

the same way as changes in development, or may simply be a consequence of changes in development. Differences at the cell membrane may be a result of the changes described above or may be due to the cell surface being directly exposed to the compounds with which the worms were treated. Cell surface proteins are typically involved in cellular signalling or cell adhesion. Cellular signalling may be essential in successful ageing to communicate external signals such as life-extending treatments or cellular signals from other cells exposed to such treatment to coordinate a global response.

Were this study to be continued, the compounds of interest would be administered to older worms to avoid the possibility that the compounds are simply delaying the rate at which the worms are developing. A longer period of drug treatment could be studied to identify the effects of chronic exposure and how this affects normal age-associated changes in gene expression.

Secondly, we studied in detail skin fibroblasts derived from the NMR and mice. In Chapter 3 we found that NMR fibroblasts were significantly more resistant to two DNA-damaging compounds, camptothecin and chromium (vi) oxide. The NMR cells required a higher dose of these compounds to kill half the cells in the sample. Additionally, treatment with these compounds resulted in a large increase in cellular senescence in mouse but not NMR cells. An increased capacity to handle genotoxic stress may contribute to the NMR's long lifespan and cancer-resistant phenotype. DNA damage is largely considered a key cause of ageing and cancer. Cells that prevent the accumulation of DNA damage through quick or successful repair of this damage or by otherwise successfully managing such damage will age slower and will be less inclined to become cancerous. Senescent cells which are irreversibly exited from the cell cycle are often considered to be simply off. This is not the case; such cells continue to perform their cellular function and signal to neighbouring cells. Senescent cells can secrete pro-inflammatory cytokines, and growth factors that disrupt normal cellular architecture and function and have been found to promote cancer development (562). Additionally, senescent cells often show increased secretion of metalloproteinases, disrupting extracellular proteins and promoting cancer as a result (563). Furthermore, senescent cells have been associated with ageing and other ageing related pathologies (406, 564) with one study that selectively removed senescent cells from a prematurely ageing mouse model resulting in delays in ageing-associated disorders (565). As such, reduced accumulation of senescent cells could delay ageing and cancer onset. Higher base levels of senescent cells were seen in NMRs, however, this may be a result of such cells accumulating between less frequent passages due to slower growth in NMRs or sub-optimal growth conditions in the relatively new model organisms. To assess this, cells taken directly from mice or NMRs should be assessed to evaluate the number of senescent cells found in vivo.

An RNAseq analysis of NMR and mouse primary skin fibroblasts responding to treatment with these genotoxic stressors was performed in Chapter 4. A large difference in cell surface proteins, particularly cell adhesion proteins, was observed between mouse and NMR cells under all conditions. NMRs show significantly higher expression of cell adhesion genes. Functional enrichment showed similar differences between control and treated NMR cells, potentially indicating a role in the stress response. Cell adhesion is involved in an array of different cellular processes as well as cancer development and prognosis (510, 516). Differences in such gene expression may explain the NMR's pronounced cancer-resistant phenotype. Increased cell adhesion may physically inhibit the growth of a tumour, and can prevent metastasis (516, 517). A decrease in cell adhesion may prevent metastasising cells from establishing in new areas of the body (519, 520). These differences in cellular adhesion in the skin of NMRs may have originally evolved to aid skin elasticity for squeezing through tight tunnels, or to aid defence and repair of bite wounds that NMRs often inflict upon one another to assert dominance and maintain the colonies hierarchy (566). A previous RNAseq study found the most highly upregulated gene in NMRs to be EPCAM a cell adhesion molecule which further hints at the importance of cell adhesion molecules in the NMR (192).

This analysis found that NMRs had either significantly lower or similar expression of DNA damage repair associated genes than mice. Given the finding that NMRs appear more resistant to DNA damaging agents, we would expect the opposite to be true. Additionally, this finding is a direct contradiction of previous work (193). This work suggested that NMR showed greater levels of gene expression relating to homologous recombination, NHEJ, MMR and DNA damage response signalling. However, our results show no significant difference between NHEJ, MMR or homologous recombination and showed that genes they termed DNA damage response signalling and NER had significantly lower expression in NMRs. This difference may be explained by the difference in cell type, as the previous study used liver cells. This highlights a potential issue with using only one cell type, as factors affecting an organism's lifespan may be due to the activity of specific organs or tissues that are not studied in this thesis. The finding that NMRs are more susceptible to NER may explain why NMRs appear sensitive to UV-induced DNA damage that has been observed in previous studies (175) as this type of DNA repair is the key means of repairing such damage. This work brings into question the prevailing theory that NMR's long life, cancer resistance and DNA damage resistance is due to increase DNA damage repair gene expression.

Additionally, cell-cycle-related genes were enriched in differentially expressed genes. This may be indicative of the slower growth rate of NMR cells. As discussed above, differences in cell cycle may contribute to increases in lifespan. Particularly, increased delays in cell cycle progression may indicate and facilitate increased DNA damage detection and repair, preventing damage being

transferred to daughter cells. As mitosis can result in mutations becoming permanent in daughter cells, preventing this damage from being passed on is vital to ensure the integrity of the genome within a population of cells.

In response to the results of the RNAseq analysis, assays to detect variations in cell adhesion and cell cycle progression were performed in Chapter 5. Cell attachment and detachment assays were conducted. It was found that, despite the increased expression of cellular adhesion genes, NMR cells showed significantly slower attachment than mouse cells after genotoxic treatment. NMR cells treated with genotoxic stressors appeared to show slower attachment than control cells, but mouse cells showed the opposite trend, though these observations were not statistically significant. Such slow attachment may contribute to the NMR's cancer resistance by inhibiting metastasising cells from establishing new tumours. Attachment assays indicated a slight increase in adhesion strength of NMR cells, but this was very small (2%-8% difference). As discussed above, increases in cell adhesion can inhibit cancer growth and may contribute to the NMR's cancer-resistant phenotype. Increased resistance to cancer, a key source of mortality in mice (567), would help facilitate increased lifespan. These assays serve as a phenotypic validation to our RNAseq analysis. Flow cytometry indicated no significant difference in cell cycle progression, though NMR appeared to show an increase in the proportion of cells in G2 in one replicate, this was not repeatable. It is surprising that no difference in cell cycle progression was observed as this has been shown in mouse cells previously. However, this was using different doses and exposure times (568). Further work is needed to validate these results and if this experiment were to be repeated, different time points post-genotoxic insult would be analysed to ensure differences in cell cycle progression were not being overlooked.

This project has made use of transcriptomic techniques that are becoming increasingly accessible to direct research into successful ageing. Particularly we have identified a potentially key difference between the long-lived NMR and short-lived mouse that has not been studied in detail. The differences in cell adhesion between these two species may serve as a key factor in cancer resistance in the NMR. It will be of interest to perform gene expression analyses on tissues directly extracted from whole organisms to determine if these differences are still present when cells are grown in their native environment. Ideally, the expression of cell adhesion protein would be confirmed through western blot analysis. Excellent work is being done using chick embryos as a model to study metastasis of cancer cells (569). Such a system could be used to evaluate differences in metastasis between transformed NMR and mouse cells. Malignant mouse cells with changes in cell adhesion gene expression to mimic NMR cells, by increasing *Selplg* expression, for example, could be generated and the cells' capacity to leave the primary tumour and form secondary tumours would be evaluated.

The overall aim of this thesis was to better our understanding of successful ageing and avoidance of age-related morbidities, notably cancer. The work that makes up this thesis has addressed this aim in a number of ways. The work has identified a number of candidate genes that may be important in successful ageing. Differences in cellular adhesion between the long-lived, cancer-resistant NMR and the short-lived, cancer-prone mouse were discovered. Based on this observation and the established literature that has shown a complex role of cellular adhesion in cancer, we hypothesise that this cellular adhesion plays a key role in the NMR's cancer resistance. The idea that differences in cell cycle progression are responsible for differences in DNA damage resistance has been challenged by the observed similarities in the proportion of cells in each stage of the cell cycle. Furthermore, our understanding of NMR cell biology has improved with assays never before performed on this organism, such a flow cytometry, being undertaken as well as validation of the available literature. Finally, vast amounts of data that are available for others to study has been generated.

In summary, we have identified a number of candidate genes that may be integral to successful ageing, and have identified cellular adhesion as a key component in the long-lived rodent, the NMR.

6.2 Future work

Were this work to be repeated or continued, a number of experiments would be changed, repeated or added to the set of work outlined in this thesis. A number of such experiments have been outlined throughout this thesis. Key experiments already discussed will be repeated in brief here and additional experiments proposed.

High baseline levels of senescence were observed in the NMR, which was not seen in mice. This could be a caveat of the NMR's slow growth that would result in more time for such cells to accumulate between the less frequent passaging required to maintain the cell stocks. Alternatively, this could imply suboptimal growth conditions. Were this work to be repeated or continued, the effect of growth conditions on growth rate and senescence would be evaluated. Key factors to be assessed would include FBS content, temperature and oxygen content. Other variables to assess could include culture media pH, starting cell density and the frequency with which the media was replaced. Using traditional experimental approaches, the above work would be a major undertaking, however by using a definitive screening design all 6 of the above variables can be analysed as well as assessing interactions between the variable in only 14 experimental conditions (Appendix Figure 15).

The number of experimental runs this type of design of experiment (DoE) requires is two times the number of variables to assess plus one, providing the number of variables is greater than or equal to 6 (for more detail of definitive screening design the reader is directed to (570)). Cells would be grown under the conditions detailed in Appendix Figure 15, and the growth rate and level of baseline senescence would be recorded. This would be input into a statistical package, and a model generated based on the data. This model would predict the effect of each variable and second-order effects (the effect of one variable on another) on senescence and growth rate. The design could be extended to include treatment with either the DNA-damaging agent studied in this thesis or even species could be included as a variable so that one study would be taken as opposed to running the design twice (once per species). Midpoints are included to allow the assessment of curvature within the variable effect. Such curvature is likely as cells grow best at an optimal condition (top of the curve) and this growth deteriorates as the cells move away from this condition. This analysis would help predict optimal growth conditions for both cell lines that would facilitate future work. By comparing and contrasting how this varies between species we can make predictions about how the conditions within the animals themselves may vary. If including the frequency of media change as a variable in this analysis this would give insight not only to rate of nutrient depletion and waste accumulation but may also relate to the release of proteins into the growth media by the cells that may help or hinder cell growth. By including DNA-damaging agents in the study, we could identify optimal conditions to avoid DNA damage which may play into the mechanisms used by the organisms to avoid such damage. This model will assign statistical significance values to each variable. Those that are insignificant are considered to be having little or no impact on the rate of growth and can be kept constant for further work. Those that are deemed significant are having an effect on the rate of growth or senescence in the cells. More traditional experimental methods would be employed to look into specific conditions of interest to fine tune the conditions. Taking values from NMR and mice allows the identification of an optimal compromise as conditions that maximise the growth rate of both species can be selected which is ideal for small labs that only have limited access to incubators.

This thesis focuses on only one cell type, and though such an approach can provide general insights, it may result in biased conclusions as we have not factored in variation due to cell type. For example, a key finding in this thesis is that NMRs show similar or lower gene expression than mice. However, a previous study looking at liver cells found the opposite to be true (193), indicating variation between these cell types. The easiest way to address this is to extend the scope of this analysis to other cell types from both mice and NMRs. This would prove logistically challenging to obtain such cells from NMR, but once cell stocks were obtained such work would be relatively simple

to perform. As a minimum, I would extend this study to include hepatocytes which have been shown to have a different gene expression profile to that observed in skin fibroblasts in this study.

This study only utilised two DNA damaging agents: chromium (vi) oxide which causes a large array of DNA damage and camptothecin which specifically causes single-strand and double-strand breaks. As discussed in Section 3.5.1 camptothecin acts in a topoisomerase 1 dependent fashion, and hence differences in resistance to camptothecin may be dependent on differences in topoisomerase 1 activity. To assess this, the resistance to compounds such as bleomycin which specifically causes single-strand DNA damage in a topoisomerase 1 independent fashion, should be assessed. Additionally inducing other forms of DNA damage to mouse and NMR cells and monitoring how the cells respond would also prove interesting, especially given our results that showed lower or equal levels of gene expression in genes associated with each type of DNA damage repair mechanism.

We have looked at gene expression in detail, but the obvious next step would be to confirm these findings at the protein level through western blot analysis. Additionally, such an approach could be used to identify post-translational modifications by using antibodies specific to such modifications, which if present could indicate the activity of the protein of interest. By performing immunohistochemistry, we could also identify the cellular localisation of our protein of interest which could also give us an indication of activity. If we were studying a transcription factor, for example, a nuclear localisation might indicate activity, and a cytosolic localisation may indicate inactivity or alternate activity. A combination of these techniques would provide more insight into what is actually happening within the cell. Gene expression profiling does not take into account post-translational modifications or translational repression of transcripts by factors such as RNA interference.

To build on the findings that adhesion-associated genes are upregulated in the NMR and the hypothesis that these genes are, in part, responsible for the NMR's cancer resistance, a number of approaches could be taken. Firstly, altering the expression of such genes in mice and monitoring the effect on ageing and cancer incidence or the spread of induced tumours. This could include reducing expression through knock down/out studies of genes thought to be beneficial and assaying for a negative impact, or increasing such expression and monitoring for benefits. Though possible a more feasible alternative, particularly as a starting point to assess which specific gene to manipulate would be to perform such manipulations on a short-lived animal. Assessing the effects of ageing on mice is difficult and expensive due to the need to maintain mice for a long period of time. Performing such work on short-lived animals such as *C. elegans* would be faster, cheaper and could

be done with greater sample sizes to give robust results. This approach could be applied to other genes of interest such as the DNA damage repair associated genes that were upregulated in NMR for example.

An alternative approach outlined in Section 6.1 could utilise the chick embryo as a model of study to directly monitor metastasis of cancerous cells with modifications in our adhesion gene of choice. As I hypothesise that alteration of adhesion genes could act principally to affect cancer development and progression, such an approach would be ideal to confirm this. By injecting genetically modified cells (to increase or decrease the gene expression of the selected adhesion gene) we would see if this modification aided or impeded the cell's ability to metastasise. It is of note that these cells would need to be transformed into cancerous cells prior to injection. Alternatively, genetically modified chick embryos could be produced so that normal cancer cells are transplanted into tissue that has altered expression of the adhesion gene of choice. If the cancer cells showed reduced metastasis, we would know that metastasis required any gene that had its expression reduced and is impeded by any gene that had its expression increased.

If such genetic interventions showed promise the next logical step would be to treat model organisms in a manner that is applicable to humans. Typically, genetic modification in animal requires alteration of embryos and selective breeding. Such methods would not be possible in humans, and so alternative methods would be required such as the use of viral vectors to genetically modify a subset of cells or the extraction of key cells to facilitate genetic modification before transplanting back into the patient. For adhesion genes, we would likely wish to target fibroblasts and hence would ideally extract and modify MSCs which would then go on to produce modified fibroblasts in the patient. If the alteration of adhesion genes proved successful in preventing tumour cells from spreading and growing, one could hypothetically compromise by genetically modifying cells in specific areas to form barriers or traps to reduce the spread of cancerous cells and facilitate conventional anti-cancer treatments. Such hypothetical approaches could be tested in mouse models.

A preferable approach would be to treat patients with a drug or protein that would promote the expression of our gene of choice while having minimal effects on other genes' expressions. Such a compound would likely be difficult to identify, however.

A different approach that could build on this thesis work is to look at the environment of the cells after treatment with genotoxic stressors. A number of genes identified through the functional enrichment studies are secreted and hence examining these proteins may prove beneficial. The first experiment would be to collect conditioned media (this was already performed throughout the

above work and frozen for future experimentation) that cells recovering from genotoxic insult were grown in. Cells could then be grown in this conditioned media and treated with genotoxic insults and the level of mortality and senescence evaluated relative to cells grown in unconditioned media. If cells grown in the conditioned media showed reduced mortality and/or senescence, this would indicate that the cells are secreting something that protects the cells and/or aids recovery of the damaged cells. Identifying what proteins are produced would be difficult, but by producing knock out cell lines for secreted proteins identified as highly expressed in the expression data presented in Chapter 4 and monitoring how this affects the ability of media conditioned by these cells to aid wild-type cells exposed to genotoxic stress beneficial proteins could be identified. If a protein was identified through this method, its usefulness could be confirmed by upregulating the gene's expression and monitoring how this affects cell survival in response to stress. In addition, condition media could be collected and purified through column chromatography to isolate the protein of choice. This could then be administered to cell media to create conditioned media that lacks other secreted proteins to confirm that the protein under study is actually causing the effect. This would likely require upregulation of the gene to increase protein content in the media. Secreted proteins that provide beneficial effects to DNA damage resistance, cancer or ageing would be useful as they could simply be administered to individuals directly to gain the beneficial effect. The protein could be expressed in *E. coli* for example, and produced in a fermenter. This would then be purified and sterilised before being administered to patients. Such a treatment would need to show efficacy in a model organism, but the process would require little alteration to be performed in humans if it was shown to be effective.

References

1. Harman D. Aging - a Theory Based on Free-Radical and Radiation-Chemistry. J Gerontol. 1956;11(3):298-300.
2. Kandola K, Bowman A, Birch-Machin MA. Oxidative stress - a key emerging impact factor in health, ageing, lifestyle and aesthetics. Int J Cosmetic Sci. 2015;37:1-8.
3. Marnett LJ. Lipid peroxidation - DNA damage by malondialdehyde. Mutat Res-Fund Mol M. 1999;424(1-2):83-95.
4. Cabiscol E, Piulats E, Echave P, Herrero E, Ros J. Oxidative stress promotes specific protein damage in Saccharomyces cerevisiae. Journal of Biological Chemistry. 2000;275(35):27393-8.
5. Wu DF, Cederbaum AI. Alcohol, oxidative stress, and free radical damage. Alcohol Res Health. 2003;27(4):277-84.
6. Hayakawa M, Hattori K, Sugiyama S, Ozawa T. Age-Associated Oxygen Damage and Mutations in Mitochondrial-DNA in Human Hearts. Biochem Bioph Res Co. 1992;189(2):979-85.
7. Barja G, Herrero A. Oxidative damage to mitochondrial DNA is inversely related to maximum life span in the heart and brain of mammals. Faseb J. 2000;14(2):312-8.
8. Barja G. Rate of generation of oxidative stress-related damage and animal longevity. Free Radical Bio Med. 2002;33(9):1167-72.
9. Driver C, Georgeou A. Variable effects of vitamin E on Drosophila longevity. Biogerontology. 2003;4(2):91-5.
10. Fischer F, Hamann A, Osiewacz HD. Mitochondrial quality control: an integrated network of pathways. Trends Biochem Sci. 2012;37(7):284-92.
11. Linnane AW, Kios M, Vitetta L. Healthy aging: regulation of the metabolome by cellular redox modulation and prooxidant signaling systems: The essential roles of superoxide anion and hydrogen peroxide. Biogerontology. 2007;8(5):445-67.
12. Lewis KN, Andziak B, Yang T, Buffenstein R. The Naked Mole-Rat Response to Oxidative Stress: Just Deal with It. Antioxid Redox Sign. 2013;19(12):1388-99.
13. Walker RF. Developmental Theory of Aging Revisited: Focus on Causal and Mechanistic Links Between Development and Senescence. Rejuv Res. 2011;14(4):429-36.
14. Tacutu R, Craig T, Budovsky A, Wuttke D, Lehmann G, Taranukha D. Human Ageing Genomic Resources: Integrated databases and tools for the biology and genetics of ageing. Nucleic acids research. 2013;41(D1):D1027-D33.
15. Lopez-Otin C, Blasco MA, Partridge L, Serrano M, Kroemer G. The Hallmarks of Aging. Cell. 2013;153(6):1194-217.
16. Moskalev AA, Shaposhnikov MV, Plyusnina EN, Zhavoronkov A, Budovsky A, Yanai H. The role of DNA damage and repair in aging through the prism of Koch-like criteria. Ageing Res Rev. 2013;12(2):661-84.
17. Martin GM. Genetic modulation of senescent phenotypes in Homo sapiens. Cell. 2005;120(4):523-32.
18. Talens RP, Christensen K, Putter H, Willemsen G, Christiansen L, Kremer D. Epigenetic variation during the adult lifespan: cross-sectional and longitudinal data on monozygotic twin pairs. Aging Cell. 2012;11(4):694-703.
19. Greer EL, Maures TJ, Hauswirth AG, Green EM, Leeman DS, Maro GS. Members of the H3K4 trimethylation complex regulate lifespan in a germline-dependent manner in C. elegans. Nature. 2010;466(7304):383-U137.
20. Powers ET, Morimoto RI, Dillin A, Kelly JW, Balch WE. Biological and Chemical Approaches to Diseases of Proteostasis Deficiency. Annual review of biochemistry. 2009;78:959-91.
21. Min JN, Whaley RA, Sharpless NE, Lockyer P, Portbury AL, Patterson C. CHIP deficiency decreases longevity, with accelerated aging phenotypes accompanied by altered protein quality control. Mol Cell Biol. 2008;28(12):4018-25.

22. Swindell WR, Masternak MM, Kopchick JJ, Conover CA, Bartke A, Miller RA. Endocrine regulation of heat shock protein mRNA levels in long-lived dwarf mice. Mech Ageing Dev. 2009;130(6):393-400.
23. Morrow G, Samson M, Michaud S, Tanguay RM. Overexpression of the small mitochondrial Hsp22 extends Drosophila life span and increases resistance to oxidative stress. Faseb J. 2004;18(1):598-+.
24. Rubinsztein DC, Marino G, Kroemer G. Autophagy and Aging. Cell. 2011;146(5):682-95.
25. Tomaru U, Takahashi S, Ishizu A, Miyatake Y, Gohda A, Suzuki S. Decreased Proteasomal Activity Causes Age-Related Phenotypes and Promotes the Development of Metabolic Abnormalities. Am J Pathol. 2012;180(3):963-72.
26. Bjedov I, Toivonen JM, Kerr F, Slack C, Jacobson J, Foley A. Mechanisms of Life Span Extension by Rapamycin in the Fruit Fly Drosophila melanogaster. Cell Metab. 2010;11(1):35-46.
27. Green DR, Galluzzi L, Kroemer G. Mitochondria and the Autophagy-Inflammation-Cell Death Axis in Organismal Aging. Science. 2011;333(6046):1109-12.
28. Nishimura EK, Granter SR, Fisher DE. Mechanisms of hair graying: Incomplete melanocyte stem cell maintenance in the niche. Science. 2005;307(5710):720-4.
29. Bergman RJ, Gazit D, Kahn AJ, Gruber H, Mcdougall S, Hahn TJ. Age-related changes in osteogenic stem cells in mice. J Bone Miner Res. 1996;11(5):568-77.
30. Molofsky AV, Slutsky SG, Joseph NM, He S, Pardal R, Krishnamurthy J. Increasing p16INK4a expression decreases forebrain progenitors and neurogenesis during ageing. Nature. 2006;443(7110):448-52.
31. Shaw AC, Joshi S, Greenwood H, Panda A, Lord JM. Aging of the innate immune system. Curr Opin Immunol. 2010;22(4):507-13.
32. Beerman I, Bhattacharya D, Zandi S, Sigvardsson M, Weissman IL, Bryder D. Functionally distinct hematopoietic stem cells modulate hematopoietic lineage potential during aging by a mechanism of clonal expansion. P Natl Acad Sci USA. 2010;107(12):5465-70.
33. Sintes J, Engel P. Bacterial recognition SLAM (CD150) is a multitasking immunoreceptor: from cosignalling to bacterial recognition. Immunol Cell Biol. 2011;89(2):161-3.
34. Rossi DJ, Bryder D, Seita J, Nussenzweig A, Hoeijmakers J, Weissman IL. Deficiencies in DNA damage repair limit the function of haematopoietic stem cells with age. Nature. 2007;447(7145):725-U15.
35. Janzen V, Forkert R, Fleming HE, Saito Y, Waring MT, Dombkowski DM. Stem-cell ageing modified by the cyclin-dependent kinase inhibitor p16INK4a. Nature. 2006;443(7110):421-6.
36. Kippin TE, Martens DJ, van der Kooy D. P21 loss compromises the relative quiescence of forebrain stem cell proliferation leading to exhaustion of their proliferation capacity. Gene Dev. 2005;19(6):756-67.
37. Cheng T, Rodrigues N, Shen H, Yang Y, Dombkowski D, Sykes M. Hematopoietic stem cell quiescence maintained by p21cip1/waf1. Science. 2000;287(5459):1804-8.
38. Chakkalakal JV, Jones KM, Basson MA, Brack AS. The aged niche disrupts muscle stem cell quiescence. Nature. 2012;490(7420):355-+.
39. Lavasani M, Robinson AR, Lu AP, Song MJ, Feduska JM, Ahani B. Muscle-derived stem/progenitor cell dysfunction limits healthspan and lifespan in a murine progeria model. Nat Commun. 2012;3.
40. Conboy IM, Conboy MJ, Wagers AJ, Girma ER, Weissman IL, Rando TA. Rejuvenation of aged progenitor cells by exposure to a young systemic environment. Nature. 2005;433(7027):760-4.
41. Villeda SA, Luo J, Mosher KI, Zou BD, Britschgi M, Bieri G. The ageing systemic milieu negatively regulates neurogenesis and cognitive function. Nature. 2011;477(7362):90-U157.
42. Cerletti M, Jang YC, Finley LWS, Haigis MC, Wagers AJ. Short-Term Calorie Restriction Enhances Skeletal Muscle Stem Cell Function. Cell Stem Cell. 2012;10(5):515-9.
43. Chen C, Liu Y, Liu Y, Zheng P. mTOR Regulation and Therapeutic Rejuvenation of Aging Hematopoietic Stem Cells. Sci Signal. 2009;2(98).

44. Ito K, Hirao A, Arai F, Matsuoka S, Takubo K, Hamaguchi I. Regulation of oxidative stress by ATM is required for self-renewal of haematopoietic stem cells. Nature. 2004;431(7011):997-1002.
45. Miyamoto K, Araki KY, Naka K, Arai F, Takubo K, Yamazaki S. Foxo3a is essential for maintenance of the hematopoietic stem cell pool. Cell Stem Cell. 2007;1(1):101-12.
46. Pont AR, Sadri N, Hsiao SJ, Smith S, Schneider RJ. mRNA Decay Factor AUF1 Maintains Normal Aging, Telomere Maintenance, and Suppression of Senescence by Activation of Telomerase Transcription. Mol Cell. 2012;47(1):5-15.
47. Adler AS, Sinha S, Kawahara TLA, Zhang JY, Segal E, Chang HY. Motif module map reveals enforcement of aging by continual NF-kappa B activity. Gene Dev. 2007;21(24):3244-57.
48. Wei J, Xu HM, Davies JL, Hemmings GP. Increase of Plasma Il-6 Concentration with Age in Healthy-Subjects. Life Sci. 1992;51(25):1953-6.
49. Ershler WB, Sun WH, Binkley N, Gravenstein S, Volk MJ, Kamoske G. Interleukin-6 and Aging - Blood-Levels and Mononuclear Cell Production Increase with Advancing Age and in-Vitro Production Is Modifiable by Dietary Restriction. Lymphokine Cytok Res. 1993;12(4):225-30.
50. Harris TB, Ferrucci L, Tracy RP, Corti MC, Wacholder S, Ettinger WH. Associations of elevated interleukin-6 and C-reactive protein levels with mortality in the elderly. Am J Med. 1999;106(5):506-12.
51. Ferrucci L, Harris TB, Guralnik JM, Tracy RP, Corti MC, Cohen HJ. Serum IL-6 level and the development of disability in older persons. J Am Geriatr Soc. 1999;47(6):639-46.
52. McCay CM, Crowell MF, Maynard LA. The effect of retarded growth upon the length of life span and upon the ultimate body size. J Nutr. 1935;10(1):63-79.
53. Jiang JC, Jaruga E, Repnevskaya MV, Jazwinski SM. An intervention resembling caloric restriction prolongs life span and retards aging in yeast. Faseb J. 2000;14(14):2135-7.
54. Klass MR. Aging in Nematode Caenorhabditis-Elegans - Major Biological and Environmental-Factors Influencing Life-Span. Mech Ageing Dev. 1977;6(6):413-29.
55. Weindruch R, Walford RL, Fligiel S, Guthrie D. The Retardation of Aging in Mice by Dietary Restriction - Longevity, Cancer, Immunity and Lifetime Energy-Intake. J Nutr. 1986;116(4):641-54.
56. Longo VD, Fontana L. Calorie restriction and cancer prevention: metabolic and molecular mechanisms. Trends Pharmacol Sci. 2010;31(2):89-98.
57. Weindruch R, Walford RL. Dietary Restriction in Mice Beginning at 1 Year of Age - Effect on Life-Span and Spontaneous Cancer Incidence. Science. 1982;215(4538):1415-8.
58. Weindruch R, Gottesman SRS, Walford RL. Modification of Age-Related Immune Decline in Mice Dietarily Restricted from or after Mid-Adulthood. P Natl Acad Sci-Biol. 1982;79(3):898-902.
59. Swindell WR. Dietary restriction in rats and mice: A meta-analysis and review of the evidence for genotype-dependent effects on lifespan. Ageing Res Rev. 2012;11(2):254-70.
60. Mattison JA, Roth GS, Beasley TM, Tilmont EM, Handy AM, Herbert RL. Impact of caloric restriction on health and survival in rhesus monkeys from the NIA study. Nature. 2012;489(7415):318-+.
61. Greer EL, Brunet A. Different dietary restriction regimens extend lifespan by both independent and overlapping genetic pathways in C-elegans. Aging Cell. 2009;8(2):113-27.
62. Carlisle DL, Pritchard DE, Singh J, Patierno SR. Chromium(VI) induces p53-dependent apoptosis in diploid human lung and mouse dermal fibroblasts. Mol Carcinogen. 2000;28(2):111-8.
63. Redman LM, Ravussin E. Caloric Restriction in Humans: Impact on Physiological, Psychological, and Behavioral Outcomes. Antioxid Redox Sign. 2011;14(2):275-87.
64. Zimin AV, Cornish AS, Maudhoo MD, Gibbs RM, Zhang X, Pandey S. A new rhesus macaque assembly and annotation for next-generation sequencing analyses. Biol Direct. 2014;9.
65. Uno H. Age-related pathology and biosenescent markers in captive rhesus macaques. Age. 1997;20(1):1-13.
66. Colman RJ, Beasley TM, Kemnitz JW, Johnson SC, Weindruch R, Anderson RM. Caloric restriction reduces age-related and all-cause mortality in rhesus monkeys. Nat Commun. 2014;5.

67. Nutrition A. Nutrient requirements of nonhuman primates. International Perspectives: The Future of Nonhuman Primate Resources. 2003:99-104.
68. Kanthaswamy S, Johnson Z, Trask JS, Smith DG, Ramakrishnan R, Bahk J. Development and Validation of a SNP-Based Assay for Inferring the Genetic Ancestry of Rhesus Macaques (Macaca mulatta). Am J Primatol. 2014;76(11):1105-13.
69. Clarke MR, O'Neil JAS. Morphometric comparison of Chinese-Origin and Indian-derived rhesus monkeys (Macaca mulatta). Am J Primatol. 1999;47(4):335-46.
70. Mattison JA, Ottinger MA, Powell D, Longo DL, Ingram DK. Endometriosis: clinical monitoring and treatment procedures in rhesus Monkeys. J Med Primatol. 2007;36(6):391-8.
71. de Cabo R, Furer-Galban S, Anson RM, Gilman C, Gorospe M, Lane MA. An in vitro model of caloric restriction. Exp Gerontol. 2003;38(6):631-9.
72. Calvert S, Tacutu R, Sharifi S, Teixeira R, Ghosh P, de Magalhaes JP. A network pharmacology approach reveals new candidate caloric restriction mimetics in C. elegans. Aging Cell. 2016;15(2):256-66.
73. Li J, Bonkowski MS, Moniot S, Zhang D, Hubbard BP, Ling AJY. AGING A conserved NAD(+) binding pocket that regulates protein-protein interactions during aging. Science. 2017;355(6331):1312-+.
74. Guan Y, Wang SR, Huang XZ, Xie QH, Xu YY, Shang D. Nicotinamide Mononucleotide, an NAD(+) Precursor, Rescues Age-Associated Susceptibility to AKI in a Sirtuin 1-Dependent Manner. J Am Soc Nephrol. 2017;28(8):2337-52.
75. Tsubota K. The first human clinical study for NMN has started in Japan. NPJ Aging Mech Dis. 2016;2:16021.
76. Speakman JR, Mitchell SE. Caloric restriction. Mol Aspects Med. 2011;32(3):159-221.
77. Kenyon C, Chang J, Gensch E, Rudner A, Tabtiang R. A C-Elegans Mutant That Lives Twice as Long as Wild-Type. Nature. 1993;366(6454):461-4.
78. Hannenhalli S, Kaestner KH. The evolution of Fox genes and their role in development and disease. Nat Rev Genet. 2009;10(4):233-40.
79. Breese CR, Ingram RL, Sonntag WE. Influence of Age and Long-Term Dietary Restriction on Plasma Insulin-Like Growth Factor-I (Igf-1), Igf-1 Gene-Expression, and Igf-1 Binding-Proteins. J Gerontol. 1991;46(5):B180-B7.
80. Ikeno Y, Hubbard GB, Lee S, Cortez LA, Lew CM, Webb CR. Reduced Incidence and Delayed Occurrence of Fatal Neoplastic Diseases in Growth Hormone Receptor/Binding Protein Knockout Mice. J Gerontol a-Biol. 2009;64(5):522-9.
81. Vergara M, Smith-Wheelock M, Harper JM, Sigler R, Miller RA. Hormone-treated snell dwarf mice regain fertility but remain long lived and disease resistant. J Gerontol a-Biol. 2004;59(12):1244-50.
82. Kachra Z, Barash I, Yannopoulos C, Khan MN, Guyda HJ, Posner BI. The Differential Regulation by Glucagon and Growth-Hormone of Insulin-Like Growth-Factor (Igf)-I and Igf Binding-Proteins in Cultured Rat Hepatocytes. Endocrinology. 1991;128(4):1723-30.
83. Uhlen M, Fagerberg L, Hallstrom BM, Lindskog C, Oksvold P, Mardinoglu A. Tissue-based map of the human proteome. Science. 2015;347(6220).
84. Alessi DR, Andjelkovic M, Caudwell B, Cron P, Morrice N, Cohen P. Mechanism of activation of protein kinase B by insulin and IGF-1. Embo Journal. 1996;15(23):6541-51.
85. Ogg S, Paradis S, Gottlieb S, Patterson GI, Lee L, Tissenbaum HA. The Fork head transcription factor DAF-16 transduces insulin-like metabolic and longevity signals in C-elegans. Nature. 1997;389(6654):994-9.
86. Paradis S, Ruvkun G. Caenorhabditis elegans Akt/PKB transduces insulin receptor-like signals from AGE-1 PI3 kinase to the DAF-16 transcription factor. Gene Dev. 1998;12(16):2488-98.
87. Tang ED, Nunez G, Barr FG, Guan KL. Negative regulation of the forkhead transcription factor FKHR by Akt. Journal of Biological Chemistry. 1999;274(24):16741-6.

88. Brunet A, Bonni A, Zigmond MJ, Lin MZ, Juo P, Hu LS. Akt promotes cell survival by phosphorylating and inhibiting a forkhead transcription factor. Cell. 1999;96(6):857-68.
89. Guo SD, Rena G, Cichy S, He XW, Cohen P, Unterman T. Phosphorylation of serine 256 by protein kinase B disrupts transactivation by FKHR and mediates effects of insulin on insulin-like growth factor-binding protein-1 promoter activity through a conserved insulin response sequence. Journal of Biological Chemistry. 1999;274(24):17184-92.
90. Jacobs FMJ, van der Heide LP, Wijchers PJEC, Burbach JPH, Hoekman MFM, Smidt MP. FoxO6, a novel member of the FoxO class of transcription factors with distinct shuttling dynamics. Journal of Biological Chemistry. 2003;278(38):35959-67.
91. Shimokawa I, Komatsu T, Hayashi N, Kim SE, Kawata T, Park S. The life-extending effect of dietary restriction requires Foxo3 in mice. Aging Cell. 2015;14(4):707-9.
92. Yamaza H, Komatsu T, Wakita S, Kijogi C, Park S, Hayashi H. FoxO1 is involved in the antineoplastic effect of calorie restriction. Aging Cell. 2010;9(3):372-82.
93. Motta MC, Divecha N, Lemieux M, Kamel C, Chen D, Gu W. Mammalian SIRT1 represses forkhead transcription factors. Cell. 2004;116(4):551-63.
94. Cohen HY, Miller C, Bitterman KJ, Wall NR, Hekking B, Kessler B. Calorie restriction promotes mammalian cell survival by inducing the SIRT1 deacetylase. Science. 2004;305(5682):390-2.
95. Ma LN, Dong W, Wang R, Li Y, Xu BL, Zhang JS. Effect of caloric restriction on the SIRT1/mTOR signaling pathways in senile mice. Brain Res Bull. 2015;116:67-72.
96. Mercken EM, Hu J, Krzysik-Walker S, Wei M, Li Y, McBurney MW. SIRT1 but not its increased expression is essential for lifespan extension in caloric-restricted mice. Aging Cell. 2014;13(1):193-6.
97. Chen WS, Xu PZ, Gottlob K, Chen ML, Sokol K, Shiyanova T. Growth retardation and increased apoptosis in mice with homozygous disruption of the akt1 gene. Gene Dev. 2001;15(17):2203-8.
98. Lin SJ, Defossez PA, Guarente L. Requirement of NAD and SIR2 for life-span extension by calorie restriction in Saccharomyces cerevisiae. Science. 2000;289(5487):2126-8.
99. Gong ZW, Kennedy O, Sun H, Wu YJ, Williams GA, Klein L. Reductions in serum IGF-1 during aging impair health span. Aging Cell. 2014;13(3):408-18.
100. Wilicox BJ, Donlon TA, He Q, Chen R, Grove JS, Yano K. FOXO3A genotype is strongly associated with human longevity. P Natl Acad Sci USA. 2008;105(37):13987-92.
101. Flachsbart F, Caliebeb A, Kleindorp R, Blanche H, von Eller-Eberstein H, Nikolaus S. Association of FOXO3A variation with human longevity confirmed in German centenarians. P Natl Acad Sci USA. 2009;106(8):2700-5.
102. Li Y, Wang WJ, Cao HQ, Lu JH, Wu C, Hu FY. Genetic association of FOXO1A and FOXO3A with longevity trait in Han Chinese populations. Hum Mol Genet. 2009;18(24):4897-904.
103. Tepper RG, Ashraf J, Kaletsky R, Kleemann G, Murphy CT, Bussemaker HJ. PQM-1 Complements DAF-16 as a Key Transcriptional Regulator of DAF-2-Mediated Development and Longevity. Cell. 2013;154(3):676-90.
104. Webb AE, Kundaje A, Brunet A. Characterization of the direct targets of FOXO transcription factors throughout evolution. Aging Cell. 2016;15(4):673-85.
105. Inoki K, Li Y, Zhu TQ, Wu J, Guan KL. TSC2 is phosphorylated and inhibited by Akt and suppresses mTOR signalling. Nature cell biology. 2002;4(9):648-57.
106. Vellai T, Takacs-Vellai K, Zhang Y, Kovacs AL, Orosz L, Muller F. Genetics - Influence of TOR kinase on lifespan in C-elegans. Nature. 2003;426(6967):620-.
107. Fok WC, Zhang YQ, Salmon AB, Bhattacharya A, Gunda R, Jones D. Short-Term Treatment With Rapamycin and Dietary Restriction Have Overlapping and Distinctive Effects in Young Mice. J Gerontol a-Biol. 2013;68(2):108-16.
108. Lamming DW, Ye L, Katajisto P, Goncalves MD, Saitoh M, Stevens DM. Rapamycin-Induced Insulin Resistance Is Mediated by mTORC2 Loss and Uncoupled from Longevity. Science. 2012;335(6076):1638-43.

109. Yu K, Toral-Barza L, Shi C, Zhang WG, Lucas J, Shor B. Biochemical, Cellular, and In vivo Activity of Novel ATP-Competitive and Selective Inhibitors of the Mammalian Target of Rapamycin. Cancer Res. 2009;69(15):6232-40.
110. Madeo F, Zimmermann A, Maiuri MC, Kroemer G. Essential role for autophagy in life span extension. J Clin Invest. 2015;125(1):85-93.
111. Toth ML, Sigmond T, Borsos E, Barna J, Erdelyi P, Takacs-Vellai K. Longevity pathways converge on autophagy genes to regulate life span in Caenorhabditis elegans. Autophagy. 2008;4(3):330-8.
112. Simonsen A, Cumming RC, Brech A, Isakson P, Schubert DR, Finley KD. Promoting basal levels of autophagy in the nervous system enhances longevity and oxidant resistance in adult Drosophila. Autophagy. 2008;4(2):176-84.
113. Liu Y, Shi SZ, Gu ZY, Du YZ, Liu MY, Yan ST. Impaired autophagic function in rat islets with aging. Age. 2013;35(5):1531-44.
114. Cuervo AM, Dice JF. Age-related decline in chaperone-mediated autophagy. Journal of Biological Chemistry. 2000;275(40):31505-13.
115. Mai S, Muster B, Bereiter-Hahn J, Jendrach M. Autophagy proteins LC3B, ATG5 and ATG12 participate in quality control after mitochondrial damage and influence life span. Autophagy. 2012;8(1):47-62.
116. Lapierre LR, De Magalhaes CD, McQuary PR, Chu CC, Visvikis O, Chang JT. The TFEB orthologue HLH-30 regulates autophagy and modulates longevity in Caenorhabditis elegans. Nat Commun. 2013;4.
117. Xie LL, Jiang Y, Ping OY, Chen J, Doan H, Herndon B. Effects of dietary calorie restriction or exercise on the PI3K and Ras signaling pathways in the skin of mice (vol 282, pg 28025, 2007). Journal of Biological Chemistry. 2008;283(23):16268-.
118. Castellano E, Downward J. RAS Interaction with PI3K: More Than Just Another Effector Pathway. Genes Cancer. 2011;2(3):261-74.
119. Yang JY, Zong CS, Xia WY, Yamaguchi H, Ding QQ, Xie XM. ERK promotes tumorigenesis by inhibiting FOXO3a via MDM2-mediated degradation. Nature cell biology. 2008;10(2):138-U22.
120. Ma L, Chen ZB, Erdjument-Bromage H, Tempst P, Pandolfi PP. Phosphorylation and functional inactivation of TSC2 by Erk: Implications for tuberous sclerosis and cancer pathogenesis. Cell. 2006;127(3):67-82.
121. Williamson D, Gallagher P, Harber M, Hollon C, Trappe S. Mitogen-activated protein kinase (MAPK) pathway activation: effects of age and acute exercise on human skeletal muscle. J Physiol-London. 2003;547(3):977-87.
122. Ratajczak MZ, Kucia M, Liu R, Shin DM, Bryndza E, Masternak MM. RasGrf1: genomic imprinting, VSELs, and aging. Aging-Us. 2011;3(7):692-7.
123. Suter M, Riek U, Tuerk R, Schlattner U, Wallimann T, Neumann D. Dissecting the role of 5 '-AMP for allosteric stimulation, activation, and deactivation of AMP-activated protein kinase. Journal of Biological Chemistry. 2006;281(43):32207-16.
124. Kurth-Kraczek EJ, Hirshman MF, Goodyear LJ, Winder WW. 5 ' AMP-activated protein kinase activation causes GLUT4 translocation in skeletal muscle. Diabetes. 1999;48(8):1667-71.
125. Carling D, Hardie DG. The Substrate and Sequence Specificity of the Amp-Activated Protein-Kinase - Phosphorylation of Glycogen-Synthase and Phosphorylase-Kinase. Biochim Biophys Acta. 1989;1012(1):81-6.
126. Hardie DG, Pan DA. Regulation of fatty acid synthesis and oxidation by the AMP-activated protein kinase. Biochem Soc T. 2002;30:1064-70.
127. Greer EL, Dowlatshahi D, Banko MR, Villen J, Hoang K, Blanchard D. An AMPK-FOXO pathway mediates longevity induced by a novel method of dietary restriction in C-elegans. Current Biology. 2007;17(19):1646-56.

128. Pallottini V, Montanari L, Cavallini G, Bergamini E, Gori Z, Trentalance A. Mechanisms underlying the impaired regulation of 3-hydroxy-3-methylglutaryl coenzyme A reductase in aged rat liver. Mech Ageing Dev. 2004;125(9):633-9.
129. Fulco M, Cen Y, Zhao P, Hoffman EP, McBurney MW, Sauve AA. Glucose restriction inhibits skeletal myoblast differentiation by activating SIRT1 through AMPK-mediated regulation of Nampt. Dev Cell. 2008;14(5):661-73.
130. Greer EL, Oskoui PR, Banko MR, Maniar JM, Gygi MP, Gygi SP. The energy sensor AMP-activated protein kinase directly regulates the mammalian FOXO3 transcription factor. Journal of Biological Chemistry. 2007;282(41):30107-19.
131. Inoki K, Zhu TQ, Guan KL. TSC2 mediates cellular energy response to control cell growth and survival. Cell. 2003;115(5):577-90.
132. Gwinn DM, Shackelford DB, Egan DF, Mihaylova MM, Mery A, Vasquez DS. AMPK phosphorylation of raptor mediates a metabolic checkpoint. Mol Cell. 2008;30(2):214-26.
133. Pearson KJ, de Cabo R. Nrf2 Mediates Cancer Protection but Not Longevity Induced by Caloric Restriction. J Nutrigenet Nutrige. 2009;2(4-5):198-.
134. Rowe JW, Kahn RL. Successful aging. Aging-Clin Exp Res. 1998;10(2):142-4.
135. Crowther MR, Parker MW, Achenbaum WA, Larimore WL, Koenig HG. Rowe and Kahn's model of successful aging revisited: Positive spirituality - The forgotten factor. Gerontologist. 2002;42(5):613-20.
136. Araujo L, Ribeiro O, Teixeira L, Paul C. Successful aging at 100 years: the relevance of subjectivity and psychological resources. Int Psychogeriatr. 2016;28(2):179-88.
137. Lozano R, Naghavi M, Foreman K, Lim S, Shibuya K, Aboyans V. Global and regional mortality from 235 causes of death for 20 age groups in 1990 and 2010: a systematic analysis for the Global Burden of Disease Study 2010. Lancet. 2012;380(9859):2095-128.
138. Heselmeyer-Haddad K, Garcia LYB, Bradley A, Ortiz-Melendez C, Lee WJ, Christensen R. Single-Cell Genetic Analysis of Ductal Carcinoma in Situ and Invasive Breast Cancer Reveals Enormous Tumor Heterogeneity yet Conserved Genomic Imbalances and Gain of MYC during Progression. Am J Pathol. 2012;181(5):1807-22.
139. Blackadar CB. Historical review of the causes of cancer. World journal of clinical oncology. 2016;7(1):54-86.
140. Sharma S, Kelly TK, Jones PA. Epigenetics in cancer. Carcinogenesis. 2010;31(1):27-36.
141. Evan GI, Vousden KH. Proliferation, cell cycle and apoptosis in cancer. Nature. 2001;411(6835):342-8.
142. Hayflick L, Moorhead PS. Serial Cultivation of Human Diploid Cell Strains. Exp Cell Res. 1961;25(3):585-&.
143. Bodnar AG, Ouellette M, Frolkis M, Holt SE, Chiu CP, Morin GB. Extension of life-span by introduction of telomerase into normal human cells. Science. 1998;279(5349):349-52.
144. Ouyang L, Shi Z, Zhao S, Wang FT, Zhou TT, Liu B. Programmed cell death pathways in cancer: a review of apoptosis, autophagy and programmed necrosis. Cell Proliferat. 2012;45(6):487-98.
145. Teng MWL, Swann JB, Koebel CM, Schreiber RD, Smyth MJ. Immune-mediated dormancy: an equilibrium with cancer. J Leukocyte Biol. 2008;84(4):988-93.
146. Kim R, Emi M, Tanabe K. Cancer immunoediting from immune surveillance to immune escape. Immunology. 2007;121(1):1-14.
147. Yang L, Pang YL, Moses HL. TGF-beta and immune cells: an important regulatory axis in the tumor microenvironment and progression. Trends Immunol. 2010;31(6):220-7.
148. Shields JD, Kourtis IC, Tomei AA, Roberts JM, Swartz MA. Induction of Lymphoidlike Stroma and Immune Escape by Tumors That Express the Chemokine CCL21. Science. 2010;328(5979):749-52.
149. Mougiakakos D, Choudhury A, Lladser A, Kiessling R, Johansson CC. Regulatory T Cells in Cancer. Adv Cancer Res. 2010;107:57-117.
150. Martinez-Outschoorn UE, Peiris-Pages M, Pestell RG, Sotgia F, Lisanti MP. Cancer metabolism: a therapeutic perspective. Nature reviews Clinical oncology. 2016.

151. Nishida N, Yano H, Nishida T, Kamura T, Kojiro M. Angiogenesis in cancer. Vascular health and risk management. 2006;2(3):213-9.
152. Muers MF, Round CE. Palliation of symptoms in non-small cell lung cancer: a study by the Yorkshire Regional Cancer Organisation Thoracic Group. Thorax. 1993;48(4):339-43.
153. Roodman GD. Mechanisms of disease: Mechanisms of bone metastasis. New Engl J Med. 2004;350(16):1655-64.
154. de Magalhaes JP, Costa J, Church GM. An analysis of the relationship between metabolism, developmental schedules, and longevity using phylogenetic independent contrasts. J Gerontol a-Biol. 2007;62(2):149-60.
155. Healy K, Guillerme T, Finlay S, Kane A, Kelly SBA, McClean D. Ecology and mode-of-life explain lifespan variation in birds and mammals. P Roy Soc B-Biol Sci. 2014;281(1784).
156. Corsi AK, Wightman B, Chalfie M. A Transparent Window into Biology: A Primer on Caenorhabditis elegans. Genetics. 2015;200(2):387-407.
157. Cassada RC, Russell RL. The dauerlarva, a post-embryonic developmental variant of the nematode Caenorhabditis elegans. Developmental biology. 1975;46(2):326-42.
158. Sternberg PW, Horvitz HR. Post-Embryonic Non-Gonadal Cell Lineages of the Nematode Panagrellus-Redivivus - Description and Comparison with Those of Caenorhabditis Elegans. Developmental biology. 1982;93(1):181-205.
159. Sulston JE, Schierenberg E, White JG, Thomson JN. The Embryonic-Cell Lineage of the Nematode Caenorhabditis-Elegans. Developmental biology. 1983;100(1):64-119.
160. Tatar M, Bartke A, Antebi A. The endocrine regulation of aging by insulin-like signals. Science. 2003;299(5611):1346-51.
161. Altun ZFaH, D. H. . Handbook of C. elegans Anatomy. In WormAtlas2005.
162. Raizen DM, Lee RYN, Avery L. Interacting Genes Required for Pharyngeal Excitation by Motor-Neuron Mc in Caenorhabditis-Elegans. Genetics. 1995;141(4):1365-82.
163. Avery L. The Genetics of Feeding in Caenorhabditis-Elegans. Genetics. 1993;133(4):897-917.
164. Lakowski B, Hekimi S. The genetics of caloric restriction in Caenorhabditis elegans. P Natl Acad Sci USA. 1998;95(22):13091-6.
165. Garigan D, Hsu AL, Fraser AG, Kamath RS, Ahringer J, Kenyon C. Genetic analysis of tissue aging in Caenorhabditis elegans: A role for heat-shock factor and bacterial proliferation. Genetics. 2002;161(3):1101-12.
166. Gems D, Riddle DL. Genetic, behavioral and environmental determinants of male longevity in Caenorhabditis elegans. Genetics. 2000;154(4):1597-610.
167. Smith ED, Kaeberlein TL, Lydum BT, Sager J, Welton KL, Kennedy BK. Age- and calorie-independent life span extension from dietary restriction by bacterial deprivation in Caenorhabditis elegans. Bmc Dev Biol. 2008;8.
168. Williams SA, Shattuck MR. Ecology, longevity and naked mole-rats: confounding effects of sociality? P Roy Soc B-Biol Sci. 2015;282(1802).
169. Buffenstein R. The naked mole-rat? A new long-living model for human aging research. J Gerontol a-Biol. 2005;60(11):1369-77.
170. Buffenstein R, Yahav S. Is the Naked Mole-Rat Heterocephalus-Glaber an Endothermic yet Poikilothermic Mammal. J Therm Biol. 1991;16(4):227-32.
171. Goldman BD, Goldman SL, Lanz T, Magaurin A, Maurice A. Factors influencing metabolic rate in naked mole-rats (Heterocephalus glaber). Physiol Behav. 1999;66(3):447-59.
172. Park TJ, Reznick J, Peterson BL, Blass G, Omerbasic D, Bennett NC. Fructose-driven glycolysis supports anoxia resistance in the naked mole-rat. Science. 2017;356(6335):305-8.
173. Delaney MA, Nagy L, Kinsel MJ, Treuting PM. Spontaneous Histologic Lesions of the Adult Naked Mole Rat (Heterocephalus glaber): A Retrospective Survey of Lesions in a Zoo Population. Vet Pathol. 2013;50(4):607-21.
174. Buffenstein R. Negligible senescence in the longest living rodent, the naked mole-rat: insights from a successfully aging species. J Comp Physiol B. 2008;178(4):439-45.

175. Salmon AB, Akha AAS, Buffenstein R, Miller RA. Fibroblasts from naked mole-rats are resistant to multiple forms of cell injury, but sensitive to peroxide, ultraviolet light, and endoplasmic reticulum stress. J Gerontol a-Biol. 2008;63(3):232-41.
176. Tian X, Azpurua J, Hine C, Vaidya A, Myakishev-Rempel M, Ablaeva J. High-molecular-mass hyaluronan mediates the cancer resistance of the naked mole rat. Nature. 2013;499(7458):346-U122.
177. Azpurua J, Ke ZH, Chen IX, Zhang QW, Ermolenko DN, Zhang ZDD. Naked mole-rat has increased translational fidelity compared with the mouse, as well as a unique 28S ribosomal RNA cleavage. P Natl Acad Sci USA. 2013;110(43):17350-5.
178. Li WG, Kong AN. Molecular Mechanisms of Nrf2-Mediated Antioxidant Response. Mol Carcinogen. 2009;48(2):91-104.
179. Lewis KN, Mele J, Hornsby PJ, Buffenstein R. Stress Resistance in the Naked Mole-Rat: The Bare Essentials - A Mini-Review. Gerontology. 2012;58(5):453-62.
180. Garcia-Cao I, Garcia-Cao M, Martin-Caballero J, Criado LM, Klatt P, Flores JM. 'Super p53' mice exhibit enhanced DNA damage response, are tumor resistant and age normally. Embo Journal. 2002;21(22):6225-35.
181. Matheu A, Maraver A, Klatt P, Flores I, Garcia-Cao I, Borras C. Delayed ageing through damage protection by the Arf/p53 pathway. Nature. 2007;448(7151):375-U14.
182. Weinberg RA. Oncogenes, antioncogenes, and the molecular bases of multistep carcinogenesis. Cancer Res. 1989;49(14):3713-21.
183. Fanning E. Simian Virus-40 Large T-Antigen - the Puzzle, the Pieces, and the Emerging Picture. J Virol. 1992;66(3):1289-93.
184. Seluanov A, Hine C, Azpurua J, Feigenson M, Bozzella M, Mao ZY. Hypersensitivity to contact inhibition provides a clue to cancer resistance of naked mole-rat. P Natl Acad Sci USA. 2009;106(46):19352-7.
185. Liang ST, Mele J, Wu YH, Buffenstein R, Hornsby PJ. Resistance to experimental tumorigenesis in cells of a long-lived mammal, the naked mole-rat (Heterocephalus glaber). Aging Cell. 2010;9(4):626-35.
186. Eagle H, Levine EM. Growth Regulatory Effects of Cellular Interaction. Nature. 1967;213(5081):1102-&.
187. Seluanov A, Hine C, Bozzella M, Hall A, Sasahara THC, Ribeiro AACM. Distinct tumor suppressor mechanisms evolve in rodent species that differ in size and lifespan. Aging Cell. 2008;7(6):813-23.
188. Patrick A, Seluanov M, Hwang C, Tam J, Khan T, Morgenstern A. Sensitivity of primary fibroblasts in culture to atmospheric oxygen does not correlate with species lifespan. Aging-Us. 2016;8(5):841-7.
189. Kim EB, Fang XD, Fushan AA, Huang ZY, Lobanov AV, Han LJ. Genome sequencing reveals insights into physiology and longevity of the naked mole rat. Nature. 2011;479(7372):223-7.
190. vanSteensel B, deLange T. Control of telomere length by the human telomeric protein TRF1. Nature. 1997;385(6618):740-3.
191. Bhattacharyya S, Keirsey J, Russell B, Kavecansky J, Lillard-Wetherell K, Tahmaseb K. Telomerase-associated protein 1, HSP90, and topoisomerase IIalpha associate directly with the BLM helicase in immortalized cells using ALT and modulate its helicase activity using telomeric DNA substrates. The Journal of biological chemistry. 2009;284(22):14966-77.
192. Yu CF, Li Y, Holmes A, Szafranski K, Faulkes CG, Coen CW. RNA Sequencing Reveals Differential Expression of Mitochondrial and Oxidation Reduction Genes in the Long-Lived Naked Mole-Rat When Compared to Mice. Plos One. 2011;6(11).
193. MacRae SL, Croken MM, Calder RB, Aliper A, Milholland B, White RR. DNA repair in species with extreme lifespan differences. Aging-Us. 2015;7(12):1171-84.
194. Altschul SF, Gish W, Miller W, Myers EW, Lipman DJ. Basic local alignment search tool. Journal of molecular biology. 1990;215(3):403-10.

195. Ma H, Li R, Zhang Z, Tong T. mRNA level of alpha-2-macroglobulin as an aging biomarker of human fibroblasts in culture. Exp Gerontol. 2004;39(3):415-21.
196. Blacker D, Wilcox MA, Laird NM, Rodes L, Horvath SM, Go RC. Alpha-2 macroglobulin is genetically associated with Alzheimer disease. Nat Genet. 1998;19(4):357-60.
197. Ishii N, Fujii M, Hartman PS, Tsuda M, Yasuda K, Senoo-Matsuda N. A mutation in succinate dehydrogenase cytochrome b causes oxidative stress and ageing in nematodes. Nature. 1998;394(6694):694-7.
198. Ishii T, Yasuda K, Akatsuka A, Hino O, Hartman PS, Ishii N. A mutation in the SDHC gene of complex II increases oxidative stress, resulting in apoptosis and tumorigenesis. Cancer Res. 2005;65(1):203-9.
199. Perez VI, Buffenstein R, Masamsetti V, Leonard S, Salmon AB, Mele J. Protein stability and resistance to oxidative stress are determinants of longevity in the longest-living rodent, the naked mole-rat. Proc Natl Acad Sci U S A. 2009;106(9):3059-64.
200. Andziak B, O'Connor TP, Qi W, DeWaal EM, Pierce A, Chaudhuri AR. High oxidative damage levels in the longest-living rodent, the naked mole-rat. Aging Cell. 2006;5(6):463-71.
201. Andziak B, Buffenstein R. Disparate patterns of age-related changes in lipid peroxidation in long-lived naked mole-rats and shorter-lived mice. Aging Cell. 2006;5(6):525-32.
202. Litvinov SV, Balzar M, Winter MJ, Bakker HA, Briaire-de Bruijn IH, Prins F. Epithelial cell adhesion molecule (Ep-CAM) modulates cell-cell interactions mediated by classic cadherins. J Cell Biol. 1997;139(5):1337-48.
203. Vilenchik MM, Knudson AG. Inverse radiation dose-rate effects on somatic and germ-line mutations and DNA damage rates. P Natl Acad Sci USA. 2000;97(10):5381-6.
204. De Bont R, van Larebeke N. Endogenous DNA damage in humans: a review of quantitative data. Mutagenesis. 2004;19(3):169-85.
205. Yasui M, Kanemaru Y, Kamoshita N, Suzuki T, Arakawa T, Honma M. Tracing the fates of site-specifically introduced DNA adducts in the human genome. DNA repair. 2014;15:11-20.
206. Krokan HE, Standal R, Slupphaug G. DNA glycosylases in the base excision repair of DNA. Biochem J. 1997;325:1-16.
207. Lindahl T, Nyberg B. Rate of Depurination of Native Deoxyribonucleic Acid. Biochemistry-Us. 1972;11(19):3610-&.
208. Boiteux S, Guillet M. Abasic sites in DNA: repair and biological consequences in Saccharomyces cerevisiae. DNA repair. 2004;3(1):1-12.
209. Loeb LA. Apurinic Sites as Mutagenic Intermediates. Cell. 1985;40(3):483-4.
210. Thompson LH, Brookman KW, Dillehay LE, Mooney CL, Carrano AV. Hypersensitivity to Mutation and Sister-Chromatid-Exchange Induction in Cho Cell Mutants Defective in Incising DNA Containing Uv Lesions. Somat Cell Genet. 1982;8(6):759-73.
211. Vamvakas S, Vock EH, Lutz WK. On the role of DNA double-strand breaks in toxicity and carcinogenesis. Crit Rev Toxicol. 1997;27(2):155-74.
212. Richardson C, Jasin M. Frequent chromosomal translocations induced by DNA double-strand breaks. Nature. 2000;405(6787):697-700.
213. Rabbitts TH. Chromosomal Translocations in Human Cancer. Nature. 1994;372(6502):143-9.
214. Korsmeyer SJ. Chromosomal Translocations in Lymphoid Malignancies Reveal Novel Protooncogenes. Annu Rev Immunol. 1992;10:785-807.
215. Randerath K, Zhou GD, Somers RL, Robbins JH, Brooks PJ. A P-32-Postlabeling assay for the oxidative DNA lesion 8,5 '-cyclo-2 '-deoxyadenosine in mammalian tissues - Evidence that four type II I-compounds are dinucleotides containing the lesion in the 3 ' nucleotide. Journal of Biological Chemistry. 2001;276(38):36051-7.
216. Yuan BF, Wang JS, Cao HC, Sun RB, Wang YS. High-throughput analysis of the mutagenic and cytotoxic properties of DNA lesions by next-generation sequencing. Nucleic acids research. 2011;39(14):5945-54.

217. Huang H, Das RS, Basu AK, Stone MP. Structure of (5 ' S)-8,5 '-Cyclo-2 '-deoxyguanosine in DNA. J Am Chem Soc. 2011;133(50):20357-68.
218. Goodsell DS. The molecular perspective: Ultraviolet light and pyrimidine dimers. Stem Cells. 2001;19(4):348-9.
219. Hemminki K. DNA-Adducts, Mutations and Cancer. Carcinogenesis. 1993;14(10):2007-12.
220. Hutchinson F. Use of Data from Bacteria to Interpret Data on DNA Damage Processing in Mammalian-Cells. Mutat Res. 1989;220(2-3):269-78.
221. Iyer RR, Pluciennik A, Burdett V, Modrich PL. DNA mismatch repair: functions and mechanisms. Chem Rev. 2006;106(2):302-23.
222. Balajee AS, Bohr VA. Genomic heterogeneity of nucleotide excision repair. Gene. 2000;250(1-2):15-30.
223. Fu D, Calvo JA, Samson LD. Balancing repair and tolerance of DNA damage caused by alkylating agents. Nat Rev Cancer. 2012;12(2):104-20.
224. Fahrer J, Kaina B. O-6-methylguanine-DNA methyltransferase in the defense against N-nitroso compounds and colorectal cancer. Carcinogenesis. 2013;34(11):2435-42.
225. Bellon S, Gasparutto D, Saint-Pierre C, Cadet J. Guanine-thymine intrastrand cross-linked lesion containing oligonucleotides: from chemical synthesis to in vitro enzymatic replication. Org Biomol Chem. 2006;4(20):3831-7.
226. Gu CN, Wang YS. Thermodynamic and in vitro replication studies of an intrastrand G[8-5]C cross-link lesion. Biochemistry-Us. 2005;44(24):8883-9.
227. Odonovan A, Davies AA, Moggs JG, West SC, Wood RD. Xpg Endonuclease Makes the 3' Incision in Human DNA Nucleotide Excision-Repair. Nature. 1994;371(6496):432-5.
228. Cole RS. Repair of Interstrand Crosslinks in DNA Induced by Psoralen Plus Light. Yale J Biol Med. 1973;46(5):492-.
229. Sarkar S, Davies AA, Ulrich HD, McHugh PJ. DNA interstrand crosslink repair during G1 involves nucleotide excision repair and DNA polymerase zeta. Embo Journal. 2006;25(6):1285-94.
230. Zheng HY, Wang X, Warren AJ, Legerski RJ, Nairn RS, Hamilton JW. Nucleotide excision repair- and polymerase eta-mediated error-prone removal of mitomycin C interstrand cross-links. Mol Cell Biol. 2003;23(2):754-61.
231. Shen X, Jun S, O'Neal LE, Sonoda E, Bemark M, Sale JE. REV3 and REV1 play major roles in recombination-independent repair of DNA interstrand cross-links mediated by monoubiquitinated proliferating cell nuclear antigen (PCNA). Journal of Biological Chemistry. 2006;281(20):13869-72.
232. Sugasawa K, Ng JM, Masutani C, Iwai S, van der Spek PJ, Eker AP. Xeroderma pigmentosum group C protein complex is the initiator of global genome nucleotide excision repair. Mol Cell. 1998;2(2):223-32.
233. Araki M, Masutani C, Takemura M, Uchida A, Sugasawa K, Kondoh J. Centrosome protein centrin 2/caltractin 1 is part of the xeroderma pigmentosum group C complex that initiates global genome nucleotide excision repair. The Journal of biological chemistry. 2001;276(22):18665-72.
234. Shimizu Y, Iwai S, Hanaoka F, Sugasawa K. Xeroderma pigmentosum group C protein interacts physically and functionally with thymine DNA glycosylase. The EMBO journal. 2003;22(1):164-73.
235. Sugasawa K, Okamoto T, Shimizu Y, Masutani C, Iwai S, Hanaoka F. A multistep damage recognition mechanism for global genomic nucleotide excision repair. Genes Dev. 2001;15(5):507-21.
236. Takao M, Abramic M, Moos M, Jr., Otrin VR, Wootton JC, McLenigan M. A 127 kDa component of a UV-damaged DNA-binding complex, which is defective in some xeroderma pigmentosum group E patients, is homologous to a slime mold protein. Nucleic acids research. 1993;21(17):4111-8.
237. Keeney S, Chang GJ, Linn S. Characterization of a human DNA damage binding protein implicated in xeroderma pigmentosum E. The Journal of biological chemistry. 1993;268(28):21293-300.

238. Wittschieben BO, Iwai S, Wood RD. DDB1-DDB2 (xeroderma pigmentosum group E) protein complex recognizes a cyclobutane pyrimidine dimer, mismatches, apurinic/apyrimidinic sites, and compound lesions in DNA. The Journal of biological chemistry. 2005;280(48):39982-9.
239. Scrima A, Fischer ES, Lingaraju GM, Bohm K, Cavadini S, Thoma NH. Detecting UV-lesions in the genome: The modular CRL4 ubiquitin ligase does it best! FEBS Lett. 2011;585(18):2818-25.
240. Goosen N. Scanning the DNA for damage by the nucleotide excision repair machinery. DNA repair. 2010;9(5):593-6.
241. Zotter A, Luijsterburg MS, Warmerdam DO, Ibrahim S, Nigg A, van Cappellen WA. Recruitment of the nucleotide excision repair endonuclease XPG to sites of UV-induced dna damage depends on functional TFIIH. Mol Cell Biol. 2006;26(23):8868-79.
242. Wakasugi M, Reardon JT, Sancar A. The non-catalytic function of XPG protein during dual incision in human nucleotide excision repair. The Journal of biological chemistry. 1997;272(25):16030-4.
243. Hermanson-Miller IL, Turchi JJ. Strand-specific binding of RPA and XPA to damaged duplex DNA. Biochemistry-Us. 2002;41(7):2402-8.
244. Kim YJ, Wilson DM, 3rd. Overview of base excision repair biochemistry. Curr Mol Pharmacol. 2012;5(1):3-13.
245. Chen DS, Herman T, Demple B. Two distinct human DNA diesterases that hydrolyze 3'-blocking deoxyribose fragments from oxidized DNA. Nucleic acids research. 1991;19(21):5907-14.
246. Winters TA, Henner WD, Russell PS, McCullough A, Jorgensen TJ. Removal of 3'-phosphoglycolate from DNA strand-break damage in an oligonucleotide substrate by recombinant human apurinic/apyrimidinic endonuclease 1. Nucleic acids research. 1994;22(10):1866-73.
247. Beard WA, Prasad R, Wilson SH. Activities and mechanism of DNA polymerase beta. Methods Enzymol. 2006;408:91-107.
248. Braithwaite EK, Prasad R, Shock DD, Hou EW, Beard WA, Wilson SH. DNA polymerase lambda mediates a back-up base excision repair activity in extracts of mouse embryonic fibroblasts. The Journal of biological chemistry. 2005;280(18):18469-75.
249. Shivji KK, Kenny MK, Wood RD. Proliferating cell nuclear antigen is required for DNA excision repair. Cell. 1992;69(2):367-74.
250. Storici F, Henneke G, Ferrari E, Gordenin DA, Hubscher U, Resnick MA. The flexible loop of human FEN1 endonuclease is required for flap cleavage during DNA replication and repair. The EMBO journal. 2002;21(21):5930-42.
251. Tomkinson AE, Vijayakumar S, Pascal JM, Ellenberger T. DNA ligases: structure, reaction mechanism, and function. Chem Rev. 2006;106(2):687-99.
252. Cappelli E, Taylor R, Cevasco M, Abbondandolo A, Caldecott K, Frosina G. Involvement of XRCC1 and DNA ligase III gene products in DNA base excision repair. The Journal of biological chemistry. 1997;272(38):23970-5.
253. Reynolds P, Cooper S, Lomax M, O'Neill P. Disruption of PARP1 function inhibits base excision repair of a sub-set of DNA lesions. Nucleic acids research. 2015;43(8):4028-38.
254. El-Khamisy SF, Masutani M, Suzuki H, Caldecott KW. A requirement for PARP-1 for the assembly or stability of XRCC1 nuclear foci at sites of oxidative DNA damage. Nucleic acids research. 2003;31(19):5526-33.
255. Ivanov EL, Sugawara N, White CI, Fabre F, Haber JE. Mutations in XRS2 and RAD50 delay but do not prevent mating-type switching in Saccharomyces cerevisiae. Mol Cell Biol. 1994;14(5):3414-25.
256. Krishna S, Wagener BM, Liu HP, Lo YC, Sterk R, Petrini JH. Mre11 and Ku regulation of double-strand break repair by gene conversion and break-induced replication. DNA repair. 2007;6(6):797-808.
257. Fiorentini P, Huang KN, Tishkoff DX, Kolodner RD, Symington LS. Exonuclease I of Saccharomyces cerevisiae functions in mitotic recombination in vivo and in vitro. Mol Cell Biol. 1997;17(5):2764-73.

258. Sugiyama T, Zaitseva EM, Kowalczykowski SC. A single-stranded DNA-binding protein is needed for efficient presynaptic complex formation by the Saccharomyces cerevisiae Rad51 protein. The Journal of biological chemistry. 1997;272(12):7940-5.
259. Galkin VE, Wu Y, Zhang XP, Qian X, He Y, Yu X. The Rad51/RadA N-terminal domain activates nucleoprotein filament ATPase activity. Structure. 2006;14(6):983-92.
260. Yonetani Y, Hochegger H, Sonoda E, Shinya S, Yoshikawa H, Takeda S. Differential and collaborative actions of Rad51 paralog proteins in cellular response to DNA damage. Nucleic acids research. 2005;33(14):4544-52.
261. New JH, Sugiyama T, Zaitseva E, Kowalczykowski SC. Rad52 protein stimulates DNA strand exchange by Rad51 and replication protein A. Nature. 1998;391(6665):407-10.
262. Chen PL, Chen CF, Chen Y, Xiao J, Sharp ZD, Lee WH. The BRC repeats in BRCA2 are critical for RAD51 binding and resistance to methyl methanesulfonate treatment. Proc Natl Acad Sci U S A. 1998;95(9):5287-92.
263. Gudmundsdottir K, Ashworth A. The roles of BRCA1 and BRCA2 and associated proteins in the maintenance of genomic stability. Oncogene. 2006;25(43):5864-74.
264. Moynahan ME. The cancer connection: BRCA1 and BRCA2 tumor suppression in mice and humans. Oncogene. 2002;21(58):8994-9007.
265. Xia F, Taghian DG, DeFrank JS, Zeng ZC, Willers H, Iliakis G. Deficiency of human BRCA2 leads to impaired homologous recombination but maintains normal nonhomologous end joining. Proc Natl Acad Sci U S A. 2001;98(15):8644-9.
266. Moynahan ME, Cui TY, Jasin M. Homology-directed dna repair, mitomycin-c resistance, and chromosome stability is restored with correction of a Brca1 mutation. Cancer Res. 2001;61(12):4842-50.
267. Zhang J, Ma Z, Treszezamsky A, Powell SN. MDC1 interacts with Rad51 and facilitates homologous recombination. Nat Struct Mol Biol. 2005;12(10):902-9.
268. Moynahan ME, Pierce AJ, Jasin M. BRCA2 is required for homology-directed repair of chromosomal breaks. Mol Cell. 2001;7(2):263-72.
269. Feng Z, Zhang J. A dual role of BRCA1 in two distinct homologous recombination mediated repair in response to replication arrest. Nucleic acids research. 2012;40(2):726-38.
270. Wright WD, Heyer WD. Rad54 functions as a heteroduplex DNA pump modulated by its DNA substrates and Rad51 during D loop formation. Mol Cell. 2014;53(3):420-32.
271. Wyatt HD, West SC. Holliday junction resolvases. Cold Spring Harb Perspect Biol. 2014;6(9):a023192.
272. Goetz JD, Motycka TA, Han M, Jasin M, Tomkinson AE. Reduced repair of DNA double-strand breaks by homologous recombination in a DNA ligase I-deficient human cell line. DNA repair. 2005;4(6):649-54.
273. Schultz N, Lopez E, Saleh-Gohari N, Helleday T. Poly(ADP-ribose) polymerase (PARP-1) has a controlling role in homologous recombination. Nucleic acids research. 2003;31(17):4959-64.
274. Lieber MR. The mechanism of human nonhomologous DNA end joining. The Journal of biological chemistry. 2008;283(1):1-5.
275. Ma Y, Pannicke U, Schwarz K, Lieber MR. Hairpin opening and overhang processing by an Artemis/DNA-dependent protein kinase complex in nonhomologous end joining and V(D)J recombination. Cell. 2002;108(6):781-94.
276. West RB, Yaneva M, Lieber MR. Productive and nonproductive complexes of Ku and DNA-dependent protein kinase at DNA termini. Mol Cell Biol. 1998;18(10):5908-20.
277. Uematsu N, Weterings E, Yano K, Morotomi-Yano K, Jakob B, Taucher-Scholz G. Autophosphorylation of DNA-PKCS regulates its dynamics at DNA double-strand breaks. J Cell Biol. 2007;177(2):219-29.
278. Goodarzi AA, Yu Y, Riballo E, Douglas P, Walker SA, Ye R. DNA-PK autophosphorylation facilitates Artemis endonuclease activity. The EMBO journal. 2006;25(16):3880-9.

279. Gu J, Lu H, Tippin B, Shimazaki N, Goodman MF, Lieber MR. XRCC4:DNA ligase IV can ligate incompatible DNA ends and can ligate across gaps. The EMBO journal. 2007;26(4):1010-23.
280. Li Z, Otevrel T, Gao Y, Cheng HL, Seed B, Stamato TD. The XRCC4 gene encodes a novel protein involved in DNA double-strand break repair and V(D)J recombination. Cell. 1995;83(7):1079-89.
281. Grawunder U, Wilm M, Wu X, Kulesza P, Wilson TE, Mann M. Activity of DNA ligase IV stimulated by complex formation with XRCC4 protein in mammalian cells. Nature. 1997;388(6641):492-5.
282. Gu J, Lu H, Tsai AG, Schwarz K, Lieber MR. Single-stranded DNA ligation and XLF-stimulated incompatible DNA end ligation by the XRCC4-DNA ligase IV complex: influence of terminal DNA sequence. Nucleic acids research. 2007;35(17):5755-62.
283. Ma Y, Lu H, Tippin B, Goodman MF, Shimazaki N, Koiwai O. A biochemically defined system for mammalian nonhomologous DNA end joining. Mol Cell. 2004;16(5):701-13.
284. Tsai CJ, Kim SA, Chu G. Cernunnos/XLF promotes the ligation of mismatched and noncohesive DNA ends. Proc Natl Acad Sci U S A. 2007;104(19):7851-6.
285. Larrea AA, Lujan SA, Kunkel TA. SnapShot: DNA Mismatch Repair. Cell. 2010;141(4).
286. Li GM, Modrich P. Restoration of mismatch repair to nuclear extracts of H6 colorectal tumor cells by a heterodimer of human MutL homologs. Proc Natl Acad Sci U S A. 1995;92(6):1950-4.
287. Gu L, Hong Y, McCulloch S, Watanabe H, Li GM. ATP-dependent interaction of human mismatch repair proteins and dual role of PCNA in mismatch repair. Nucleic acids research. 1998;26(5):1173-8.
288. Guo S, Presnell SR, Yuan F, Zhang Y, Gu L, Li GM. Differential requirement for proliferating cell nuclear antigen in 5' and 3' nick-directed excision in human mismatch repair. The Journal of biological chemistry. 2004;279(17):16912-7.
289. Zhang Y, Yuan F, Presnell SR, Tian K, Gao Y, Tomkinson AE. Reconstitution of 5'-directed human mismatch repair in a purified system. Cell. 2005;122(5):693-705.
290. Kadyrov FA, Dzantiev L, Constantin N, Modrich P. Endonucleolytic function of MutLalpha in human mismatch repair. Cell. 2006;126(2):297-308.
291. Ramilo C, Gu L, Guo S, Zhang X, Patrick SM, Turchi JJ. Partial reconstitution of human DNA mismatch repair in vitro: characterization of the role of human replication protein A. Mol Cell Biol. 2002;22(7):2037-46.
292. Bernstein C, Bernstein H. Epigenetic reduction of DNA repair in progression to gastrointestinal cancer. World journal of gastrointestinal oncology. 2015;7(5):30-46.
293. Khil PP, Camerini-Otero RD. Over 1000 genes are involved in the DNA damage response of Escherichia coli. Mol Microbiol. 2002;44(1):89-105.
294. Murphy CT, McCarroll SA, Bargmann CI, Fraser A, Kamath RS, Ahringer J. Genes that act downstream of DAF-16 to influence the lifespan of Caenorhabditis elegans. Nature. 2003;424(6946):277-84.
295. Wang Z, Gerstein M, Snyder M. RNA-Seq: a revolutionary tool for transcriptomics. Nat Rev Genet. 2009;10(1):57-63.
296. Ozsolak F, Milos PM. RNA sequencing: advances, challenges and opportunities. Nat Rev Genet. 2011;12(2):87-98.
297. Wood SH, Craig T, Li Y, Merry B, de Magalhaes JP. Whole transcriptome sequencing of the aging rat brain reveals dynamic RNA changes in the dark matter of the genome. Age. 2013;35(3):763-76.
298. Mortazavi A, Williams BA, Mccue K, Schaeffer L, Wold B. Mapping and quantifying mammalian transcriptomes by RNA-Seq. Nat Methods. 2008;5(7):621-8.
299. Marioni JC, Mason CE, Mane SM, Stephens M, Gilad Y. RNA-seq: An assessment of technical reproducibility and comparison with gene expression arrays. Genome Res. 2008;18(9):1509-17.

300. Sultan M, Schulz MH, Richard H, Magen A, Klingenhoff A, Scherf M. A global view of gene activity and alternative splicing by deep sequencing of the human transcriptome. Science. 2008;321(5891):956-60.
301. Berezikov E, Thuemmler F, van Laake LW, Kondova I, Bontrop R, Cuppen E. Diversity of microRNAs in human and chimpanzee brain. Nat Genet. 2006;38(12):1375-7.
302. Cloonan N, Forrest ARR, Kolle G, Gardiner BBA, Faulkner GJ, Brown MK. Stem cell transcriptome profiling via massive-scale mRNA sequencing. Nat Methods. 2008;5(7):613-9.
303. Bartel DP. MicroRNAs: Target Recognition and Regulatory Functions. Cell. 2009;136(2):215-33.
304. Gygi SP, Rochon Y, Franza BR, Aebersold R. Correlation between protein and mRNA abundance in yeast. Mol Cell Biol. 1999;19(3):1720-30.
305. Schwanhausser B, Busse D, Li N, Dittmar G, Schuchhardt J, Wolf J. Global quantification of mammalian gene expression control. Nature. 2011;473(7347):337-42.
306. de Magalhaes JP, Toussaint O. How bioinformatics can help reverse engineer human aging. Ageing Res Rev. 2004;3(2):125-41.
307. Weindruch R, Kayo T, Lee CK, Prolla TA. Gene expression profiling of aging using DNA microarrays. Mech Ageing Dev. 2002;123(2-3):177-93.
308. H. KABJHAMOT. The Biology of Human Starvation. Minneapolis: University of Minnesota Press. 1950.
309. Lamb J. The connectivity map: Using gene-expression profiling to identify new therapeutics and potential adverse drug effects. Chem Res Toxicol. 2007;20(12):2018-.
310. Harrison DE, Strong R, Sharp ZD, Nelson JF, Astle CM, Flurkey K. Rapamycin fed late in life extends lifespan in genetically heterogeneous mice. Nature. 2009;460(7253):392-U108.
311. Kenyon CJ. The genetics of ageing. Nature. 2010;464(7288):504-12.
312. Stanfel MN, Shamieh LS, Kaeberlein M, Kennedy BK. The TOR pathway comes of age. Bba-Gen Subjects. 2009;1790(10):1067-74.
313. Dumont FJ, Su QX. Mechanism of action of the immunosuppressant rapamycin. Life Sci. 1995;58(5):373-95.
314. Hansen M, Taubert S, Crawford D, Libina N, Lee SJ, Kenyon C. Lifespan extension by conditions that inhibit translation in Caenorhabditis elegans. Aging Cell. 2007;6(1):95-110.
315. Wullschleger S, Loewith R, Hall MN. TOR signaling in growth and metabolism. Cell. 2006;124(3):471-84.
316. Blagosklonny MV. Rapamycin extends life- and health span because it slows aging. Aging-Us. 2013;5(8):592-8.
317. Blagosklonny MV. Rapamycin and quasi-programmed aging Four years later. Cell cycle. 2010;9(10):1859-62.
318. Niu CS, Wu HT, Cheng KC, Lin KC, Chen CT, Cheng JT. A Novel Mechanism for Decreasing Plasma Lipid Level from Imidazoline I-1 Receptor Activation in High Fat Diet-fed Mice. Horm Metab Res. 2011;43(7):458-63.
319. Yang TT, Chiu NH, Chung HH, Hsu CT, Lee WJ, Cheng JT. Stimulatory Effect of Allantoin on Imidazoline I-1 Receptors in Animal and Cell Line. Horm Metab Res. 2012;44(12):879-84.
320. Chen MF, Yang TT, Yeh LR, Chung HH, Wen YJ, Lee WJ. Activation of Imidazoline I-2B Receptors by Allantoin to Increase Glucose Uptake into C2C12 Cells. Horm Metab Res. 2012;44(4):268-72.
321. Yang TT, Ku PM, Hsu CT, Chung HH, Lee WJ, Cheng JT. Mediation of AMP Kinase in the Increase of Glucose Uptake in L6 Cells Induced by Activation of Imidazoline I-2 Receptors. Horm Metab Res. 2013;45(5):359-63.
322. Ko WC, Liu IM, Chung HH, Cheng JT. Activation of I(2)-imidazoline receptors may ameliorate insulin resistance in fructose-rich chow-fed rats. Neurosci Lett. 2008;448(1):90-3.
323. Alexander B. Artyukhin CID, Frank C. Schroeder, Young-Jai You and Leon Avery. Effect of parent history on purine metabolism in L1-arrested C. elegans. The Worm Breeder's Gazette. 2013.

324. Consortium CeS. Genome sequence of the nematode C-elegans: A platform for investigating biology. Science. 1998;282(5396):2012-8.
325. Stiernagle T. Maintenance of *C. elegans.* In WormBook, doi/101895/wormbook11011, e.T.*C.e.*R.C. *WormBook*, ed. 2006.
326. Moskalev AA, Shaposhnikov MV. Pharmacological Inhibition of Phosphoinositide 3 and TOR Kinases Improves Survival of Drosophila melanogaster. Rejuv Res. 2010;13(2-3):246-7.
327. Wang XM, Wang XY, Li LD, Wang DQ. Lifespan extension in Caenorhabditis elegans by DMSO is dependent on sir-2.1 and daf-16. Biochem Bioph Res Co. 2010;400(4):613-8.
328. Benjamini Y, Hochberg Y. Controlling the False Discovery Rate - a Practical and Powerful Approach to Multiple Testing. J Roy Stat Soc B Met. 1995;57(1):289-300.
329. de Magalhaes JP, Curado J, Church GM. Meta-analysis of age-related gene expression profiles identifies common signatures of aging. Bioinformatics. 2009;25(7):875-81.
330. Huang da W, Sherman BT, Lempicki RA. Systematic and integrative analysis of large gene lists using DAVID bioinformatics resources. Nature protocols. 2009;4(1):44-57.
331. Pearson K. Notes on regression and inheritance in the case of two parents. Proceedings of the Royal Society of London. 1895;58:240–2.
332. Team RDC. R: A language and environment for statistical computing. R Foundation for Statistical Computing, Vienna, Austria. 2008;ISBN 3-900051-07-0, URL http://www.R-project.org.
333. Gomez-Amaro RL, Valentine ER, Carretero M, LeBoeuf SE, Rangaraju S, Broaddus CD. Measuring Food Intake and Nutrient Absorption in Caenorhabditis elegans. Genetics. 2015;200(2):443-+.
334. Nelson WJ. Regulation of cell-cell adhesion by the cadherin-catenin complex. Biochem Soc T. 2008;36:149-55.
335. Chen BJ, Liu P, Wang SJ, Ge QA, Zhan HY, Mohler WA. alpha-Catulin CTN-1 is required for BK channel subcellular localization in C. elegans body-wall muscle cells. Embo Journal. 2010;29(18):3184-95.
336. Oh HJ, Abraham LS, van Hengel J, Stove C, Proszynski TJ, Gevaert K. Interaction of alpha-Catulin with Dystrobrevin Contributes to Integrity of Dystrophin Complex in Muscle. Journal of Biological Chemistry. 2012;287(26):21717-28.
337. Werner ME, Zvara P, Meredith AL, Aldrich RW, Nelson MT. Erectile dysfunction in mice lacking the large-conductance calcium-activated potassium (BK) channel. J Physiol-London. 2005;567(2):545-56.
338. Brenner R, Perez GJ, Bonev AD, Eckman DM, Kosek JC, Wiler SW. Vasoregulation by the beta 1 subunit of the calcium-activated potassium channel. Nature. 2000;407(6806):870-6.
339. Fan LC, Chiang WF, Liang CH, Tsai YT, Wong TY, Chen KC. alpha-Catulin knockdown induces senescence in cancer cells. Oncogene. 2011;30(23):2610-21.
340. Sapir A, Choi J, Leikina E, Avinoam O, Valansi C, Chernomordik LV. AFF-1, a FOS-1-regulated fusogen, mediates fusion of the anchor cell in C-elegans. Dev Cell. 2007;12(5):683-98.
341. Howe KL, Bolt BJ, Cain S, Chan J, Chen WJ, Davis P. WormBase 2016: expanding to enable helminth genomic research. Nucleic acids research. 2016;44(D1):D774-D80.
342. Kim Y, Sun H. ASM-3 Acid Sphingomyelinase Functions as a Positive Regulator of the DAF-2/AGE-1 Signaling Pathway and Serves as a Novel Anti-Aging Target. Plos One. 2012;7(9).
343. Page APaJ, I.L. The cuticle WormBook, ed. The C. elegans Research Community, WormBook, doi/10.1895/wormbook.1.138.1, http://www.wormbook.org. 2007.
344. Craig KL, Tyers M. The F-box: a new motif for ubiquitin dependent proteolysis in cell cycle regulation and signal transduction. Prog Biophys Mol Bio. 1999;72(3):299-328.
345. Hsu AL, Murphy CT, Kenyon C. Regulation of aging and age-related disease by DAF-16 and heat-shock factor. Science. 2003;300(5622):1142-5.
346. Morley JF, Morimoto RI. Regulation of longevity in Caenorhabditis elegans by heat shock factor and molecular chaperones. Mol Biol Cell. 2004;15(2):657-64.

347. Williamson EA, Wray JW, Bansal P, Hromas R. Overview for the histone codes for DNA repair. Prog Mol Biol Transl Sci. 2012;110:207-27.
348. Hsieh EA, Chai CM, Hellerstein MK. Effects of caloric restriction on cell proliferation in several tissues in mice: role of intermittent feeding. Am J Physiol Endocrinol Metab. 2005;288(5):E965-72.
349. Wuttke D, Connor R, Vora C, Craig T, Li Y, Wood S. Dissecting the Gene Network of Dietary Restriction to Identify Evolutionarily Conserved Pathways and New Functional Genes. Plos Genet. 2012;8(8).
350. Iorio F, Bosotti R, Scacheri E, Belcastro V, Mithbaokar P, Ferriero R. Discovery of drug mode of action and drug repositioning from transcriptional responses. P Natl Acad Sci USA. 2010;107(33):14621-6.
351. Carrella D, Napolitano F, Rispoli R, Miglietta M, Carissimo A, Cutillo L. Mantra 2.0: an online collaborative resource for drug mode of action and repurposing by network analysis. Bioinformatics. 2014;30(12):1787-8.
352. de Magalhaes JP. Programmatic features of aging originating in development: aging mechanisms beyond molecular damage? Faseb J. 2012;26(12):4821-6.
353. Atwood CS, Bowen RL. The reproductive-cell cycle theory of aging: An update. Exp Gerontol. 2011;46(2-3):100-7.
354. Lee HG, Chen Q, Wolfram JA, Richardson SL, Liner A, Siedlak SL. Cell Cycle Re-Entry and Mitochondrial Defects in Myc-Mediated Hypertrophic Cardiomyopathy and Heart Failure. Plos One. 2009;4(9).
355. Sun L, Peng Y, Sharrow AC, Iqbal J, Zhang Z, Papachristou DJ. FSH directly regulates bone mass. Cell. 2006;125(2):247-60.
356. Matuoka K, Mitsui Y. Changes in cell-surface glycosaminoglycans in human diploid fibroblasts during in vitro aging. Mech Ageing Dev. 1981;15(2):153-63.
357. Kelley RO, Azad R, Vogel KG. Development of the aging cell surface: concanavalin A-mediated intercellular binding and the distribution of binding sites with progressive subcultivation of human embryo fibroblasts. Mech Ageing Dev. 1978;8(3):203-17.
358. Onken B, Driscoll M. Metformin Induces a Dietary Restriction-Like State and the Oxidative Stress Response to Extend C. elegans Healthspan via AMPK, LKB1, and SKN-1. Plos One. 2010;5(1).
359. de Magalhaes JP. Why genes extending lifespan in model organisms have not been consistently associated with human longevity and what it means to translation research. Cell cycle. 2014;13(17):2671-3.
360. Hill CS, Treisman R. Transcriptional Regulation by Extracellular Signals - Mechanisms and Specificity. Cell. 1995;80(2):199-211.
361. Gstraunthaler G. Alternatives to the use of fetal bovine serum: Serum-free cell culture. Altex-Altern Tierexp. 2003;20(4):275-81.
362. Guadagno TM, Assoian RK. G1/S Control of Anchorage-Independent Growth in the Fibroblast Cell-Cycle. J Cell Biol. 1991;115(5):1419-25.
363. Amstein CF, Hartman PA. Adaptation of Plastic Surfaces for Tissue-Culture by Glow-Discharge. J Clin Microbiol. 1975;2(1):46-54.
364. Curtis ASG, Forrester JV, Mcinnes C, Lawrie F. Adhesion of Cells to Polystyrene Surfaces. J Cell Biol. 1983;97(5):1500-6.
365. Ramsey WS, Hertl W, Nowlan ED, Binkowski NJ. Surface Treatments and Cell Attachment. In Vitro Cell Dev B. 1984;20(10):802-8.
366. Kim NG, Koh E, Chen X, Gumbiner BM. E-cadherin mediates contact inhibition of proliferation through Hippo signaling-pathway components. P Natl Acad Sci USA. 2011;108(29):11930-5.
367. Perrais M, Chen X, Perez-Moreno M, Gumbiner BM. E-cadherin homophilic ligation inhibits cell growth and epidermal growth factor receptor signaling independently of other cell interactions. Mol Biol Cell. 2007;18(6):2013-25.

368. Schlegelmilch K, Mohseni M, Kirak O, Pruszak J, Rodriguez JR, Zhou DW. Yap1 Acts Downstream of alpha-Catenin to Control Epidermal Proliferation. Cell. 2011;144(5):782-95.
369. Olovnikov AM. Telomeres, telomerase, and aging: Origin of the theory. Exp Gerontol. 1996;31(4):443-8.
370. Olovniko.Am. Theory of Marginotomy - Incomplete Copying of Template Margin in Enzymic-Synthesis of Polynucleotides and Biological Significance of Phenomenon. J Theor Biol. 1973;41(1):181-90.
371. Lorenzini A, Tresini M, Austad SN, Cristofalo VJ. Cellular replicative capacity correlates primarily with species body mass not longevity. Mech Ageing Dev. 2005;126(10):1130-3.
372. Bennett NC FC. African mole-rats: ecology and eusociality. Cambridge: Cambridge University Press;. 2000.
373. de Souza N. Too much of a good thing. Nat Methods. 2007;4(5):386-.
374. Guzy RD, Schumacker PT. Oxygen sensing by mitochondria at complex III: the paradox of increased reactive oxygen species during hypoxia. Exp Physiol. 2006;91(5):807-19.
375. Richter A, Sanford KK, Evans VJ. Influence of Oxygen and Culture Media on Plating Efficiency of Some Mammalian Tissue Cells. J Natl Cancer I. 1972;49(6):1705-12.
376. Bates MK. Culturing Cells Under Hypoxic Conditions for Biologically Relevant Results. American Laboratory. 2012.
377. Chromium, nickel and welding. IARC monographs on the evaluation of carcinogenic risks to humans / World Health Organization, International Agency for Research on Cancer. 1990;49:1-648.
378. Hayes RB. The carcinogenicity of metals in humans. Cancer Cause Control. 1997;8(3):371-85.
379. Buttner B, Beyersmann D. Modification of the Erythrocyte Anion Carrier by Chromate. Xenobiotica. 1985;15(8-9):735-41.
380. Arslan P, Beltrame M, Tomasi A. Intracellular Chromium Reduction. Biochim Biophys Acta. 1987;931(1):10-5.
381. Quievryn G, Peterson E, Messer J, Zhitkovich A. Genotoxicity and mutagenicity of chromium(VI)/ascorbate-generated DNA adducts in human and bacterial cells. Biochemistry-Us. 2003;42(4):1062-70.
382. Stearns DM, Wetterhahn KE. Reaction of chromium(VI) with ascorbate produces chromium(V), chromium(IV), and carbon-based radicals. Chem Res Toxicol. 1994;7(2):219-30.
383. Wise JP, Orenstein JM, Patierno SR. Inhibition of Lead Chromate Clastogenesis by Ascorbate - Relationship to Particle Dissolution and Uptake. Carcinogenesis. 1993;14(3):429-34.
384. Voitkun V, Zhitkovich A, Costa M. Complexing of Amino-Acids to DNA by Chromate in Intact-Cells. Environ Health Persp. 1994;102:251-5.
385. Zhitkovich A, Voitkun V, Costa M. Formation of the amino acid-DNA complexes by hexavalent and trivalent chromium in vitro: Importance of trivalent chromium and the phosphate group. Biochemistry-Us. 1996;35(22):7275-82.
386. Miller CA, Costa M. Characterization of DNA-Protein Complexes Induced in Intact-Cells by the Carcinogen Chromate. Mol Carcinogen. 1988;1(2):125-33.
387. Krupa R, Stanczak M, Walter Z. Chromium incorporated in RNA and DNA. Z Naturforsch C. 2002;57(9-10):951-3.
388. O'Brien T, Xu J, Patierno SR. Effects of glutathione on chromium-induced DNA crosslinking and DNA polymerase arrest. Molecular and cellular biochemistry. 2001;222(1-2):173-82.
389. Zhitkovich A, Shrager S, Messer J. Reductive metabolism of Cr(VI) by cysteine leads to the formation of binary and ternary Cr-DNA adducts in the absence of oxidative DNA damage. Chem Res Toxicol. 2000;13(11):1114-24.
390. Casadevall M, Fresco PD, Kortenkamp A. Chromium(VI)-mediated DNA damage: oxidative pathways resulting in the formation of DNA breaks and abasic sites. Chem-Biol Interact. 1999;123(2):117-32.

391. Bose RN, Moghaddas S, Mazzer PA, Dudones LP, Joudah L, Stroup D. Oxidative damage of DNA by chromium(V) complexes: relative importance of base versus sugar oxidation. Nucleic acids research. 1999;27(10):2219-26.
392. O'Brien TJ, Ceryak S, Patierno SR. Complexities of chromium carcinogenesis: role of cellular response, repair and recovery mechanisms. Mutat Res-Fund Mol M. 2003;533(1-2):3-36.
393. Hertzberg RP, Caranfa MJ, Hecht SM. On the Mechanism of Topoisomerase-I Inhibition by Camptothecin - Evidence for Binding to an Enzyme DNA Complex. Biochemistry-Us. 1989;28(11):4629-38.
394. Hsiang YH, Hertzberg R, Hecht S, Liu LF. Camptothecin Induces Protein-Linked DNA Breaks Via Mammalian DNA Topoisomerase-I. Journal of Biological Chemistry. 1985;260(27):4873-8.
395. Roca J. The Mechanisms of DNA Topoisomerases. Trends Biochem Sci. 1995;20(4):156-60.
396. Svejstrup JQ, Christiansen K, Gromova, II, Andersen AH, Westergaard O. New technique for uncoupling the cleavage and religation reactions of eukaryotic topoisomerase I. The mode of action of camptothecin at a specific recognition site. Journal of molecular biology. 1991;222(3):669-78.
397. Hsiang YH, Lihou MG, Liu LF. Arrest of Replication Forks by Drug-Stabilized Topoisomerase I-DNA Cleavable Complexes as a Mechanism of Cell Killing by Camptothecin. Cancer Res. 1989;49(18):5077-82.
398. Ryan AJ, Squires S, Strutt HL, Johnson RT. Camptothecin Cytotoxicity in Mammalian-Cells Is Associated with the Induction of Persistent Double Strand Breaks in Replicating DNA. Nucleic acids research. 1991;19(12):3295-300.
399. Tsao YP, Russo A, Nyamuswa G, Silber R, Liu LF. Interaction between Replication Forks and Topoisomerase-I-DNA Cleavable Complexes - Studies in a Cell-Free Sv40 DNA-Replication System. Cancer Res. 1993;53(24):5908-14.
400. Nitiss J, Wang JC. DNA Topoisomerase-Targeting Antitumor Drugs Can Be Studied in Yeast. P Natl Acad Sci USA. 1988;85(20):7501-5.
401. Seluanov A, Vaidya A, Gorbunova V. Establishing primary adult fibroblast cultures from rodents. J Vis Exp. 2010(44).
402. Strutz F, Okada H, Lo CW, Danoff T, Carone RL, Tomaszewski JE. Identification and characterization of a fibroblast marker: FSP1. J Cell Biol. 1995;130(2):393-405.
403. Randhawa MA. Calculation of LD50 values from the method of Miller and Tainter, 1944. Journal of Ayub Medical College, Abbottabad : JAMC. 2009;21(3):184-5.
404. Galvao J, Davis B, Tilley M, Normando E, Duchen MR, Cordeiro MF. Unexpected low-dose toxicity of the universal solvent DMSO. Faseb J. 2014;28(3):1317-30.
405. Jamalzadeh L, Ghafoori, H., Sariri, R., Rabuti, H., Nasirzade, J., Hasani,H., and Aghamaali, M. Cytotoxic Effects of Some Common Organic Solvents on MCF-7, RAW-264.7 and Human Umbilical Vein Endothelial Cells. Avicenna Journal of Medical Biochemistry. 2016;4(1).
406. Jeyapalan JC, Sedivy JM. Cellular senescence and organismal aging. Mech Ageing Dev. 2008;129(7-8):467-74.
407. Anders S, Huber W. Differential expression analysis for sequence count data. Genome biology. 2010;11(10):R106.
408. Dragan AI, Pavlovic R, McGivney JB, Casas-Finet JR, Bishop ES, Strouse RJ. SYBR Green I: Fluorescence Properties and Interaction with DNA. J Fluoresc. 2012;22(4):1189-99.
409. Vannini A, Cramer P. Conservation between the RNA Polymerase I, II, and III Transcription Initiation Machineries. Mol Cell. 2012;45(4):439-46.
410. Turabelidze A, Guo SJ, DiPietro LA. Importance of housekeeping gene selection for accurate reverse transcription-quantitative polymerase chain reaction in a wound healing model. Wound Repair Regen. 2010;18(5):460-6.
411. Amable PR, Teixeira MVT, Carias RBV, Granjeiro JM, Borojevic R. Identification of Appropriate Reference Genes for Human Mesenchymal Cells during Expansion and Differentiation. Plos One. 2013;8(9).

412. Dobin A, Davis CA, Schlesinger F, Drenkow J, Zaleski C, Jha S. STAR: ultrafast universal RNA-seq aligner. Bioinformatics. 2013;29(1):15-21.
413. van Dam S, Craig T, de Magalhaes JP. GeneFriends: a human RNA-seq-based gene and transcript co-expression database. Nucleic acids research. 2015;43(Database issue):D1124-32.
414. Keane M, Craig T, Alfoeldi J, Berlin AM, Johnson J, Seluanov A. The Naked Mole Rat Genome Resource: facilitating analyses of cancer and longevity-related adaptations. Bioinformatics. 2014;30(24):3558-60.
415. Flicek P, Amode MR, Barrell D, Beal K, Billis K, Brent S. Ensembl 2014. Nucleic acids research. 2014;42(D1):D749-D55.
416. Love MI, Huber W, Anders S. Moderated estimation of fold change and dispersion for RNA-seq data with DESeq2. Genome biology. 2014;15(12).
417. Ye J, Coulouris G, Zaretskaya I, Cutcutache I, Rozen S, Madden TL. Primer-BLAST: A tool to design target-specific primers for polymerase chain reaction. Bmc Bioinformatics. 2012;13.
418. Valadan R, Hedayatizadeh-Omran A, Alhosseini-Abyazani MN, Amjadi O, Rafiei A, Tehrani M. Data supporting the design and evaluation of a universal primer pair for pseudogene-free amplification of HPRT1 in real-time PCR. Data in brief. 2015;4:384-9.
419. Romero IG, Pai AA, Tung J, Gilad Y. RNA-seq: impact of RNA degradation on transcript quantification. Bmc Biol. 2014;12.
420. Chen ZT, Duan XP. Ribosomal RNA Depletion for Massively Parallel Bacterial RNA-Sequencing Applications. Methods Mol Biol. 2011;733:93-103.
421. Casellas J. Inbred mouse strains and genetic stability: a review. Animal. 2011;5(1):1-7.
422. Faulkes CG, Abbott DH, Mellor AL. Investigation of Genetic Diversity in Wild Colonies of Naked Mole-Rats (Heterocephalus-Glaber) by DNA Fingerprinting. J Zool. 1990;221:87-97.
423. Reeve HK, Westneat DF, Noon WA, Sherman PW, Aquadro CF. DNA Fingerprinting Reveals High-Levels of Inbreeding in Colonies of the Eusocial Naked Mole-Rat. P Natl Acad Sci USA. 1990;87(7):2496-500.
424. Clarke FM, Faulkes CG. Dominance and queen succession is captive colonies of the eusocial naked mole-rat, Heterocephalus glaber. P Roy Soc B-Biol Sci. 1997;264(1384):993-1000.
425. Grishin NV. The R3H motif: A domain that binds single-stranded nucleic acids. Trends Biochem Sci. 1998;23(9):329-30.
426. Huang da W, Sherman BT, Lempicki RA. Bioinformatics enrichment tools: paths toward the comprehensive functional analysis of large gene lists. Nucleic acids research. 2009;37(1):1-13.
427. Haslam RJ, Koide HB, Hemmings BA. Pleckstrin domain homology. Nature. 1993;363(6427):309-10.
428. Mayer BJ, Baltimore D. Signalling through SH2 and SH3 domains. Trends in cell biology. 1993;3(1):8-13.
429. Cordeiro RM, Stirling S, Fahy GM, de Magalhaes JP. Insights on cryoprotectant toxicity from gene expression profiling of endothelial cells exposed to ethylene glycol. Cryobiology. 2015;71(3):405-12.
430. Konstantinova I, Nikolova G, Ohara-Imaizumi M, Meda P, Kucera T, Zarbalis K. EphA-ephrin-A-mediated beta cell communication regulates insulin secretion from pancreatic islets. Cell. 2007;129(2):359-70.
431. Hao YB, Wu W, Shi FC, Dalmolin RJS, Yan M, Tian F. Prediction of long noncoding RNA functions with co-expression network in esophageal squamous cell carcinoma. Bmc Cancer. 2015;15.
432. van Bree C, Rodermond HM, ten Cate R, de Vos J, Stalpers LJ, Haveman J. G0 cell cycle arrest alone is insufficient for enabling the repair of ionizing radiation-induced potentially lethal damage. Radiat Res. 2008;170(2):184-91.
433. Moffatt P, Thomas G, Sellin K, Bessette MC, Lafreniere F, Akhouayri O. Osteocrin is a specific ligand of the natriuretic peptide clearance receptor that modulates bone growth. Journal of Biological Chemistry. 2007;282(50):36454-62.

434. Ataman B, Boulting GL, Harmin DA, Yang MG, Baker-Salisbury M, Yap EL. Evolution of Osteocrin as an activity-regulated factor in the primate brain. Nature. 2016;539(7628):242-+.
435. Gehring WJ, Affolter M, Burglin T. Homeodomain proteins. Annual review of biochemistry. 1994;63:487-526.
436. Gabellini D, Colaluca IN, Vodermaier HC, Biamonti G, Giacca M, Falaschi A. Early mitotic degradation of the homeoprotein HOXC10 is potentially linked to cell cycle progression. The EMBO journal. 2003;22(14):3715-24.
437. Rommel C, Camps M, Ji H. PI3K delta and PI3K gamma: partners in crime in inflammation in rheumatoid arthritis and beyond? Nature reviews Immunology. 2007;7(3):191-201.
438. Liang J, Slingerland JM. Multiple roles of the PI3K/PKB (Akt) pathway in cell cycle progression. Cell cycle. 2003;2(4):339-45.
439. Collado M, Medema RH, Garcia-Cao I, Dubuisson ML, Barradas M, Glassford J. Inhibition of the phosphoinositide 3-kinase pathway induces a senescence-like arrest mediated by p27Kip1. The Journal of biological chemistry. 2000;275(29):21960-8.
440. Shtivelman E, Sussman J, Stokoe D. A role for PI 3-kinase and PKB activity in the G2/M phase of the cell cycle. Current biology : CB. 2002;12(11):919-24.
441. Kanehisa M, Goto S. KEGG: kyoto encyclopedia of genes and genomes. Nucleic acids research. 2000;28(1):27-30.
442. Kanehisa M, Goto S, Sato Y, Kawashima M, Furumichi M, Tanabe M. Data, information, knowledge and principle: back to metabolism in KEGG. Nucleic acids research. 2014;42(Database issue):D199-205.
443. Tsukagoshi H, Kawata T, Shimizu Y, Ishizuka T, Dobashi K, Mori M. 4-Hydroxy-2-nonenal enhances fibronectin production by IMR-90 human lung fibroblasts partly via activation of epidermal growth factor receptor-linked extracellular signal-regulated kinase p44/42 pathway. Toxicology and applied pharmacology. 2002;184(3):127-35.
444. Ha UH, Lim JH, Kim HJ, Wu W, Jin S, Xu H. MKP1 regulates the induction of MUC5AC mucin by Streptococcus pneumoniae pneumolysin by inhibiting the PAK4-JNK signaling pathway. The Journal of biological chemistry. 2008;283(45):30624-31.
445. Oliveros JC. Venny. An interactive tool for comparing lists with Venn's diagrams. http://bioinfogp.cnb.csic.es/tools/venny/index.html2007-2015 [
446. Kastner S, Voss T, Keuerleber S, Glockel C, Freissmuth M, Sommergruber W. Expression of G protein-coupled receptor 19 in human lung cancer cells is triggered by entry into S-phase and supports G(2)-M cell-cycle progression. Molecular cancer research : MCR. 2012;10(10):1343-58.
447. Caruso R, Fedele F, Luciano R, Branca G, Parisi C, Paparo D. Mitotic catastrophe in malignant epithelial tumors: the pathologist's viewpoint. Ultrastructural pathology. 2011;35(2):66-71.
448. Adamson B, Smogorzewska A, Sigoillot FD, King RW, Elledge SJ. A genome-wide homologous recombination screen identifies the RNA-binding protein RBMX as a component of the DNA-damage response. Nature cell biology. 2012;14(3):318-28.
449. Bhattacharya S, Ray RM, Johnson DA, Johnson LR. Camptothecin induced expression and phosphorylation of p53 regulates apoptosis in epithelial cells. Faseb J. 2008;22.
450. Hill R, Leidal AM, Madureira PA, Gillis LD, Cochrane HK, Waisman DM. Hypersensitivity to chromium-induced DNA damage correlates with constitutive deregulation of upstream p53 kinases in p21-/- HCT116 colon cancer cells. DNA repair. 2008;7(2):239-52.
451. Pritchard DE, Ceryak S, Ramsey KE, O'Brien TJ, Ha L, Fornsaglio JL. Resistance to apoptosis, increased growth potential, and altered gene expression in cells that survived genotoxic hexavalent chromium [Cr(VI)] exposure. Molecular and cellular biochemistry. 2005;279(1-2):169-81.
452. Brugarolas J, Moberg K, Boyd SD, Taya Y, Jacks T, Lees JA. Inhibition of cyclin-dependent kinase 2 by p21 is necessary for retinoblastoma protein-mediated G(1) arrest after gamma-irradiation. P Natl Acad Sci USA. 1999;96(3):1002-7.

453. Mandal M, Bandyopadhyay D, Goepfert TM, Kumar R. Interferon-induces expression of cyclin-dependent kinase-inhibitors p21WAF1 and p27Kip1 that prevent activation of cyclin-dependent kinase by CDK-activating kinase (CAK). Oncogene. 1998;16(2):217-25.
454. Deng CX, Zhang PM, Harper JW, Elledge SJ, Leder P. Mice Lacking P21(C/P1/Waf1) Undergo Normal Development, but Are Defective in G1 Checkpoint Control. Cell. 1995;82(4):675-84.
455. Smits VAJ, Klompmaker R, Vallenius T, Rijksen G, Makela TP, Medema RH. p21 Inhibits Thr(161) phosphorylation of Cdc2 to enforce the G(2) DNA damage checkpoint. Journal of Biological Chemistry. 2000;275(39):30638-43.
456. Charrier-Savournin FB, Chateau MT, Gire V, Sedivy J, Piette J, Dulic V. p21-mediated nuclear retention of cyclin B1-Cdk1 in response to genotoxic stress. Mol Biol Cell. 2004;15(9):3965-76.
457. Lee J, Kim JA, Barbier V, Fotedar A, Fotedar R. DNA Damage Triggers p21(WAF1)-dependent Emi1 Down-Regulation That Maintains G2 Arrest. Mol Biol Cell. 2009;20(7):1891-902.
458. Gillis LD, Leidal AM, Hill R, Lee PWK. p21(Cip1/WAF1) mediates cyclin B1 degradation in response to DNA damage. Cell cycle. 2009;8(2):253-6.
459. Tillhon M CO, Dutto I, Stivala LA, Prosperi E p21CDKN1A and DNA repair systems: recent findings and future perspectives. Recent Findings and Future Perspectives, New Research Directions in DNA Repair, Prof Clark Chen (Ed), ISBN: 978-953-51-1114-6, InTech, DOI: 105772/54173 Available from: http://wwwintechopencom/books/new-research-directions-in-dna-repair/p21cdkn1a-and-dna-repair-systems-recent-findings-and-future-perspectives. 2013.
460. Coqueret O. New roles for p21 and p27 cell-cycle inhibitors: a function for each cell compartment? Trends in cell biology. 2003;13(2):65-70.
461. Cmielova J, Rezacova M. p21Cip1/Waf1 protein and its function based on a subcellular localization [corrected]. Journal of cellular biochemistry. 2011;112(12):3502-6.
462. Forsberg K, Wuttke A, Quadrato G, Chumakov PM, Wizenmann A, Di Giovanni S. The Tumor Suppressor p53 Fine-Tunes Reactive Oxygen Species Levels and Neurogenesis via PI3 Kinase Signaling. J Neurosci. 2013;33(36):14318-30.
463. Dekker P, Gunn D, McBryan T, Dirks RW, van Heemst D, Lim FL. Microarray-based identification of age-dependent differences in gene expression of human dermal fibroblasts. Mech Ageing Dev. 2012;133(7):498-507.
464. Nordlind K, Johansson O, Liden S, Hokfelt T. Glutamate-Like and Aspartate-Like Immunoreactivities in Human Normal and Inflamed Skin. Virchows Arch B. 1993;64(2):75-82.
465. Jurk D, Wilson C, Passos JF, Oakley F, Correia-Melo C, Greaves L. Chronic inflammation induces telomere dysfunction and accelerates ageing in mice. Nat Commun. 2014;5.
466. Shin S, Cha HJ, Lee EM, Lee SJ, Seo SK, Jin HO. Alteration of miRNA profiles by ionizing radiation in A549 human non-small cell lung cancer cells. Int J Oncol. 2009;35(1):81-6.
467. Bae S, Lee EM, Cha HJ, Kim K, Yoon Y, Lee H. Resveratrol Alters microRNA Expression Profiles in A549 Human Non-Small Cell Lung Cancer Cells. Mol Cells. 2011;32(3):243-9.
468. Martinez-Morales PL, Quiroga AC, Barbas JA, Morales AV. SOX5 controls cell cycle progression in neural progenitors by interfering with the WNT-beta-catenin pathway. Embo Rep. 2010;11(6):466-72.
469. Wang RJ, Liang HQ. MiR-132, miR-15a and miR-16 synergistically inhibit pituitary tumor cell proliferation, invasion and migration by targeting Sox5. Cancer Lett. 2015;356(2):568-78.
470. Guo H, Lv Y, Tian T, Hu TH, Wang WJ, Sui X. Downregulation of p57 accelerates the growth and invasion of hepatocellular carcinoma. Carcinogenesis. 2011;32(12):1897-904.
471. Jerng HH, Qian Y, Pfaffinger PJ. Modulation of Kv4.2 channel expression and gating by dipeptidyl peptidase 10 (DPP10). Biophys J. 2004;87(4):2380-96.
472. Chang ALS, Atzmon G, Bergman A, Brugmann S, Atwood SX, Chang HY. Identification of Genes Promoting Skin Youthfulness by Genome-Wide Association Study. J Invest Dermatol. 2014;134(3):651-7.
473. Pardo LA, Bruggemann A, Camacho J, Stuhmer W. Cell cycle-related changes in the conducting properties of r-eag K+ channels. J Cell Biol. 1998;143(3):767-75.

474. Takahashi A, Yamaguchi H, Miyamoto H. Change in K+ Current of Hela-Cells with Progression of the Cell-Cycle Studied by Patch-Clamp Technique. Am J Physiol. 1993;265(2):C328-C36.
475. Lee JA, Yerbury JJ, Farrawell N, Shearer RF, Constantinescu P, Hatters DM. SerpinB2 (PAI-2) Modulates Proteostasis via Binding Misfolded Proteins and Promotion of Cytoprotective Inclusion Formation. Plos One. 2015;10(6).
476. Schroder WA, Major LD, Le TT, Gardner J, Sweet MJ, Janciauskiene S. Tumor cell-expressed SerpinB2 is present on microparticles and inhibits metastasis. Cancer Med-Us. 2014;3(3):500-13.
477. Tinkum KL, White LS, Marpegan L, Herzog E, Piwnica-Worms D, Piwnica-Worms H. Forkhead Box O1 (FOXO1) Protein, but Not p53, Contributes to Robust Induction of p21 Expression in Fasted Mice. Journal of Biological Chemistry. 2013;288(39):27999-8008.
478. Nakae J, Kitamura T, Kitamura Y, Biggs WH, Arden KC, Accili D. The forkhead transcription factor Foxo1 regulates adipocyte differentiation. Dev Cell. 2003;4(1):119-29.
479. Huang HJ, Regan KM, Lou ZK, Chen JJ, Tindall DJ. CDK2-dependent phosphorylation of FOXO1 as an apoptotic response to DNA damage. Science. 2006;314(5797):294-7.
480. Yuan ZQ, Becker EBE, Merlo P, Yamada T, DiBacco S, Konishi Y. Activation of FOXO1 by Cdk1 in cycling cells and postmitotic neurons. Science. 2008;319(5870):1665-8.
481. Seoane J, Le HV, Shen LJ, Anderson SA, Massague J. Integration of Smad and Forkhead pathways in the control of neuroepithelial and glioblastoma cell proliferation. Cell. 2004;117(2):211-23.
482. Tachibana K, Haghparast SMA, Miyake J. Inhibition of cell adhesion by phosphorylated Ezrin/Radixin/Moesin. Cell Adhes Migr. 2015;9(6):502-12.
483. Gottesman MM. Mechanisms of cancer drug resistance. Annu Rev Med. 2002;53:615-27.
484. Kawai K, Kamatani N, Georges E, Ling V. Identification of a Membrane Glycoprotein Overexpressed in Murine Lymphoma Sublines Resistant to Cis-Diamminedichloroplatinum(Ii). Journal of Biological Chemistry. 1990;265(22):13137-42.
485. Torok Z, Tsvetkova NM, Balogh G, Horvath I, Nagy E, Penzes Z. Heat shock protein coinducers with no effect on protein denaturation specifically modulate the membrane lipid phase. P Natl Acad Sci USA. 2003;100(6):3131-6.
486. Nagy E, Balogi Z, Gombos I, Akerfelt M, Bjorkbom A, Balogh G. Hyperfluidization-coupled membrane microdomain reorganization is linked to activation of the heat shock response in a murine melanoma cell line. P Natl Acad Sci USA. 2007;104(19):7945-50.
487. Milanowska K, Krwawicz J, Papaj G, Kosinski J, Poleszak K, Lesiak J. REPAIRtoire-a database of DNA repair pathways. Nucleic acids research. 2011;39:D788-D92.
488. Abbas T, Sivaprasad U, Terai K, Amador V, Pagano M, Dutta A. PCNA-dependent regulation of p21 ubiquitylation and degradation via the CRL4(Cdt2) ubiquitin ligase complex. Gene Dev. 2008;22(18):2496-506.
489. Daley JM, Laan RL, Suresh A, Wilson TE. DNA joint dependence of pol X family polymerase action in nonhomologous end joining. The Journal of biological chemistry. 2005;280(32):29030-7.
490. Lee JW, Blanco L, Zhou T, Garcia-Diaz M, Bebenek K, Kunkel TA. Implication of DNA polymerase lambda in alignment-based gap filling for nonhomologous DNA end joining in human nuclear extracts. The Journal of biological chemistry. 2004;279(1):805-11.
491. Steen HB. Light scattering measurement in an arc lamp-based flow cytometer. Cytometry. 1990;11(2):223-30.
492. Avagyan S, Churchill M, Yamamoto K, Crowe JL, Li C, Lee BJ. Hematopoietic stem cell dysfunction underlies the progressive lymphocytopenia in XLF/Cernunnos deficiency. Blood. 2014;124(10):1622-5.
493. Tilgner K, Neganova I, Singhapol C, Saretzki G, Al-Aama JY, Evans J. Brief report: a human induced pluripotent stem cell model of cernunnos deficiency reveals an important role for XLF in the survival of the primitive hematopoietic progenitors. Stem Cells. 2013;31(9):2015-23.
494. Cichoz-Lach H, Michalak A. Oxidative stress as a crucial factor in liver diseases. World J Gastroentero. 2014;20(25):8082-91.

495. Nigel C. Bennett CGF. African Mole-Rats: Ecology and Eusociality: Cambridge University Press; 2000.
496. Gillet LCJ, Scharer OD. Molecular mechanisms of mammalian global genome nucleotide excision repair. Chem Rev. 2006;106(2):253-76.
497. Cavallaro U, Christofori G. Cell adhesion and signalling by cadherins and Ig-CAMs in cancer. Nat Rev Cancer. 2004;4(2):118-32.
498. Martin TA, Mansel RE, Jiang WG. Loss of occludin leads to the progression of human breast cancer. Int J Mol Med. 2010;26(5):721-32.
499. Kanehisa M, Sato Y, Kawashima M, Furumichi M, Tanabe M. KEGG as a reference resource for gene and protein annotation. Nucleic acids research. 2016;44(D1):D457-D62.
500. Moore KL, Eaton SF, Lyons DE, Lichenstein HS, Cummings RD, Mcever RP. The P-Selectin Glycoprotein Ligand from Human Neutrophils Displays Sialylated, Fucosylated, O-Linked Poly-N-Acetyllactosamine. Journal of Biological Chemistry. 1994;269(37):23318-27.
501. Yang J, Hirata T, Croce K, Merrill-Skoloff G, Tchernychev B, Williams E. Targeted gene disruption demonstrates that P-selectin glycoprotein ligand 1 (PSGL-1) is required for P-selectin-mediated but not E-selectin-mediated neutrophil rolling and migration. J Exp Med. 1999;190(12):1769-82.
502. Xia LJ, Sperandio M, Yago S, McDaniel JM, Cummings RD, Pearson-White S. P-selectin glycoprotein ligand-1-deficient mice have impaired leukocyte tethering to E-selectin under flow. J Clin Invest. 2002;109(7):939-50.
503. Kim YJ, Borsig L, Varki NM, Varki A. P-selectin deficiency attenuates tumor growth and metastasis. P Natl Acad Sci USA. 1998;95(16):9325-30.
504. Tinoco R, Carrette F, Barraza ML, Otero DC, Magana J, Bosenberg MW. PSGL-1 Is an Immune Checkpoint Regulator that Promotes T Cell Exhaustion. Immunity. 2016;44(5):1190-203.
505. Ludwig RJ, Boehme B, Podda M, Henschler R, Jager E, Tandi C. Endothelial P-selectin as a target of heparin action in experimental melanoma lung metastasis. Cancer Res. 2004;64(8):2743-50.
506. Andersen CL, Jensen JL, Orntoft TF. Normalization of real-time quantitative reverse transcription-PCR data: A model-based variance estimation approach to identify genes suited for normalization, applied to bladder and colon cancer data sets. Cancer Res. 2004;64(15):5245-50.
507. Xie FL, Xiao P, Chen DL, Xu L, Zhang BH. miRDeepFinder: a miRNA analysis tool for deep sequencing of plant small RNAs. Plant Mol Biol. 2012;80(1):75-84.
508. Nigro JM, Aldape KD, Hess SM, Tlsty TD. Cellular adhesion regulates p53 protein levels in primary human keratinocytes. Cancer Res. 1997;57(17):3635-9.
509. Sosa-Garcia B, Gunduz V, Vazquez-Rivera V, Cress WD, Wright G, Bian H. A Role for the Retinoblastoma Protein As a Regulator of Mouse Osteoblast Cell Adhesion: Implications for Osteogenesis and Osteosarcoma Formation. Plos One. 2010;5(11).
510. Cohen MB, Griebling TL, Ahaghotu CA, Rokhlin OW, Ross JS. Cellular adhesion molecules in urologic malignancies. Am J Clin Pathol. 1997;107(1):56-63.
511. Buxton RS, Magee AI. Structure and interactions of desmosomal and other cadherins. Seminars in cell biology. 1992;3(3):157-67.
512. Tenchini ML, Adams JC, Gilberty C, Steel J, Hudson DL, Malcovati M. Evidence against a Major Role for Integrins in Calcium-Dependent Intercellular-Adhesion of Epidermal-Keratinocytes. Cell Adhes Commun. 1993;1(1):55-66.
513. OConnell D, Koenig A, Jennings S, Hicke B, Han HL, Fitzwater T. Calcium-dependent oligonucleotide antagonists specific for L-selectin. P Natl Acad Sci USA. 1996;93(12):5883-7.
514. Brown RC, Davis TP. Calcium modulation of adherens and tight junction function - A potential mechanism for blood-brain barrier disruption after stroke. Stroke. 2002;33(6):1706-11.
515. Wong V, Gumbiner BM. A synthetic peptide corresponding to the extracellular domain of occludin perturbs the tight junction permeability barrier. J Cell Biol. 1997;136(2):399-409.

516. Martin TA, Jiang WG. Loss of tight junction barrier function and its role in cancer metastasis. Bba-Biomembranes. 2009;1788(4):872-91.
517. Hollande F, Blanc EM, Bali JP, Whitehead RH, Pelegrin A, Baldwin GS. HGF regulates tight junctions in new nontumorigenic gastric epithelial cell line. Am J Physiol-Gastr L. 2001;280(5):G910-G21.
518. Yonemura S, Itoh M, Nagafuchi A, Tsukita S. Cell-to-Cell Adherens Junction Formation and Actin Filament Organization - Similarities and Differences between Non-Polarized Fibroblasts and Polarized Epithelial-Cells. J Cell Sci. 1995;108:127-42.
519. Hsu MY, Meier FE, Nesbit M, Hsu JY, Van Belle P, Elder DE. E-cadherin expression in melanoma cells restores keratinocyte-mediated growth control and down-regulates expression of invasion-related adhesion receptors. Am J Pathol. 2000;156(5):1515-25.
520. Vleminckx K, Vakaet L, Mareel M, Fiers W, Vanroy F. Genetic Manipulation of E-Cadherin Expression by Epithelial Tumor-Cells Reveals an Invasion Suppressor Role. Cell. 1991;66(1):107-19.
521. Bates RC, Lincz LF, Burns GF. Involvement of Integrins in Cell-Survival. Cancer Metast Rev. 1995;14(3):191-203.
522. Frisch SM, Francis H. Disruption of Epithelial Cell-Matrix Interactions Induces Apoptosis. J Cell Biol. 1994;124(4):619-26.
523. Chen YQ, Hsieh JT, Yao FY, Fang BL, Pong RC, Cipriano SC. Induction of apoptosis and G2/M cell cycle arrest by DCC. Oncogene. 1999;18(17):2747-54.
524. Okegawa T, Pong RC, Li YM, Bergelson JM, Sagalowsky AI, Hsieh JT. The mechanism of the growth-inhibitory effect of coxsackie and adenovirus receptor (CAR) on human bladder cancer: A functional analysis of CAR protein structure. Cancer Res. 2001;61(17):6592-600.
525. Lu JG, Li Y, Li L, Kan X. Overexpression of osteopontin and integrin alpha v in laryngeal and hypopharyngeal carcinomas associated with differentiation and metastasis. J Cancer Res Clin. 2011;137(11):1613-8.
526. van den Hoogen C, van der Horst G, Cheung H, Buijs JT, Pelger RCM, van der Pluijm G. Integrin alpha v Expression Is Required for the Acquisition of a Metastatic Stem/Progenitor Cell Phenotype in Human Prostate Cancer. Am J Pathol. 2011;179(5):2559-68.
527. Richter U, Schroder C, Wicklein D, Lange T, Geleff S, Dippel V. Adhesion of small cell lung cancer cells to E- and P-Selectin under physiological flow conditions: implications for metastasis formation. Histochem Cell Biol. 2011;135(5):499-512.
528. LeBaron RG, Athanasiou KA. Ex vivo synthesis of articular cartilage. Biomaterials. 2000;21(24):2575-87.
529. Hong S, Ergezen E, Lec R, Barbee KA. Real-time analysis of cell-surface adhesive interactions using thickness shear mode resonator. Biomaterials. 2006;27(34):5813-20.
530. Horwitz AF. Integrins and health. Sci Am. 1997;276(5):68-75.
531. Geiger B, Bershadsky A, Pankov R, Yamada KM. Transmembrane crosstalk between the extracellular matrix--cytoskeleton crosstalk. Nature reviews Molecular cell biology. 2001;2(11):793-805.
532. Rawlings ND, Barrett AJ. Families of Serine Peptidases. Method Enzymol. 1994;244:19-61.
533. Zhang B, Shan H, Li D, Li ZR, Zhu KS, Jiang ZB. Different methods of detaching adherent cells significantly affect the detection of TRAIL receptors. Tumori. 2012;98(6):800-3.
534. Vermeulen K, Van Bockstaele DR, Berneman ZN. The cell cycle: a review of regulation, deregulation and therapeutic targets in cancer. Cell Proliferat. 2003;36(3):131-49.
535. Lee MG, Nurse P. Complementation Used to Clone a Human Homolog of the Fission Yeast-Cell Cycle Control Gene Cdc2. Nature. 1987;327(6117):31-5.
536. Sherr CJ, Roberts JM. Inhibitors of mammalian G1 cyclin-dependent kinases. Genes Dev. 1995;9(10):1149-63.
537. Blagosklonny MV, Pardee AB. The restriction point of the cell cycle. Cell cycle. 2002;1(2):103-10.

538. Bartek J, Lukas J. Mammalian G1- and S-phase checkpoints in response to DNA damage. Curr Opin Cell Biol. 2001;13(6):738-47.
539. Yam CH, Fung TK, Poon RYC. Cyclin A in cell cycle control and cancer. Cell Mol Life Sci. 2002;59(8):1317-26.
540. Cimprich KA, Cortez D. ATR: an essential regulator of genome integrity. Nat Rev Mol Cell Bio. 2008;9(8):616-27.
541. Katou Y, Kanoh Y, Bando M, Noguchi H, Tanaka H, Ashikari T. S-phase checkpoint proteins Tof1 and Mrc1 form a stable replication-pausing complex. Nature. 2003;424(6952):1078-83.
542. Cortez D, Glick G, Elledge SJ. Minichromosome maintenance proteins are direct targets of the ATM and ATR checkpoint kinases. P Natl Acad Sci USA. 2004;101(27):10078-83.
543. Alberts B, Johnson A, Lewis J, Morgan D, Raff M, Roberts K. Molecular Biology of the Cell, Sixth Edition. Molecular Biology of the Cell, Sixth Edition. 2015:1-1342.
544. Liskay RM. Absence of a measurable G2 phase in two Chinese hamster cell lines. Proc Natl Acad Sci U S A. 1977;74(4):1622-5.
545. Porter LA, Donoghue DJ. Cyclin B1 and CDK1: nuclear localization and upstream regulators. Prog Cell Cycle Res. 2003;5:335-47.
546. Mailand N, Podtelejnikov AV, Groth A, Mann M, Bartek J, Lukas J. Regulation of G(2)/M events by Cdc25A through phosphorylation-dependent modulation of its stability. Embo Journal. 2002;21(21):5911-20.
547. Taylor WR, Stark GR. Regulation of the G2/M transition by p53. Oncogene. 2001;20(15):1803-15.
548. Xiao Z, Chen Z, Gunasekera AH, Sowin TJ, Rosenberg SH, Fesik S. Chk1 mediates S and G2 arrests through Cdc25A degradation in response to DNA-damaging agents. The Journal of biological chemistry. 2003;278(24):21767-73.
549. Peters JM. SCF and APC: the Yin and Yang of cell cycle regulated proteolysis. Curr Opin Cell Biol. 1998;10(6):759-68.
550. Ciosk R, Zachariae W, Michaelis C, Shevchenko A, Mann M, Nasmyth K. An ESP1/PDS1 complex regulates loss of sister chromatid cohesion at the metaphase to anaphase transition in yeast. Cell. 1998;93(6):1067-76.
551. Darzynkiewicz Z, Halicka HD, Zhao H. Analysis of Cellular DNA Content by Flow and Laser Scanning Cytometry. Adv Exp Med Biol. 2010;676:137-47.
552. Schneider EL, Fowlkes BJ. Measurement of DNA Content and Cell-Volume in Senescent Human Fibroblasts Utilizing Flow Multiparameter Single Cell Analysis. Exp Cell Res. 1976;98(2):298-302.
553. Wlodkowic D, Telford W, Skommer J, Darzynkiewicz Z. Apoptosis and Beyond: Cytometry in Studies of Programmed Cell Death. Method Cell Biol. 2011;103:55-98.
554. Loffek S, Hurskainen T, Jackow J, Sigloch FC, Schilling O, Tasanen K. Transmembrane Collagen XVII Modulates Integrin Dependent Keratinocyte Migration via PI3K/Rac1 Signaling. Plos One. 2014;9(2).
555. Heitman J, Movva NR, Hall MN. Targets for Cell-Cycle Arrest by the Immunosuppressant Rapamycin in Yeast. Science. 1991;253(5022):905-9.
556. Bruss MD, Thompson ACS, Aggarwal I, Khambatta CF, Hellerstein MK. The effects of physiological adaptations to calorie restriction on global cell proliferation rates. Am J Physiol-Endoc M. 2011;300(4):E735-E45.
557. Long XM, Spycher C, Han ZS, Rose AM, Muller F, Avruch J. TOR deficiency in C-elegans causes developmental arrest and intestinal atrophy by inhibition of mRNA translation. Current Biology. 2002;12(17):1448-61.
558. Murakami M, Ichisaka T, Maeda M, Oshiro N, Hara K, Edenhofer F. mTOR is essential for growth and proliferation in early mouse embryos and embryonic stem cells. Mol Cell Biol. 2004;24(15):6710-8.

559. Oldham S, Montagne J, Radimerski T, Thomas G, Hafen E. Genetic and biochemical characterization of dTOR, the Drosophila homolog of the target of rapamycin. Gene Dev. 2000;14(21):2689-94.
560. Ross MH. Length of life and nutrition in the rat. J Nutr. 1961;75:197-210.
561. Baugh LR. To Grow or Not to Grow: Nutritional Control of Development During Caenorhabditis elegans L1 Arrest. Genetics. 2013;194(3):539-55.
562. Krtolica A, Parrinello S, Lockett S, Desprez PY, Campisi J. Senescent fibroblasts promote epithelial cell growth and tumorigenesis: A link between cancer and aging. P Natl Acad Sci USA. 2001;98(21):12072-7.
563. Liu D, Hornsby PJ. Senescent human fibroblasts increase the early growth of xenograft tumors via matrix metalloproteinase secretion. Cancer Res. 2007;67(7):3117-26.
564. Minamino T, Yoshida T, Tateno K, Miyauchi H, Zou YZ, Toko H. Ras induces vascular smooth muscle cell senescence and inflammation in human atherosclerosis. Circulation. 2003;108(18):2264-9.
565. Baker DJ, Wijshake T, Tchkonia T, LeBrasseur NK, Childs BG, van de Sluis B. Clearance of p16Ink4a-positive senescent cells delays ageing-associated disorders. Nature. 2011;479(7372):232-6.
566. Clarke FM, Faulkes CG. Dominance and queen succession in captive colonies of the eusocial naked mole-rat, Heterocephalus glaber. Proc Biol Sci. 1997;264(1384):993-1000.
567. Pompei F, Polkanov M, Wilson R. Age distribution of cancer in mice: the incidence turnover at old age. Toxicol Ind Health. 2001;17(1):7-16.
568. Hu Y, Lu X, Zhou G, Barnes EL, Luo G. Recql5 plays an important role in DNA replication and cell survival after camptothecin treatment. Mol Biol Cell. 2009;20(1):114-23.
569. Cimpean AM, Ribatti D, Raica M. The chick embryo chorioallantoic membrane as a model to study tumor metastasis. Angiogenesis. 2008;11(4):311-9.
570. Jones B, Nachtsheim CJ. A Class of Three-Level Designs for Definitive Screening in the Presence of Second-Order Effects. J Qual Technol. 2011;43(1):1-15.

Appendix

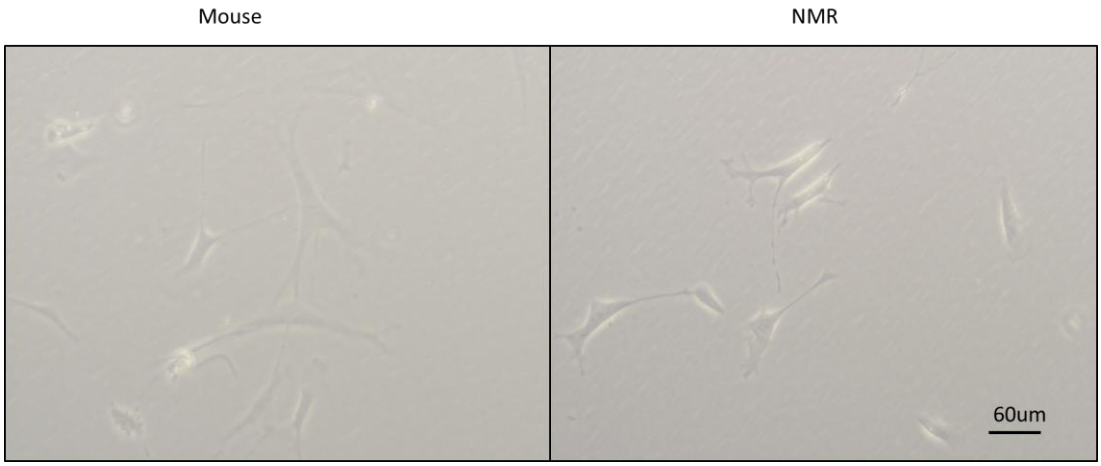

Appendix Figure 1. Representative images of untreated mouse and NMR cells from the beta cell stock. Grown for 48 hours before imaging. Mouse cell line 2 and NMR cell line 2 displayed.

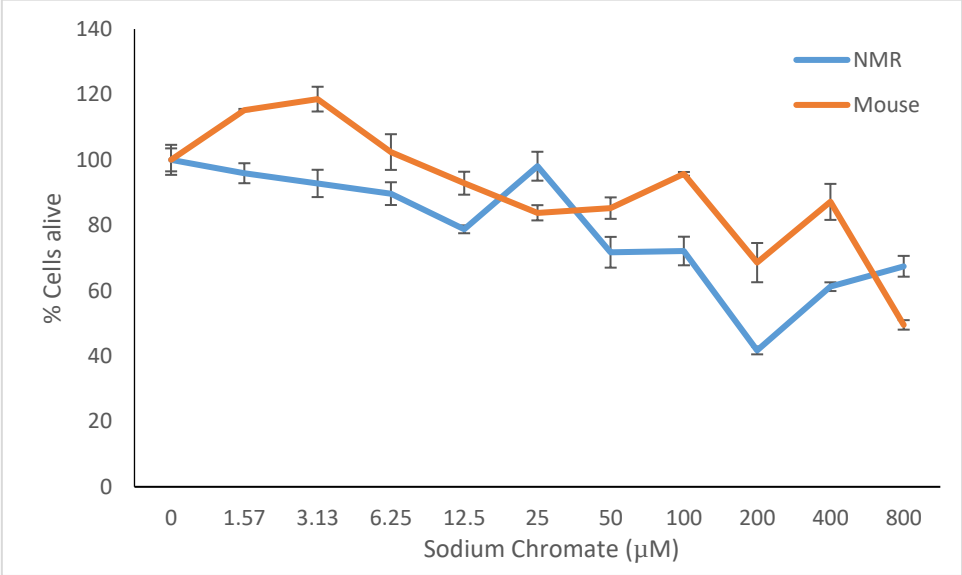

Appendix Figure 2. Percentage survival of NMR or mouse skin fibroblast (alpha cell stock), treated with sodium chromate. Error bars indicate +/- one standard error of the mean between three cell lines, each cell line value consisted of one replicate only.

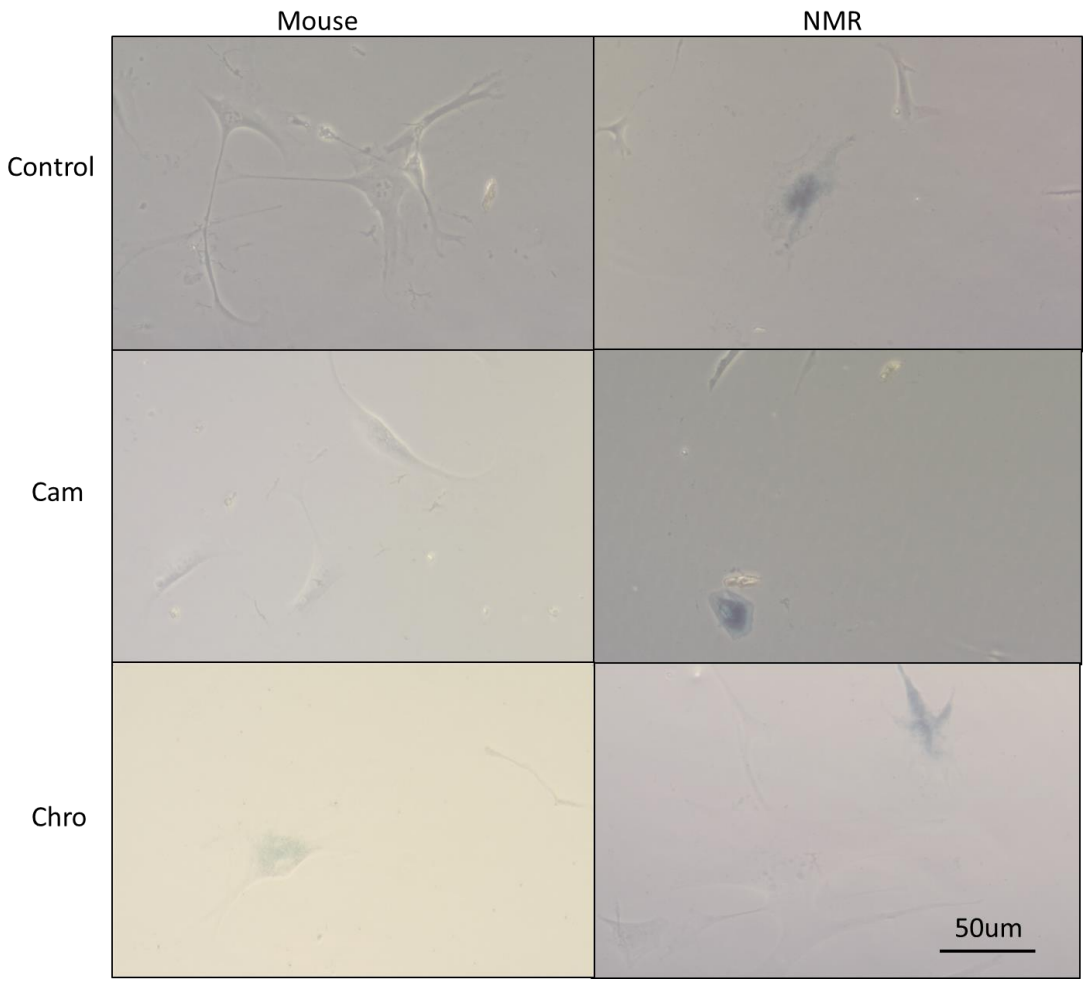

Appendix Figure 3. Non-representative images of Mouse and NMR cell line 1 (beta cell stock) after 2-hour treatment with control conditions, 160μM chromium (vi) oxide or 120μM camptothecin and incubated in beta galactosidase staining solution at pH6 for 3 days at 37°C at atmospheric CO_2. Cam – camptothecin, Chro – chromium (vi) oxide. Marker indicates approximately 50μm. Despite the prevalence of stained cells in camptothecin-treated mouse cells, the only clear images taken did not contain any such cells hence the absence of staining in the image.

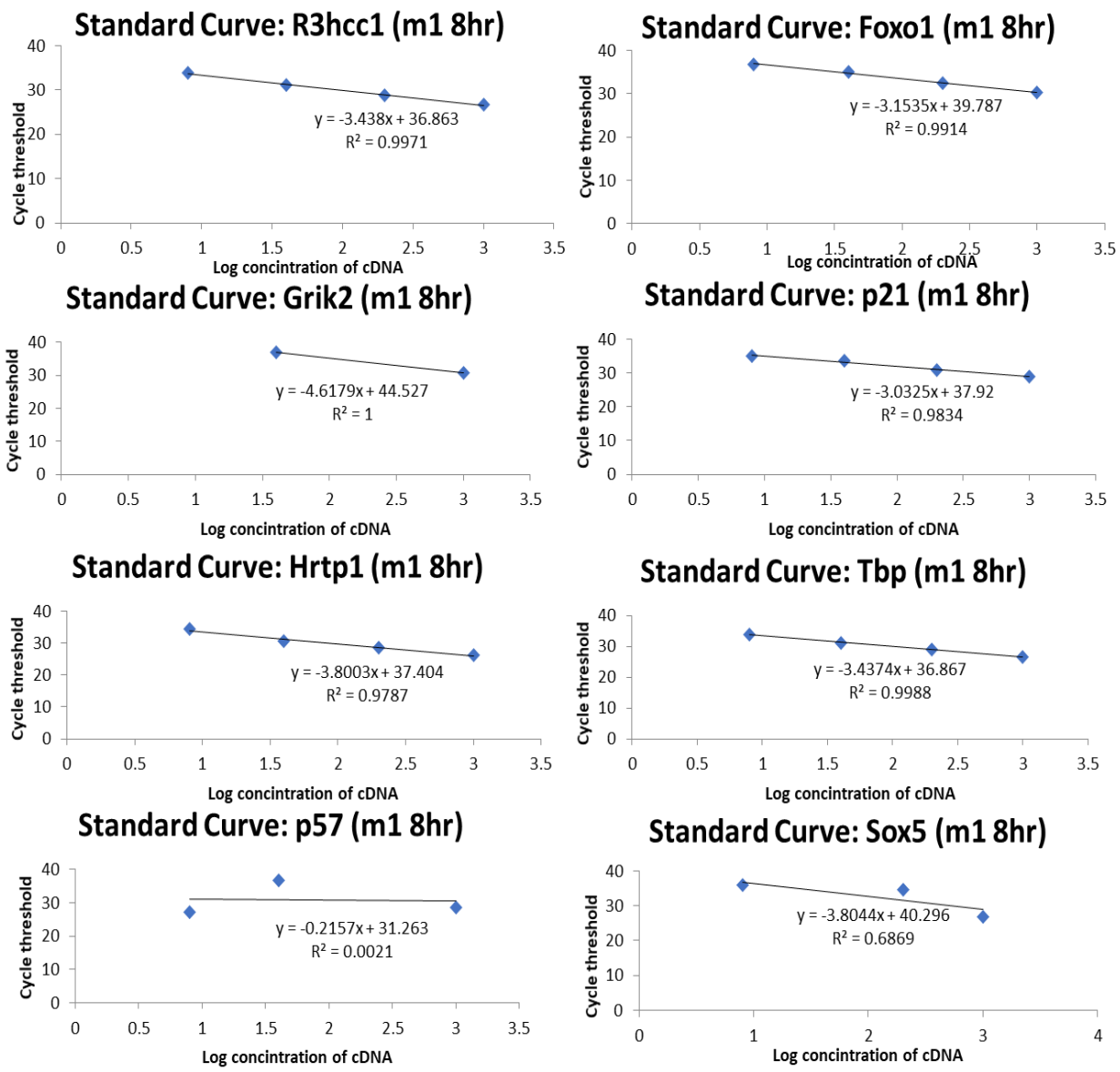

Appendix Figure 4. Standard curves generated from control cDNA samples from mouse cell line 1 after 8 hours post genotoxin treatment. Missing points in samples are due to poor amplification during the qPCR analysis. Concentration in ng.

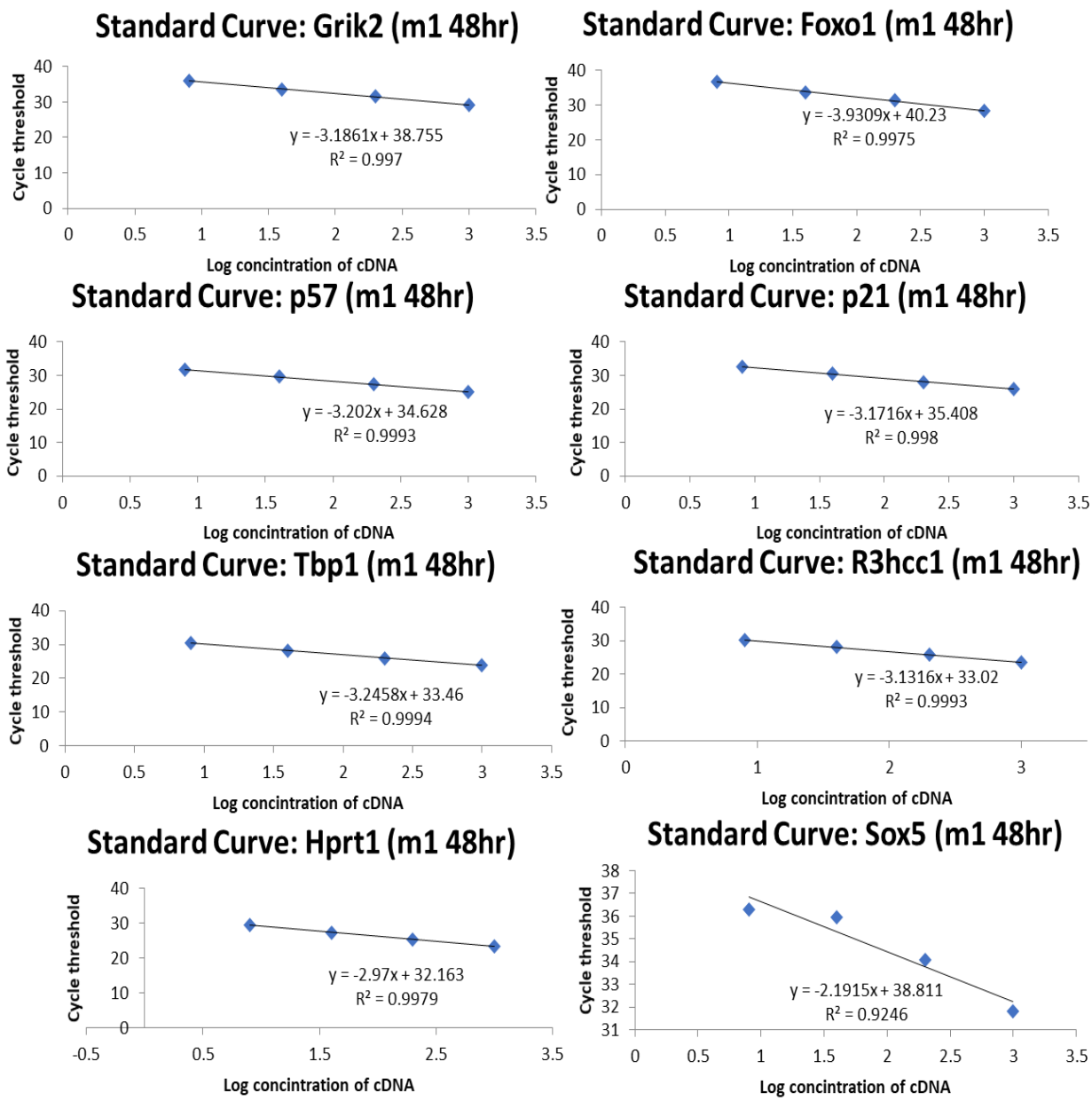

Appendix Figure 5. Standard curves generated from control cDNA samples from mouse cell line 1 after 48 hours post genotoxin treatment. Missing points in samples are due to poor amplification during the qPCR analysis. Concentration in ng.

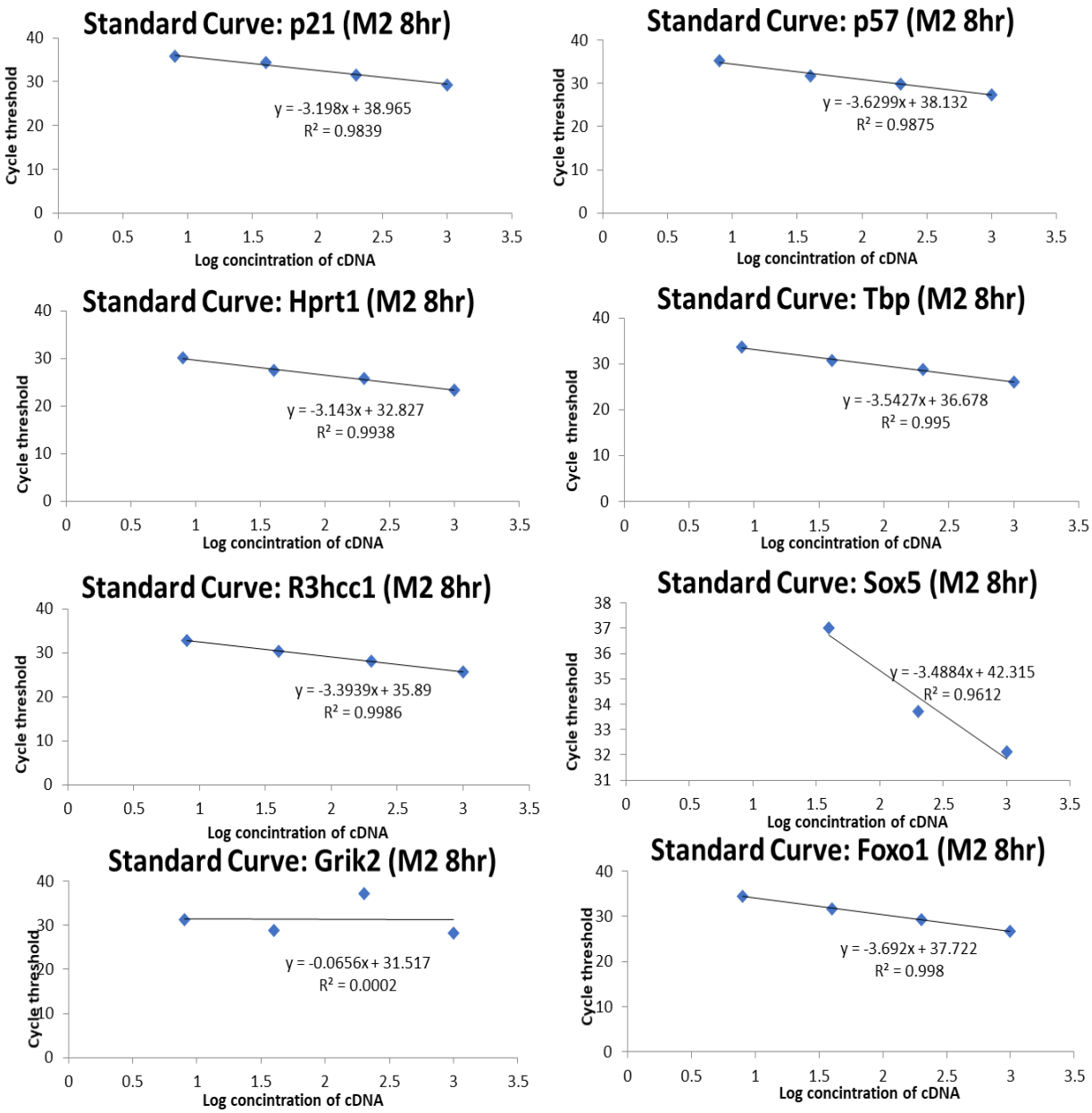

Appendix Figure 6. Standard curves generated from control cDNA samples from mouse cell line 2 after 8 hours post genotoxin treatment. Missing points in samples are due to poor amplification during the qPCR analysis. Concentration in ng.

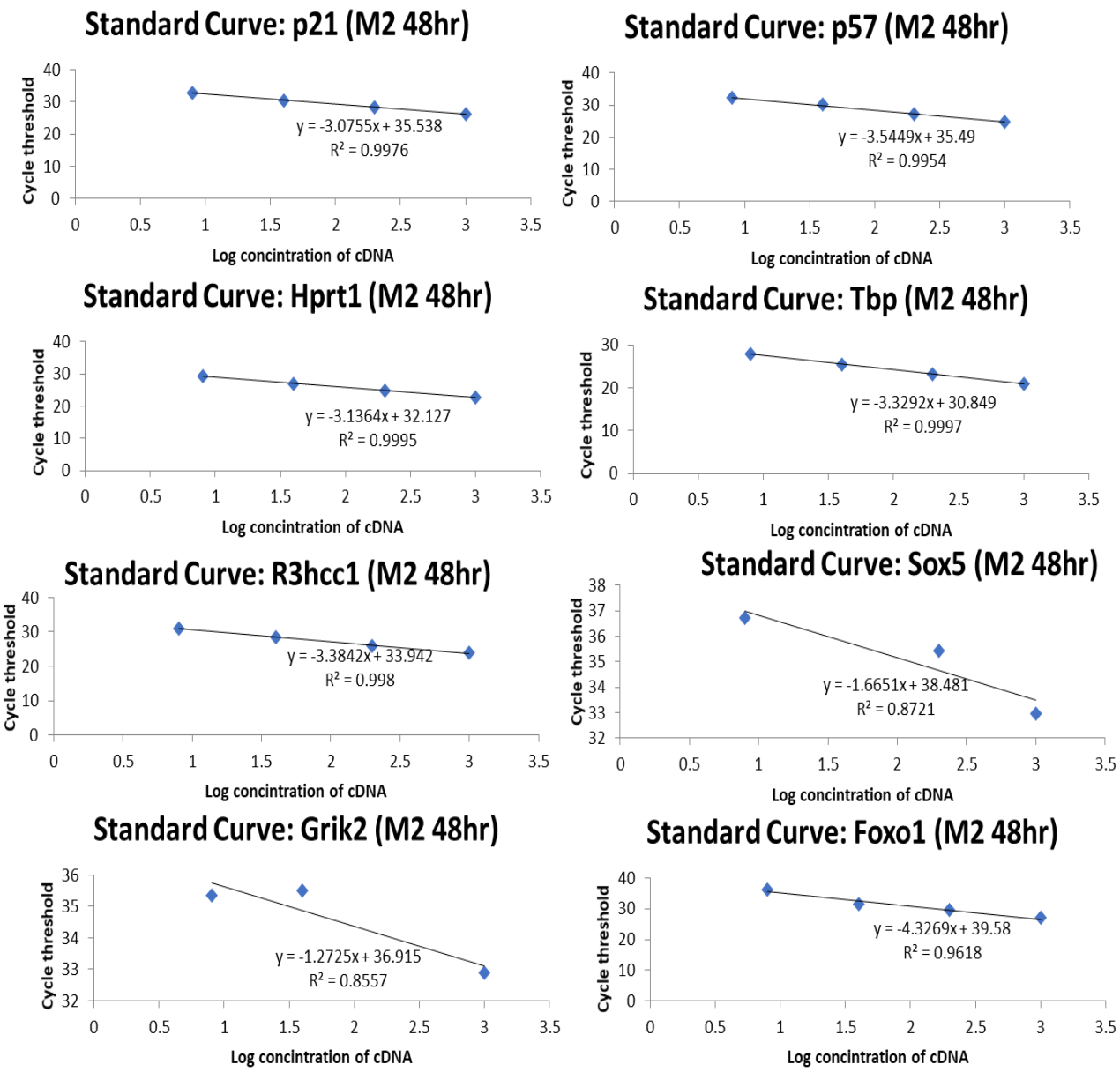

Appendix Figure 7. Standard curves generated from control cDNA samples from mouse cell line 2 after 8 hours post genotoxin treatment. Missing points in samples are due to poor amplification during the qPCR analysis. Concentration in ng.

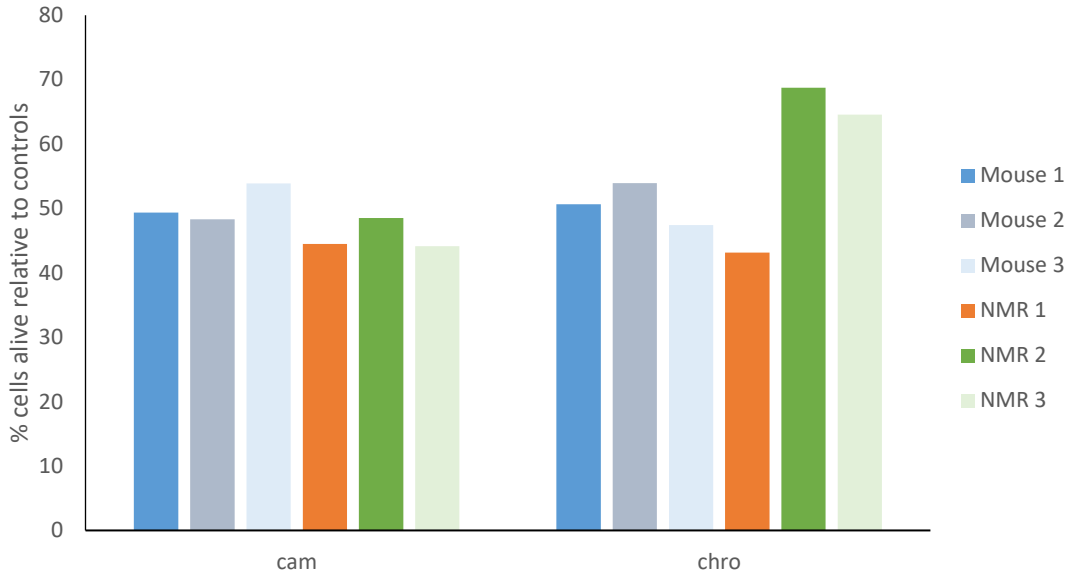

Appendix Figure 8. The proportion of cells alive relative to untreated controls of treated samples after 48 hours. This count was performed prior to RNA extraction for RNAseq. Key, cam - camptothecin, chro – chromium (vi) oxide, con - control.

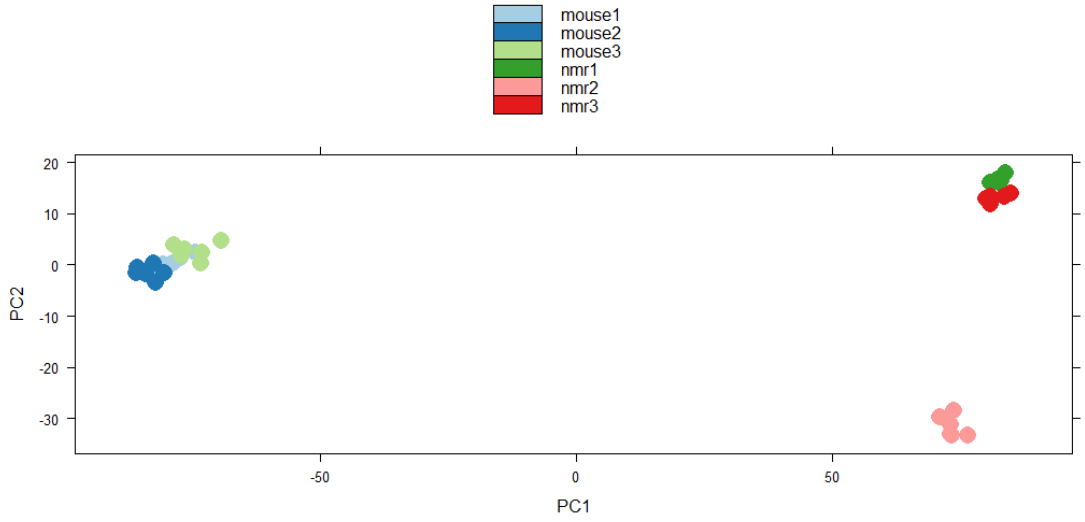

Appendix Figure 9. PCA plot of mouse and NMR RNA samples. Mouse samples can be seen to cluster to the left, while NMR samples from two distinct clusters of the right, the top being formed by NMR cell lines 1 and 3 and the bottom being made of NMR cell line 2 samples.

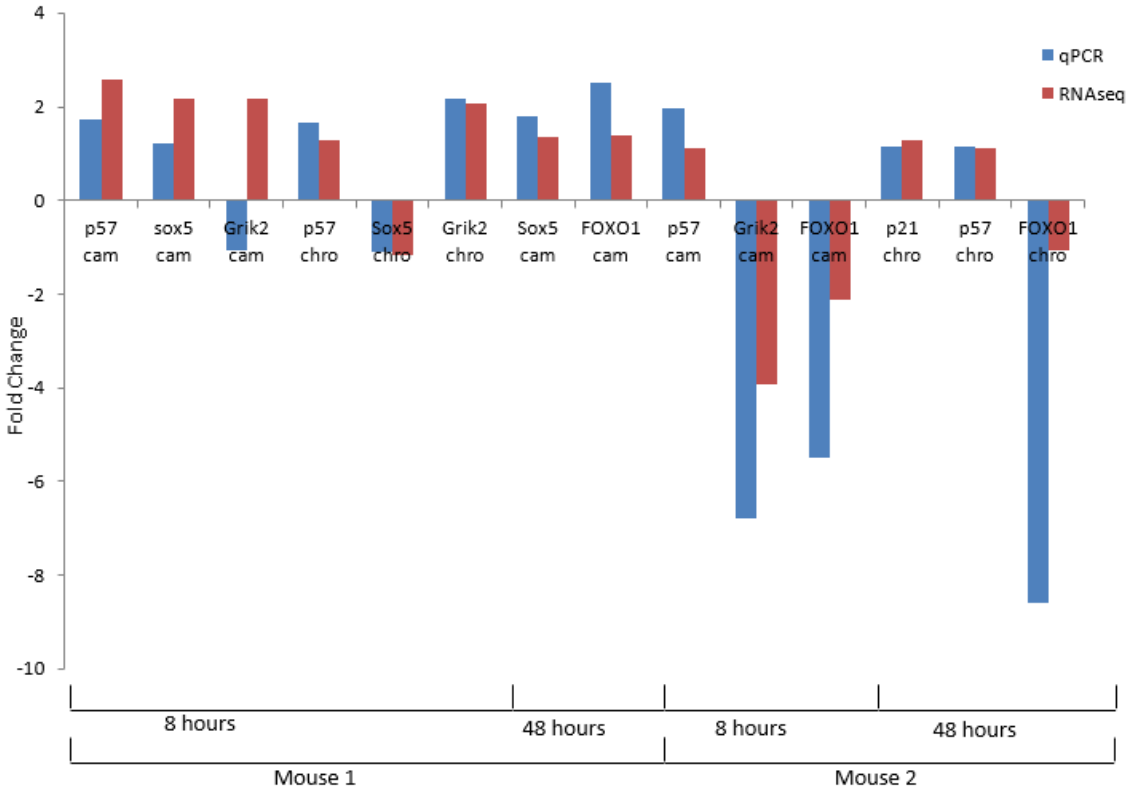

Appendix Figure 10. The fold change in gene expression between control and treated samples as determined by RNAseq (red) and qPCR (blue) for samples that failed to meet the cut off for efficiency (95-105%) and/or R^2 (≥0.98). For most samples the change in gene expression is the same in both RNAseq and qPCR however m1 samples from camptothecin-treated samples after 8hrs for Grik2 show reduced expression from qPCR and increased expression from RNAseq. The following samples are not included due to excessively large fold changes; all showed a decrease in both RNAseq and qPCR, but qPCR samples showed a much greater decrease: m2 8hr Sox5 camptothecin-treated and 48hr treated with chromium for Sox5 and Foxo1. Tbp was used as the housekeeping gene in this analysis.

Appendix Table 1. Amplification efficiency of each primer pair used in the qPCR analysis.

Cell line	Sample	Gene	Efficiency
M1	8hr	P21	113.6785
		p57	4325722
		Hrtp1	83.2893
		Tbp	95.39685
		r3hcc1	95.37401
		sox5	83.16966
		grik2	64.64504
		foxo1	107.5429
	48hr	p21	106.6799
		p57	105.2602
		Hrtp1	117.1203
		tbp1	103.278
		r3hcc1	108.6054
		sox5	186.168
		grik2	105.9982
		foxo1	79.63653
M2	8hr	p21	105.4449
		p57	88.57742
		Hprt1	108.0498
		Tbp	91.5449
		R3hcc1	97.08169
		Sox5	93.49261
		Grik2	1.75E+17
		Foxo1	86.57605
	48hr	p21	111.4221
		p57	91.46765
		Hprt1	108.3708
		Tbp	99.69742
		R3hcc1	97.46531
		Sox5	298.625
		Grik2	510.7375
		Foxo1	70.27874

Appendix Table 2. Ct values for housekeeping genes Tbp and Hprt1. Key, m1 - mouse cell line 1, m2 - mouse cell line 2.

			Tbp	*Hprt1*
Cell line	Sample time	Treatment	Mean ± SD	Mean ± SD
m1	8hour	control	26.6 ± 0.38	26.29 ± 0.05
		camptothecin	25.94 ± 0.37	25.82 ± 0.27
		chromium	27.22 ± 0.02	26.71 ± 0.13
	48hour	control	23.79 ± 0.13	23.36 ± 0.06
		camptothecin	25.27 ± 0.1	23.94 ± 0.01
m2	8hour	control	26.04 ± 0.23	23.34 ± 0.2
		camptothecin	27.36 ± 0.02	23.81 ± 0.06
	48hour	control	20.87 ± 0.32	22.76 ± 0.04
		chromium	21.69 ± 0.04	23 ± 0.1

Appendix Table 3. All DNA repair genes that are present in the NMR RNAseq dataset. Arrows indicate up (↑) and down (↓) regulation between mouse and NMR cells in the presented conditions, dash (-) indicates the gene was not significantly differentially expressed at the p=0.05 level. Continues over three pages.

	8 hour post stimuli			48 hour post stimuli		
Gene	Control	Camptothecin	Chromium (vi) oxide	Control	Camptothecin	Chromium (vi) oxide
Alkbh2	↑	↑	↑	↑	↑	↑
Alkbh3	-	-	-	-	-	-
Apex1	-	-	-	-	-	-
Apex2	-	-	-	-	-	-
Aplf	↓	↓	↓	↓	↓	↓
Aptx	-	-	↓	-	-	↓
Atm	↓	↓	↓	↓	↓	↓
Atr	↓	↓	↓	↓	↓	↓
Atrip	↓	↓	↓	↓	↓	↓
Brca1	-	-	-	-	-	↑
Brca2	-	↓	-	↓	↓	-
Brip1	-	↓	-	↓	↓	-
Ccnh	-	-	-	-	-	-
Cdkn1a	-	-	↑	↑	-	↑
Chaf1a	↓	↓	-	↓	↓	-
Chek1	-	-	-	-	-	↑
Chek2	-	-	↑	-	-	-
Clk2	-	-	-	-	-	-
Cops5	↓	↓	↓	↓	↓	↓
Cul4a	-	-	-	-	-	-
Dclre1a	-	-	↑	-	-	↑
Dclre1b	-	-	-	-	-	-
Dclre1c	↑	↑	↑	↑	↑	↑
Ddb1	↓	↓	↓	↓	↓	↓
Ddb2	-	-	-	-	-	-
Dmc1	↑	↑	↑	↑	↑	↑
Dut	↓	↓	↓	↓	↓	↓
Eme1	-	-	-	-	-	-
Endov	↓	↓	↓	↓	↓	↓
Ercc1	-	-	-	-	-	-
Ercc2	-	-	-	-	-	-
Ercc3	↓	↓	↓	↓	↓	↓
Ercc4	↑	↑	↑	↑	↑	↑
Ercc6	↓	↓	↓	-	↓	-
Ercc8	-	-	-	-	-	-
Exo1	-	↓	-	-	↓	-
Fan1	↑	↑	↑	↑	↑	↑
Fanca	-	-	-	-	-	-
Fancb	↓	↓	↓	↓	↓	↓
Fancc	↓	↓	↓	↓	↓	↓
Fancd2	↑	↑	↑	↑	↑	↑
Fancg	-	-	-	-	-	-
Fanci	-	-	-	-	-	-
Fancl	-	-	-	-	↓	-
Fen1	↓	↓	-	↓	↓	-
Gen1	↑	-	↑	↑	-	↑
Gps1	↓	↓	↓	-	-	-
Gtf2h1	↓	↓	↓	↓	↓	↓
Gtf2h3	↓	↓	↓	↓	↓	↓
Gtf2h4	-	↓	-	-	-	-
Helq	↓	↓	↓	↓	↓	↓
Hltf	↑	↑	↑	↑	↑	↑
Hus1	-	-	-	-	-	-
Lig3	-	-	-	-	-	-
Lig4	↓	↓	↓	↓	↓	↓
Mad2l2	↑	-	↑	↑	↑	↑

	8 hour post stimuli			48 hour post stimuli		
Gene	Control	Camptothecin	Chromium (vi) oxide	Control	Camptothecin	Chromium (vi) oxide
Mbd4	↑	↑	↑	↑	↑	↑
Mdc1	-	-	-	-	-	-
Mgmt	-	-	↓	-	-	↓
Mlh1	↑	↑	-	↑	↑	-
Mlh3	↑	↑	↑	↑	↑	↑
Mms19	-	-	-	-	-	-
Mnat1	↓	↓	↓	↓	↓	↓
Mpg	↑	↑	↑	↑	↑	↑
Mre11a	↓	↓	↓	↓	↓	↓
Msh2	↓	↓	↓	↓	↓	-
Msh3	↑	-	-	-	-	-
Msh4	-	-	↑	-	-	-
Msh5	-	-	-	-	-	-
Msh6	-	-	-	-	-	-
Mus81	-	-	-	-	-	-
Mutyh	↓	↓	↓	↓	↓	↓
Neil1	↑	↑	↑	↑	↑	↑
Neil2	↑	↑	↑	↑	↑	↑
Neil3	-	-	-	-	-	-
Nhej1	↑	↑	↑	↑	↑	↑
Nthl1	↑	↑	↑	↑	↑	↑
Nudt1	↑	↑	↑	↑	↑	↑
Ogg1	-	-	-	-	-	-
Parp3	↓	↓	↓	↓	↓	↓
Pcna	↓	↓	-	↓	↓	-
Per1	↑	↑	↑	↑	↑	↑
Pms2	-	-	-	-	-	-
Pnkp	-	-	↓	-	-	↓
Polb	-	-	-	-	-	-
Pold1	-	↓	-	↓	↓	-
Pole	-	↓	-	↓	↓	-
Polh	↓	↓	↓	↓	↓	↓
Polk	↓	↓	↓	↓	↓	↓
Poll	↑	-	↑	-	-	↑
Polm	-	-	-	-	-	-
Polq	-	↓	-	-	↓	-
Prkdc	-	-	-	-	-	-
Prpf19	-	-	-	-	-	-
Rad1	↓	↓	↓	↓	↓	↓
Rad17	-	-	-	-	-	-
Rad18	↓	↓	↓	↓	↓	↓
Rad23b	-	-	-	-	-	-
Rad50	-	↓	-	↓	↓	-
Rad51	-	-	-	-	-	-
Rad51b	↑	↑	↑	↑	↑	↑
Rad51d	↑	↑	↑	↑	-	-
Rad52	-	-	-	-	-	-
Rbbp8	↓	↓	↓	↓	↓	↓
Rfc1	-	-	-	-	-	-
Rfc2	↓	↓	↓	↓	↓	-
Rfc3	↓	↓	-	↓	↓	-
Rfc5	-	-	-	-	-	-
Rif1	↑	-	↑	↑	-	↑
Rnf168	↓	↓	↓	↓	↓	↓
Rnf4	↓	↓	↓	↓	↓	↓
Rpa1	-	-	-	-	↓	-
Rpa2	-	-	↑	↑	-	↑
Rpa3	↓	↓	↓	↓	↓	↓
Shprh	↓	↓	↓	↓	↓	↓
Slx4	↑	↑	↑	↑	↑	↑
Smug1	↓	-	↓	↓	-	↓
Tdg	-	-	-	-	-	-
Tdp1	↑	↑	↑	↑	↑	↑
Topbp1	↓	↓	↓	↓	↓	↓

	8 hour post stimuli			48 hour post stimuli		
Gene	Control	Camptothecin	Chromium (vi) oxide	Control	Camptothecin	Chromium (vi) oxide
Trex1	-	-	-	-	-	-
Trex2	↑	↑	↑	↑	↑	↑
Trp53	↑	↑	↑	↑	↑	↑
Ube2a	↑	↑	↑	↑	↑	↑
Ube2b	↓	↓	↓	↓	↓	↓
Ube2n	↓	↓	↓	↓	↓	↓
Ung	-	-	-	-	-	↑
Uvssa	-	-	-	-	-	-
Wrn	-	-	-	↓	↓	-
Xab2	↓	↓	↓	↓	-	↓
Xpa	-	-	↓	-	-	↓
Xpc	↑	↑	↑	↑	↑	↑
Xrcc1	-	-	-	-	-	-
Xrcc4	-	↓	↓	-	↓	↓
Xrcc5	-	-	-	-	-	-
Xrcc6	-	-	-	-	-	-

Appendix Table4The number of DNA repair genes associated with a given pathway up (↑) or down (↓) regulated in NMR cells compared to mouse cells for different treatments and time points. Genes significant at the 0.05 level after correcting for multiple testing. Key, NHEJ, non-homologous end join, HR homologous recombination, MMR miss match repair, NER nucleotide excision repair, BER base excision repair, DDS DNA damage signalling.

		Control	Camptothecin	Chromium (vi) oxide
8hr	NHEJ	2↑ 1↓	1↑ 1↓	2↑ 1↓
	HR	3↑ 3↓	3↑ 4↓	4↑ 4↓
	MMR	3↑ 1↓	2↑ 4↓	1↑ 0↓
	NER	1↑ 4↓	1↑ 7↓	1↑ 4↓
	BER	6↑ 5↓	5↑ 6↓	6↑ 5↓
	DDS	0↑ 13↓	0↑ 14↓	1↑ 12↓
48hr	NHEJ	1↑ 1↓	1↑ 1↓	2↑ 1↓
	HR	3↑ 5↓	2↑ 5↓	3↑ 3↓
	MMR	2↑ 2↓	2↑ 4↓	1↑ 0↓
	NER	1↑ 6↓	1↑ 7↓	1↑ 4↓
	BER	5↑ 7↓	5↑ 6↓	7↑ 5↓
	DDS	0↑ 13↓	0↑ 13↓	2↑ 10↓

Appendix Table 5. All cell adhesion molecule genes from KEGG that are present in the NMR RNAseq dataset. Arrows indicate up (↑) and down (↓) regulation between mouse and NMR cells in the presented conditions, dash (-) indicates the gene was not significantly differentially expressed at the p=0.05 level. Continues over two pages.

	8 hour post stimuli			48 hour post stimuli		
Gene	Control	Camptothecin	Chromium (vi) oxide	Control	Camptothecin	Chromium (vi) oxide
Vtcn1	↑	↑	↑	↑	↑	-
Vcan	↑	↑	↑	↑	↑	↑
Vcam1	↓	-	↓	↓	↓	↓
Tigit	↑	↑	↑	↑	↑	↑
Spn	-	-	↓	-	-	↓
Siglec1	-	-	-	-	-	-
Selplg	↑	↑	↑	↑	↑	↑
Selp	↓	↓	↓	↓	↓	↓
Sele	↓	↓	-	↓	↓	↓
Sdc3	-	-	-	-	-	↓
Sdc2	↓	↓	↓	↓	↓	↓
Sdc1	-	-	↑	-	-	-
Pvr	↓	-	-	-	-	-
Ptprf	-	-	-	-	-	↓
Ptprc	-	-	-	-	-	-
Pdcd1	↑	↑	↑	↑	↑	↑
Ocln	-	-	-	-	-	-
Ntng2	↑	↑	↑	↑	↑	↑
Ntng1	↑	↑	↑	↑	↑	↑
Nrxn2	-	-	-	-	-	-
Nrcam	-	-	-	-	-	-
Nlgn3	-	↑	-	-	-	-
Nlgn2	-	-	-	-	-	-
Nlgn1	↑	↑	↑	↑	↑	↑
Nfasc	↑	↑	-	↑	↑	-
Neo1	↓	↓	↓	↓	↓	↓
Negr1	-	-	-	-	-	↓
Ncam2	↑	↑	↑	↑	↑	↑
Ncam1	↑	↑	-	↑	↑	-
Mpzl1	-	-	↑	-	-	↑
Mpz	-	-	-	-	-	-
Mag	-	-	↑	-	-	↑
Lrrc4c	↓	↓	-	↓	↓	↓
Lrrc4	↓	-	-	-	↓	-
L1cam	-	-	-	-	-	-
Jam3	-	-	-	-	-	-
Jam2	↓	↓	↓	↓	↓	↓
Itgb8	↑	↑	↑	↑	↑	↑
Itgb7	↓	↓	↓	↓	↓	↓
Itgb2	-	-	-	-	-	-
Itgb1	↓	-	↓	↓	↓	↓
Itgav	↓	-	↓	-	↓	↓
Itgal	↑	↑	↑	↑	↑	↑
Itga9	↑	↑	-	↑	↑	↓
Itga8	↓	↓	↓	↓	↓	↓
Itga6	↑	↑	-	-	↑	-
Itga4	↑	↑	↑	↑	↑	↑
Icos	-	-	-	-	-	-
Icam2	↑	↑	↑	↑	↑	↑
Icam1	↑	↑	↑	↑	↑	↑
Glg1	↑	-	↑	-	-	↑
F11r	↓	↓	↓	↓	↓	↓
Esam	↓	-	-	-	↓	↓
Ctla4	-	-	-	-	-	-
Cntnap1	↓	↓	-	↓	↓	-
Cntn2	-	-	-	-	-	-
Cntn1	↑	↑	-	-	-	-

	8 hour post stimuli			48 hour post stimuli		
Gene	Control	Camptothecin	Chromium (vi) oxide	Control	Camptothecin	Chromium (vi) oxide
Cldn9	-	-	-	-	-	-
Cldn8	-	-	-	-	-	-
Cldn7	-	-	↑	-	-	-
Cldn6	↑	↑	↑	↑	↑	↑
Cldn5	-	-	-	-	-	-
Cldn22	↑	↑	↑	↑	↑	↑
Cldn2	↑	↑	↑	↑	↑	↑
Cldn19	-	-	-	-	-	-
Cldn18	-	-	-	-	-	-
Cldn17	-	-	-	-	-	-
Cldn16	↑	↑	↑	↑	↑	↑
Cldn15	-	↓	-	-	-	↓
Cldn14	-	-	-	-	-	-
Cldn11	-	-	-	-	-	-
Cldn10	↑	↑	↑	↑	↑	↑
Cldn1	↑	↑	↑	↑	↑	↑
Cdh5	↑	↑	↑	↑	↑	↑
Cdh4	↑	↑	↑	↑	↑	-
Cdh3	-	-	-	-	-	↓
Cdh2	↑	↑	↑	↑	↑	↑
Cdh15	↑	↑	↑	↑	↑	↑
Cdh1	-	-	-	-	-	-
Cd8a	-	-	-	-	-	-
Cd86	-	-	-	-	-	-
Cd6	-	-	-	-	-	-
Cd40lg	-	-	-	-	-	-
Cd40	↑	↑	↑	↑	↑	↑
Cd4	-	-	-	-	-	-
Cd34	↓	↓	↓	↓	↓	↓
Cd28	-	-	-	-	↓	-
Cd276	↓	↓	↓	↓	↓	↓
Cd274	↑	↑	↑	↑	↑	↑
Cd226	-	-	-	-	-	-
Cd22	-	-	-	-	-	-
Cd2	-	-	-	-	-	-
Cadm3	↑	↑	↑	↑	↑	↑
Cadm1	↑	↑	↑	↑	↑	↑
Alcam	↑	↑	-	↑	↑	-

Appendix Table 6. PCR products produced with different primers in cDNA samples from the m2 mouse primary cells after 8hr treatment with camptothecin (cam) in media with 2% DMSO or media with 2% DMSO as control. These were run on a 3% agarose gel containing 0.006% Midori Green. Single bands indicate that no unspecific amplification has taken place. Bands in Hprt1 and Tbp blank samples indicate DNA contamination. The size of each band on the ladder is given to the left of the image.

				3% Agarose, 6µl Midori Green
Lane	Sample	Predicted size (bp)	Load	
1	Ladder	100-1,000	5µl	
2	P21 control	111	8µl	
3	P21 camptothecin	111	8µl	
4	P57 control	111	8µl	
5	P57 camptothecin	141	8µl	
6	Hprt1 control	141	8µl	
7	Hprt1 camptothecin	141	8µl	
8	Tbp control	195	8µl	
9	Tbp camptothecin	195	8µl	
10	R3hcc1 control	195	8µl	
11	R3hcc1 camptothecin	109	8µl	
12	Sox5 control	109	8µl	
13	Sox5 camptothecin	109	8µl	
14	Grik2 control	100	8µl	
15	Grik2 camptothecin	100	8µl	
16	FOXO1 control	100	8µl	
17	FOXO1 camptothecin	124	8µl	
18	P21 blank	124	8µl	
19	P57 blank	124	8µl	
20	Hprt1 blank	145	8µl	
21	Tbp blank	145	8µl	
22	R3hcc1 blank	145	8µl	
23	Sox5 blank	124	8µl	
24	Grik2 blank	124	8µl	
25	FOXO1 blank	124	8µl	

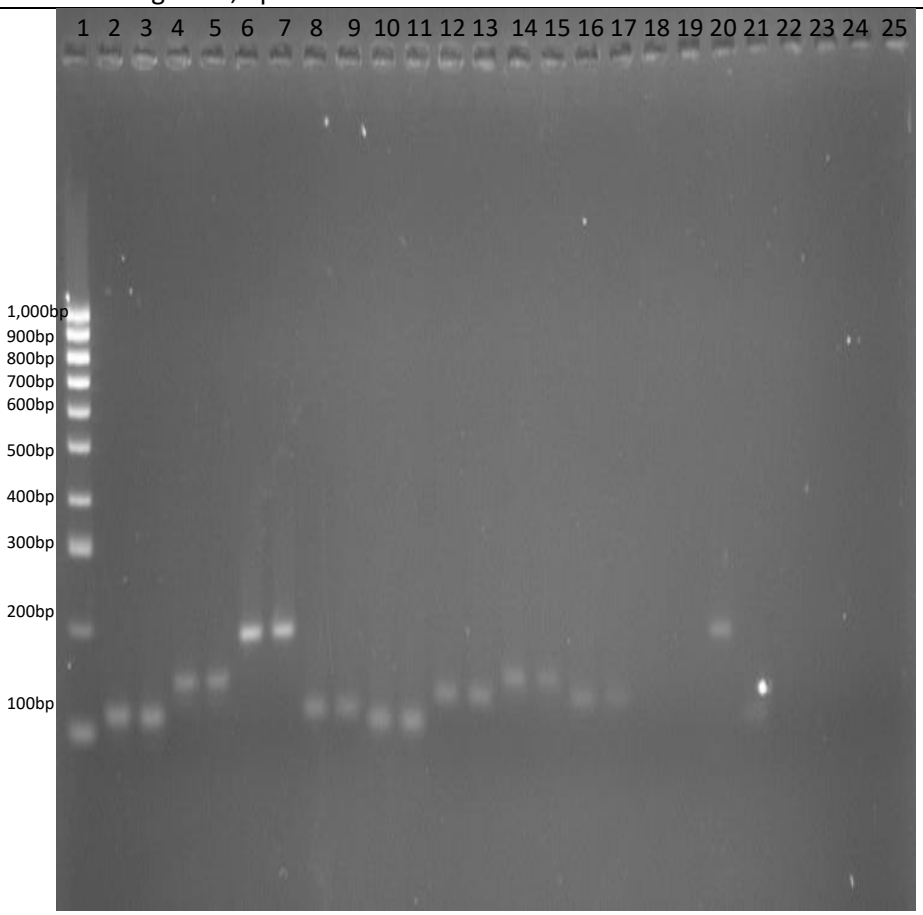

Appendix Table 7. PCR products produced with different primers in cDNA samples from the m2 mouse primary cells after 48hr treatment with chromium (vi) oxide (chro) in media with 2% DMSO or media with 2% DMSO as control. These were run on a 3% agarose gel containing 0.006% Midori Green. Single bands indicate that no unspecific amplification has taken place. Bands in p21 and Hprt1 blank samples indicate DNA contamination. The size of each band on the ladder is given to the left of the image.

				3% Agarose, 6µl Midori Green
Lane	Sample	Predicted size (bp)	Load	
1	Ladder	100-1,000	5µl	
2	P21 control	111	8µl	
3	P21 camptothecin	111	8µl	
4	P57 control	111	8µl	
5	P57 camptothecin	141	8µl	
6	Hprt1 control	141	8µl	
7	Hprt1 camptothecin	141	8µl	
8	Tbp control	195	8µl	
9	Tbp camptothecin	195	8µl	
10	R3hcc1 control	195	8µl	
11	R3hcc1 camptothecin	109	8µl	
12	Sox5 control	109	8µl	
13	Sox5 camptothecin	109	8µl	
14	Grik2 control	100	8µl	
15	Grik2 camptothecin	100	8µl	
16	FOXO1 control	100	8µl	
17	FOXO1 camptothecin	124	8µl	
18	P21 blank	124	8µl	
19	P57 blank	124	8µl	
20	Hprt1 blank	145	8µl	
21	Tbp blank	145	8µl	
22	R3hcc1 blank	145	8µl	
23	Sox5 blank	124	8µl	
24	Grik2 blank	124	8µl	
25	FOXO1 blank	124	8µl	

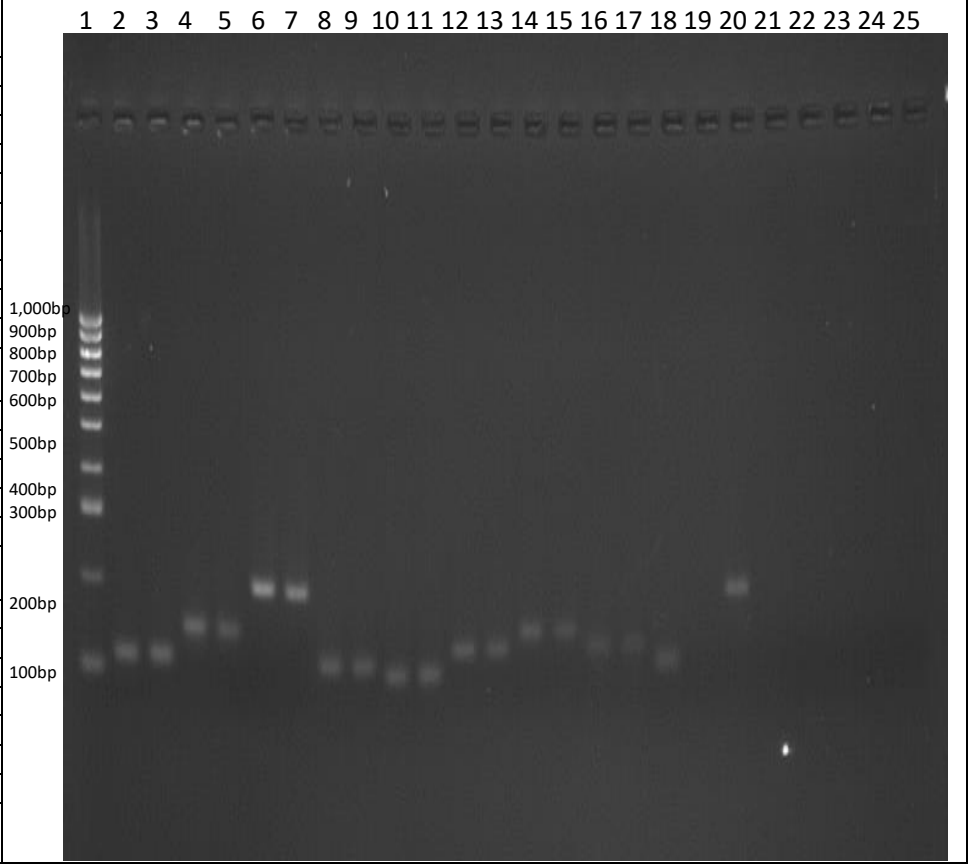

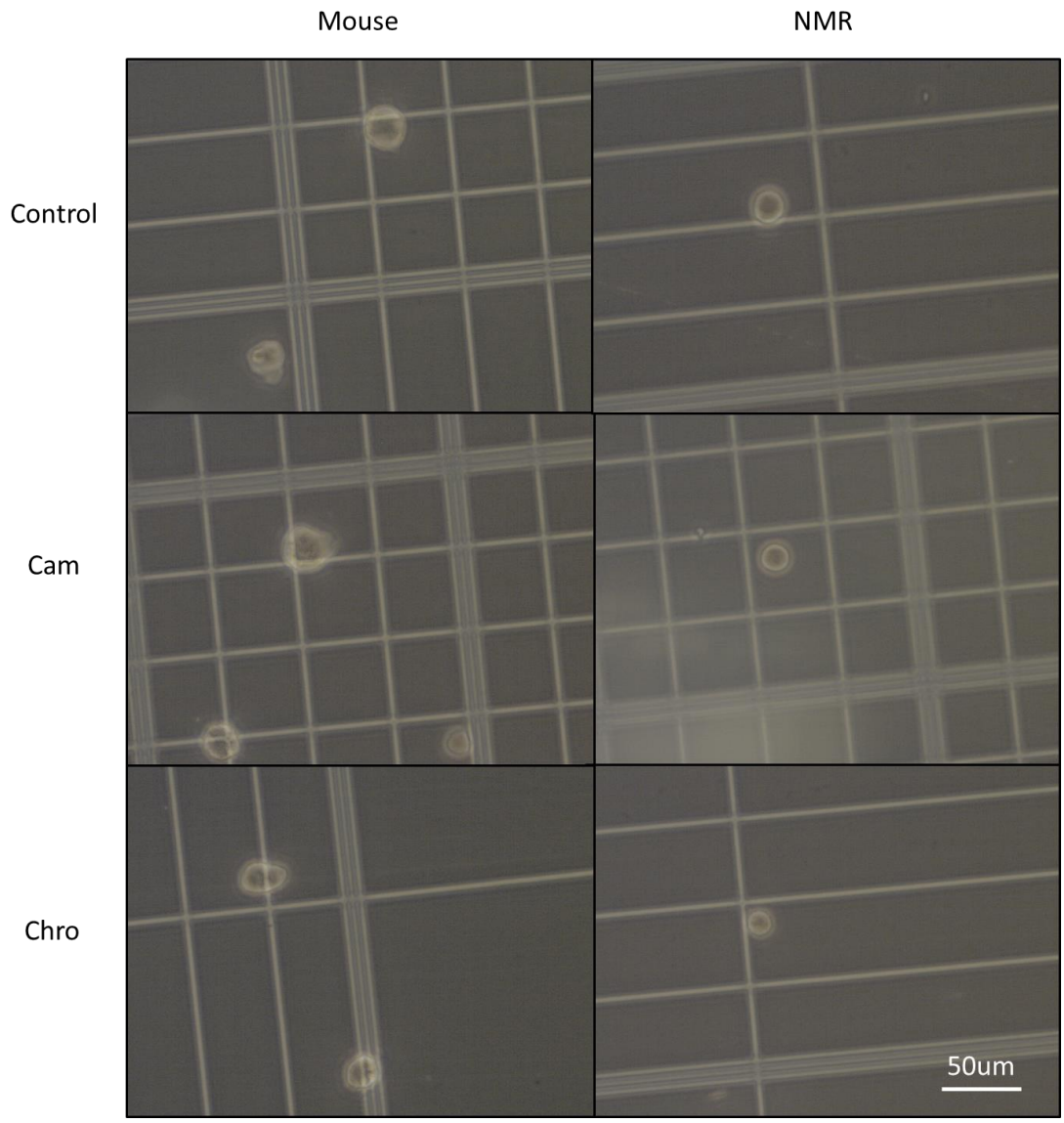

Appendix Figure 11. Representative images of trypsinised Mouse and NMR samples under each treatment prior used to estimate cell surface area. Cam – camptothecin treatment, Chro – chromium (vi) oxide treatment. White bar indicates ~50um.

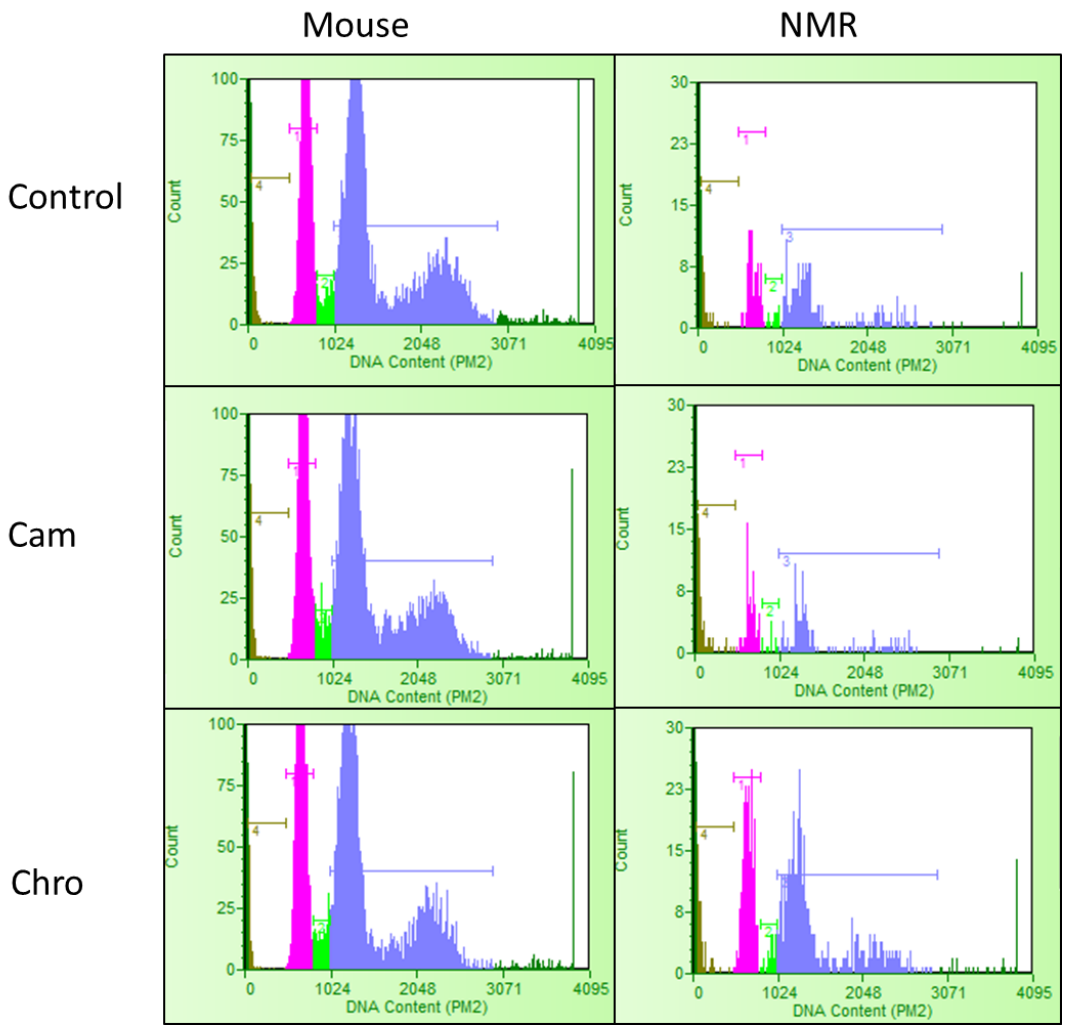

Appendix Figure 12. Representative histograms of Mouse and NMR samples under each treatment from flow cytometry. Mouse samples shown are of mouse cell line 3, NMR samples are of NMR cell line 3. NMR samples have been scaled up 3 fold to make the image clearer. Cells relating to a given section of the cell cycle have been highlighted. Pink indicates G1, green indicates S phase, blue indicates G2 and olive green indicates G4. Cam – camptothecin treatment, Chro – chromium (vi) oxide treatment.

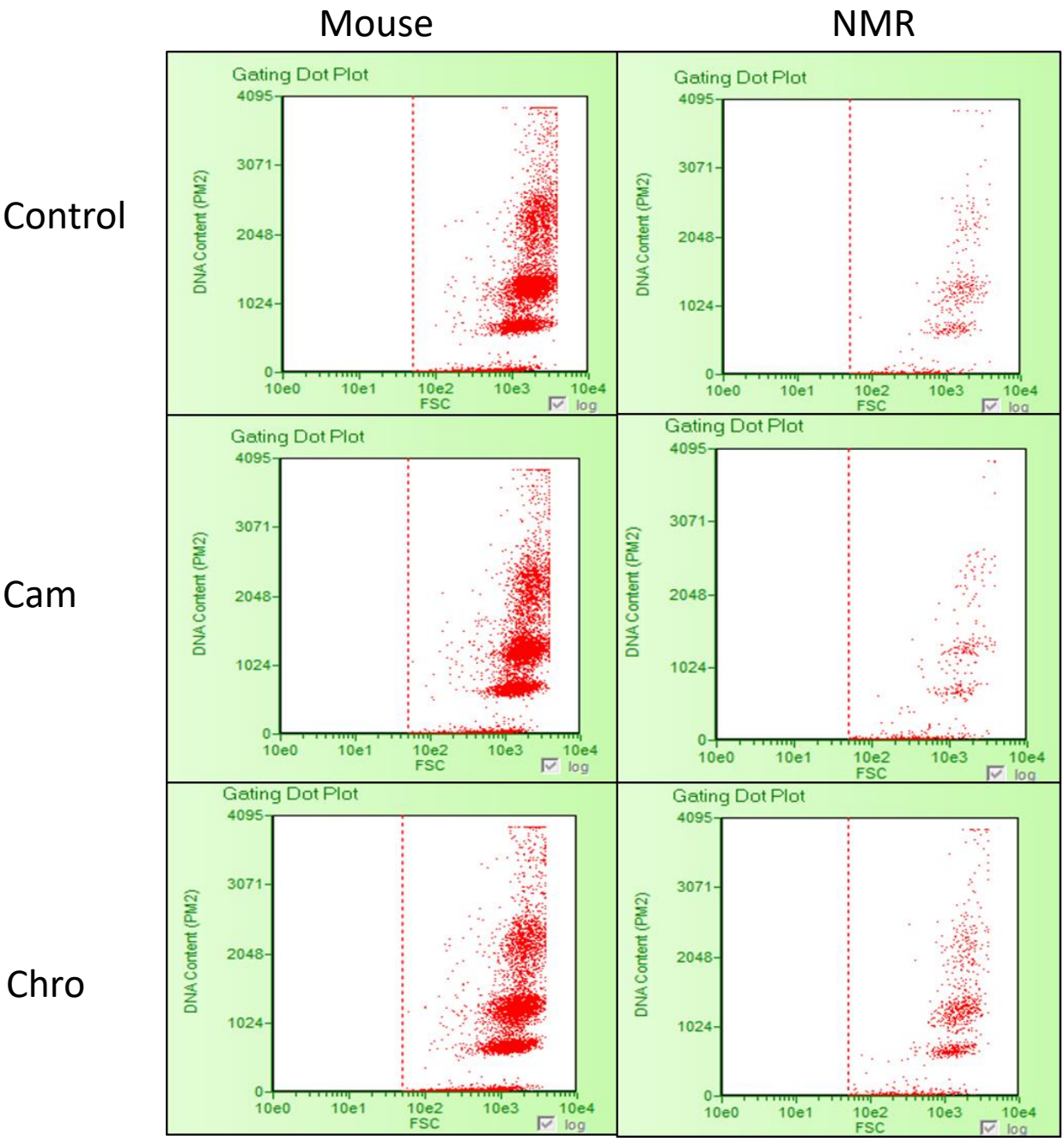

Appendix Figure 13. Representative scatter plots of Mouse and NMR samples under each treatment from flow cytometry. Mouse samples shown are of mouse cell line 3, NMR samples are of NMR cell line 3. Cam – camptothecin treatment, Chro – chromium (vi) oxide treatment.

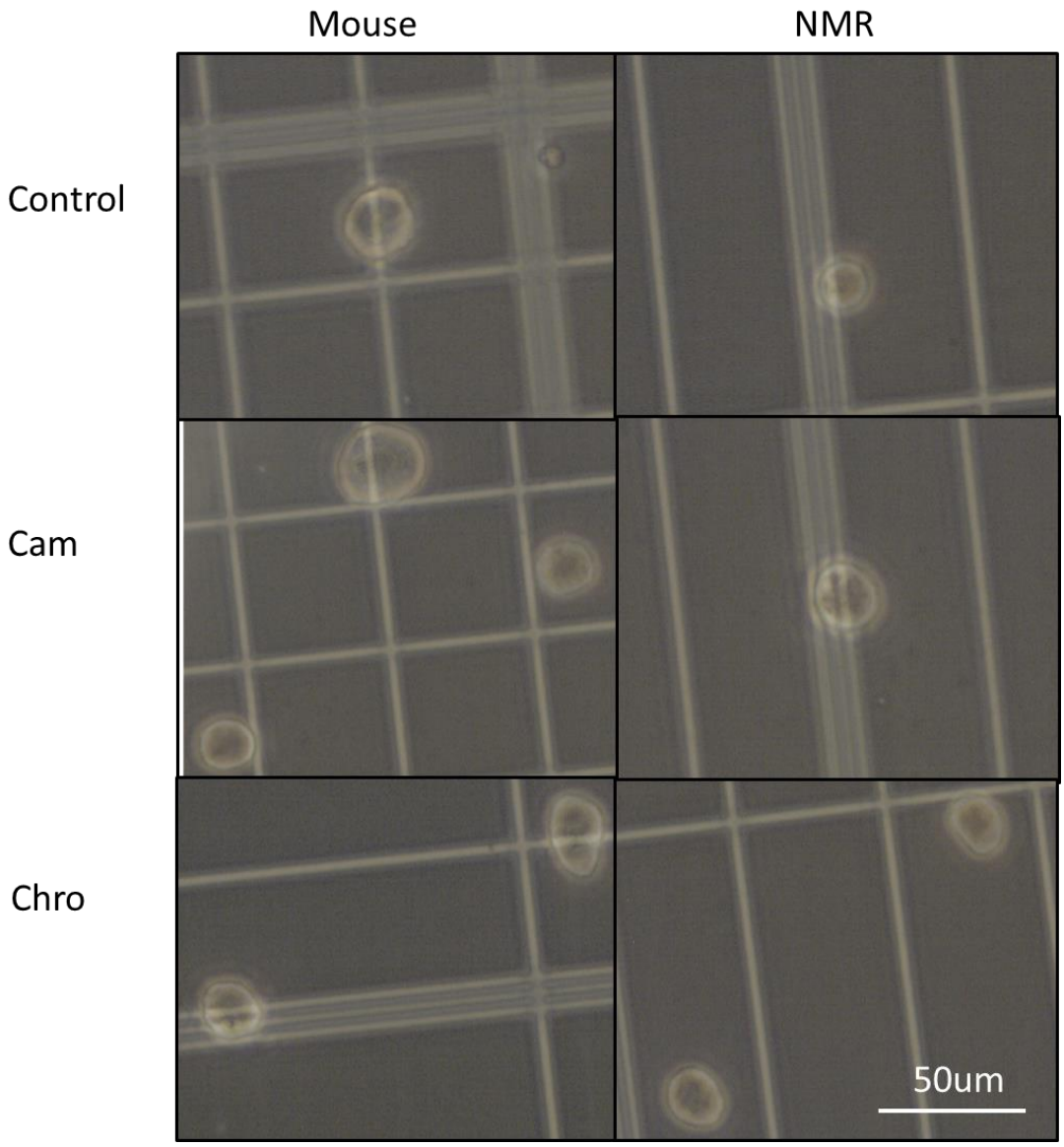

Appendix Figure 14. Representative images of trypsinised Mouse and NMR samples under each treatment prior to flow cytometry. Cam – camptothecin treatment, Chro – chromium (vi) oxide treatment. White bar indicates ~50um.

Appendix Table 8. The total number of cells analysed through flow cytometry for each cell line and treatment. Con – control, cam – camptothecin, chro – chromium (vi) oxide.

	Mouse 1	Mouse 2	Mouse 3	NMR 1	NMR 2	NMR 3
con	24,374	15,070	10,937	3,215	10,518	250
cam	13,046	18,149	8,474	2,847	18,532	262
chro	19,274	7,470	9,108	3,692	6,518	235

	Block	FBS %	Temperiture	Oxygen content	pH	starting cell count	Media change frequency
1	1	5	37	12	7	5000	low
2	1	10	37	21	7	50000	high
3	1	10	30	3	6	5000	low
4	1	10	33.5	12	6.5	27500	high
5	1	5	30	3	7	27500	high
6	1	15	37	21	6	27500	low
7	1	15	30	12	6	50000	high
8	1	10	33.5	12	6.5	27500	low
9	2	5	37	3	6	50000	low
10	2	15	37	3	6.5	5000	high
11	2	5	30	21	6.5	50000	low
12	2	5	33.5	21	6	5000	high
13	2	15	30	21	7	5000	high
14	2	15	33.5	3	7	50000	low

Appendix Figure 15. A definitive screening design to evaluate the effect of growing conditions on the cell. By default, a block is added to define which experiment should be carried out at the same time. Due to limitations with the incubator availability, this would be removed, and the temperature and oxygen content would dictate the blocking. Cells would be grown under the above conditions, and the growth rate and levels of senescence would be evaluated. These data points would be used to create a model to predict the effects of each condition.